



Universidade do Minho
Escola de Engenharia

**Development of a New Technique for Manufacturing
Biodegradable Magnesium Stents**

Vitor Emanuel Rebelo Lopes

**Development of a New Technique for
Manufacturing Biodegradable
Magnesium Stents**

Vitor Emanuel Rebelo Lopes

UMinho | 2022

janeiro de 2022



Universidade do Minho

Escola de Engenharia

Vitor Emanuel Rebelo Lopes

**Development of a New Technique for
Manufacturing Biodegradable Magnesium
Stents**

Tese de Doutoramento

Programa Doutoral em Engenharia Mecânica

Trabalho realizado sob a orientação de

Professor Doutor Hélder Jesus Fernandes Puga

Professor Doutor José Carlos Fernandes Teixeira

Janeiro de 2022

DIREITOS DE AUTOR E CONDIÇÕES DE UTILIZAÇÃO DO TRABALHO POR TERCEIROS

Este é um trabalho académico que pode ser utilizado por terceiros desde que respeitadas as regras e boas práticas internacionalmente aceites, no que concerne aos direitos de autor e direitos conexos.

Assim, o presente trabalho pode ser utilizado nos termos previstos na licença abaixo indicada.

Caso o utilizador necessite de permissão para poder fazer um uso do trabalho em condições não previstas no licenciamento indicado, deverá contactar o autor, através do RepositóriUM da Universidade do Minho.

Licença concedida aos utilizadores deste trabalho



**Atribuição-NãoComercial
CC BY-NC**

<https://creativecommons.org/licenses/by-nc/4.0/>

ACKNOWLEDGMENTS

The support and assistance I received during this work were crucial for the accomplishment of this objective. Over the past few years, with my commitment and resilience, I have been able to learn so much and grow up at a professional and personal level. However, this was only possible with the accompaniment and support of different individuals and institutions. To all of them, I would like to express my deepest gratitude.

My supervisor, Professor Hélder Puga, I thank him for believing in my potential and for making this opportunity possible. As a result of his work capacity and nonconformist character, I was always motivated to improve. He was always present and available, which was crucial for the success of this project.

To my co-supervisor, Professor José Carlos Teixeira, I am thankful for his wise and friendly advice. His knowledge, care, and friendship contributed greatly to the success of the project.

I would like to thank Fundação para a Ciência e a Tecnologia (FCT) for funding this work through the Ph.D. grant SFRH/BD/129223/2017, in the context of the Mechanical Engineering Doctoral Program at University of Minho.

I am very grateful to the Department of Mechanical Engineering of the University of Minho for all institutional support and for providing me with the opportunity to serve as an assistant lecturer. A special thanks to all departmental Professors and technical workers for their unceasing support and constant welfare. I would like to extend my sincere thanks to Professor Joaquim Barbosa for his wise pieces of advice, friendship and for supporting me along this academic journey.

To all my academic colleagues and friends over the past years, I really appreciated their unique friendship at every moment. To all my laboratory colleagues, I want to express my gratitude for their support and pleasant working hours. Special thanks to my friends Flávia and Filipe for being my true partners on this journey. It was an honor to share these moments with them.

Finally, I owe and dedicate this work to my parents, my brothers, my nephews, and my girlfriend. They are the most important people in my life.

Agradeço a Deus por tudo!

STATEMENT OF INTEGRITY

I hereby declare having conducted this academic work with integrity. I confirm that I have not used plagiarism or any form of undue use of information or falsification of results along the process leading to its elaboration.

I further declare that I have fully acknowledged the Code of Ethical Conduct of the University of Minho.

RESUMO

Desenvolvimento de uma nova tecnologia para a fabricação de *stents* biodegradáveis de magnésio

Nos últimos anos, o magnésio e as suas ligas têm sido o principal foco de vários estudos, tanto a nível académico como industrial. As propriedades mecânicas deste material, devido à sua natureza metálica e inerente baixa densidade, proporcionam altos valores de força específica e módulo específico. Contudo, as ligas de magnésio são de grande dificuldade de processamento quando fundidas. Isto deve-se à autoignição de alguns dos seus elementos constituintes abaixo da temperatura de *liquidus* e à sua elevada reatividade com os elementos circundantes acima desta temperatura. Todos estes fatores tornam a fabricação de estruturas em magnésio de paredes finas um processo extremamente complexo de difícil controlo, sendo normalmente evitado na indústria.

Relativamente à fundição de ligas de magnésio, algumas técnicas têm sido desenvolvidas para superar essas dificuldades, havendo, principalmente, um esforço considerável na mitigação das reações existentes. As abordagens estudadas e propostas incluem o uso de atmosferas protetivas, a aplicação de carapaças e revestimentos refratários, bem como a melhoria dos atuais processos de fabrico a que estas ligas são sujeitas. Embora um progresso significativo tenha sido feito para garantir vazamentos bem-sucedidos, a produção de componentes com estruturas de paredes finas continua a ser considerado um processo pouco desenvolvido e confiável.

O presente estudo aborda o desenvolvimento de uma nova metodologia de fundição por modelo perdido de paredes finas da liga de magnésio AZ91D-1 wt. % CaO em moldação de gesso, especificamente otimizada para a fabricação de *stents*. Métodos como manufatura aditiva, revestimento à base de Ítria e fundição com assistência de vácuo são investigados e aplicados para melhorar o processo. Para isso, diferentes estudos experimentais são realizados para estudo e compreensão dos fenómenos que podem ocorrer em cada etapa do processo. A interface molde-metal é devidamente caracterizada e um estudo de fluidez é realizado para perceção da influência de cada variável termodinâmica no comprimento total de enchimento das cavidades.

A obtenção de geometrias de *stents* vazados em liga de magnésio com 0,4 mm e 0,8 mm de espessura de parede demonstra o bom desempenho das técnicas propostas na mitigação das reações molde-metal, permitindo confirmar a eficácia da metodologia desenvolvida.

Palavras-chave: Fundição por modelo perdido; Ligas de magnésio; Stents; Manufatura aditiva; Reações molde-metal; Revestimento à base de Ítria; Vácuo.

ABSTRACT

Development of a new technique for manufacturing biodegradable magnesium stents

In the last years, magnesium and its alloys have been the focus of many studies in both academic and industrial fields. The mechanical properties of this material, due to its metallic nature and inherent low density, yield high values of specific strength and modulus. However, Mg alloys are known for their relatively difficult processing in casting. This is due to its auto-ignition prior to liquidus temperature in some of its constituent elements and their high reactivity above this temperature. All these factors imply that manufacturing of thin-walled magnesium structures is an extremely complex process and hard to control, which is generally avoided in industry.

Regarding the casting of magnesium alloys, some techniques have been developed to surpass this inherent difficulty. Hence, there has been essentially a considerable effort in the reactions mitigation. The studied and proposed approaches include the use of protective atmospheres, the application of refractory shells and coatings, as well as the improvement of current manufacturing processes that these alloys are subjected to. Despite of the significant progress to guarantee successful castings, the production of thin-walled magnesium structures is still considered an unreliable and not well-established process.

The present study addresses a thin-walled investment casting methodology of AZ91D-1 wt.% CaO magnesium alloy in plaster molding, specially optimized for stent fabrication. Additive manufacturing, Yttria-based coating, and vacuum-assisted casting are investigated and applied to optimize the process. To do this, different experimental studies are conducted in order to better understand all of the phenomena that may occur during each stage of the process. In this work, the mold-metal interface is extensively explored, and the effect of each thermodynamic variable on the cavity filling length is evaluated on thin-walled samples.

Magnesium stents with wall thicknesses of 0.4 mm and 0.8 mm have been obtained using the developed techniques for mitigating mold-metal reactions, demonstrating the effectiveness of the proposed methodology.

Keywords: Investment casting; Magnesium alloys; Stents; Additive manufacturing; Mold-metal reactions; Yttria-based coating; Vacuum.

TABLE OF CONTENTS

ACKNOWLEDGMENTS	III
RESUMO.....	V
ABSTRACT	VI
TABLE OF CONTENTS	VII
LIST OF FIGURES	IX
LIST OF TABLES	XIV
LIST OF ABBREVIATIONS.....	XVI
LIST OF SYMBOLS.....	XVIII
CHAPTER 1. INTRODUCTION	1
1.1. Overview and Motivation	2
1.2. Statement of the Problem	7
1.3. Research Objectives (RO).....	8
1.4. Thesis Structure.....	9
1.5. Overall Contributions of the Work	10
CHAPTER 2. BACKGROUND LITERATURE	12
2.1. Processing of Magnesium Alloys.....	13
2.2. Magnesium Investment Casting in Ceramic Molding	19
2.3. Thin-walled Magnesium Structures	22
2.4. Stent Manufacturing.....	24
2.5. Summary and Conclusions	36

CHAPTER 3. MODEL-MOLD-METAL INTERFACE CHARACTERIZATION	40
3.1. Additive Manufacturing of Models	41
3.2. Coating and Molding Making	45
3.3. Experimental Procedure	48
3.4. Case Study 1 – Effect of model’s coating on mold-metal reactions	52
3.5. Summary and Conclusions	62
CHAPTER 4. THERMODYNAMIC ANALYSIS IN MAGNESIUM INVESTMENT CASTING	64
4.1. Molding Thermal Cycle Optimization.....	65
4.2. Casting Parameters	68
4.3. Case Study 2 – Enhancement of AZ91D-1 wt.% CaO Magnesium Alloy Fluidity in Thin-walled Investment Casting.....	74
4.4. Influence of Casting Variables	85
4.5. Summary and Conclusions	89
CHAPTER 5. PROCESS VALIDATION: MAGNESIUM STENTS MANUFACTURING	93
5.1. Model’s Production: CAD and Printing.....	94
5.2. Coating, Molding, and Casting Procedures.....	99
5.3. Casting’s Characterization.....	102
5.4. Processing Methodology Overview	117
5.5. Summary and Conclusions	124
CHAPTER 6. CONCLUDING REMARKS	128
6.1. Final Conclusions.....	128
6.2. Future Work.....	131
REFERENCES.....	132
SCIENTIFIC CONTRIBUTIONS.....	154

LIST OF FIGURES

Figure 1.1: Top 5 causes of death ([2]).	2
Figure 1.2: Stent delivery system (Abbott Laboratories).	3
Figure 2.1: Degassing scheme: (A) dissolution of the argon (Ar) bubbles by the US system; (B) diffusion of hydrogen atoms and inclusions; and (C) flotation of the gas bubbles and release of the hydrogen gas to the atmosphere.	16
Figure 2.2: The main characteristics of biodegradable stents.	26
Figure 2.3: Conventional stent's fabrication: (a) primary steps; (b) initial machined minitube and stent design; (c) laser-cut minitube; and (d) electropolishing process (adapted from [156]).	27
Figure 2.4: Principal defects of laser cutting: (a) deformations; (b) burrs; and (c) porosities (adapted from [15, 208, 209]).	32
Figure 2.5: Stent manufacturing from a metallic alloy.	38
Figure 2.6: A proposed hybrid methodology for magnesium manufacturing.	39
Figure 3.1: FDM printing.	42
Figure 3.2: SLA printing.	43
Figure 3.3: Measurement of the contact angles.	44
Figure 3.4: Additive manufacturing: (a) FDM with support material; (b) FDM using cleaning tower; and (c) SLA.	48
Figure 3.5: Contact angles measurement for PLA and resin.	49
Figure 3.6: Castings after different coating applications: (a) Yttria; (b) Alumina; and (c) Sand-based slip.	50
Figure 3.7: Application of dip and spray coating methods.	51
Figure 3.8: Application of different coating thicknesses.	52

Figure 3.9: Models geometry (dimensions in mm): (a) tree assembly, and (b) analyzed sectioned part.....	53
Figure 3.10: Experimental setup of vacuum-assisted casting: 1- AZ91D-1 wt.% CaO; 2- crucible; 3- cavity of the assembled model; 4- plaster molding; 5- vacuum atmosphere, and 6- furnace.	54
Figure 3.11: Casting samples: (a) obtained results for tests performed on both uncoated and coated models, and (b) sectioned parts for characterization of the A and B points (scale in mm).....	56
Figure 3.12: The reaction mechanism proposed for the occurrence of porosity defects.	57
Figure 3.13: OM analysis of the mold-metal interaction zone (A and B areas in Figure 3.11): (a) performed test without no model coating, and (b) performed test using Y_2O_3 layers to coat the initial model.	58
Figure 3.14: Schematic mold-metal interface: (a) no use of models coating, and (b) use of Y_2O_3 to coat the models: 1- before pouring; 2- after pouring.	60
Figure 3.15: SEM analysis of the samples obtained without coating: (a) backscattered FESEM images in the periphery; (b) EDS analysis of point Z2; and (c) EDS analysis of point Z1.....	61
Figure 3.16: (a) backscattered FESEM images of the samples obtained using Y_2O_3 to coat the models, and (b) EDS analysis of point Z3.....	61
Figure 4.1: Weight loss and DTG: (a) resin; (b) PLA; and (c) plaster.	66
Figure 4.2: Thermal processing for curing the plaster moldings.	66
Figure 4.3: Application of both normal and optimized thermal cycles in plaster molding.	67
Figure 4.4: Induction furnace equipped with 1- 12 g of AZ91D-1 wt.% CaO, 2- crucible, 3- thermocouple, 4- induction coil, 5- plaster molding, 6- argon/vacuum atmosphere, and 7- external structure.....	68
Figure 4.5: Magnesium investment casting in metallic molding: (a) vacuum casting, and (b) non-vacuum casting.	71
Figure 4.6: Microstructures of the vacuum and non-vacuum cast samples in Figure 4.5.....	72

Figure 4.7: Mg stent investment casting in plaster molding of vacuum and non-vacuum castings.	73
Figure 4.8: Spiral specimen for fluidity testing.	75
Figure 4.9: Experimental casting samples resulting from fluidity studies.....	77
Figure 4.10: Steps for spirals' angle measurement.....	77
Figure 4.11: Filling length percentage for all samples obtained.	80
Figure 4.12: Filling length comparison between the different sizes of the squared cross-sections.	81
Figure 4.13: Filling length comparison between both temperatures.....	81
Figure 4.14: Filling length comparison between casting conditions: (a) condition N; (b) condition Y; and (c) condition YV.....	82
Figure 4.15: 2D μ CT images of the samples with 1.5 mm of thickness: (a) N660; (b) N720; (c) Y660; (d) Y720; (e) YV660; and (f) YV720.....	84
Figure 4.16: 3D μ CT models of the Yttria 'cracking husks' for samples: (a) 1.5Y660, and (b) 1.5YV720.....	85
Figure 4.17: SEM analysis of the mold-metal interface of sample 1.5YV720: (a) backscattered FESEM image, and EDS elemental mapping of the element (b) Y, (c) Mg, and (d) O.....	85
Figure 4.18: Response of the filling length to the variation of the factors.	87
Figure 4.19: Evaluation of the filling length comparing all the studied variables.	92
Figure 5.1: CAD stent geometry (mm): (a) design unit cell, and (b) models for testing.	94
Figure 5.2: Additive manufacturing of stents Model 1: (a) construction of support material, and (b) printing maximization.	95
Figure 5.3: Molding cooling (after pouring): (a) placement of thermocouples, and (b) recording of temperatures.....	98
Figure 5.4: Schematic representation of molding temperature distribution during pouring.	99
Figure 5.5: Schematic representation of molding temperature distribution 3 minutes after pouring.	99

Figure 5.6: Model 1 processing: (a) additive manufacturing; (b) tree assembly; and (c) Yttria coating	100
Figure 5.7: Thermal cycle optimized and applied to the plaster moldings when Yttria coating is used in stent manufacturing.	101
Figure 5.8: Experimental setup used for stent manufacturing.....	102
Figure 5.9: Yttria-coated cast stents.	103
Figure 5.10: Volume ratio of coated stents during the process.	105
Figure 5.11: Uncoated cast stents and preparation of samples for microscopic characterization.	105
Figure 5.12: Model 1 SEM analysis.	106
Figure 5.13: Model 2 SEM analysis.	106
Figure 5.14: Backscattered FESEM images of the Model 2 uncoated unit cell.	107
Figure 5.15: Backscattered FESEM images of the Model 2 coated unit cell.	108
Figure 5.16: Values of oxygen concentrations in all castings.	110
Figure 5.17: Hardness analysis of the Model 2 unit cell.....	110
Figure 5.18: XRD analysis of the Model 2 unit cell.....	111
Figure 5.19: Study of the influence of the molding and pouring temperatures for condition N.	112
Figure 5.20: Influence of pouring temperature for condition N.	113
Figure 5.21: Stent obtained for both models through casting condition N: (a) printed Model 1; (b) printed Model 2; and (c) cast stents for both models.	114
Figure 5.22: Comparison of conditions YV and N for indirect filling stent casting.	115
Figure 5.23: SEM analysis of the Model 1 unit cell for condition N.	116
Figure 5.24: Comparison of Model 1 stent casting applying different casting conditions.	117
Figure 5.25: Micro-CT for both cast stents: (a) Model 1, and (b) Model 2.	118
Figure 5.26: Micro-CT of the Model 1 printed stent: (a) 3D model reconstruction showing printing failures, such as (b) scars, (c) excess material, and (d) small pits.	119

Figure 5.27: Micro-CT of the Model 2 printed stent: (a) 3D model reconstruction showing printing failures, such as (b)(d) excess material, (c) small pits, and (e) dimensional inaccuracies.....	119
Figure 5.28: micro-CT of the Model 1 cast stent for condition YV: (a) X-Z plane, (b) isometric view of X-Z plane, (c) X-Y plane, and (d) Z-Y plane.	121
Figure 5.29: MgO formed on the crucible during the investment casting for condition YV.....	123
Figure 5.30: Stent investment casting using the commercial AZ91D magnesium alloy for condition YV: (a) during melting, and (b) after pouring.	124
Figure 5.31: Optimal range of temperatures for stent manufacturing under the casting condition N.	127

LIST OF TABLES

Table 1.1: Main properties of pure magnesium [29].	5
Table 1.2: Relative power and comparative machinability (According to Luxfer MEL Technologies*).	6
Table 2.1: Advantages and drawbacks of different processing methods for obtaining biomedical devices.	37
Table 3.1: Comparison between FDM and SLA characteristics.	43
Table 3.2: Coating application characteristics.	46
Table 3.3: Acquisition data for wettability analysis (one measurement reading).	49
Table 3.4: Chemical composition of AZ91D-1 wt.% CaO magnesium alloy (mass%).	55
Table 3.5: Key parameters adopted during processing.	55
Table 3.6: Possible mold-metal reactions on Mg-SiO ₂ interface [48].	58
Table 4.1: Technical data of the experimental setup (according to the manual).	69
Table 4.2: Optimal safe casting parameters (experimentally optimized).	70
Table 4.3: The main variables and values used in evaluating fluidity.	75
Table 4.4: Calculated values from the experimental fluidity study.	78
Table 4.5: Selected factors and their levels.	86
Table 4.6: Results of Analysis of Variance.	88
Table 5.1: Filling design optimization using condition YV and 720 °C pouring temperature.	96
Table 5.2: Optimized painting characteristics.	100
Table 5.3: EDS analysis of the points indicated in Figure 5.14.	107
Table 5.4: EDS analysis of the points indicated in Figure 5.15.	108

Table 5.5: EDS analysis of the points indicated in Figure 5.23.	116
Table 5.6: X-ray μ -CT scan parameters in Figure 5.25.	118

LIST OF ABBREVIATIONS

2D	Two-dimensional
3D	Three-dimensional
ABE	Accumulative Back Extrusion
ABS	Acrylonitrile Butadiene Styrene
ANOVA	Analysis of Variance
CAD	Computer-aided Design
CEC	Cyclic Extrusion and Compression
CEE	Cyclic Expansion Extrusion
CNC	Computerized Numerical Control
DoE	Design of Experiments
DoF	Degrees of Freedom
DTG	Derivative Thermo Gravimetry
ECAP	Equal Channel Angular Pressing
ECO-Mg	Environment-Conscious Magnesium
EDS	Energy-dispersive X-ray Spectroscopy
EX	Direct Extrusion
FDM	Fused Deposition Modelling
FESEM	Field Emission Scanning Electron Microscopy
HPDC	High Pressure Die Casting
HPT	High-Pressure Torsion
MAP	Magnetic Abrasive Polishing

Micro-CT (μ -CT)	Micro-computed Tomography
MIM	Metal Injection Molding
MSA	Mobile Surface Analyzer
MTE	Microtube Extrusion
OM	Optical Microscopy
OWRK	Owens-Wendt-Rabel-Kaelble
PLA	Polylactic Acid
PM	Powder Metallurgy
PVA	Polyvinyl Alcohol
RE	Rare Earth
SEM	Scanning Electron Microscopy
SLA	Stereolithography
SLM	Selective Laser Melting
SMA's	Shape Memory Alloys
SPD	Severe Plastic Deformation
SS	Sequential Sum of Squares
SS'	Pure Sum of Squares
STL	Standard Triangle Language
TCAP	Tubular Channel Angular Pressing
TGA	Thermal Gravimetric Analysis
UST	Ultrasound Technique
UV	Ultraviolet
WHO	World Health Organization
XRD	X-ray Diffraction

LIST OF SYMBOLS

Symbol	Unit (SI)	Description
l	m	Length of the squared cross-section (spiral)
L	m	Filling length (spiral) and total length (stent)
\emptyset	m	Diameter
p	m	Spiral pitch
$R(\theta)$	m	Radius of the spiral in position θ
R_0	m	Initial radius of the spiral center
T	K	Temperature
t	m	Stent wall thickness
ΔG_f°	m	Gibbs free energy of formation
θ	rad	Angular parameter along the spiral
x, y, z X, Y, Z	-	Cartesian coordinates

There is a scientific publication of 1997 entitled "The origin of the word stent". Although it remains uncertain, it seems likely that the word originated with the dentist Charles T. Stent (1807-1885) [1].

Chapter 1. INTRODUCTION

As engineering applies to various knowledge fields, society have become accustomed to significant innovations, constructions, and improvements. Engineering is synonymous with development and will continue to be. It continues to be critically important in every knowledge area and major market sector to optimize processes and products in order to minimize resources employed, namely time, costs, and manpower.

Considering its scientific and innovative focus, the main objective of this study is to develop an innovative methodology for casting Mg (magnesium) alloys in plaster molding, as well as its optimization for thin-walled magnesium alloy parts, especially stents.

Magnesium Alloy (material), Investment Casting (process), and Stent device (application) are the three major pillars of this research, which is of great interest to both the scientific community and the industry, thereby presenting an added value to the advancement of this theme in the field of engineering.

1.1. Overview and Motivation

Ischemic heart disease currently ranks as the world's biggest killer, as can be observed in Figure 1.1. According to recent data collected from the WHO (World Health Organization) and displayed on their website, in the last 21 years, this disease has been the leading cause of death increase, rising by more than 2 million to 8.9 million deaths in 2019, which represents 16 % of all global deaths [2]. The issue is a grave and real one, which has intensified over the years and has not undergone significant evolution regarding the search for new solutions or the enhancement of existing ones. It is necessary to act predictively and not only in a corrective and/or preventative manner.

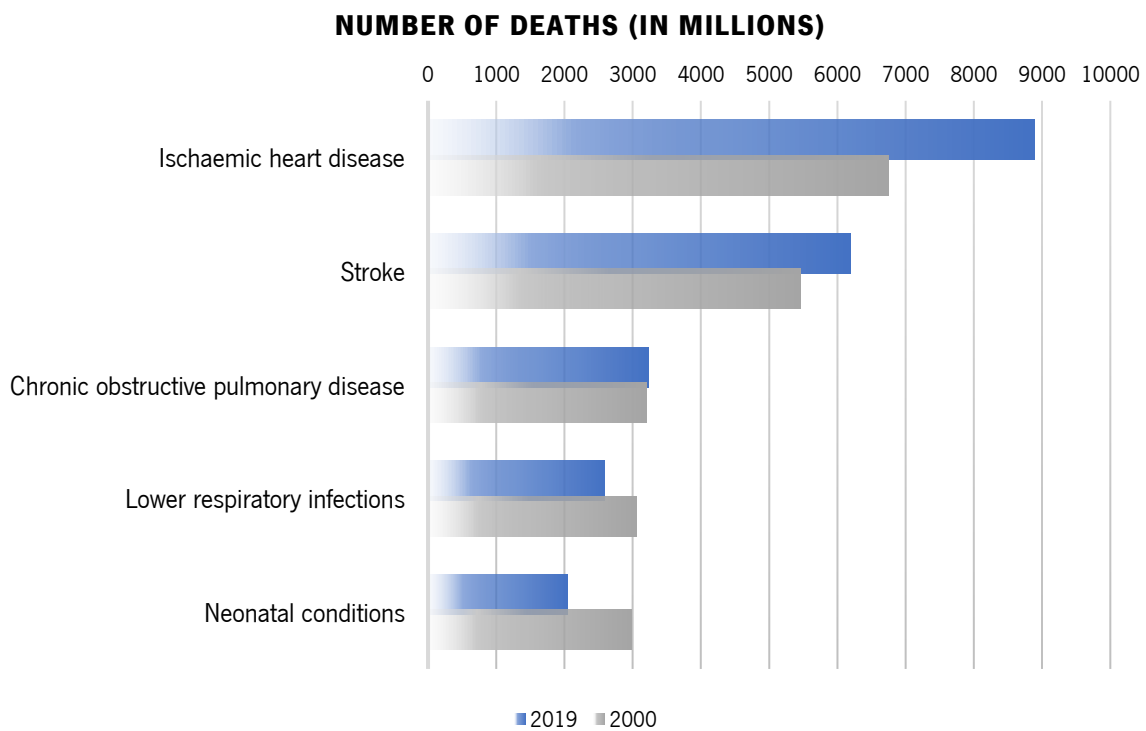


Figure 1.1: Top 5 causes of death [2].

Atherosclerosis is the most common cause of coronary artery disease. The thickness increase and the elasticity loss of the arterial walls can lead to artery blockages, limiting the normal blood flow. A complete blockage of arteries can lead to serious health problems, including angina, myocardial infarction, arrhythmias, and even death caused by heart failure.

According to the severity of the injury and the clinical history of the patient [3], percutaneous coronary interventions (also called coronary angioplasty) with stent deployment have constituted one of the main methods to combat this problem and the most appropriate to apply

over time [4, 5]. A stent is a metallic expandable knitted medical device introduced into veins and arteries. Through its radial expansion, it unclogs such vessels to increase blood flow to the organs and prevent complications generated therein [6, 7]. In-stent angioplasty, a medical device is mounted in a flask with the orientation of a catheter system. As shown in Figure 1.2, the balloon-stent system is introduced as a compressed form into the clogged region, after which it is inflated to compress the plaque against the vessel walls. The balloon is removed after angioplasty, and the stent remains in the artery to support maintaining the vessel walls open, ensuring correct blood circulation. Therefore, the application of the stent has sparked interest by the scientific community in this thematic, and there have been several studies conducted on the design and manufacture of this medical device.

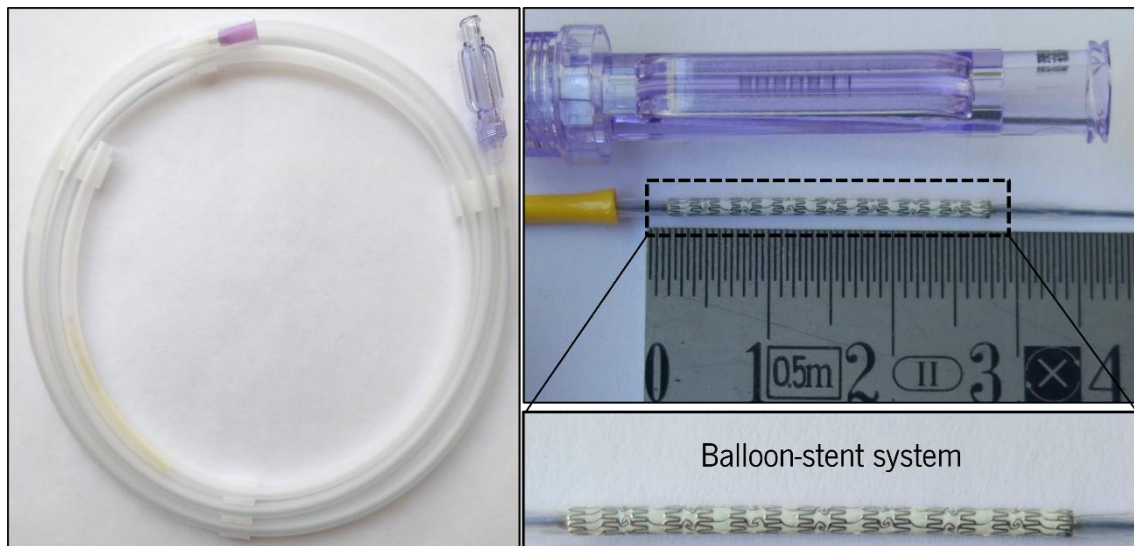


Figure 1.2: Stent delivery system (Abbott Laboratories).

Nowadays, most metal stents are manufactured in stainless steel and alloys based on nickel and titanium, cobalt and chromium, platinum, and others [4, 8-12]. As a result, these materials provide mechanical properties that enable the stents to perform a structural role within vessel walls without compromising the blood flow [13]. Regarding the manufacturing process, and according to studies reported by Demir and Previtali [10], Hermawan *et al.* [14], and Moravej and Mantovani [15], laser cutting is the usual method used for fabricating metallic stents, even though some subsequent finishing operations (deburring, chemical finishing, electropolishing, electroplating, and others) are required to improve, essentially, the superficial quality of the stents [10, 16]. Although actual stent fabrication requires sophisticated manufacturing processes and materials offering better properties, the need for metal stents to remain permanently in the same region where they are placed remains a barrier to biocompatibility between stents and the human

organism, compromising the implant success [17, 18]. A stent's long-term presence inside the artery can lead to complications, such as restenosis [4, 19], late thrombosis [20, 21], and other complications, for instance, the internal artery lining in response to arterial wall injuries and inflammatory reactions, which raises questions about the evolution of treatments for heart disease [22].

In some cases, a second surgery is required to remove the stent or insert an alternative, resulting in serious health problems, even death. Additionally, the manufacturing process can also be cause-related to some health complications in stent' applications. The laser cutting process, for example, can induce thermal problems that cause insufficient surface quality to the manufactured stents [6]. Even more, if the stent does not have good visibility under fluoroscopy, the actual stent placement procedure can also pose problems associated with stent placement and interaction [23, 24].

Therefore, addressing stent models improvement presents a clear opportunity for progress in addressing the growth and benefits of engineering advances [14]. Stents made of biodegradable materials, such as magnesium, and through methods that can overcome some of the current manufacturing limitations, can be considered a field that presents an enormous potential for success in combating the deadliest diseases in today's world [25-27]. On the other hand, the limited information about processing techniques applied to magnesium applications has been an important catalyst for the scientific community to develop this theme, which has sparked an increasing interest in lightweight materials. Magnesium has indeed been the subject of increasing interest both at the academic and industrial levels. This can be justified by the growing knowledge of applying its excellent properties (Table 1.1) and by the compelling need for continuous improvement of engineering systems. In addition to being one of the most abundant elements on the planet, which avoids problems in its exploitation, magnesium has a density value of 1.7 g/cm^3 , which is 33 % lighter than Al (aluminum) and 75 % lighter than steel, presenting as well good mechanical performance [28].

Table 1.1: Main properties of pure magnesium [29].

Property	Unit	Value
Atomic mass		24.31
Atomic number		12
Boiling point	°C	1107
Crystalline structure		A3
Density at 20 °C	g/ cm ³	1.74
Elastic modulus	GPa	40
Elongation	%	2-10*
Hardness	HBW	45-47*
Thermal conductivity	W/ (m·K)	418
Melting point	°C	650
Resistivity	nΩ·m	44.5
Specific heat capacity	kJ/ (kg·K)	1.025
Tensile strength	MPa	180-220*
Thermal expansion coefficient	10 ⁻⁵ 1/ K	25.2
Yield point, 0.2	MPa	115-140*

*rolling

Magnesium has gained its largest application area by creating alloys in combination with other elements. Currently, magnesium alloys have ceased to be future materials and have become present in some specific areas [30]. This fact was recently corroborated by Xu *et al* [31], which reported that the ongoing interest in studying and exploring magnesium alloys resulted in a growth rate of 491 % of publications in the 21st century. In addition to being one of the lightest metals, these alloys have an excellent strength-to-weight ratio, which helps justify the high investments carried out by the scientific community and the industrial sector. Moreover, the demand for these kinds of alloys is driven by their distinct and attractive engineering properties. As a result of their low density, good castability, and high damping capacity, there has been a continuous demand for their use in a wider range of applications, such as aerospace industry [32], as well as for automotive applications [33, 34]. Thus, magnesium and its alloys (Mg alloys) have tremendous potential to replace materials such as steel, aluminum, and plastic-based materials, increasing the research interest to improve further their properties [35, 36]. Science has continued to investigate emerging technologies for magnesium alloys and increase their use for a significant evolution in these industries [37, 38]. According to Lara-Rodriguez *et al.* [39] and Kucharczyk *et al.* [40], the functional properties of Mg foams, such as sound and energy absorption and excellent vibration

reduction capacity, allow promising applications of porous metal structures for medical purposes. In addition, due to these lightweight materials' biodegradable and biocompatible characteristics in combination with the previous properties, Mg alloys have been the subject of several investigations for the production of temporary implants and orthopedic applications [41]. Yang *et. al* [42] also considered recently that Mg alloys have a high potential as heat sink materials due to their thermal properties. Furthermore, magnesium is also advantageous in its ability to be machinable compared to other commonly used metals, as shown in Table 1.2.

Table 1.2: Relative power and comparative machinability (According to Luxfer MEL Technologies*).

Metal	Relative Power	AISI – B1112 Machinability** Index (%)
Magnesium alloys	1.0	500
Aluminum alloys	1.8	300
Mild steel	6.3	50
Titanium alloys	7.6	20

*www.luxfermeltechnologies.com

**Machinability can be defined as the capability of one material to be cut by another. Cannot be quantified.

Hence, magnesium and its alloys, along with aluminum and its alloys, are currently considered ideal materials to be applied in structural applications. Moreover, resources for magnesium-based alloys, are not abundant but unlimited, because these materials are inherently recyclable.

Nevertheless, improving materials also requires the demand for new and improved manufacturing processes. So, developing a methodology for making stents from magnesium alloys is the main purpose of this research, to address the current stent's problems and needs. Bearing that in mind, the application of the investment casting process in plaster molding will be investigated. The casting technique is used to overcome some limitations that are evident in traditional methods, primarily poor surface quality caused by laser cutting. This process is capable of obtaining parts from practically any metal or alloy. It is economically advantageous in comparison to other manufacturing processes because it is a low-cost method that allows easy manipulation and control of various sizes and shapes [43]. Furthermore, the use of ceramic moldings allows producing near-net-shape parts with a high surface finish (roughness below 3.2 μm) and a high capacity for reproducing details [44].

1.2. Statement of the Problem

Engineering has played a significant role in the treatment of coronary artery disease and the stents' deployment in blood vessels is considered the most appropriate method to be used. Although the current ones used, called permanent stents, possess high mechanical properties and biocompatibility, their introduction into the vessels is definitive. This limits the long-term success of these applications since they may be difficult to remove, resulting in the necessity for a new procedure and the introduction of additional stents.

As seen in the previous subchapter, there is a clear need to use biodegradable materials to manufacture temporary implants, such as stents, in order to prevent these problems. In this sense, magnesium's biodegradable properties provide a promising solution for treating coronary artery disease in the future [26]. After completing its function of clearing the vessels, Mg-based stents gradually disintegrate themselves until their complete dissolution in physiological environments, not representing a threat to the patient's health. However, despite their benefits and suitable properties, the use of magnesium alloys in the manufacture of stents does have some disadvantages. Since magnesium is a very reactive material and corrodes very quickly, it is challenging to be processed and control its corrosion rate at controlled intervals. Additionally, magnesium's practical and clinical use has been affected by obstacles related to this disadvantage, such as insufficient mechanical stability over time [45, 46].

Investment casting thus appears to be a feasible and practical solution for producing magnesium-based castings. However, the processing of magnesium alloys by casting technologies, especially investment casting, remains a challenge due to magnesium's high ability to react with the molding materials and with the environmental atmosphere, as reported by Jafari *et al.* [47-49]. According to these authors, the oxidation and reaction rates that may occur during the entire process can be a consequence of reactions between the liquid metal and the surrounding atmosphere during the melting phase, and/or by the contact between the liquid metal and the molding walls during the pouring and filling phases.

The presence of oxygen is fundamental to the occurrence of oxidation and reaction, as well as the remaining effect. During the melting phase, inert protective atmospheres may prevent oxidation since the cover gas is not involved in a chemical reaction, but merely serves as a protection from oxygen/air, so flow rates are not critical. As a result of the high affinity of magnesium for oxygen, the main challenge during the investment casting process is preventing

mold-metal interaction. The severe reaction may have been caused by Mg's interaction with the SiO_2 in the plaster composition. Combining these elements can trigger a series of chemical reactions that give rise to different types of reaction products [47, 50]. The direct interaction allows Mg and SiO_2 to diffuse, forming a greater reaction zone as metal and molding temperatures rise, significantly increasing cooling time and allowing continuing reactions for longer periods.

Many approaches have been developed to mitigate these interface reactions. Different techniques, including shell investment moldings, refractory coatings, and protective inert atmospheres, continue to attract the attention of researchers.

1.3. Research Objectives (RO)

This work has been developed under the Doctoral Program of Mechanical Engineering at the University of Minho, Portugal. Its vision includes two main lines. i.e., training highly qualified specialists capable of autonomous research, development, and innovation work in a university and/or business environment, and preparing new human resources to produce new knowledge and disruptive innovation.

Considering this, the main goal of this work is **to develop an innovative processing methodology to obtain magnesium thin-walled parts**. Hence, it is expected that the developed methodology based on the combination of additive manufacturing and investment casting process in plaster molding must be used to obtain stents and other thin-walled parts from a magnesium alloy, resulting in final casting parts with good metal sanity and high dimensional and detail precision. To accomplish that, a set of multidisciplinary goals was established to:

- RO.1** Provide a better understanding of the mold-metal reactions in the investment casting of AZ91D-1 wt.% CaO magnesium alloy, studying the occurrence of reactions between the liquid metal and the molding walls, as well as the effect of model's coating;
- RO.2** Propose and apply a novel methodology to mitigate/reduce the reaction's rate on the process, identifying the factors affecting thin-walled manufacturing the most;
- RO.3** Study the effect of various factors, such as the printing quality from additive manufacturing, the coating application, the protective atmosphere, and the casting parameters on both the dimensional and surface characterization, as well as the microstructure of the final cast parts;

RO.4 Characterize the casting variables' effects on the fluidity alloy, evaluating the process' effectiveness in different contexts;

RO.5 Establish the optimal casting parameters for manufacturing Mg stents, namely those related to the thermodynamic analysis.

As demonstrated in subchapter 1.2, the study of processing Mg alloys through the combination of additive manufacturing and investment casting is still a very recent issue and in full development, especially for thin-walled parts. The accomplishment of the objectives proposed in this work could have a great impact on the scientific community. So, this could be a starting point for further research in this area, providing a strong connection with the industrial context. Additionally, this thesis explores the issue of the "file drawer problem," also known as "publication bias," in which results with positive results are more likely to be published. In that sense, all of the steps taken throughout this work are justified regardless of whether their influence on the outcome is significant or not.

1.4. Thesis Structure

Using a combination of additive manufacturing and investment casting, the present thesis addresses all the steps necessary for achieving the defined objective of creating thin-walled magnesium stents. Among these steps are the state of the art of the main subject, the definition and optimization procedures used, and the analysis for validation. Thus, this document is divided into six main chapters.

The contextualization of the theme and the motivation to develop this research work are provided in the first chapter. Here, the problem statement is described, and the main objectives are defined. The overall contributions of this thesis are also highlighted.

The second chapter examines the background literature on magnesium processing. The convergence of Mg alloys processing for manufacturing stents is discussed. In the sequel of this process, different techniques for handling magnesium alloys are presented, as well as the process for casting magnesium in ceramic molding. An overview of thin-walled magnesium structures is also provided, followed by the definition and description of the proposed method for manufacturing magnesium parts.

Chapter three details the initial steps of the proposed experimental methodology in detail. Additive manufacturing contributes to creating the molding cavities by printing three-dimensional polymer models. Moreover, the sequence of procedures for applying the coating to the initial models is described, as well as the steps involved in making plaster moldings. In this chapter, a case study is conducted to determine the effect of the coating model on the mold-metal reaction interface.

Chapter four describes the last steps of the proposed methodology, including optimizing the thermal treatment used for curing moldings, and defining the casting parameters that can guarantee a safe Mg casting process. Regarding magnesium handling, different casting conditions are defined, used, analyzed, and correlated in the investment casting of thin-walled magnesium parts. An evaluation of fluidity is presented in this chapter for the AZ91D-1 wt.% CaO magnesium alloy under all defined casting conditions. The results analyzed indicate an improved perception of the process effectiveness and how each variable contributes to the obtained results.

Following all the optimized processes from previous chapters, the proposed methodology for stent manufacturing is applied in chapter five. Different casting conditions are applied for two different stent models made by additive manufacturing, with the results compared and correlated to help clarify the occurrences. In addition to the surface quality characterization of the castings, microstructural characterization and micro-CT (Micro-computed Tomography) analysis are conducted to evaluate the metal quality of the stents, as well as its geometric and dimensional accuracy. A description of the method's effectiveness is also presented, depending on the casting condition applied.

Finally, chapter six summarises the most relevant conclusions of this work. Additionally, some future research proposals are outlined to complement this project, which can contribute to a higher magnesium alloy acceptance in the foundry industry.

1.5. Overall Contributions of the Work

This Ph.D. thesis provides a general methodology to respond to the extreme difficulty in handling magnesium alloys through the combination of additive manufacturing and investment casting process in plaster molding. Many aspects of processing Mg alloys are investigated, namely, the reaction phenomena that can occur between magnesium and the surrounding atmosphere during the melting phase, as well as between liquid melt and the plaster from the moldings during

the pouring and cooling stages. Some of the most important studies published by the scientific community, related to this thematic, are taken into consideration and described in the next chapter.

An experimental study concerning the influence of coating on magnesium models is outlined in this work. Different coating materials and applications techniques are presented and tested in order to optimize the process. The results demonstrate that Yttria coating is a very effective solution for mitigating mold-metal contact and, consequently, preventing the reaction rate resulting from the castings.

Different casting conditions are tested and compared regarding the reactions occurring during the magnesium melting phase, considering some relevant thermodynamic and model variables, such as pressure, temperature, and filling thickness. In order to analyze the casting reactions, a fluidity analysis is performed based on the variables' variances described above on the magnesium alloy used. This approach provides in-depth knowledge about the relationship between metal sanity and the filling quality of magnesium cast parts. There is a clear compromise between casting effectiveness (absence of reactions and oxidations) and metal fluidity (filling length), which is influenced by the balance between the pouring and molding temperatures, the filling thickness, and the processing conditions (use of refractory coating and vacuum assistance). This development is vital for a better understanding of reactions that take place in the processing of Mg alloys, and it is very promising for an increasingly safe introduction of magnesium alloys into industrial foundries.

In order to characterize the thin-walled process developed in this work, some analyzes are performed evaluating the casting quality and the microstructure sanity of both stent models, using different types of equipment. Depending on the casting condition used, the results allow to ascertain which optimal casting parameters are needed that guarantee a safe and effective Mg casting.

Several publications related to the themes presented in this thesis have been published in both academic journals and at international conferences. A list of these publications is provided at the end of this document.

According to the authoritative scientific literature database Web of Science Core Collection, the number of publications on magnesium alloys has increased from 1344 in 2008 to 3034 in 2020.

Chapter 2. BACKGROUND LITERATURE

With the coverage of the literature review on biodegradable medical devices, one may conclude that, although the mechanical and medical properties of the material applied are important, finding a focus should be placed on finding the best fabrication process to manufacture those devices. The processing methods greatly impact the final device's characteristics, especially in stent manufacturing [51]. Additionally, when developing metallic biodegradable applications, the fabrication process determines whether a piece of starting stock can be converted into a functional medical device in a cost-effective manner, which is an exceptionally critical factor [11]. In the case of stent manufacturing, different fabrication processes may be used to improve the mechanical and structural properties and control the degradation rate of the devices, which becomes a disadvantage when using biodegradable materials. Therefore, several techniques for strengthening the properties of magnesium alloys have been studied, and different processes for manufacturing them have been developed according to their end use.

In this work, the stent processing is directly correlated to the material, i.e., magnesium alloys. Thus, the topic of this chapter relates to the materials and manufacturing processes used in magnesium processing, and how they relate to the use of stents. Various approaches to stent manufacturing are analyzed, and a new promising method as a potential solution is described.

2.1. Processing of Magnesium Alloys

Magnesium alloys have a large margin of progress in obtaining better and higher engineering properties, increasing their interest in constantly growing sectors. Emerging studies have highlighted some methodologies that enhance the mechanical properties of magnesium alloys, focusing on alloying, microstructure control, and others.

The addition of elements is one of the most commonly used methods to achieve higher properties, as referred to by Wang *et al.* [52] and Razzaghi *et al.* [53], following the studies of Xue *et al.* [54] and Wang *et al.* [55]. Particularly regarding the manufacturing of stents and other medical devices, the addition of suitable magnesium elements ensures they can perform their biomechanical role of supporting the vessel walls during the remodeling process, which occurs within 6 to 12 months [11]. Once the stent completes its purpose, the corrosion product of the Mg alloy generated by the electrochemical reaction is absorbed or excreted by the surrounding tissues and by the metabolic system of the human body [12].

Different magnesium alloys can be made by adding different elements, depending on the desired properties. It is common to add aluminum (AZ31, AZ91, LAE422, AM60, etc.) and rare earth elements (WE43, AE21, etc.) to magnesium alloys in order to optimize grain size, improve corrosion resistance, provide mechanical strength through intermetallic formation, and facilitate their processing [56, 57]. As an example, finer grain size alloys promote improved ductility, because they activate deformation mechanisms other than those commonly observed for basal slip and twinning [58]. Growth restriction can also achieve grain refinement during solidification, contributing to a homogeneous distribution of intermetallic constituents and facilitating subsequent thermo-mechanical processing [59, 60].

According to numerous scientific publications, Al, Ca, Mn, Y, and Ce are the most used chemical elements in magnesium. These elements can react with Mg to form intermetallic phases, which can dissolve in the grain matrix or distribute along the grain boundary, thereby influencing their mechanical properties and corrosion behavior.

Aluminum is the most used alloying element for Mg alloys, presenting a maximum solubility of 12.7 wt.% in Mg and constituting several Mg-Al-based alloy systems that have been used for industrial applications. Dobrzanski *et al.* [29] and Agarwal *et al.* [56] report that only Al additions of 1-5 % can affect the grain size, making them smaller. The as-cast Mg-Al alloys show α -Mg matrix

and β -phases predominantly in the form of $Mg_{17}Al_{12}$ phases, which precipitate along the grain boundaries as a result of the Al dissolution in Mg solid solutions. These secondary phases increase with increasing Al contents, exhibiting a 'net-shaped' distribution when Al amounts exceed 3 % [29]. The influence of the $Mg_{17}Al_{12}$ phase on the corrosion resistance is not linear. It can either accelerate the corrosion of the alloy by acting as a cathode concerning the α -Mg matrix [56, 61], or it can reduce corrosion by acting as a corrosive barrier with respect to the β -phase volume fraction, which is higher and distributed along the grain boundary [56, 62]. Moreover, high Al contents can improve the castability of Mg alloys by lowering the liquidus and solidus temperature lines [63].

The addition of calcium (Ca) promotes grain refinement. According to Li *et al.* [64], the optimal concentration should be less than 1 %. When Mg-Ca alloys have a high Ca content, the Mg_2Ca secondary phase which forms at grain boundaries is brittle, reducing ductility and corrosion resistance due to the formation of micro-galvanic cells [56, 64]. Additionally, CaO can be added to Mg alloys to produce ECO-Mg (Environment-Conscious Magnesium) alloys. According to the purpose, these master alloys with a high weight percentage of CaO are prepared in advance and then mixed and diluted to produce ECO-Mg alloys in the CaO range of 0.2 % and 1.5 % [29]. Numerous studies have already shown that adding CaO to Mg alloys has several advantages, including no-SF₆ processing, improved melt cleanliness, improved mechanical properties through grain refinement, improved oxidation and ignition resistance, improved recyclability, and cost reduction [65-69].

Likewise, manganese (Mn) is a very common alloying element used in Mg alloys to reduce the grain size. According to Ding *et al.* [61], Song and Atrens [70], and Walker *et al.* [71], Mn addition can also improve the mechanical and corrosion properties of extruded Mg alloys, but at controlled levels.

Moravej and Mantovani [15] and Wang *et al.* [55] also report the addition of RE (rare earth) elements such as Y and Ce, as well as other metallic elements including niobium, lithium, zirconium, and calcium. It aims to manipulate and control the microstructure of the magnesium alloy (grain size and intermetallic morphology - $Mg_{17}Al_{12}$ refinement) in order to increase their corrosion resistance and mechanical properties [72, 73]. The RE elements are a group of 17 elements, typically added to Mg alloys as master alloys [29]. Master alloys, also commonly referred to as hardeners, are pre-alloyed concentrates or mixtures of alloying elements used to add all the major alloying elements in one form to the melt to produce a particular alloy, to modify a melt, or

to alter processing characteristics to achieve desired properties. For instance, Al-Ti-B (aluminum-titanium-boron) master alloys are known to be grain refiners in aluminum alloys. Indeed, some reports have also evaluated its effect on the mechanical properties of AZ (aluminum-zinc) magnesium alloys, concluding that the grain sizes can be reduced effectively [74-76].

The application of an ultrasound technique (UST) is also pointed as a solution for grain refinement, melt cleanliness and degassing, as well as molding filling [77]. Acoustic energy has been the subject of many scientific studies, including studies of magnesium alloys. For instance, higher mechanical properties were achieved with the AZ91D magnesium alloy by microstructure refinement, ultrasound melt treatment [78], and degassing techniques [79]. In fact, one of the most used ultrasound applications is the degassing process, which involves the release of gas. This operation is particularly important when processing light metals and their alloys. These materials, when in the liquid state, present great affinity to the absorption of gas through their surface layer. Indeed, magnesium alloys' melts are characterized by a high hydrogen solubility, making them very suited to pick up gases from the atmosphere. Studies conducted by Lee [80] and Mikucki and Shearouse [81] have found that even a small portion of hydrogen may affect the formation of microporosities, while larger pores may form at the grain boundaries or near the second phase if hydrogen content exceeds the solubility limit at the heading face of liquid-solid [79]. This issue is more common in high alloyed magnesium alloys, such as AZ91, since these materials exhibit a wider solidification range, allowing for more time and space for the nucleation and growth of gas pores – the weak spots of the alloy.

Argon degassing itself in magnesium alloys can cause a strong disturbance, increasing the number of melt slags, as these materials are highly reactive, oxidize, and burn. The use of ultrasonic vibrations allows the breaking of the large argon bubbles into smaller ones and disperse them uniformly in the melt, leading to an efficient degassing process that reduces the melt loss, as well as the intense flow turbulence. The high-intensity ultrasonic vibration promotes oscillating pressures that create multiple small cavities in the liquid, which grow fast in response to the alternating pressure and the unidirectional diffusion of the dissolved hydrogen from the melt to the available cavities. This phenomenon, schematically described in Figure 2.1, results in the formation of cavitation bubbles, which then coalesce and float to the surface, driven by the differential density and acoustically induced flows in the melt. This process leads to the release of hydrogen gas produced by the interaction of hydrogen atoms inside bubbles, as well as the reduction of the porosity of the casting [82].

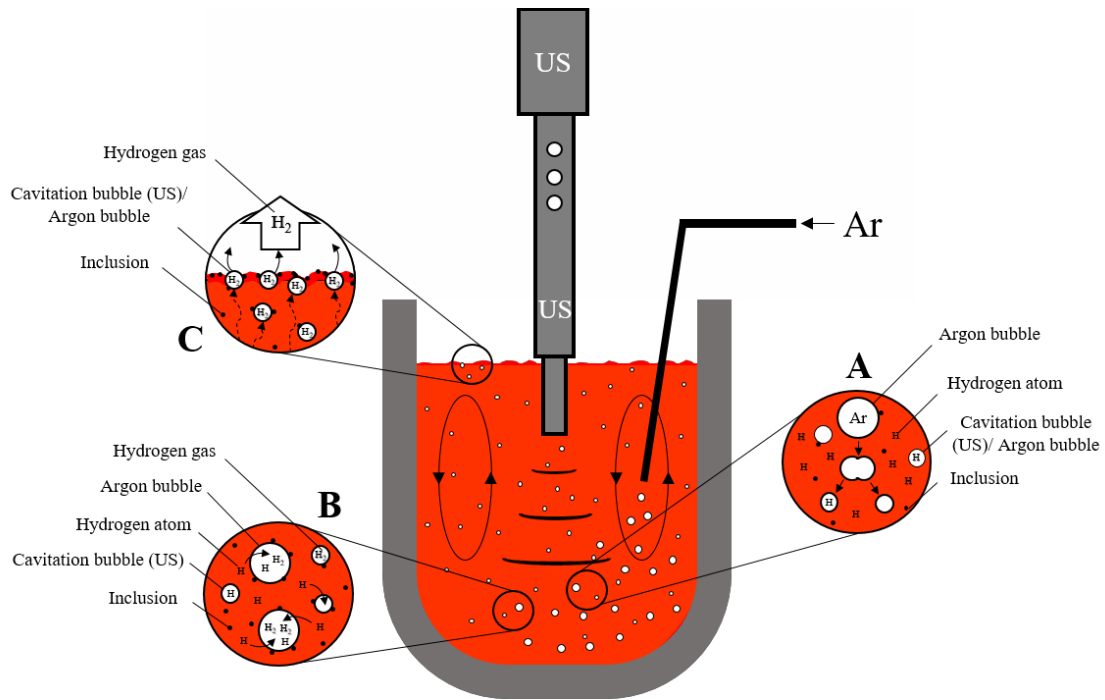


Figure 2.1: Degassing scheme: (A) dissolution of the argon (Ar) bubbles by the US system; (B) diffusion of hydrogen atoms and inclusions; and (C) flotation of the gas bubbles and release of the hydrogen gas to the atmosphere.

According to Liu *et al.* [79], applying ultrasonic argon degassing allows the ultimate strength to be highest while maintaining the yield strength. Additionally, the ultrasound treatment greatly impacts grain refinement, noticing the size reduction and shape modification of the $\beta\text{-Mg}_{17}\text{Al}_{12}$ phase, the instigation of a spherical shape, as well as improved uniformity and distribution in the $\alpha\text{-Mg}$ matrix. Du and Zhang [83] showed that the uniform distribution of the fine $\beta\text{-Mg}_{17}\text{Al}_{12}$ intermetallic phase enhances mechanical properties, while gas pores and microstructural non-uniformity lower them. Stress concentration in bulk materials can be reduced by reducing these defects, while ductility can be improved by preventing early fractures.

There are two distinct mechanisms associated with grain refinement efficiency: (i) heterogeneous nucleation at high (above liquidus) temperatures, and (ii) intermetallic compound fragmentation due to the streaming acoustic effect. The co-existence of these mechanisms suggests an enhanced refinement of dendrite cell size, thinning, and dispersion of $\beta\text{-Mg}_{17}\text{Al}_{12}$ intermetallic phase in the $\alpha\text{-Mg}$ matrix during the phase of solidification under the effect of ultrasonic vibration. During the first stage of solidification, the ultrasonic treatment improves grain refinement by heterogeneous nucleation as well as the wettability of the $\beta\text{-Mg}_{17}\text{Al}_{12}$ by the metal, further improving secondary phase refinement. During a second step, which corresponds to the formation of the first solid metal, cavitation can produce acoustic streaming due to the collapse of

bubbles in the remaining liquid, resulting in the fragmentation of grain dendrites and intermetallic clusters. As a result of the coexistence of these two mechanisms, a high density of nuclei in the melt is also promoted, resulting in a large number of smaller grains and, thus, in a significant improvement of the mechanical properties [84].

The pouring of the alloy is also improved, avoiding coarse and dendritic structure which harms the mechanical properties of the material [78, 79, 85]. This situation, associated with the increase of elongation, is favorable to the stent's manufacturing, as it decreases the probability of device collapse during the deployment procedure, providing, however, the possibility of promoting its expansion with lower pressures. In addition to this, the increased mechanical properties of the AZ91 magnesium alloy enable the use of thinner struts and lower thicknesses comparable to stainless-steel products, which would not otherwise be possible due to the inferior mechanical properties of the material as-cast.

In addition to alloying and UST techniques, other methods are used to improve the properties of magnesium alloys depending on their application. According to the literature, an in-depth investigation has been published to improve their corrosion resistance. Some studies refer that another way to control the biodegradation rate of magnesium stents is by coating the surface with biodegradable polymeric layers [86-90]. The drugs can be released during polymer breakdown or even through the coating diffusion mechanisms, thereby increasing the overall degradation time of the stent. On the other hand, the mechanical behavior and corrosion resistance of magnesium stents are strongly influenced by the geometry and dimensions of the stents, as well as the microstructure of the alloys [91-93].

All of these types of methodologies can be of great assistance in the development and modification of new magnesium alloys with higher physical, chemical, and mechanical properties, making them ideal, among others, for the replacement of the most used metallic structural materials (iron, steel, and aluminum). However, improving materials also requires the demand for new and improved manufacturing processes. Given the decreasing cost of aluminum and magnesium alloys, there has been a higher investment in improving the manufacturing processes of these materials [33, 94, 95]. The purpose of this is to improve the quality and complexity of the obtained castings [96] and improve their mechanical properties directly, for instance, by modifying the gating system, which reduces porosity [97]. Although the industrial process is constantly evolving and researchers are learning more about the advantages of using magnesium alloys, there

is a need for improvement and the creation of new manufacturing processes, capable of meeting the market's high expectations both in terms of final product quality and quantity. Mahi Sahoo [98] stated that most of the magnesium alloys' processing was done through HPDC (High Pressure Die Casting) in the previous decade, being directed to large volume part productions. This observation was later corroborated by Luo [99] and has remained until today, as confirmed by Dobrzanski *et al.* [29]. The possibility of high production volume and low production cost can justify this fact, but magnesium and its alloys can be processed through solid, powder, or liquid phases. A variety of stent manufacturing processes are discussed at the end of this chapter. Nevertheless, despite all the advantages, solid-phase processing has high processing costs, limitations on thickness, and the need for complex handling of fine powders, so liquid phase processing is more common.

Casting is a millennial technology that, although still a widely used process to obtain all kinds of casting pieces using the same concepts over the years, has tried to adapt to the demands of industry and technological development. Depending on the type of application and the final component to be obtained, the casting process also comprises different forms of processing. Magnesium alloys can be cast by gravity, by low pressure, by injection, among other methods. According to Carvalho Ferreira [100], the casting process can be classified based on the permanence or perishability of models and moldings. In this thesis, the **model**, obtained by additive manufacturing, is considered the printed part presenting the geometric form of the final piece to be obtained, **molding** is referred to the manufactured part containing the cavities in which the metal is poured, and **mold-metal** is related to the interaction zone between the liquid melt and the molding walls during the pouring phase. In permanent molding casting, there is no model production, and the desired final form is achieved by pouring metal directly into the molding. In this case, the molding is not destroyed and has appropriate mechanical characteristics that are generally made of metal or other materials with high wear resistance. In this process, although many parts can be cast without their characteristics or shape being significantly changed, the drawback is that permanent molds are required for each component to be cast, which is a more time-consuming and more expensive process than ceramic molding. For non-permanent moldings and permanent models, it is necessary to use ceramic or sand moldings that can be removed from their interior before the liquid metal is poured. The molding is destroyed after the metal is poured, i.e., the metal is removed from the molding. Lastly, casting with non-permanent molding and non-permanent model is characterized by the fact that the model is involved in the construction of the ceramic molding and is also destroyed, usually by sublimation, in order to create the cavities in

which the liquid metal will be poured. It is also known as investment casting, and it is the only type of processing employed throughout this work.

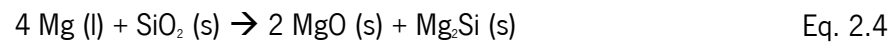
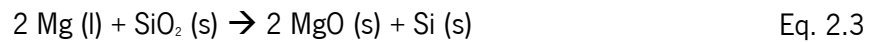
2.2. Magnesium Investment Casting in Ceramic Molding

Investment casting is a manufacturing process capable of producing pieces from practically any metal or alloy and economically, compared to other manufacturing processes [43]. However, nowadays it is not normally used to manufacture medical devices, including biodegradable ones, such as stents. The high reactivity of biodegradable alloys, especially magnesium and its alloys, as well as the disadvantages the process can present in terms of surface quality, dimensional accuracy, and filling capacity for thin and complex walls that require complementary finishing operations have made this process unsuitable for the manufacture of small biomedical devices. However, the increasing development of technologies in recent years has altered the landscape of manufacturing processes and the knowledge about them as well. New technologies and equipment have been developed, allowing to redesign and improve many existing processes. As part of the near-net-shape stent's processing, a new approach can be defined that uses investment casting (using non-permanent models and molding) as a potential and practical solution to manufacture magnesium-based castings.

Dobrzanski *et al.* [29] report that besides offering high-quality complicated shapes with a broader range of dimensions and geometries [94], investment casting is also seen as a promising process for the manufacture of thin-walled components that require a good surface finish and a high degree of dimensional tolerance [101]. There are, however, some barriers to overcome in magnesium investment casting using plaster moldings.

Due to the significant reactions between magnesium and the ceramic moldings used in the conventional investment casting process, magnesium alloys are not widely applied in these industries. The fact that there are not yet suitable and effective inhibitors to control these reactions makes it impossible to handle magnesium alloys in foundries. The reactions can strongly affect the surface finish of the castings, reducing their final quality. Therefore, it becomes imperative to prevent mold-metal interactions during investment casting. It remains the biggest challenge to overcome due to the high affinity of magnesium for oxygen, specifically for the silicon dioxide (SiO_2) present in the plaster composition, which causes a set of strong exothermic reactions [47-49]. The most common reactions, which can occur during the interaction of the liquid (from magnesium

and its alloys) are represented by Eqs. 2.1-2.4, but other reactions may also take place, depending on the affinity of the liquid magnesium reaction with the constituent elements of the ceramic materials used and the surrounding atmosphere [50]:



The amount and intensity of reactions occurring during the melting and pouring phases of liquid magnesium are also strongly influenced by pressure and temperature conditions. High pressure and temperature significantly increase reaction formation. These reactions can occur due to different situations during the investment casting process, caused by the interaction between the liquid metal with the ceramic molding walls or the surrounding atmosphere.

Some approaches have been suggested and implemented in the last decade to minimize the reaction issue. The use of protective atmospheres was reported by Lee *et al.* [102], while Jafari *et al.* [47, 103] described the use of shell investment molds as an effective way to reduce these phenomena.

Based on silica or zirconia binders, ceramic shell moldings were applied by Zhang and Morin [104] to avoid mold-metal reactions. It was concluded that an atmosphere of SF₆ in CO₂ is absolutely necessary under an inhibitor gas atmosphere. Furthermore, these techniques are highly dependent on the materials used for the moldings and the alloys used for casting. More recently, it was proposed by Jafari *et al.* [49] the application of an *in situ* melting technique for AZ91D magnesium alloy casting, applying a slurry composed of zircon flour and colloidal silica, along with fine alumino-silicate stucco sand. Moreover, a flux of MgCl₂, KCl, and CaF₂ was used in combination with small-sized granules of the alloy. Although the processing conditions avoided magnesium reactions, the obtained castings revealed defects such as micro-shrinkage porosity, inclusions, and non-fused metal parts.

The application of refractory coatings in the investment casting of highly reactive alloys has also been proven successful in overcoming the inherent difficulties of this process, as shown by the use of ZrO₂·SiO₂-based crucibles with an inner layer of Y₂O₃ to melt a Ti-48Al alloy [105, 106]. It was concluded that chemical composition and alloy homogeneity are strongly influenced by

processing conditions such as processing melting pressure and superheating time and temperature.

A protective flux or protective gas must cover the molten magnesium to prevent it from burning. Flux protects from burning, but flux inclusions trapped in the casting can pose a problem [107]. In terms of protective gases, there are a few available in use today, but SF₆ (sulfur hexafluoride) is still the most efficient at protecting molten magnesium. It is non-toxic, non-corrosive, and provides adequate protection against molten magnesium at very low concentrations. Typically, it is mixed with a carrier gas such as dry air and/or CO₂. However, even though it is possible to reduce its concentration by combining important processing conditions, such as mold and pouring temperatures, SF₆ is a powerful greenhouse gas that negatively impacts the environment [32]. Consequently, it was reported by Ha and Kim [108] that using the HFC-134a gas (1,1,1,2-tetrafluoroethane) provides an effective alternative to SF₆. Nevertheless, a gas mixture must be used to prevent the formation of highly corrosive hydrogen fluoride, which can reduce the process' effectiveness. On the other hand, it has been demonstrated that the addition of a small amount of CaO to Mg alloys, forming Eco-Mg alloys (as mentioned in the previous subchapter), is a non-SF₆ process during melting and casting of Mg alloys that significantly increases the ductility and strength of these alloys [66, 67].

Nevertheless, none of these studies reported effective solutions to overtake the reactivity between ceramic-based moldings and magnesium alloys, which is still poorly understood. According to Jafari *et al.* [47], the progress that has been made does not correspond to a practical and economical alternative to encourage the investment casting foundries to handle magnesium. Thus, searching for a process that effectively mitigates the interfacial reactions and allows obtaining complex and thin-walled magnesium alloy parts constitutes a great stimulus of investigation for the scientific community. To overtake these inherent limitations, it remains necessary to develop an economical, practical, and environmentally friendly method of avoiding mold-metal interaction and suppressing the reactions that result. In this way, the combination of additive manufacturing with investment casting process can be seen as a route for fabricating thin-walled magnesium parts in several industrial applications, such as the manufacture of medical devices.

2.3. Thin-walled Magnesium Structures

From the perspective of applications, the larger industries produce most of the magnesium alloy castings, thus justifying large-scale part productions. Indeed, although a few recent studies have been reported on the development of magnesium metal foams [39, 43] and some medical devices, such as stents [109] and biomedical prostheses [110], there is an identified need for thin-walled parts manufactured through magnesium casting. More specifically, there is insufficient information on magnesium investment casting studies for thin-wall geometries [111]. This can be explained by the difficulty in handling magnesium on magnesium casting in ceramic moldings due to its high reactivity, and the difficulty in filling thin-walled cavities using molten metal. Furthermore, despite significant progress in providing a successful investment casting process without any reactions, thin-walled magnesium alloy structures production is still a relatively unreliable process due to filling and rapid solidification challenges. This issue can be challenging, but new achievements can be very valuable to the foundry industry in the most diverse areas of thin and small parts applications, such as aerospace, aeronautics, automotive, and biomedical. In this sense, a complete and reliable study of magnesium alloys' fluidity in the investment casting process using plaster moldings is needed.

The fluidity of a metal alloy is one of the most important characteristics to consider for the microcasting process. This is a complex characteristic affected by many variables, and it is essential to ensure that the liquid metal flow fills the entire cavity before solidifying. The metal fluidity depends on variables such as viscosity, metal flow in the liquid state, and the solidification metal mode into the channels, as stated by Ferreira [100]. So, the process parameters such as pouring and molding temperatures, vacuum assistance, and metal cleaning can significantly influence the alloy's fluidity [112-114].

The pouring temperature is one of the preeminent factors in fluidity. Huang *et al.* [113] and Sin and Dube [114] have noted that with increasing temperature, the reproduction ability of the cavity details is improved since the metal remains in the liquid state for a more extended time. Indeed, this increase can also cause a decrease in viscosity and surface tension, thus increasing fluidity. In the case of magnesium alloys, the pouring temperature should be comprised between 650 °C and 750 °C in order to mitigate the oxidation and reaction rates that occur during the process.

Although with less influence, the increase in molding temperature also affects fluidity. It can reduce the heat transfer rate, slowing the material's solidification and reproducing the cavity details, increasing the metal flux fluidity. Thus, the molding temperature should also be limited in order to prevent the reactivity rate that may occur between the alloy and the molding material, which is usually comprised between 100 °C and 450 °C for magnesium alloys [113-115].

Another crucial factor promoting fluidity is the vacuum feature. It has been reported that the use of vacuum in pouring operations can prevent reactions such as oxidation, and can even prevent the introduction of dissolved gases into metals to avoid porosity [116]. Additionally, the use of vacuum is considered an effective method of better filling molding cavities, since it creates a negative pressure therein. The vacuum does not directly affect fluidity, but it may assume a preponderant role in the casting process with poorly permeable moldings since air trapped inside the molding tends to be compressed by the metal in the liquid state, making it difficult for the cavity to be completely filled. This technique is widely used, especially in casting in which thinner thicknesses are desired since it involves removing air from inside the moldings [115-117].

Metal cleaning also influences the molding filling capacity. Since gases, intermetallic phases, inclusions, and impurities decrease fluidity, procedures such as particle filtration and degassing can significantly contribute to its increase [117]. As seen in the previous subchapter, the degassing of liquid metal is very effective by applying an ultrasound technique, which helps to improve the alloy's fluidity.

Nonetheless, other factors can directly influence the alloy's fluidity, such as its chemical composition, specific heat, latent heat, thermal conductivity, density, viscosity, or surface tension [112]. Besides processing parameters, these variables can also be controlled by adding elements, which has been explored extensively by the scientific community, as reported by Fu *et al.* [118] and Hua *et al.* [119].

Therefore, it is of extreme importance to study the influence of these variables on the filling behavior of the liquid magnesium and its alloys in order to find which of them is more relevant to the ability to fill thin walls and consequently complex geometries such as stents.

2.4. Stent Manufacturing

Current medical devices require a wide range of manufacturing processes, both because of the materials advances and design complexity. Several processing techniques have been applied to improve the main characteristics of the final product, including the mechanical and structural properties. Different fabrication techniques can also improve stent's mechanical and structural properties and control the device's degradation rate, which becomes a serious problem when biodegradable materials are used. Therefore, the type of material used in fabricating stents determines the manufacturing process.

2.4.1. Materials

There are several different types of stents based on different materials that can confer different properties on the devices. Although polymer stents offer some advantages over metallic stents in some aspects, they lose credibility due to their poor mechanical properties. Depending on the material, metal stents may be considered either permanent or biodegradable.

Permanent stents

The existing metal stents are made mainly of stainless steel and nickel and titanium alloys, or chromium and cobalt materials, and remain permanently in the blood vessels after insertion [8, 9, 45, 120-123]. These alloys exhibit good mechanical properties and biocompatibility, making them the ideal material for the manufacture of stents for the human body and limiting the success of such applications over the long run. They can be challenging to remove as a consequence of resulting complications, which might be needed for the placement of additional stents [13, 124, 125]. Furthermore, the purpose of the stent within the blood vessels has been shown to be temporary and limited to an interval between 6 and 12 months after implantation, during which time arterial remodeling and healing occur [126, 127].

The stent's implantation in the blood vessels was an important step towards the minimization of problems associated with coronary artery diseases, such as advanced vessel obstruction and restenosis, which previously recurred after expansion balloon angioplasty [128]. While permanent stents have markedly improved the quality of patient care, the introduction of permanent stents poses some challenges, one of which is the occurrence of intra-stent restenosis [19, 20, 129-133] and stent thrombosis [4, 20, 21, 134]. Thus, the biological incompatibility

caused by the interaction between the arteries and the metal stents justifies the dissemination retraction of their permanent use. Without entirely dismissing this intervention method and taking advantage of its advantages against ischemic diseases, it is highly desirable and necessary that this type of medical device be improved in the future for percutaneous coronary intervention [135, 136].

Biodegradable stents

The limited duration of the stent within the body constitutes an asset because it allows the overcoming of the atherosclerosis problem and prevents any medical complications between the device and the blood vessels. Once the intervention has restored blood flow, the implant becomes dispensable, proving the practical benefits of using biodegradable stents instead of conventional ones. After a performance period, they can degrade themselves without being harmful to the patient [17, 18]. Considering this fact, several studies have been published during the last years concerning the application of biodegradable materials to stent implants [137-140].

In order to ensure that a biomedical device performs properly without being dangerous to the health of the patient, it is imperative to act on the characteristics that influence the possibility of problems. The geometrical shape and physical properties of the device as well as the chemical, physical and mechanical properties that come from the type of material and the manufacturing process are examples [141]. The materials applied to biodegradable stents, for example, need to be biocompatible since the products resulting from their degradation need to be able to remain in the body for several months before they are completely absorbed or rejected. Additionally, the force applied and the structural support of the stent in the expanded form must be sufficient to keep the blood vessel open. This will ensure normal blood flow in the intervention zone [15]. A number of studies have been conducted to meet the needs of the ideal stent [142], by fulfilling some important characteristics, depicted in Figure 2.2, and the same should apply to the development of any medical device.

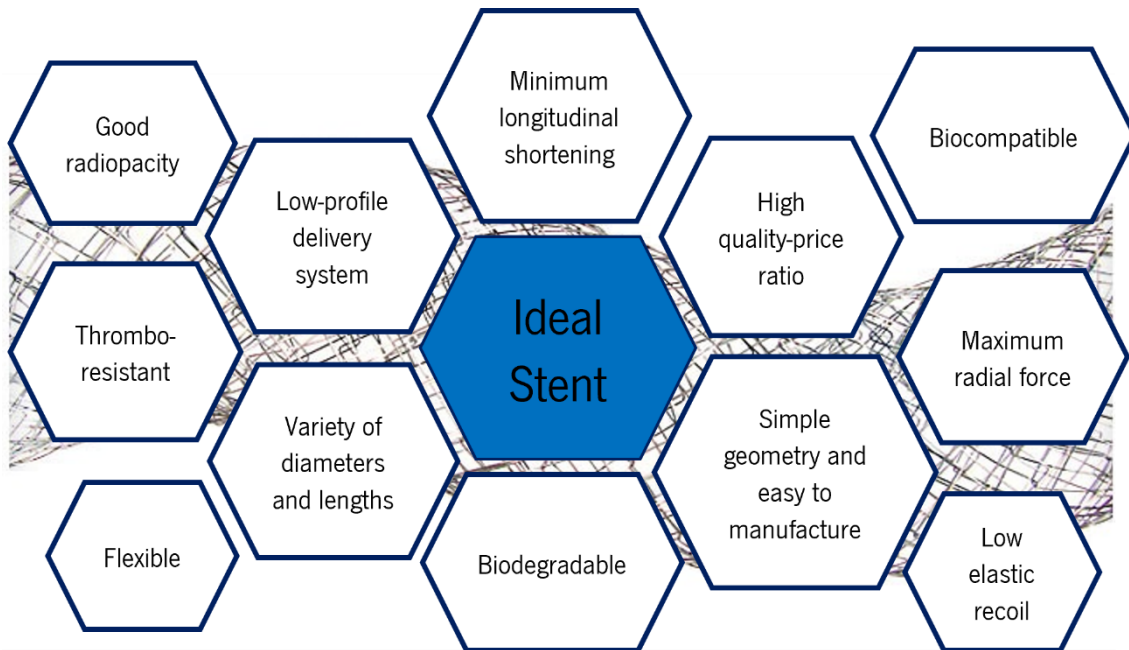


Figure 2.2: The main characteristics of biodegradable stents.

Several Mg-based alloys have been investigated as potential materials for the production of temporary stents when considering the stent properties and combating complications associated with the use of permanent stents [11, 143]. These materials have some advantages that make them a very interesting material for stent manufacturing, namely properties of biodegradability and biocompatibility [63, 144]. Furthermore, magnesium is a human tissue constituent and an essential element, not presenting a carcinogenic risk [15].

2.4.2. Processing

The greater acceptance of stent's use as the general process in the percutaneous treatment of coronary artery diseases has extended its applications to lesions of more complexity. The technological growth, which prompted immediate industry response, has led to the growth of a wide variety of vascular stent models with innovative designs and features. The coverage of the literature review on stents allows concluding that the manufacturing process has a huge influence on metal stents' properties [51]. So, the manufacture of these devices is an art that requires experience in many areas, from selecting the ideal raw material to approaching the best manufacturing process and finishing steps to ensure the highest quality of the final product.

Conventional stent processing

The current manufacture of stents, called the conventional process, does not correspond to a single sequential processing step but addresses a set of necessary procedures to obtain a high-quality final product. The manufacturing procedure comprises different steps from the bulk material to obtaining a stent in its final form with the required specifications. Figure 2.3 shows the most adopted process for the manufacture of metallic stents, highlighting its essential procedures: (a) raw material processing and heat treatments; (b) minitube formation; (c) cutting stent design; and (d) finishing operations.

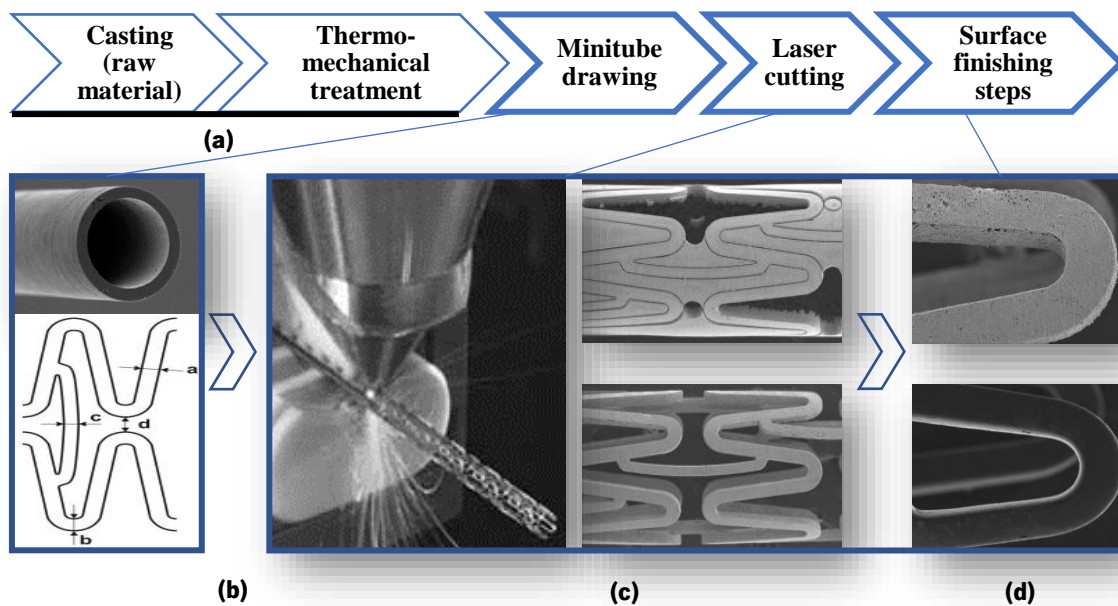


Figure 2.3: Conventional stent's fabrication: (a) primary steps; (b) initial machined minitube and stent design; (c) laser-cut minitube; and (d) electropolishing process (adapted from [145]).

Raw material processing and heat treatment

The process of manufacturing a stent begins with the processing of raw materials. The procedure consists of producing metallic ingots through melting and thermomechanical treatment [17, 59, 123, 146, 147]. For biomedical applications, most metals are melted under vacuum. As mentioned in subchapter 2.3, this procedure prevents oxidation reactions, especially with highly reactive alloys, and removes any dissolved gases in the bath, contributing to porosities' formation [15]. Additionally, melt processing greatly influences the molten alloy's homogeneity, porosity, and micro cleanliness [148].

Casting is only used as a primary process in stents' manufacturing. As a result, since the as-cast materials have a very coarse microstructure, forming and thermomechanical processes are very important to achieving the desired mechanical properties. There are many processes conducted at temperatures at which the alloy is easily shaped, to improve mechanical properties by means of plastic deformation and hardening. Some of these processes include forging, rolling, and extrusion. After hot working, metallic materials are cold worked and heat-treated to obtain ingots with higher physical and mechanical properties [149]. Ingots are then formed into tubes using forming techniques before being cut by lasers, which enables the stent's design to be defined.

Minitube formation

The next step concerns the formation of tubular components (semi-products) that will support the fabrication process. It is crucial to select a tube processing that can guarantee excellent mechanical properties in the final stent since this involves microstructural modification of the alloy used. At the industrial level, rolling, drawing, and casting processes are often used to produce seamless tubes. However, whereas these processes are used for large-scale products, the feasibility of components such as stents, that demand high dimensional and geometry quality, does not have the required viability.

For fabricating permanent metallic stents, there are basically four steps to follow, including extrusion, machining, and drawing to form tubes [150]: (1) obtaining a solid rod by hot extrusion of the molten feedstock; (2) drilling a deep hole in the rod to obtain the tubular shape; (3) indirect extrusion of the tube; and (4) reduction of the diameter and wall thickness by multiple drawing and intermediate tube annealing. Tube drawing is a typical metal forming procedure that involves stretching a hollow billet under tensile stresses to reduce its cross-sectional area and increase its surface finish and dimensional accuracy. Therefore, this type of procedure requires that the material exhibit high ductility and sufficient tensile strength allowing plastic deformation to occur before fracture.

Metallic biodegradable stents require advanced fabrication technologies, which have not received enough attention. For biodegradable Mg-based alloys, which are materials presenting low formability, it is challenging to produce cold-drawn seamless tubes with extremely dimensional rigor due to their poor plasticity at room temperature. Due to its closed hexagonal crystalline structure characteristic and poor room temperature workability, it is common to use hot drawing to form semi-products of this material [151]. However, using a hot mandrel can cause

uncontrollable increases in the wall thickness of the magnesium tube and poor surface quality. Only a few studies have so far been conducted on developing fabrication technology for magnesium microtubes and improving their mechanical properties, as well as on the dimension accuracy of the stent's semi-finished products [5, 11]. The manufacture of stents requires complete control of all properties and characteristics, and this process does not necessarily satisfy these requirements. As a result, some authors have adopted other processes for the manufacture of minitubes from metallic alloys, including different drawing procedures [152-155] and other tube forming techniques, such as electric discharge machining [156, 157] and SPD (Severe Plastic Deformation) [158-166].

Concerning conventional drawing procedures, some studies have been published in order to reduce tubing size. Wall thickness reductions had been achieved by Furushima and Manabe [152] from hollow billets of the AZ31 magnesium alloy, and tubes with an outside diameter of 2 mm and a thickness of 0.5 mm were obtained through hot drawing without a die. However, it was concluded that in hot tube drawing without a die, uniformity in wall thickness could hardly be kept under control, and the inner surface of drawn tubes would not be perfectly defined. Alternatively, Yoshima and Koiwa [153] fabricated tubes with an external diameter of 3.6 mm and an apparent thickness of 0.61 mm using the AZ31 magnesium alloy at room temperature, applying the fluid as a mandrel. Through multipass cold drawing, Fang *et al.* [155] were carried out to produce magnesium alloy minitubes using the ZM21 alloy for stent manufacturing. The drawn tubes with an outside diameter of 2.9 mm and wall thickness of 0.217 mm were obtained through five passes of cold drawing with an interpass annealing procedure after the fourth pass. Accordingly, although it is technically challenging, the literature review allows to conclude that in order to obtain minitubes for biodegradable magnesium stents, the cold drawing appears more feasible than hot drawing since cold drawing is better at achieving close dimensional tolerances and a fine surface finish, as well as high mechanical properties [155]. Nevertheless, the values obtained in these studies appear insufficient to meet the stringent needs that medical devices have at the microscale level. Several improvements need to be made, mainly in reducing the thickness of the stent (corresponding to the minitubes thickness) to values close to the 0.1 mm that permanent stents can present, and controlling degradation rates of biodegradable materials, which considerably affect the final device's mechanical properties.

SPD processes are thermomechanical processing techniques with great potential for producing bulk samples with extremely small grains, improving the homogeneity of the impurity

distributions in the alloy microstructures [167]. During SPD processes, the samples' overall shape is not changed, making it possible to ensure that the repetitive severe plastic deformation refines the microstructure through a continual dynamic recrystallization process. SPD processes are therefore applied to all metals, both permanent materials such as stainless steel and aluminum [158, 159] as in biodegradable alloys such as magnesium [160, 168]. Several studies have reported that grain refinement caused by these processing techniques can enhance mechanical properties [169, 170]. Among the most studied, the ECAP (Equal Channel Angular Pressing) [161] and the HPT (High-Pressure Torsion) [162] are the most SPD promising processes. While the ECAP technique allows the production of larger samples, the HPT technique generates high hydrostatic pressures, allowing the processing of materials with low ductility. But other SPD techniques can be used, such as CEC (Cyclic Extrusion and Compression) [171], TCAP (Tubular Channel Angular Pressing) [164], and ABE (Accumulative Back Extrusion) [172]. Several studies have demonstrated the benefits of using the SPD processes in the alloy's properties for biomedical applications. Ge *et al.* [169] applied ECAP for manufacturing a biodegradable magnesium stent prior to extrusion and laser cutting. The process was used to achieve a significant grain refining in the submicrometric grain-size range and the 0.2 % yield strength increased from 180 to 340 MPa after 150 °C ECAP processing, keeping a relatively high tensile ductility. On the other hand, Figueiredo *et al.* [166] described the development of exceptional ductility in pure magnesium after HPT processing at room temperature. The results showed that grain refinement by severe plastic deformation resulted in a higher strain rate sensitivity and a more significant elongation at room temperature. All of these studies have shown that the use of SPD methods at elevated temperatures mixed with other forming processes is considered a very promising approach for improving the mechanical properties of magnesium alloys through grain refinement. According to this, Amani *et al.* [5] proposed a new combined method of SPD techniques to fabricate magnesium microtubes for biodegradable vascular stents. This method consisted of three forming processes and a drilling step. The WE43 Mg alloy was applied for three SPD techniques: CEE (Cyclic Expansion Extrusion), EX (Direct Extrusion) and MTE (Microtube Extrusion). Three microtubes with outside diameter of 3.3 mm and wall thickness of 0.22 mm were successfully fabricated in three different ways: from the initial material, and through one pass or two passes of CEE technique. In comparison with the original microstructure, the authors were able to significantly reduce the alloy grain size and reduce the cross-section of the samples. Regarding mechanical properties, a significant increase in the maximum strength and elongation was achieved, which was recorded in the final samples.

However, even though SPD processes have proved beneficial in improving mechanical properties, there is no definition or knowledge of how they impact corrosion behavior. Some studies have shown different trends in corrosion behavior using severe plastic deformation methods [173-175]. For instance, Ralston *et al.* [176] demonstrate in their study that the grain refinement achieved by SPD techniques can lead to a higher corrosion rate of the alloy, affecting the mechanical properties and compromising its use and application.

Although the minitubes fabrication for the manufacture of stents from metal alloys may encompass several different processes, considering the aforementioned, there have been no studies and consistent investigations concerning metallic minitubes for medical devices [135].

Cutting and stent design

The stent mesh design can be achieved by a number of methods, including photochemical etching, water jet cutting, and electric discharge machining. However, laser cutting is nowadays the most widely used method for metal stents production, with considerable flexibility of shapes and geometries in an extensive production line [177-179]. It is a type of material solid processing that produces small diameter minitubes and thin-walled patterns. Cutting micro stents is a demanding process in the medical device industry. A coronary stent should be between 1 mm and 10 mm in diameter and 0.1 mm in thickness. For this reason, the cutting process must be high in precision. Cutting stents must not have imperfections that can lead to infections in the blood vessels into which they are inserted. The majority of laser-cut stents are either slotted tube designs or modular constructions, and different stent designs are available on the market from different manufacturers [180]. The laser cutting manufacturing technique has many advantages that make it a viable method of obtaining stents. However, it has limitations that compromise the specificity required for biomedical devices, namely at the level of surface quality and thermal issues. These issues directly affect the metal's properties and its corrosion. The heat generated by the laser can cause thermal damage to the application area due to high thermal gradients. This causes deformations, microcracks, burrs, porosities, residual stresses, and dimensional inaccuracy (Figure 2.4), compromising stent properties [181]. Some studies proved that laser cutting can also induce loss of alloying elements from the processed material [182], and that the resulting heat from this manufacturing process is associated with the grain thickening on the stent surface, affecting its mechanical properties [6, 148, 183]. Moreover, the tubing step associated with the conventional laser cutting manufacturing process results in the formation of relatively large

inclusions in the final material. This poses a series of risks of rupture failure after stent expansion [148].

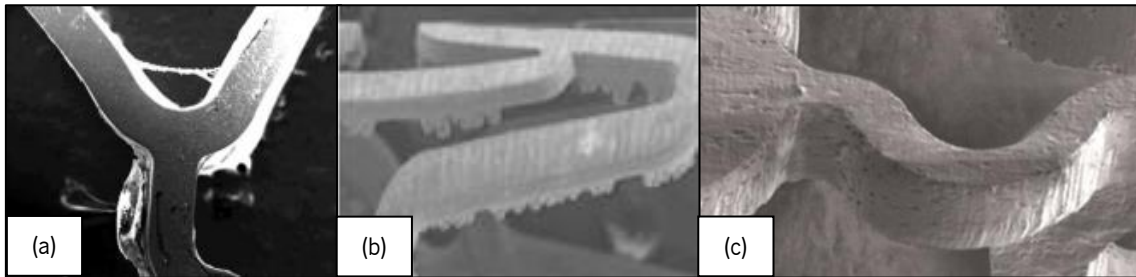


Figure 2.4: Principal defects of laser cutting: (a) deformations; (b) burrs; and (c) porosities (adapted from [15, 184, 185]).

In trying to minimize these problems, additional thermomechanical processes and finishing procedures, such as annealing, chemical etching, electropolishing, and sterilization, among others, are necessarily performed [15, 145]. Furthermore, the stents can be subjected to heat treatments such as vacuum annealing after laser cutting. This will soften the metal, induce grain growth, and relieve residual stresses created during laser cutting, which improves the stent's physical and mechanical properties [15]. In the manufacture of metal stents, the heat treatment procedure is critical because it directly influences the properties of the materials, while other processes determine the geometry, dimensional accuracy, and surface quality. In order to obtain homogeneous grain composition and distribution, as well as fine grain size, annealing requires different temperature and actuation time parameters. These parameters are according to the type of material to be treated. In addition, finishing processes are also helpful for removing any mechanical defects on the stent surface. This is designed to have a roughness value of less than $0.5 \mu\text{m}$ [10]. Hence, studies have been conducted to determine the ideal process parameters for laser cutting metallic alloys. These parameters are mainly in terms of dimensional accuracy and surface finish [15, 148], and process parameters [25, 109].

Finishing operations

Surface finishing is the final step in manufacturing stents and is very important to enhance product quality, especially in the case of biomedical devices, whose surface characteristics determine the nature of immediate and long-term tissue response [163]. Surface treatments may be electrochemical, chemical, or mechanical, depending on the application. As a result, these processes improve the surface quality of the stent and its corrosion resistance and biocompatibility,

removing contaminants and mechanical imperfections that can occur when laser cutting or other non-conventional method is used.

Once again, different finishing processes can be applied depending on the surface characteristics to be improved. As an example, Figure 2.4(c) shows the application of electropolishing after laser cutting. Electropolishing is the conventional finishing procedure used to fabricate stents and is usually used to achieve a smooth surface and remove burrs and defects generated by the heat ablation during laser cutting, etching, or forming steps [15, 163]. It is a controlled and repetitive electrochemical process that removes metal from the surface of complex geometric objects using electrolytic dissolution. As a result, the required surface finishing is ensured, and the stents' biocompatibility and corrosion resistance are improved. For example, in the manufacture of permanent NiTi (nitinol) stents, electropolishing selectively decreases the amount of nickel on the surface. The passivation is composed of titanium oxide, which improves the biocompatibility of the stent since nickel is harmful to the body due to its association with cancerous and inflammatory reactions. Although electropolishing has been considered a successful method of improving the stents' quality finish, some other techniques can be used after the laser cutting process, such as chemical etching, MAP (Magnetic Abrasive Polishing), ultrasonic cleaning, honing, sterilization, and others. By using these procedures, high-quality biocompatible stents with a bright, shiny surface, defect-free, and improved corrosion resistance are obtained.

Chemical etching with nitric acid and ethanol is applied to clean the spatter deposited on the stent surface [178].

MAP can also be applied using flexible tools, including iron powder and abrasive particles [186]. It is characterized as a super-finishing technique to achieve a nanometric level of surface finish. A controlled magnetic force of extremely small magnitude is used in ferromagnetic abrasive particles, which are a conglomerate of abrasives and iron particles for material removal. It is widely used for ultrafine polishing of non-magnetic stents.

Ultrasonic cleaning removes surfaces' contaminants such as oils, fingerprints, and dust. It is a suitable surface finishing process for stent application since it allows cleaning in difficult access and small diameter areas. During this procedure, the stent is submerged in a solution under high frequency sound waves.

Honing is an abrasive machining process performed immediately after laser cutting, producing a precision surface on the metal part to which it is applied. It consists of rubbing an

abrasive stone in the tested sample along a controlled path and is mainly used to improve the geometric shape and surface texture. In stents manufacturing, the honing process is applied to permanent stents to remove the remaining material between supports and soften the resulting laser rough edges.

Finally, sterilization is a process of eliminating or removing all forms of life and other biological agents presented on the surface product. Because it can change the surface properties, this procedure should be the last step in manufacturing a biomedical device [171]. Can be achieved through various ways, including disinfection by ethylene oxide before implantation [187], sterilization by γ -radiation exposure [188, 189], and UV (ultraviolet) radiation [190]. In terms of applications, a recent study by Liu *et al.* [191] focused on the effect of various sterilization methods on the surface characteristics and biocompatibility of pure Mg and Mg alloys. The authors concluded that the Co60 γ ray radiation sterilization may be the most appropriate technology in reaching the best properties for biomedical magnesium alloys.

Non- conventional stent processing

The biomedical sector requires better, stricter, and smaller devices, so engineers are increasingly challenged to implement better fabrication processes. Several new processes have evolved or have been improved to meet this requirement, leading to realistic alternatives for producing metallic stents that are designed to overcome the conventional laser cutting limitations.

Butt welding is a technique that involves microcutting a mesh structure from a solid metal tube or welding preformed wire sections in a composite structure. This process is typically used for permanent stainless steel or cobalt alloy stents, although there has been some interest in applying this process to materials such as magnesium for manufacturing biodegradable stents.

On the other hand, some authors favor the production of metallic stents through metallic elementary powders using near-net-shape processes, which reduces the number of manufacturing steps required and, as a result, lowers the total cost of the entire process [192]. For instance, PM (Powder Metallurgy) manufactures shaped components or semi-finished products from metal powder. Here, fine powdered materials are blended inside a mold, compacted into the desired shape, and then heated in a controlled atmosphere, referred to as sintering, in order to facilitate the bonding formation of powder particles in the final part [193]. Alternatively to this conventional PM process, SLM (Selective Laser Melting) or MIM (Metal Injection Molding) can also be used.

SLM is a powder bed fusion technique in which a laser scans the powder layer by layer to generate the desired geometry. SLM's key advantages include shape flexibility and the use of lattice structures [194, 195]. Based on powder bed fusion, this method offers an attractive way to manufacture stents directly from powder, decreasing laser cutting and minitube manufacturing steps into a single process, and reducing production times and enhancing geometrical flexibility [10]. However, additive manufacturing techniques for vascular devices have been limited to a few applications using polymeric materials. There exists an apparent need for a comprehensive analysis of available and novel additive manufacturing techniques for metallic materials with adequate geometrical precision. Wessargues *et al.* [196] used fine powder (5–20 μm) with a micro SLM system to produce prototype stents of AISI 316L stainless steel, which were subsequently finished by plasma and chemical polishing. Despite surface cracks after expansion, the prototyped stents showed promising mechanical performance.

MIM is a well-established powder metallurgy technology and a viable alternative to other processes [197]. As a near-net-shape process, it has the advantage of allowing significant reductions in production costs, as well as being considered a suitable technique to produce small and complex parts in large quantities [198, 199]. It is an invention derived from the idea of plastic injection molding, in which the metal powder particles are mixed with a binder and injected into a cavity with the desired shape [200-202]. First, powders and binders are mixed to produce feedstock, and then a green compact is formed through injection molding. Afterward, the binders are extracted through de-binding to form the sintered final compact. The MIM process seems to be a very promising manufacturing method for the commercial scale of medical devices made from biodegradable alloys, although its true potential has not yet been sufficiently explored. A significant disadvantage of this method is the presence of pores during the sintering phase, which facilitates corrosion. The corrosion resistance can thus be affected by the heat treatment applied to the material, as stated by Hamidi *et al.* [199]. However, research involving biodegradable metals for biomedical applications has been in development since the 21st century beginning [203]. In recent years, micro MIM technology has been developed to reach thin walls of 20 μm and surface roughness values of less than 0.05 μm [204]. This indicates that, from a geometric point of view, this technology can meet the requirements for stent manufacturing. Moreover, its near-net-shape concept makes it particularly suitable for developing complex geometries with high dimensional accuracy [205-210].

PM techniques can thus be considered an attractive alternative manufacturing process in stent fabrication from an economic standpoint. Furthermore, powder metallurgy might be advantageous for metallic biomaterials like titanium, magnesium, or nitinol, which are more difficult to machine with conventional methods [193]. However, the main disadvantage of these processes is that they are restricted to specific geometries and dimensions, which inhibits greater investment in their use for thin-walled medical devices.

Finally, the casting process should also be included in this section of unconventional processes for fabricating metallic stents. As discussed earlier in this chapter, casting is primarily used to manufacture stents in the conventional process, specifically in obtaining minitubes. However, it would be desirable and economically advantageous if stents could be cast as a near-net-shape process. Therefore, and avoiding procedures such as minitube formation and heat treatment, stents could be designed to meet the market's mechanical, physical, and chemical requirements by investment casting. So, due to the evolution of manufacturing processes and their adaptation for the fabrication of biomedical devices, processing metallic stents through the combination of additive manufacturing with investment casting can be viewed as a promising route for the development of these devices.

2.5. Summary and Conclusions

This chapter describes the methods and techniques used for handling and improving magnesium alloys to manufacture stents. The addition of elements and the ultrasonic technique can be applied to improve the physical, chemical, and mechanical properties of magnesium alloys. Regarding processing, it is necessary to develop new methods and improvements for the high-pressure die casting processes, usually used for magnesium alloys. In that way, and due to its advantageous dimensional and geometric characteristics, the investment casting process, combined with additive manufacturing, can be seen as a potentially effective solution for the processing of magnesium alloys, mainly in obtaining thin-walled parts, whose knowledge needs further exploration. Considering medical device manufacturing, which involves geometric complexity, different processes can be implemented, whether based on solid, powder, or liquid processes or through conventional or non-conventional methods. Most of these techniques are presented in Table 2.1.

Table 2.1: Advantages and drawbacks of different processing methods for obtaining biomedical devices.

Process	Type	Advantages	Disadvantages	References
Casting	Liquid processing	Any material can be cast Dimension and geometry complexity Economic	Poor dimensional accuracy and surface finish Waste of material	[51, 211]
Laser cutting	Solid processing	Shapes and geometries flexibility Large production lines	Insufficient surface quality Thermal issues	[14-16, 51, 180]
Machining	Solid processing	Variety of materials High mechanical strength and density Good dimensional accuracy	Unavoidable defects High cost and maintenance	[155, 157, 212, 213]
Metal Injection Molding (MIM)	Powder processing	High production rate Good mechanical properties Good shape complexity with high dimensional accuracy	Presence of pores and impurities Part size limitation	[197-199, 214]
Powder Metallurgy (PM)	Powder processing	Low cost Variety of materials High production rate Good dimensional precision Development of shape memory alloys (SMAs)	Production of pores and residual porosity Size and shape limitation Long heating time	[193]
Selective Laser Melting (SLM)	Powder processing	Shape and geometry flexibility Reduced production time	Higher energy level necessity Expensive Smaller scan velocities	[10, 194-196]
Severe Plastic Deformation (SPD)	Solid processing	Effective grain refinement Improved mechanical properties Production of semi-products	Size and shape limitation Acceleration of corrosion rate	[158, 166, 168, 170]
Surface finishing	Solid processing	Surface quality Mechanical defects removing	Low production rate and time	[163]

The current manufacturing process of stents, involving laser cutting, encompasses several processing stages, making it expensive, as stated by Hermawan and Mantovani [145]. Additionally, the thermal problems that arise from the laser can compromise the successful application of the devices, mainly if magnesium alloys are used. The sequence of operations required for each process is shown by the descriptive and summary flowchart in Figure 2.5.

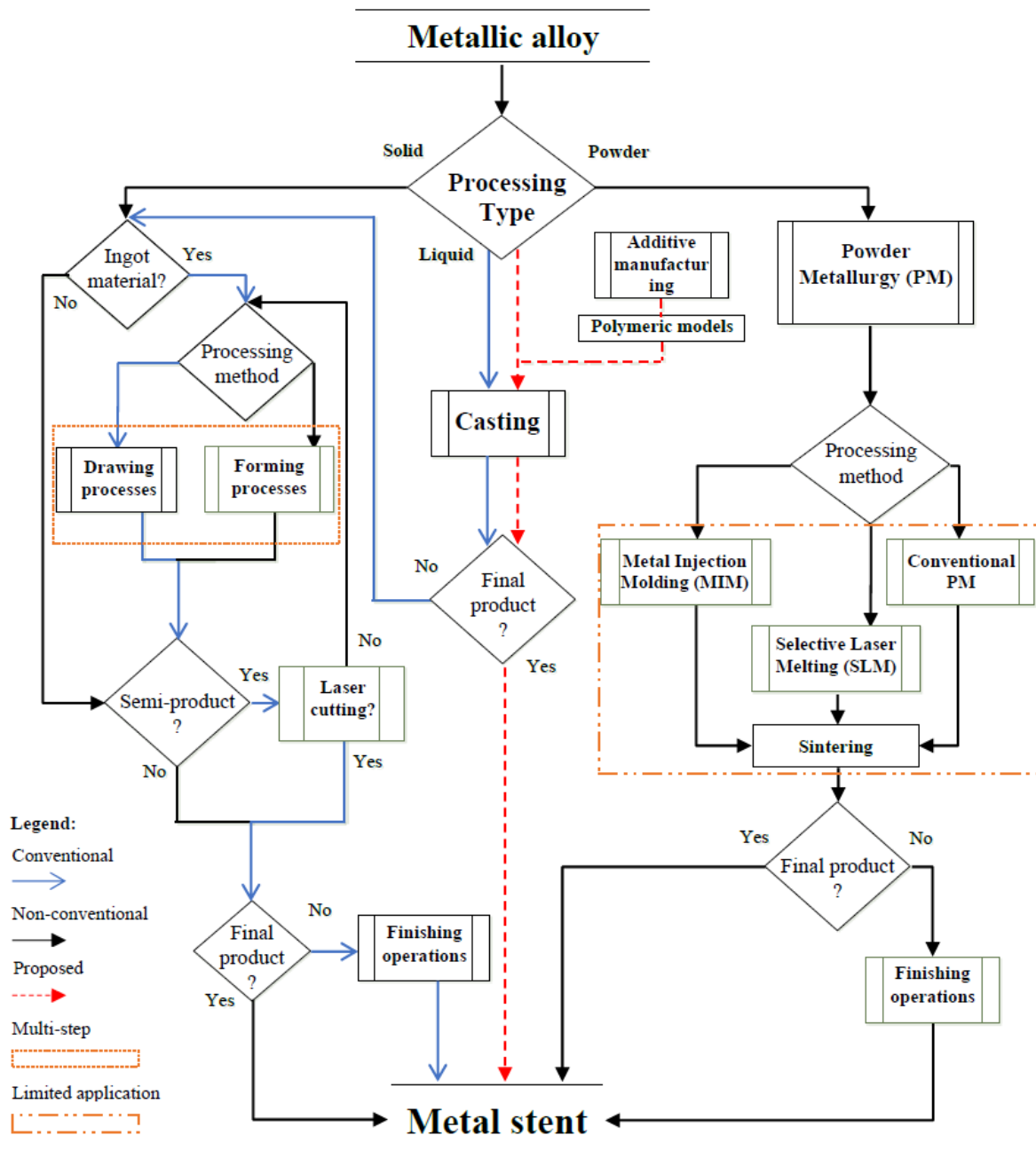


Figure 2.5: Stent manufacturing from a metallic alloy.

There is already work on alternative methods of conventional stent manufacture (blue path), as seen in subchapter 2.4, but it is desirable to explore new manufacturing methods that incorporate recent advances to make the process more efficient and more cost-effective. In addition, some drawbacks have characterized most of the known processes. While the solid route is described as a multi-step process, the geometrical and dimensional limitations can restrict the use of powder techniques.

Thus, since new and different solutions present new and different problems nowadays, the study and research for improving innovative devices and the development of new processing techniques must be recurrent and systematic procedures. There is a clear opportunity to progress in developing stent models and their manufacturing processes. The development of alloys based on biodegradable materials using methods that can overcome the shortcomings of the current manufacturing processes constitutes a field with an enormous potential for success. An approach for dealing with the interfacial reactions and ensuring cavity filling quality has been developed by Lopes *et al.* [215, 216] to eliminate the limitations of magnesium investment casting applied to thin-walled applications. Based on that, a novel proposal is presented in this work, as shown in Figure 2.5 by the red path.

This thesis aims to demonstrate the fabrication of magnesium alloy stents by using a method that combines additive manufacturing with investment casting in plaster molding. This hybrid process can significantly reduce processing steps and costs if compared to the other existent processes, especially for thin-walled casting parts requiring complex geometries, such as stents. Although there are some obstacles to overcome, such as high molten metal reactivity, several procedures are implemented and optimized to make this process an effective solution for magnesium processing, giving the foundry a preponderant role in the evolutionary context of industrial processes. Figure 2.6 illustrates all the steps involved in the proposed methodology, from design to obtaining the final magnesium part which can serve as the basis for all subsequent castings.

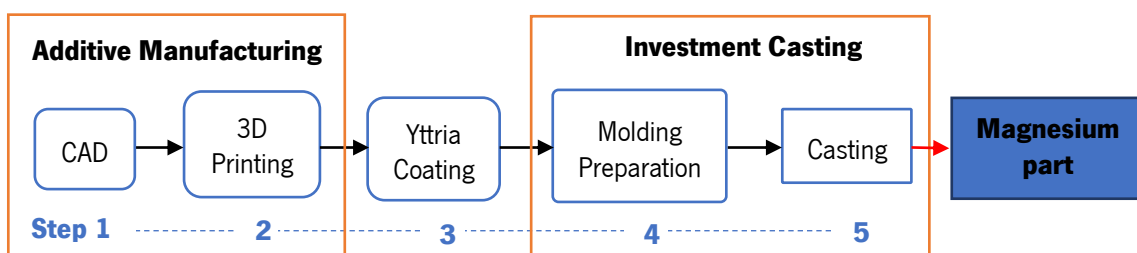


Figure 2.6: A proposed hybrid methodology for magnesium manufacturing.

Although the additive manufacturing revolution is a recent fact, this process is estimated to have emerged in 1981 in Japan for the 3D printing of plastic parts. The first registered patent is dated 1984.

Chapter 3. MODEL-MOLD-METAL INTERFACE

CHARACTERIZATION

The growing evolution regarding the knowledge of materials has led to the improvement of manufacturing processes and the emergence of new technologies that reduce production times and costs. Additive manufacturing results from years of evolution within conventional machining. Although this technology has been around for more than 30 years, it has recently revolutionized industrial processes. Through the creation of 3D models of actual parts intended to be obtained, additive manufacturing is a powerful tool in casting, especially in investment casting. Nowadays, it is possible to design and produce very complex geometries that are impossible to achieve using conventional production methods.

This chapter details the process of producing initial polymeric models using additive manufacturing, and the coatings that are applicable to those models. After that, the plaster molding production is discussed. These procedures correspond to steps 1-4 of the proposed methodology presented in Figure 2.6, and for each one, an optimization process is made to achieve the optimal set of parameters that can guarantee safe and effective thin-walled magnesium castings.

3.1. Additive Manufacturing of Models

Typically, the conventional investment casting process comprises several stages. First, the matrix (usually metallic) that will shape the model is made. The model, generally obtained from wax and through an injection process, is assembled with other parts forming a model tree. Then, the tree is immersed in a ceramic mixture to form a coating shell (ceramic molding). Concluded the defined number of coating layers, the model material is removed by heating, leading to the creation of molding cavities into which the molten metal is poured. When the metal solidifies, the molding is destroyed, and the resulting parts are removed and cleaned. Die manufacturing, still widely used in today's foundry industry, is the initial step of the process to obtain a wax model, involving high production costs and long lead times. This is due to the higher cost of machining processes and the time spent on CNC (Computerized Numerical Control) operations and other procedures necessary to ensure high dimensional and geometric precision. With additive manufacturing, however, both time and cost in die manufacturing can be reduced since the 3D printing process can directly obtain the 'models' used as templates in creating the molding cavities that help to produce the final cast parts. Die manufacturing is no longer necessary using this “new” manufacturing process. Furthermore, the use of additive manufacturing to obtain the initial models is characterized by a reduced rate of material waste, which is a disadvantage when machining poured parts.

3D printing encompasses a set of physical modeling technologies to rapidly produce models and prototypes from model drawing information, which can be generated in CAD (Computer-aided Design) through digitized CT (Computed Tomography) scanning data, MRI (magnetic resonance imaging), and data obtained by other digitization systems based on computer modeling. In a pre-processing phase, CAD model data is converted to STL (Standard Triangle Language) representation. In the 3D printing equipment, this model is translated into layers and slices to define the printing variables, which are handled almost entirely by the manufacturer's software.

Among various additive manufacturing methods, only FDM (Fused Deposition Modelling) and SLA (Stereolithography) will be discussed and implemented in this work. In addition to being the most popular techniques used by consumers, the fact that the models are made from polymeric materials makes them ideal techniques for obtaining the desired models, offering safe costs and reliable time.

FDM was one of the first technologies developed for 3D printing and remains one of the most common on the market today. This printer uses filament as a raw material for polymer variations, such as PLA (Polylactic Acid) and ABS (Acrylonitrile Butadiene Styrene), with the possibility of mixing other materials. The filaments are usually wound on spools and have constant diameters. The filament, illustrated in Figure 3.1, is extruded through a heated nozzle mounted on a print head with a linear motion system that moves around a printing area. Layer by layer, the material is deposited on the printing base, and the printing table moves at a height corresponding to each layer's thickness. FDM is an ideal process for an office environment, as it is easy to use and maintain. Additionally, consumables are relatively inexpensive compared to other methods. Double extrusion is also possible in this process, allowing the use of two materials in a single print. When the parts to be printed have more complex geometries, which require support structures, materials such as PVA (Polyvinyl Alcohol) can be used, since it is soluble in water and allows easy removal after printing.

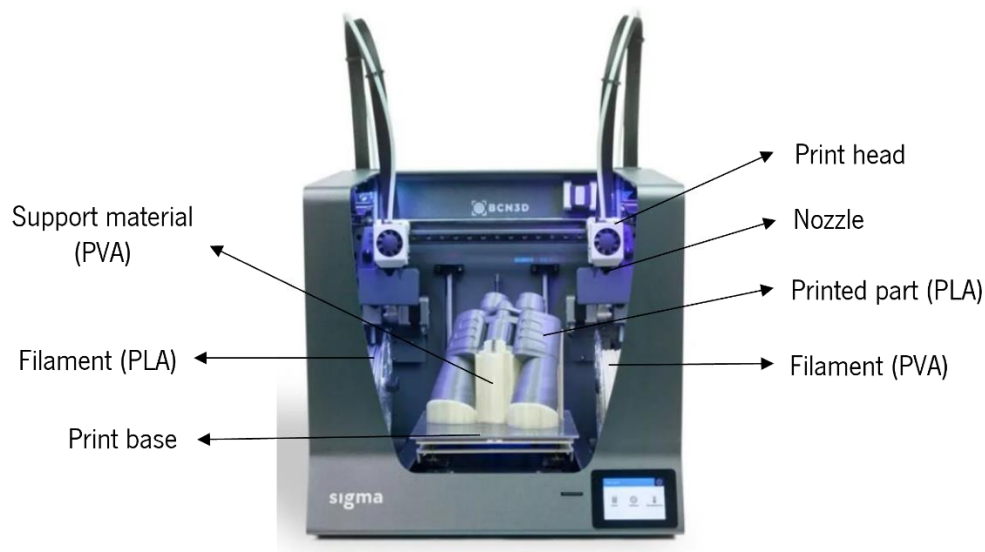


Figure 3.1: FDM printing.

SLA is another great 3D printing technology, which uses UV curing resins as raw materials. In this process, shown in Figure 3.2, the printing procedure is also made layer by layer, but the material is not deposited on the printing base. The resin is placed in a tank of glass or acrylic, which is submerged in the printing base. An ultraviolet laser cures and hardens the resin, allowing the object to be formed as the printer's base rises at the same height as the layer's thickness. This process is repeated until the object has the desired shape. SLA is, therefore, suitable for printing complex geometry parts containing fine details. However, it requires post-processing as the parts

must be cured in a UV chamber after printing. Furthermore, working resins have a higher cost when compared to the FDM method.

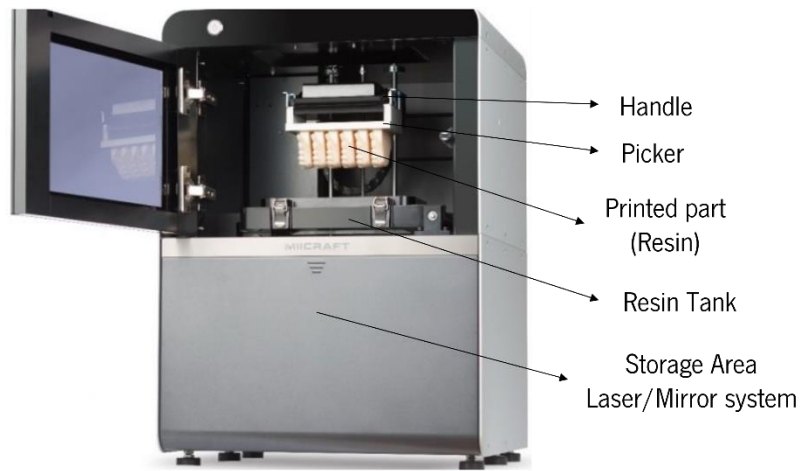


Figure 3.2: SLA printing.

Table 3.1 presents a summary of the main characteristics of each printing method. Both technologies have advantages and limitations, so their use should be based on the printing requirements.

Table 3.1: Comparison between FDM and SLA characteristics.

	FDM	SLA
Printer (Cost)	BCN3D Sigma (100 € - 15.000 €)	FabPro 1000 (3.500 € - 80.000 €)
Material (Cost)	PLA ABS PVA (50 €/kg – 200 €/kg)	Resin (150 € - 200 €/l)
Main advantages	Fast processing Low-cost equipment parts and materials Low maintenance Easy cleanliness	High accuracy Smooth surface finish High range of functional applications
Main disadvantages	Low accuracy Low precision Limited design	High cost Post-processing need Low printing volume Toxical
Wall thickness (Suitable good surface finish)	(> 0.5 mm)	(> 0.1 mm)

Wettability is another factor to consider when choosing a material for three-dimensional models. As the next step involves the application of a coating on the initial models, the printing material should present good wettability, because it is necessary that the coating adheres effectively to the model surface to ensure that all geometric details will be replicated. To assess this property, the surface tension of the liquid/solid contact needs to be determined, specifically, the surface free energy of the solid materials utilized. In order to evaluate the wettability value, it is necessary to use different types of measurement, for example, the contact angle measurements, used in the current study. Owens-Wendt-Rabel-Kaelble (OWRK) is one of the most widely used surface free energy theories based on Young's equation. It divides the interfacial interactions into two categories: polar and dispersive. To calculate the surface free energy with this model, the contact angle of two known liquids must be measured. One of them, with a dominant polar component, and the other as a dispersive liquid, since the interactions occur between similar components (if only dispersive liquid has been used, the potential polar interactions would not have been observed). Most commonly, water and diiodomethane are used.

In this research, a mobile measurement system was used to measure the surface free energy of PLA and resin. Using the MSA (Mobile Surface Analyzer - KRUSS) portable equipment, the obtained results are presented and discussed in subchapter 3.3. With a double sessile drop measurement method, the used equipment captures the contact angles of the two drops concerning the polar and dispersive components (water and diiodomethane). After the software has processed the data, the surface free energy values are recorded. A smaller contact angle indicates better wettability of the analyzed material and, consequently, better adhesion to the coating. Figure 3.3 illustrates this process straightforwardly.

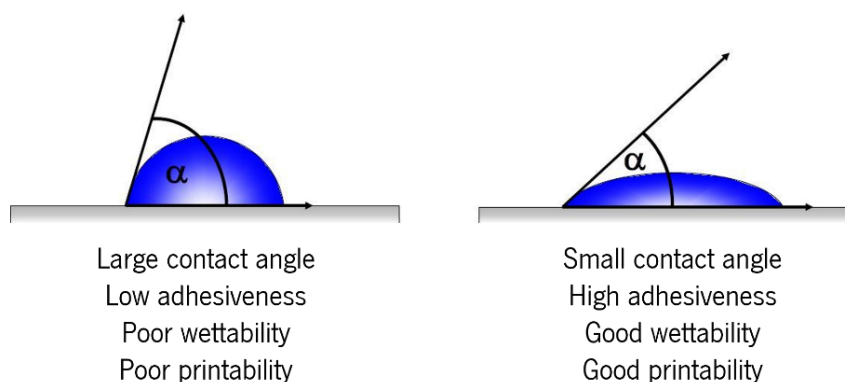


Figure 3.3: Measurement of the contact angles.

Following 3D printing, the polymer models are assembled with sprues and channels (feeding parts) through a technique known as tree making in the investment casting process [94, 217]. The printed models must be placed in a “tree” form as possible. Although high detail precision is not required, the feeding parts can also be printed using the same technique. However, FDM is recommended for time and cost savings.

There are some aspects to follow in the tree making to achieve successful castings:

- For larger trees, single models must be fixed around the main spruce in a spiral shape to facilitate removing the cast pieces;
- Spruces should be as short as possible;
- The diameter of spruces should guarantee optimal casting feeding;
- The PLA or resin connection to the spruce should be made in a hydro-dynamic style, to prevent turbulences while pouring the heavy liquid metal, breaking away thin parts of the plaster molding.

3.2. Coating and Molding Making

According to the proposed methodology (Figure 2.6), coating the model and fabricating the plaster molding are the next steps. The application of protective coatings in the investment casting process is one of the mechanisms that are employed to mitigate the reactions that occur during liquid magnesium melting and casting, as described in subchapter 2.2. A simple coating of liquid solutions is applied, followed by a cured period in which the coating dries and gains consistency. Water and investment powders are then applied over the coated sample trees to create the plaster moldings.

A variety of variables were tested in this investigation study to analyze the effect of coatings on mold-metal reactions during the investment casting of magnesium alloys. Having selected the best coating to use, other studies were examined, such as the effect of implementing different application methods and the effect of using a different number of coating layers. Based on the experimental evaluation, variables such as immersion time or curing time can be optimized during the procedure. Additionally, in order to avoid losing consistency, it is essential to ensure that the coated model is neither too dry nor too wet. Table 3.2 summarizes all the variables examined in this thesis concerning coating application.

Table 3.2: Coating application characteristics.

Coating	Application	Immersion time	Number of layers	Curing times
Yttria Fused Alumina Sand-based slip	Through dipping Through spraying	10 s*	1 layer	3 h*
			3 layers	
			5 layers	
			7 layers	

* commonly used in industry

Three different compounds were tested regarding the type of coating: Yttria, fused Alumina, and Sand-based ceramic slip. It should be noted that, in the present study, coatings were used only as face-coat slurries and not for shell production. The models were coated, followed by the production of the moldings. The main objective was to create a thin layer of refractory adhering to the plaster in order to prevent any contact between the liquid metal and the plaster from the molding that might affect the metal quality or the dimension accuracy.

Although there have been some studies on the use of Yttria (Y_2O_3) especially for coating crucibles in the casting of reactive alloys [107, 218, 219], it is not widely used in industry due to its high cost and thermal shock brittleness [218]. Yttria coatings have, however, demonstrated superior results in preventing the formation of reactions and reducing bath contamination [107, 219], mainly because of its low free energy formation ($\Delta G_f^\circ = -898,7 \text{ kJ mol O}_2^{-1}$ at 2000 K). A considerable negative value of ΔG_f° , also called Gibbs free energy, indicates a strong driving force to the compound's formation and high-compound resistance to thermal decomposition (reverse reaction). Chemical stability generally increases as the melting point increases. Indeed, the high melting point is not so important in magnesium casting because of the relatively low casting temperatures, but chemical stability is critical. Hence, at magnesium melting temperatures, and considering the very negative values of Gibbs free energy, Y_2O_3 is one of the most stable oxides, making it ideal for use as a refractory coating. In addition, its application in this work for low-volume ratio models takes some weight away from the cost disadvantage. The coating of Yttria used in this research is a liquid solution with 99.99 wt.% purity (from ZYP coatings).

Another two solutions were also tested and evaluated for the coating of 3D models. Fused Alumina (Al_2O_3) is considered an excellent cost-effective refractory product and a suitable ready-to-use binder for investment casting. In this work, the VP Disp. W 640 XC8 (EVONIK) solution was used as a coating, which is an Alumina dispersion with high solid content, anionic stabilization,

and a neutral to basic pH. A first coating layer of Yttria solution was used as a binder before applying the Sand-based slip. A low-granulometry (0.15 - 0.3 mm) sand mixture was used for the refractory material.

The models were coated according to two methods, dipping and spray painting, and were left to dry for three hours. Through dipping, the tree assembled samples were immersed in the liquid coating solution for 10 seconds and dried at a constant temperature of 30 °C in a cubic-shaped chamber (800 x 400 x 400 mm³). Applying the spray painting, the samples were coated manually using a commercial paint gun, followed by the same curing conditions. Depending on the number of layers required (Table 3.2), the procedure was repeated for each method.

After curing, the assembled models (painted or not) were involved in plaster to produce the moldings. A mixture of water and investment powder (Omega+ from Gold Star) was made according to the conventional molding technique and then left to dry at 30 °C before thermal processing. Here, a thermal cycle was applied in order to evaporate the ceramic materials (PLA and resin) from the molding interior and give consistency to the plaster, eliminating the water content.

It is important to consider several variables when making a molding, such as the type of mixture, the mixing time, the pouring time, the type of water, etc. The ability to control each variable is crucial for time savings and sample repeatability, avoiding poor castings and unnecessary raw material expenses, especially in experimentation in which the same procedure is repeated several times. According to investment manufacturers and casting industry experts, changes in these properties may be the cause of casting defects. For instance, a long pouring time increases the probability of investments' watermarks, especially if they are not mixed long enough. Having a weak investment will result in the formation of fins and a rough surface, resulting in heavy castings. The water can introduce impurities into the mixture. These properties are dependent on the water-to-powder ratio (w/p) and have a significant effect on casting results, so their control is vital.

For this reason, investment manufacturers recommend higher w/p ratios for smaller and more detailed pieces as well as de-ionized water to remove interference compounds. As a result, a 40/100 (mass%) ratio of water (de-ionized) to powder has been employed in this study. Additionally, mixing and pouring were carried out in proper machines (MC - series by Indutherm GmbH), under a vacuum atmosphere to prevent the introduction of air bubbles into the moisture.

3.3. Experimental Procedure

The application of different additive manufacturing methods is presented in Figure 3.4. In general, it is evident that SLA has a higher quality and precision than FDM. So, for complex geometries and reduced dimensions parts, it can be concluded that SLA must be used. FDM cannot obtain the higher geometric and dimensional precision required by some pieces, even when support material is needed (Figure 3.4a) or an extrusion nozzle cleaning tower is used to prevent material drag (Figure 3.4b). Despite being cheaper, FDM has a poorer surface finish than SLA, apart from thickness limitation. In this work, for example, SLA must be used for stent printing and FDM can be used to print the feeding system. This will be explained further in subchapter 5.1.

The castable resin used in the SLA method (JewelCast GRN) is an ideal green material for printing small patterns in plaster investment casting applications. Furthermore, this material provides superior casting quality with minimal ash after burnout and allows the production of finely detailed investment casting parts with a smooth surface finish.

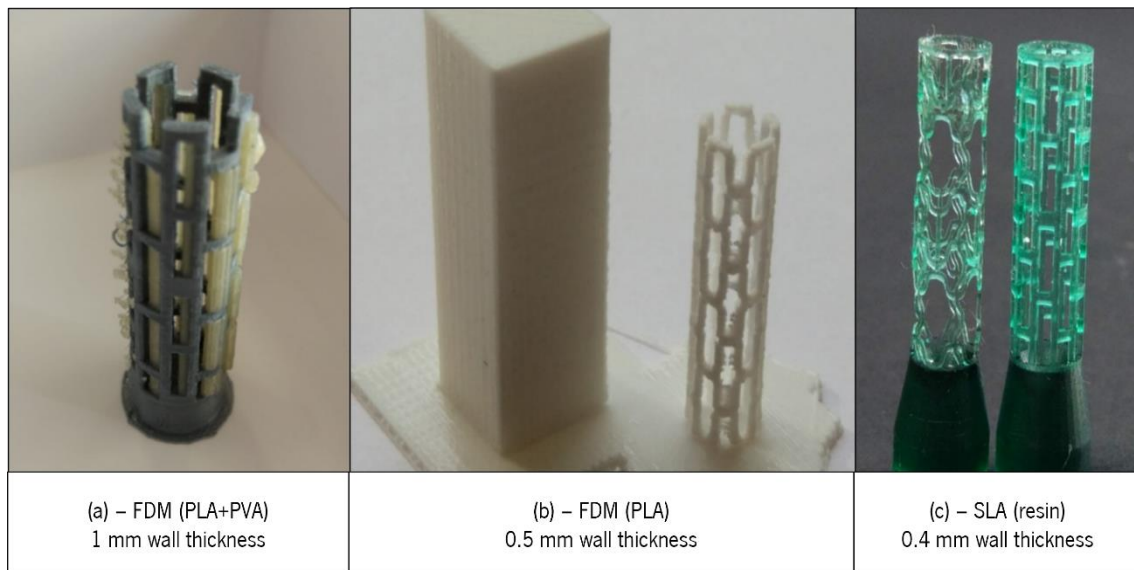


Figure 3.4: Additive manufacturing: (a) FDM with support material; (b) FDM using cleaning tower and (c) SLA.

Based on the results of the wettability assessment, depicted in Figure 3.5 and presented in Table 3.3, it appears that along with better print quality, the resin also exhibits greater wettability, favoring the subsequent application of the coating. According to the contact angles captured by the MSA equipment for both the polar component (water drop) and the dispersive component (diiodomethane drop), the resin has a greater surface free energy (63.83 mN/m) compared to PLA (42.20 mN/m), using the OWRK calculation method. This means that resin is more wettable than

PLA and ensures better adhesion to liquids, i.e., to the coating layers. As such, the use of resin must be prioritized over the PLA for better coating adhesion, unless the application does not justify the higher resource expenditure.

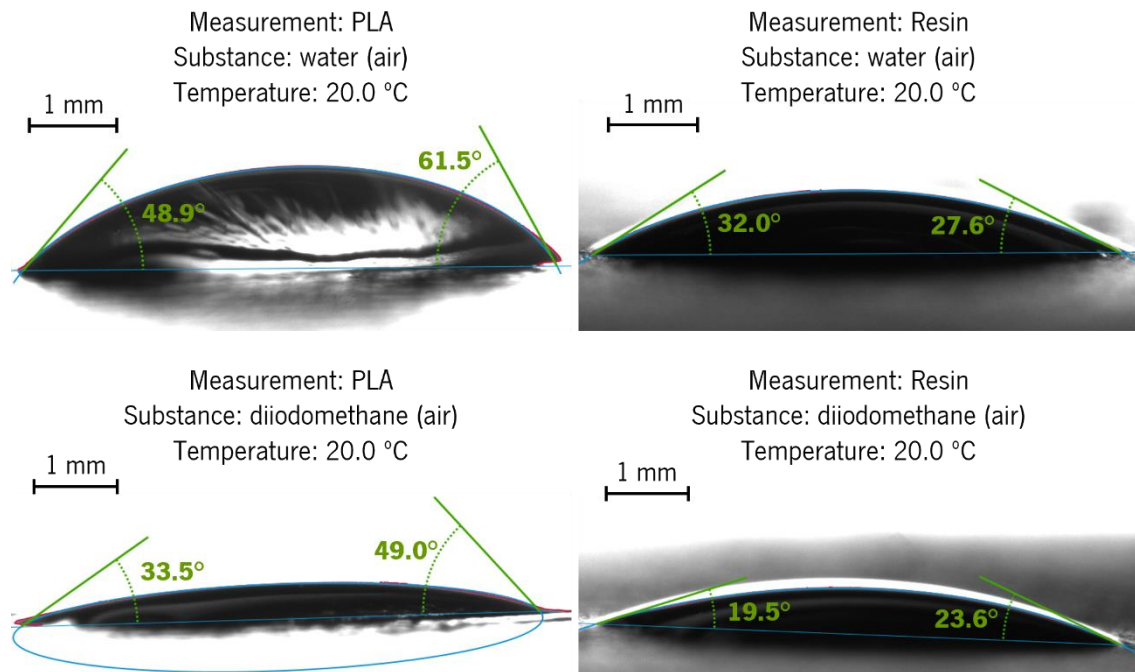


Figure 3.5: Contact angles measurement for PLA and resin.

Table 3.3: Acquisition data for wettability analysis (one measurement reading).

	PLA	Resin
Surface free energy	42.20 mN/m	63.83 mN/m
Dispersive	12.61 mN/m	45.58 mN/m
Polar	29.59 mN/m	18.26 mN/m

The coating type to be applied is shown in Figure 3.6 in accordance with the different refractories defined (Yttria, Alumina, and Sand-based slip). The samples were immersed in the liquid solutions for 10 seconds. For the Sand-based slip application, as described in the previous subsection, the sand mixture is applied after a coating layer of liquid Yttria, which is not allowed to dry in order to improve sand adhesion.

Alumina (Figure 3.6b) and Sand-based slip (Figure 3.6c) were ineffective. The coatings were unable to protect from the reactions that occurred with the liquid magnesium, which resulted in totally failed castings, characterized by the occurrence of strong exothermic reactions that compromised the process. In both cases, the cavity filling was blocked due to the reactive contact

between the magnesium and the molding walls. These experiments are not recommended for user safety and equipment preservation, so their use was not repeated in this study. On the other hand, the Yttria coating effectively acted as a barrier to reactions, and a complete cavity filling was achieved. Considering the obtained stent (Figure 3.6a), it may be concluded that the application of Yttria is an effective solution to magnesium casting using plaster molding, although further experiments and an in-depth analysis of the process are still needed.

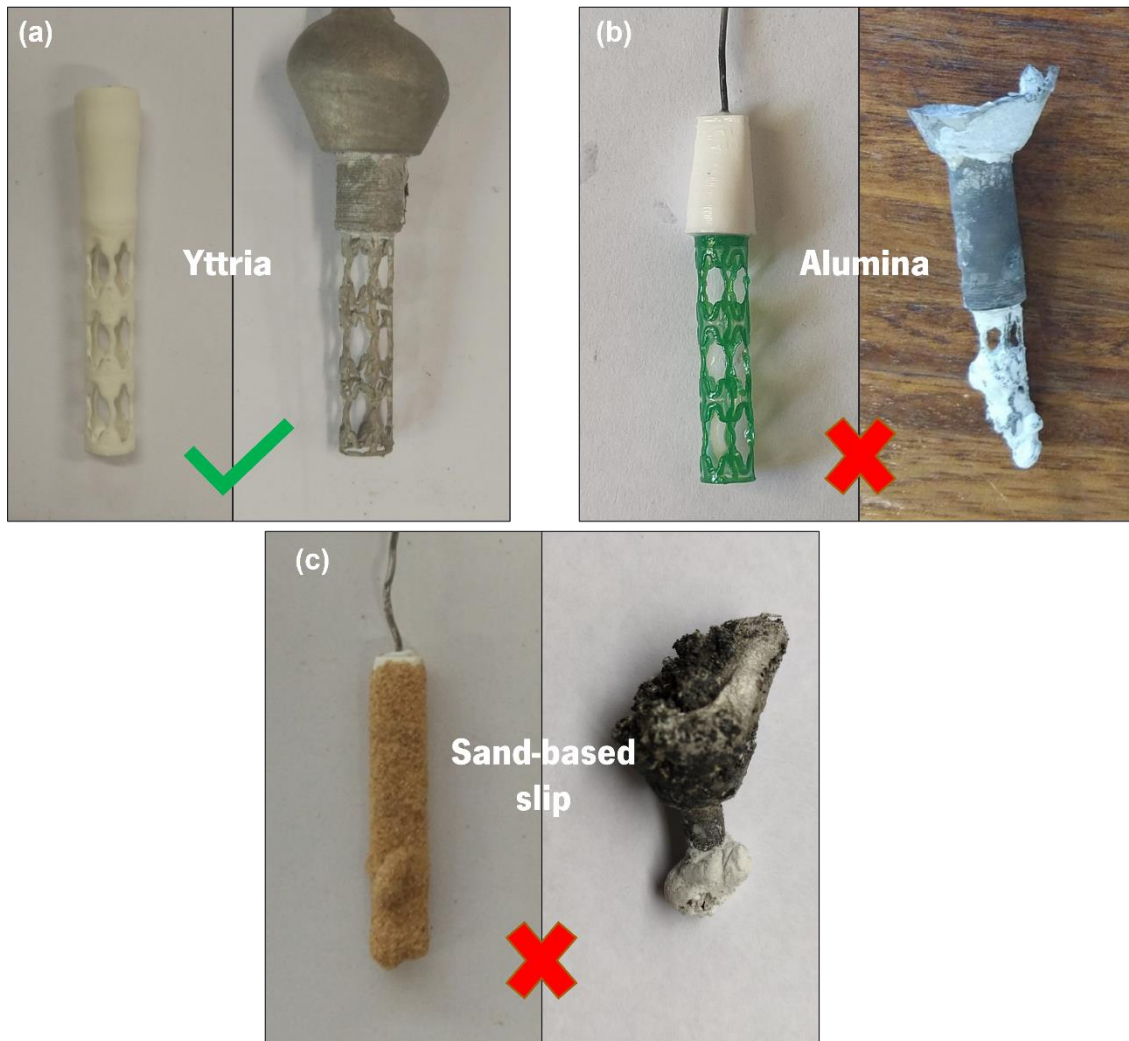


Figure 3.6: Castings after different coating applications: (a) Yttria; (b) Alumina; and (c) Sand-based slip.

The application method was tested after determining that Yttria is the appropriate protective coating to use. As displayed in Figure 3.7, both dip and spray methods fulfilled the objective of ensuring a uniform Y_2O_3 coating for the resin 3D models. In practice, however, the spray method does not appear to apply a layer as adherent to the solid as the dip method. A small degree of coating roughness can be observed when the spray was applied to coat the stent tree. The resulting castings also confirm these observations. The final cast stent showed some degree

of reaction and high surface roughness in the spray coating, although the cavity filling was not significantly affected. Alternatively, in the casting in which the model tree was dipped in Yttria, the absence of reactions and a sane molten metal is evident, resulting in a better casting. As a result, and based on the comparison of both methods, the dipping method is recommended to guarantee a more uniform coating for magnesium investment casting.

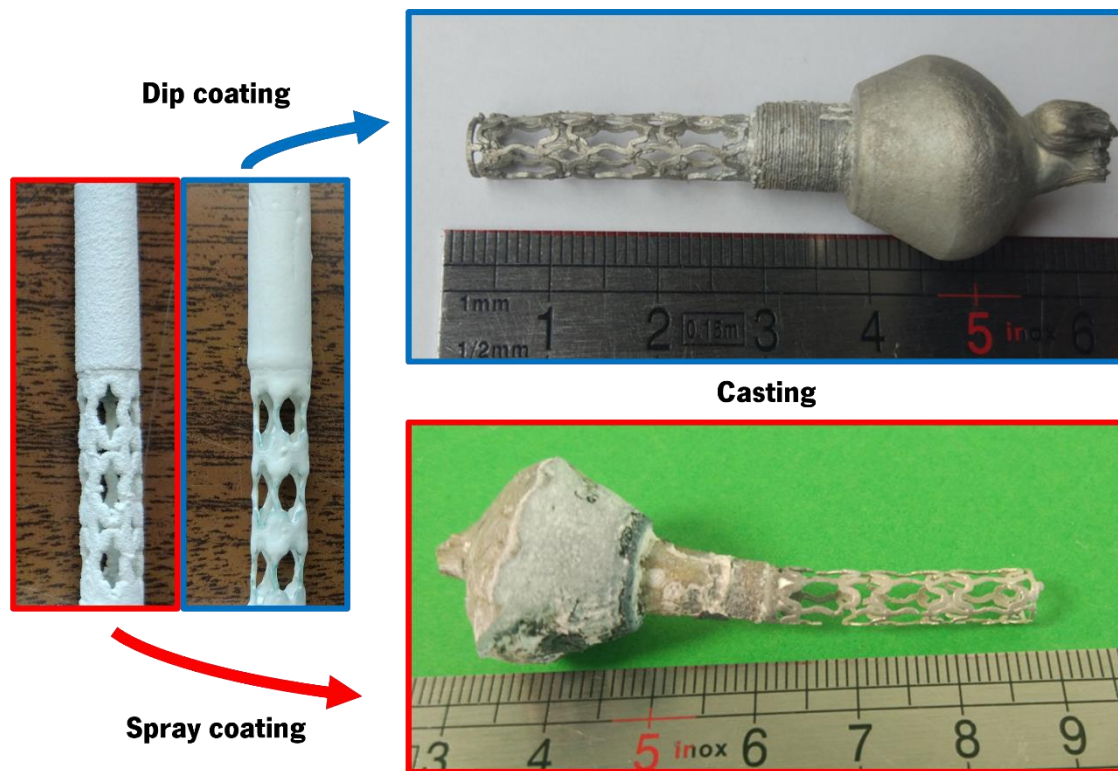


Figure 3.7: Application of dip and spray coating methods.

Finally, an experimental study was carried out to understand the influence of coating thickness. The procedure of dipping the sample and allowing it to dry was repeated several times, depending on the number of layers to be applied. Then, the plaster moldings were made. More than one coating layer is applied to reduce the Yttria permeability in order to prevent the metal from coming into contact with the molding walls. Figure 3.8. illustrates the obtained results after the thermal cycle. Increasing the number of Y_2O_3 layers led to worse results. Under the influence of thermal treatment, the outer Yttria layers detach from the inner layers, breaking up and accumulating into the molding cavities. Metal casting is considerably affected by this phenomenon, both in terms of surface roughness and metal contamination by Y_2O_3 particles released during the casting process. It can be concluded from the results of these castings that the stability of the Yttria coating can be affected by the temperature and/or by the volumetric contraction that occurs during

the thermal treatment procedure. As the thermal cycle for moldings assumes temperatures of 720 °C, the cracking is higher for thicker coating layers and larger molding cavities. Consequently, the application of coating as a refractory requires a compromise between the thickness of the layer and the temperatures involved.

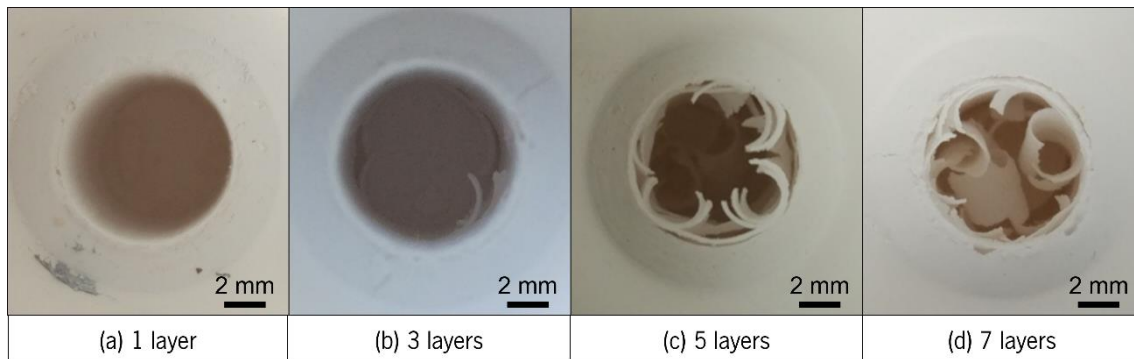


Figure 3.8: Application of different coating thicknesses.

In the following subchapter, a more detailed analysis will be conducted to the mechanisms of the reactions occurring at the metal-liquid interface between the liquid magnesium and the molding walls, as well as the effectiveness of using Yttria for casting magnesium parts.

3.4. Case Study 1 – Effect of model's coating on mold-metal reactions

3.4.1. Experimental procedure

The experimental procedure was carried out through a vacuum-assisted investment casting process, which was based on the five steps belonging to the proposed methodology (Figure 2.6): (i) production of CAD models; (ii) manufacture and assembly of polymeric models; (iii) coating of models; (iv) preparation of ceramic moldings (plaster); and (v) casting of the magnesium alloy.

The initial models were made by additive manufacturing, using the FDM process. Using the tree-making technique, models were printed in PLA and assembled with sprues and channels (also made by the same method). A disk specimen with a thickness of 2 mm was selected to ensure adequate cavity filling and evaluate the mold-metal interface. For reproducibility purposes, each tree consists of two specimens. Figure 3.9 provides the CAD corresponding to the tree assembly of the produced models (Figure 3.9a) and the cross-section of the sectioned part (Figure 3.9b) for analysis. The extension of the distribution gate in the tree assembly is justified in order to

prevent turbulent flow within the cavity. Furthermore, this extension promotes the retention of inclusions and slag that may occur as a result of the interaction of the liquid magnesium with the surrounding atmosphere during the melting phase [97].

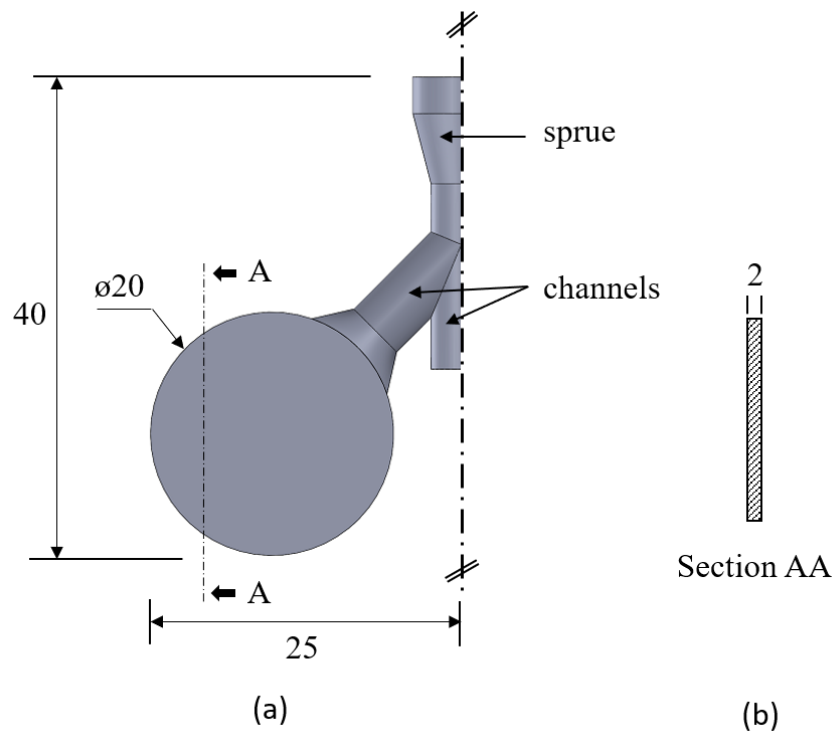


Figure 3.9: Models geometry (dimensions in mm): (a) tree assembly and (b) analyzed sectioned part.

Six castings were performed, consisting of twelve specimens for analysis, and using two different conditions (samples with models' coating and samples without coating). So, half of the samples were coated with three Ytria layers (comprising a thickness of approximately 0.3 mm each) in order to analyze the interaction between the metal and the plaster during the casting process. The PLA-assembled models were immersed in liquid Y_2O_3 for 10 seconds and then dried in a cubic chamber ($800 \times 400 \times 400 \text{ mm}^3$) at a controlled temperature of $30 \text{ }^\circ\text{C}$, accelerating the cooling process and removing moisture. This procedure was repeated twice in a one-hour interval, resulting in three layers of refractory protection for each assembled model.

As described in the previous chapter, the ceramic moldings for both models with and without coating were made from plaster. A mixture of water and investment powder (Omega + from Gold Star) was used in a ratio of 40/100 (mass%) following the conventional molding technique and following the instructions of the plaster manufacturer (Ultra-Vest, Ranson & Randolph, Maumee, OH, USA). A thermal cycle was then used to remove the water content and polymeric materials, giving consistency to the plaster [220]. It involved first heating of the moldings at $300 \text{ }^\circ\text{C}$

for 3 hours, followed by second heating at 1.6 °C/min to 720 °C. At the same temperature, an isothermal stage was followed comprising a period of 3 hours to increase the plaster moldings' mechanical strength and eliminate the PLA material. The evaporation of the polymeric material allows the creation of an empty shape into plaster moldings that corresponds to the final envisaged geometry.

A vacuum-assisted induction melting furnace was used to melt 10 grams of AZ91D-1 wt.% CaO in a SiC crucible, as depicted schematically in Figure 3.10. The melting performance was 3.5 kW, and the mains supply was 230 V/16 A at 50 or 60 Hz. Table 3.4 shows the composition of the AZ91D-CaO magnesium alloy used, which was already received with the CaO addition (commercial alloy). All tests were performed under an argon-protected atmosphere during the melting process. The metal was melted under a vacuum pressure of 1.0 bar and held inside the crucible at 700 °C for 1 minute for homogenization. Then, according to the processing parameters shown in Table 3.5, the melt was poured into the plaster molding pre-heated at 400 °C overpressure of 2.0 bar to facilitate cavity filling. Casting and pouring temperatures were controlled by the furnace display. After pouring, the plaster moldings were cooled for a period of 10 minutes and the samples were then removed, cleaned, cut according to section AA of Figure 3.9, and mounted in resin for characterization. Finally, the samples were ground using increasingly small SiC papers sizes (#320, #600, #800, and #1200), followed by polishing of 1 µm using cloths with diamond suspension.

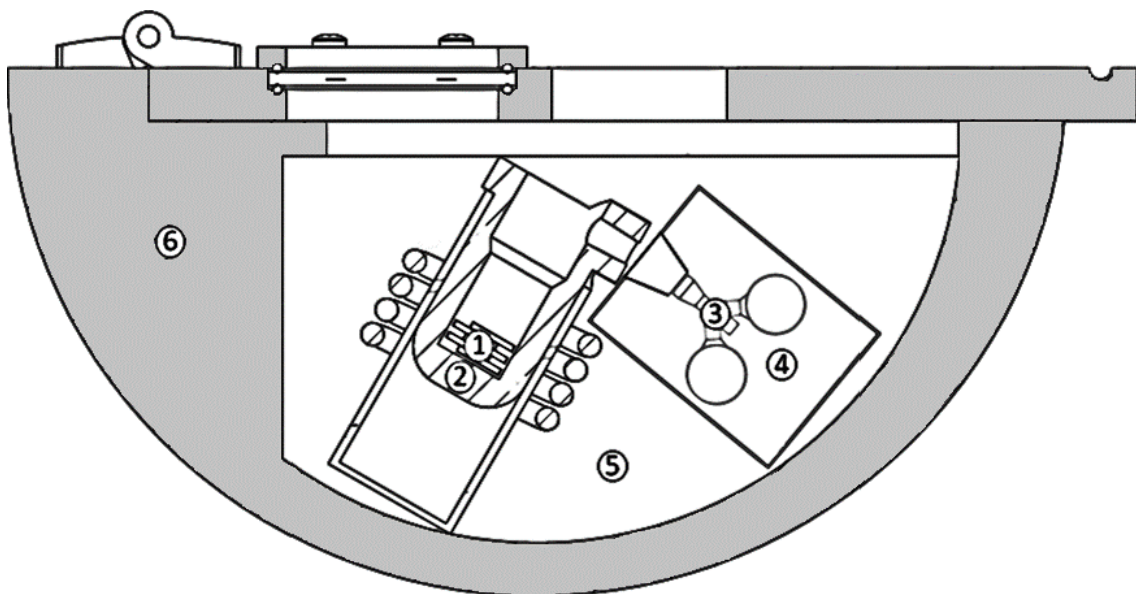


Figure 3.10: Experimental setup of vacuum-assisted casting: 1- AZ91D-1 wt.% CaO; 2- crucible; 3- cavity of the assembled model; 4- plaster molding; 5- vacuum atmosphere, and 6- furnace.

Table 3.4: Chemical composition of AZ91D-1 wt.% CaO magnesium alloy (mass%).

Element	Al	Zn	Mn	Si	Cu	Fe	CaO	Mg
Standard	8.3 - 9.7	0.35 - 1.0	0.15 - 0.5	Max. 0.01	Max. 0.003	Max. 0.005	Added 1.0	Bal
Measured	8.9	0.56	0.3	0.003	0.-	0.-	0.98	Bal

Table 3.5: Key parameters adopted during processing.

Sample	Refractory layer	No. of coating layers	Pouring temperature, °C	Molding temperature, °C	Casting pressure, bar
A	-	-	700	350	2
B	Y ₂ O ₃	3	700	350	2

In terms of characterization, the final cast samples were initially evaluated by visual inspection. After that, both the periphery and the matrix were examined by OM (Optical Microscopy) and at higher magnification by FESEM (Field Emission Scanning Electron Microscopy) equipped with EDS (Energy-dispersive X-ray Spectroscopy) in order to reveal and evaluate the mold-metal interface reaction that occurred during the investment casting process, as well as the microstructure morphology.

3.4.2. Results and Discussion

The complete cavity filling was achieved for both casting conditions. A well-defined layer of reaction products was detected through visual assessment of the castings in which the models were not coated (Figure 3.11a). This layer formed along the surface suggests the occurrence of interaction between the high-temperature melt and the plaster molding (walls). Consequently, defects such as high surface roughness and macro porosities were identified in these samples, as illustrated in Figure 3.11b. Additionally, it was observed that the surfaces of the models coated with Y₂O₃ had better surface quality and were free from reaction products, as shown in Figure 3.11. This indicates an increase in process efficiency which can be attributed to the use of Yttria as the interface coating. However, small “splinters” of the refractory were incorporated into the samples (Figure 3.11b), due to the occurrence of scaling of the innermost layer of Y₂O₃. This evidence can be explained by the poor resistance of the Yttria layers to high temperatures during the molding's thermal processing. Additionally, the poor adhesion of the coating to the molding walls was

responsible for the surface roughness observed in these castings. Figure 3.11 illustrates that similar phenomena also occurred for the other two castings per condition.

Figure 3.12 schematically explains the porosity defects that occurred in the samples in which the models were not coated. As a result of the reaction zone between the molten magnesium and the walls of plaster molding, gas was released throughout the entire filling area, which accumulated on the top of the filling channel and in the peripheral areas. Furthermore, a substantial amount is released to the exterior in the form of splashes. Then, due to the rapid cooling of the liquid metal in the upper filling zones (sprue and channels), the accumulation of gases that are not expelled to the outside, induces large defects in the poured samples, as can be seen visually in Figure 3.12(detail I). No macro casting defects were found in castings in which models were coated, as observed in Figure 3.12(detail II).

A complete characterization of the mold-metal interaction zone was completed by OM (Optical Microscopy) and SEM (Scanning Electron Microscopy) evaluation of the areas A and B marked in Figure 3.11b.

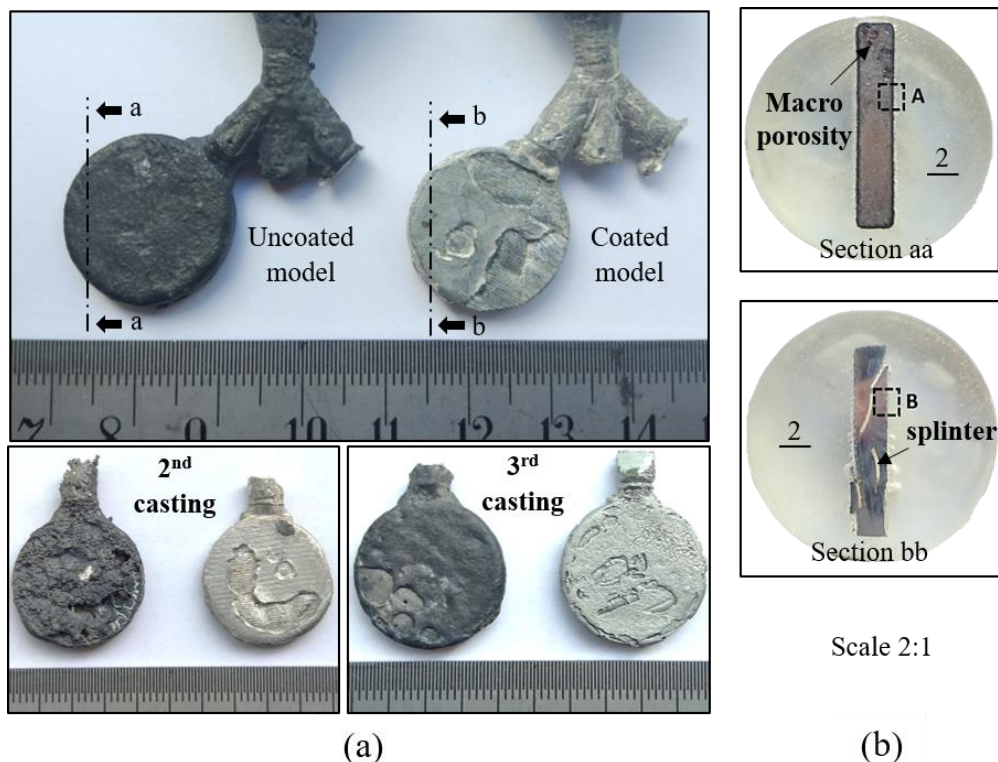


Figure 3.11: Casting samples: (a) obtained results for tests performed on both uncoated and coated models and (b) sectioned parts for characterization of the A and B points (scale in mm).

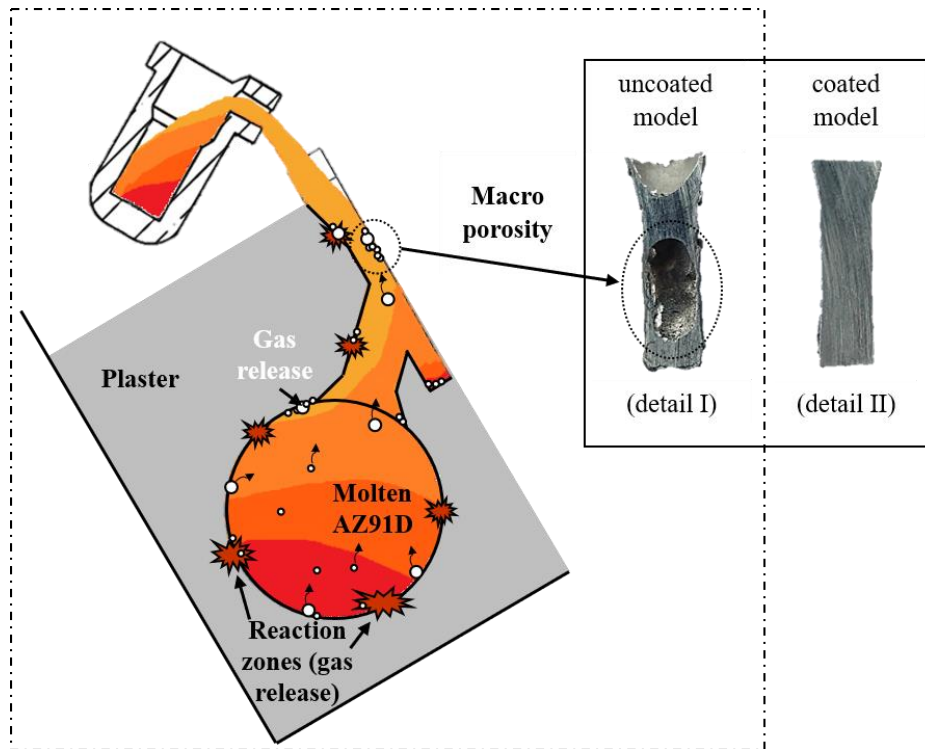


Figure 3.12: The reaction mechanism proposed for the occurrence of porosity defects.

Based on the OM analysis, it is noted in Figure 3.13a that severe reactions occurred in the experiments without coating application in the interface zone, resulting in significant casting defects, such as inclusions and porosities. A continuous layer of oxidation and reaction products (200 - 300 μm) can be found along the entire surface of the samples, as well as the formation of precipitates as a consequence of these reactions. The precipitated particles that were revealed (denoted as 'Z1' in Figure 3.13a) are distributed along with the entire matrix, representing a volume fraction of 20 % with an average area of 0.715 mm^2 . Direct contact between the liquid metal and the plaster from the molding may explain the severe reactions observed, as well as the highly heterogeneous morphology of the matrix in the castings without any coating of Y_2O_3 . In fact, the intense reaction that occurred may have been caused by the interaction of SiO_2 with magnesium. Combining these elements can trigger a series of chemical reactions that give rise to different types of reaction products, as described in Table 3.6 [48], which mainly occur at the mold-metal interface.

In contrast, a smooth and clean surface was achieved in the samples in which Yttria was used as a protective coating. In these castings, a microstructure with low inclusions and porosities was obtained, showing a more homogeneous distribution of the $\alpha\text{-Mg}$ and $\beta\text{-Mg}_{17}\text{Al}_{12}$ intermetallic phases, as shown in Figure 3.13b.

Table 3.6: Possible mold-metal reactions on Mg-SiO₂ interface [48].

Reaction	Temperature range (°C)
$2\text{Mg (l)} + \text{SiO}_2\text{(s)} \rightarrow 2\text{MgO (s)} + \text{Si (s)}$	Eq. 2.3
$4\text{Mg (l)} + \text{SiO}_2\text{(s)} \rightarrow 2\text{MgO (s)} + \text{Mg}_2\text{Si (s)}$	Eq. 2.4
$4\text{Mg (l)} + \text{SiO}_2\text{(s)} \rightarrow 2\text{MgO (s)} + \text{Mg}_2\text{Si (s)}$	Eq. 3.1
$\text{MgO (s)} + \text{SiO}_2\text{(s)} \rightarrow \text{MgSiO}_3\text{(s)}$	Eq. 3.2
$2\text{MgO (s)} + \text{SiO}_2\text{(s)} \rightarrow \text{MgSiO}_4\text{(s)}$	Eq. 3.3

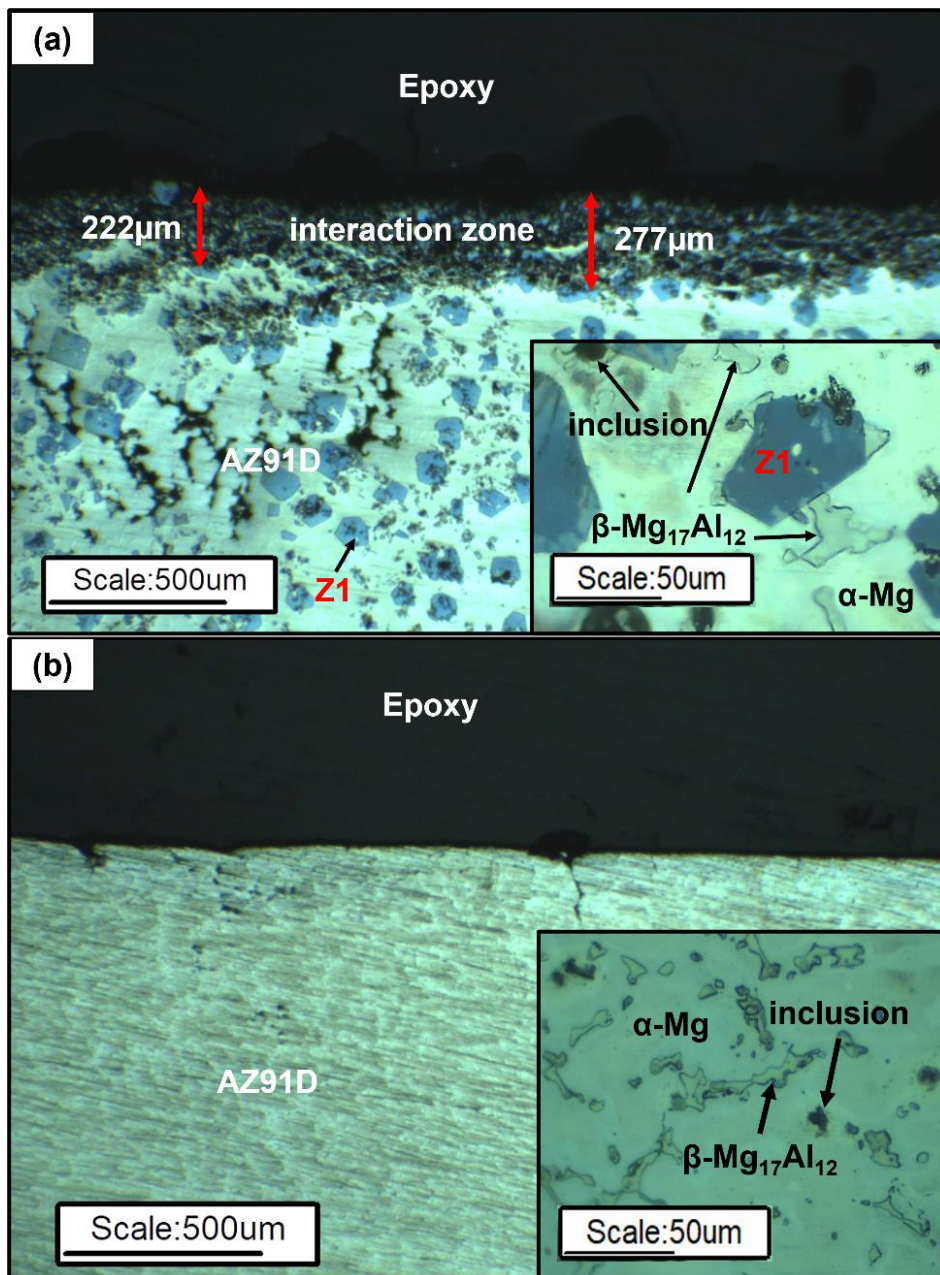


Figure 3.13: OM analysis of the mold-metal interaction zone (A and B areas in Figure 3.11): (a) performed test without no model coating and (b) performed test using Y₂O₃ layers to coat the initial model.

Figure 3.14 presents an explanation of the interaction zone for both molding preparation conditions. In the tests conducted without coating the models, Mg and SiO₂ diffusion occurs due to direct contact between the liquid metal and the walls from the plaster molding (Figure 3.14a). When Y₂O₃ is used to coat the models, this fact is not observed, indicating that Ytria acts as a barrier to prevent mold-metal contact in the interface zone. Because of the high temperatures applied during the thermal cycle, the integrity and adhesion of the coating to the plaster molding walls were compromised. This resulted in the cracking of the Y₂O₃ layer, as shown in Figure 3.14b.

The SEM analysis of the A (uncoated model) and B (coated model) areas marked in Figure 3.11b, respectively, are shown in Figures 3.15 and 3.16. Considering the experiments without the coating, the non-uniform and irregular morphology at the interface zone (Figure 3.15a) confirms the occurrence of mold-metal reactions. As can be seen, in the results of the EDS analysis of the point Z2 (Figure 3.15b), Mg (59.27 wt.%) and O (34.63 wt.%) are the dominant elements in the periphery of the mold-metal reaction products. This confirms that the most obvious layer of the mold-metal reaction products is composed of predominantly magnesium oxide, MgO. In addition, the EDS analysis performed on the precipitated particles discovered in the microstructure of these samples (Figure 3.15c), which are identified in Figures 3.13a and 3.15a as 'Z1', revealed that these particles contained significant amounts of Mg (30.76 wt.%), Si (25.49 wt.%) and Ca (26.51 wt.%). This suggests the formation of a CaMgSi phase and the matrix, lending credence to the notion that these particles were created due to the interaction between the liquid metal and the plaster from the molding.

This phenomenon is demonstrated in Figure 3.14a. The magnesium diffused through the plaster and reduced the silica present in the ceramic material of the molding. This resulted in a new phase, precipitating as a polyhedral intermetallic compound, as shown in Figures 3.13a and 3.15a. This compound was also reported by Moussa [221] and Lotfpour *et al.* [222]. In fact, these authors described the occurrence of a new CaMgSi phase after the addition of 1.0 wt.% Ca into an Mg-5 wt.% Si hyper-eutectic alloy, which is consistent with the results obtained in this case study. In addition, the detection of high O content (16.78 wt.%) indicates that extensive oxidation has occurred in the matrix of these samples. Based on the low percentage of aluminum found, it is clear that aluminum did not participate in the formation of the oxides, indicating that magnesium oxide dominated, which is in agreement with the results reported by Czerwinski [223] and by Jafari *et al.* [224].

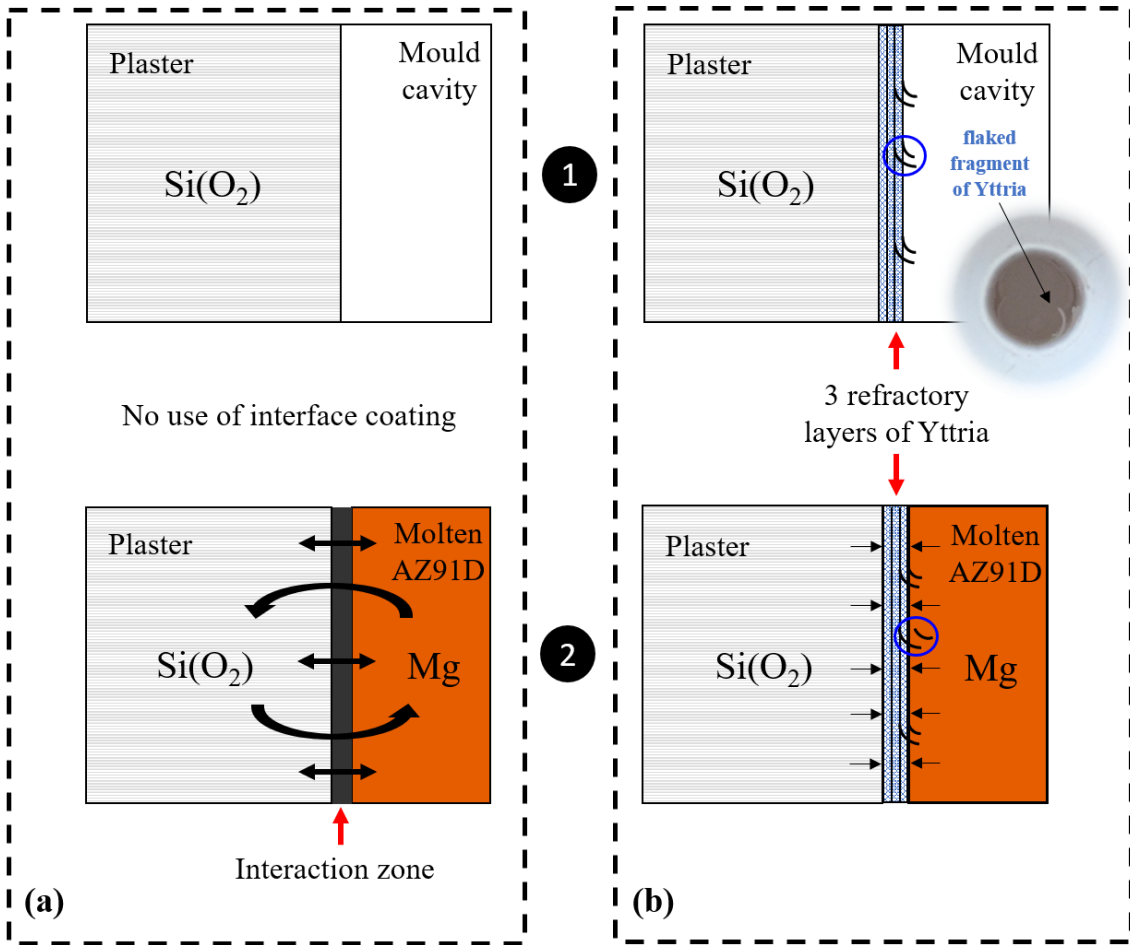


Figure 3.14: Schematic mold-metal interface: (a) no use of models coating and (b) use of Y_2O_3 to coat the models: 1- before pouring; 2- after pouring.

On the other hand, a well-defined surface free of large oxidations was denoted in the obtained samples using Y_2O_3 to coat the models, as displayed in Figure 3.16a. Microstructural analysis shows a sane matrix, free of large oxidations and reaction products, which indicates a more uniform distribution of the α -Mg and β - $\text{Mg}_{17}\text{Al}_{12}$ phases. The EDS analysis of the point Z3 (Figure 3.16b) suggests the appearance of an Mn-Al intermetallic into the matrix, given the Mg content of 34.40 wt.% detected from the surrounding matrix and the very fine size of the particles. The absence of silica in this analysis confirms that an apparent inhibition of reactions was achieved by preventing direct contact between magnesium and plaster. Furthermore, the absence of Yttrium in the analysis indicates no dilution of the Yttria layers into the castings. The presence of a small percentage of oxygen indicates that a slight degree of oxidation has occurred in the first reaction stage, during the melting process. A possible explanation for this is the presence of oxygen in the chamber atmosphere due to the handling procedures since it is required to initiate Mg reactions.

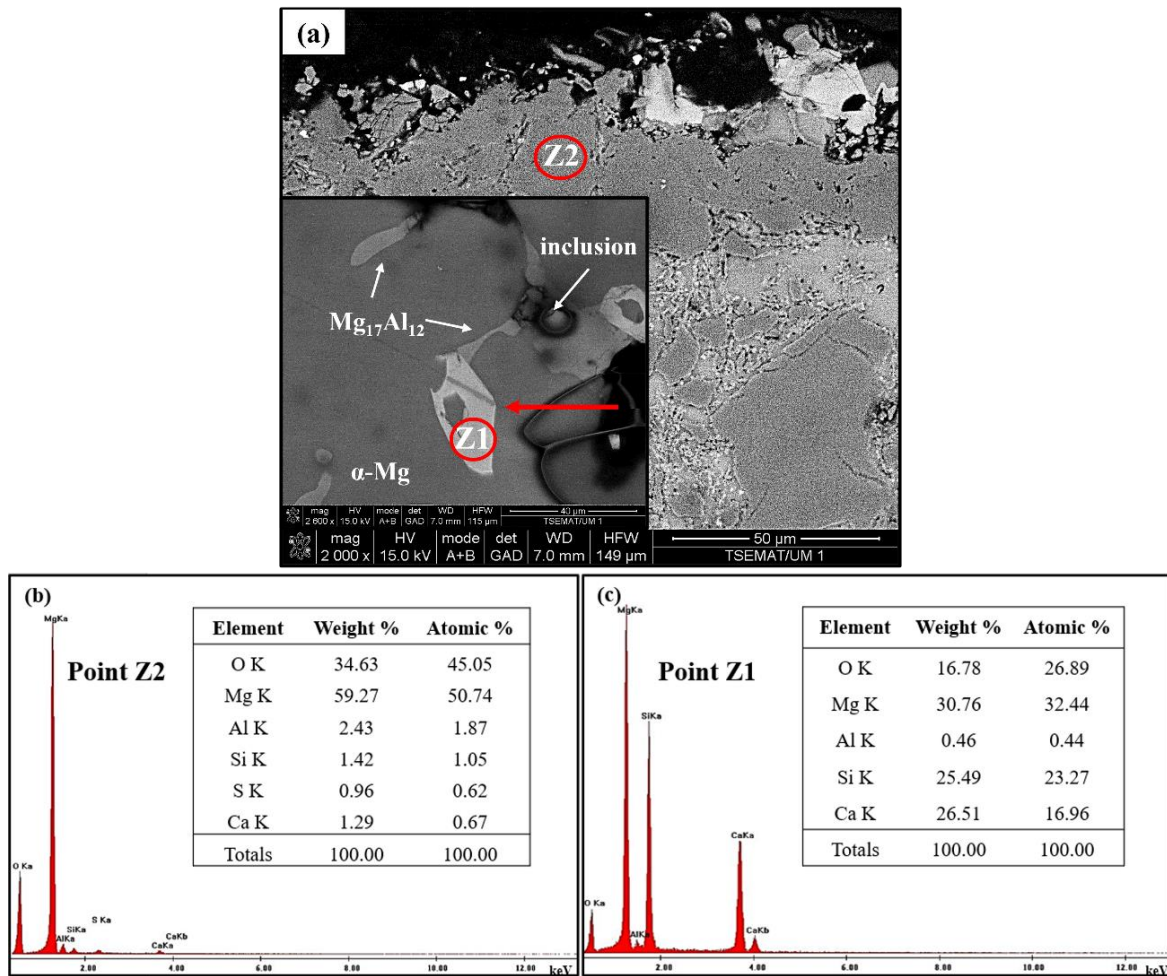


Figure 3.15: SEM analysis of the samples obtained without coating: (a) backscattered FESEM images in the periphery; (b) EDS analysis of point Z2 and (c) EDS analysis of point Z1.

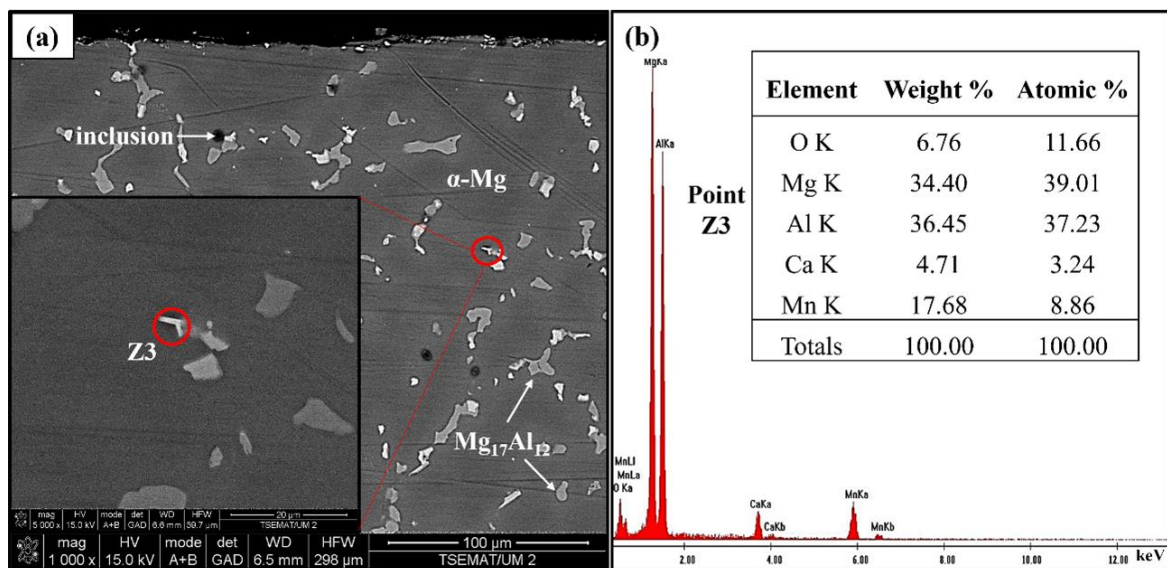


Figure 3.16: (a) backscattered FESEM images of the samples obtained using Y_2O_3 to coat the models and (b) EDS analysis of point Z3.

Based on the analysis performed in this case study, Y_2O_3 layer application in the coating of the model is an effective inhibitor of mold-metal interaction in investment casting, preventing serious reactions triggered by this interaction. Therefore, further research could have a positive impact on the magnesium alloy casting industry.

3.5. Summary and Conclusions

This chapter addresses the initial steps regarding the methodology proposed in Figure 2.6 (1-4 steps). Considering the conditions and objectives outlined, optimization approaches were explored for each stage of the conventional process.

Concerning the initial three-dimensional models, used to create the molding cavities into which the magnesium is poured, it was concluded that the SLA technology offers the best printing results, in terms of detail precision and surface roughness. Furthermore, additive manufacturing of models allows for a significant reduction in time and costs compared to conventional manufacturing processes. Aside from being capable of excellent geometric replication, the resin used in this process had also better wettability values than PLA, which indicates better adhesion to the coating.

The three-dimensional models were coated in several different ways in order to study the mitigation of mold-metal reactions. The use of Alumina and Sand-based slip as refractories led to failed castings as a result of strong exothermic reactions. On the other hand, the use of Yttria proved to be very effective in preventing these phenomena. However, the stability of the Y_2O_3 layers is compromised at elevated temperatures, resulting in cracking of the outer layers. Therefore, Yttria coatings must be applied by dipping with a few layers and a compromise between the coating's permeability and stability is needed.

A case study was performed to investigate the effectiveness of Yttria coating. Based on the experiments and analyzes carried out, the following conclusions can be drawn:

- Using Yttria (Y_2O_3) as a refractory coating on the initial models effectively prevented the mold-metal interaction that occurred in the investment casting of AZ91D-1 wt.% CaO magnesium alloy. The high precision casting process and the dimensional complexity of the samples, however, require further improvement of the coating application technique.

- Strong reaction products were detected in samples in which Y_2O_3 was not used to coat the models. An extensive oxidation layer was detected along with the mold-metal interface. The formation of specific particles along the entire matrix (new phase) can be attributed to the direct contact between the liquid metal and the plaster molding. Significant porosity defects were also originated due to the gas released by the reactions that occurred during the casting process.
- A cleaner surface and a more uniform microstructure were evidenced in the experiments performed in which the models were coated with Y_2O_3 . These experiments revealed no significant oxidation. The absence of Si and Y in the EDS analysis indicates no interaction between the liquid metal and the plaster from the molding, and therefore no dilution of the coating into the castings.
- The detection of low oxygen content in the EDS analysis of samples in which Y_2O_3 coating was applied indicates slight oxidation during the melting process, possibly attributable to residual oxygen in the chamber atmosphere. However, continuous improvement of these procedures can be a promising way to invest in casting as a near-net-shape process to perform magnesium castings.

Foundry is believed to be the industry genesis. It is perhaps the oldest known process, as there are records of objects in molten copper made more than 6000 thousand years ago.

Chapter 4. THERMODYNAMIC ANALYSIS IN MAGNESIUM INVESTMENT CASTING

A successful investment casting part requires identifying the most influential processing parameters. Variable values of these parameters should satisfy the desired final properties, making them relevant to the quality of the final product. A successful casting process cannot be achieved without knowing the influence of the casting parameters and variables related to the temperatures and pressures involved in the process. These variables assume even greater importance in the investment casting of magnesium alloys, as they are mainly responsible for the thermodynamic conditions that can trigger the occurrence of reactions. On the other hand, the use of a protective atmosphere and the timing handling of the procedures during the process are other essential characteristics to be considered.

This chapter examines and discusses the melting and pouring phases that are critical for magnesium investment casting. A thermal cycle optimization is also applied to the plaster moldings. This corresponds to steps 4 and 5 in the methodology proposed in this study (Figure 2.6). In addition, another case study is conducted to analyze and validate the performed optimizations to determine the importance of each casting variable in the fluidity and the filling length of the AZ91D-1 wt.% CaO magnesium alloy.

4.1. Molding Thermal Cycle Optimization

The investment casting process employs a thermal cycle after the manufacture of the plaster moldings to eliminate the water content and ensure consistency of the plaster, as described in case study 1 of Chapter 3. During the process, the polymeric material (fabricated by Additive Manufacturing) melts and is eliminated from the interior of the moldings, resulting in empty cavities of the same geometry that can be filled with metal.

However, it was determined that the Yttria layers' stability is compromised at high temperatures, especially when using a thermal treatment that reaches temperatures above 700 °C, as applied before. In order to determine the optimal temperature conditions, DTG (Derivative Thermo Gravimetry) and TGA (Thermal Gravimetric Analysis) were performed on the printing and molding materials to obtain a better understanding of the thermal impact. According to the results of the graphs presented in Figure 4.1, it is possible to conclude that the printed materials, resin, and PLA, started to evaporate only at temperatures around 400 °C, as shown in Figures 4.1a and 4.1b, respectively. Based on the weight loss percentage and the DTG analysis, it appears that these materials were almost completely burned. Further, the plaster analysis (Figure 4.1c) suggests that the most significant loss in weight occurs until 450 °C, due to the water's elimination, and is only 0.3 % up to that temperature. This thermal study made it possible to determine the maximum temperature that could be applied to the plaster moldings without impairing the stability of the Yttria coating.

Therefore, an optimized thermal cycle was adopted as part of the proposed methodology for curing the plaster moldings, as shown in Figure 4.2. The moldings were placed into the furnace for an initial isothermal period of 30 °C. To avoid large thermal gradients that would compromise the stability of the plaster, the heating rate for the following isothermal slopes was lowered. In light of previous analyzes, the maximum temperature of this new cycle was set at 420 °C. Thus, after 13 h, the elimination of the polymeric materials and the plaster water content was guaranteed, safeguarding the Yttria coating's stability. The thermal cycle ended at the temperature that corresponded to the temperature of the molding during the casting process, which is normally between 350 °C and 400 °C.

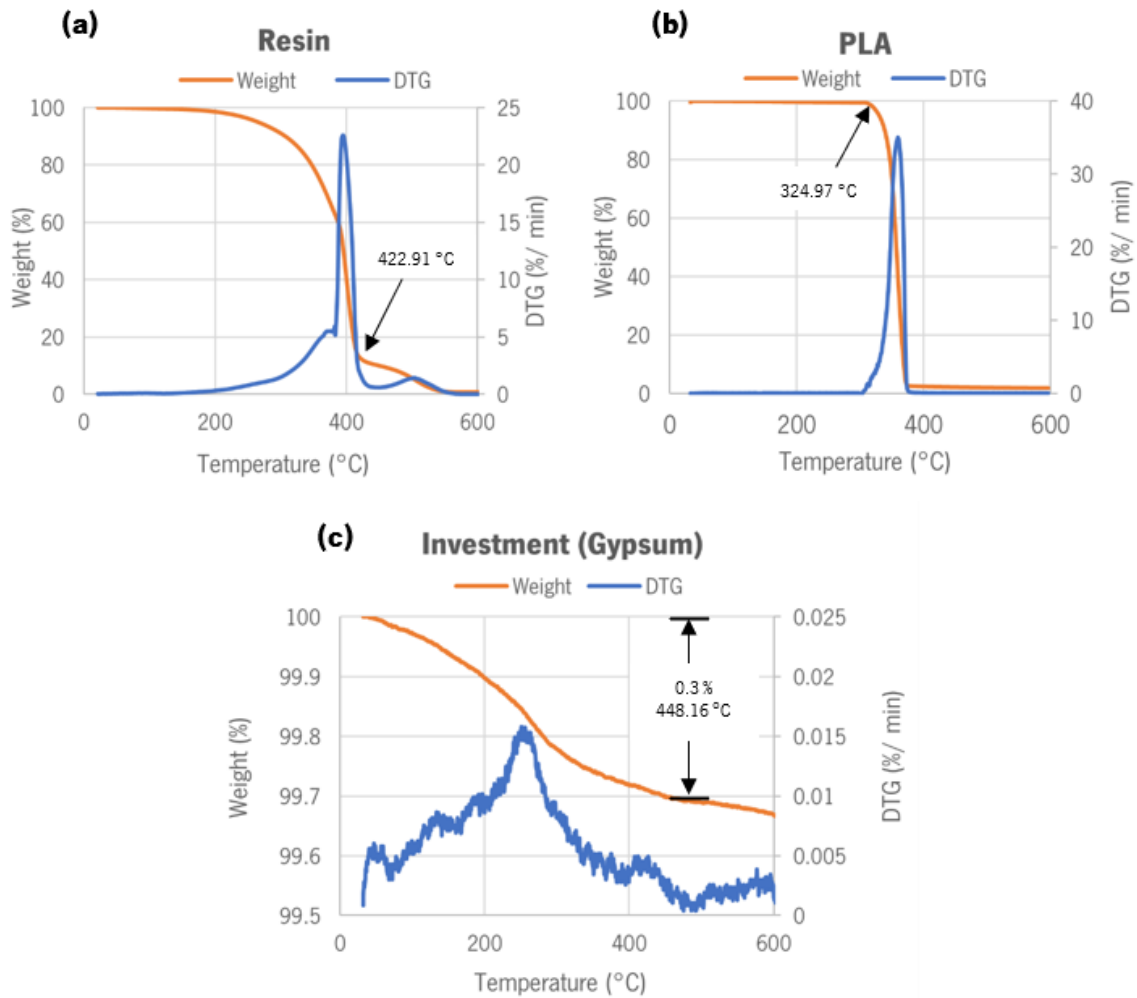


Figure 4.1: Weight loss and DTG: (a) resin; (b) PLA; and (c) plaster.

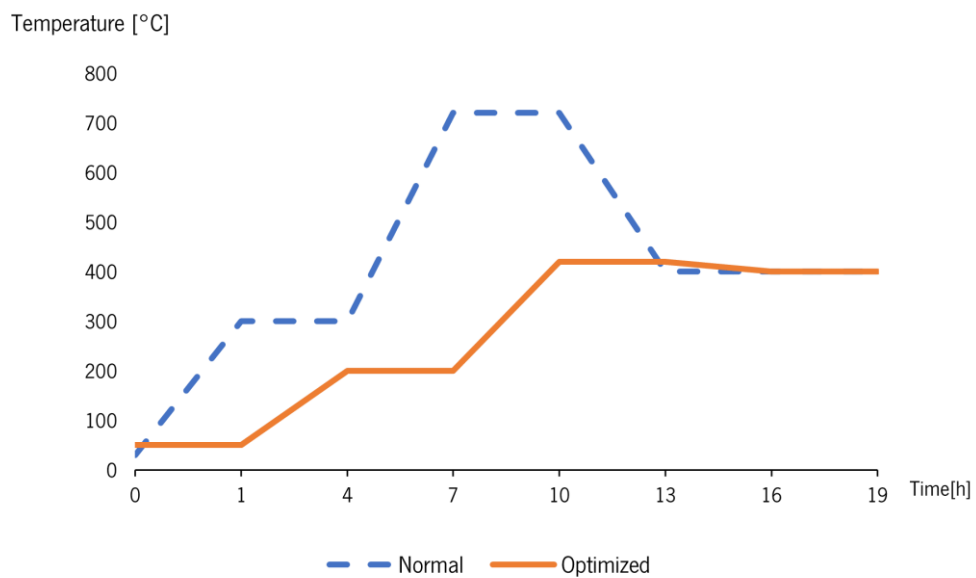


Figure 4.2: Thermal processing for curing the plaster moldings.

An experimental trial was carried out to better understand the influence of the thermal cycle optimization applied to the plaster moldings on the Yttria coating stability. For this, simplified geometry samples were used comprising different section thicknesses and coated with varying numbers of layers of Y_2O_3 . The moldings were cut according to Figure 4.3 after applying the thermal cycle for visual analysis. As shown in Figure 3.8, Yttria presents a significant degree of thermal instability when 720 °C is reached in the normal cycle, worsening as more layers are added. On the other hand, there was a significant difference in results when using the optimized thermal cycle. Despite the presence of some cracking in the Y_2O_3 layers, particularly when multiple layers are applied, the coating stability in this case improved. Using the optimized thermal cycle, where the maximum temperature reached is around 420 °C, Yttria adheres better to the molding walls and no parts are detaching from the outer coating layers into the cavities. Comparing both cases, different findings were also observed regarding coating thickness. By the use of a general thermal cycle, higher Yttria instability was observed for thicker coating layers, regardless of the number of layers applied. In contrast, when applying the optimized thermal cycle, it was not possible to establish a pattern of influence between the cavity thickness and the stability of the Y_2O_3 coating.

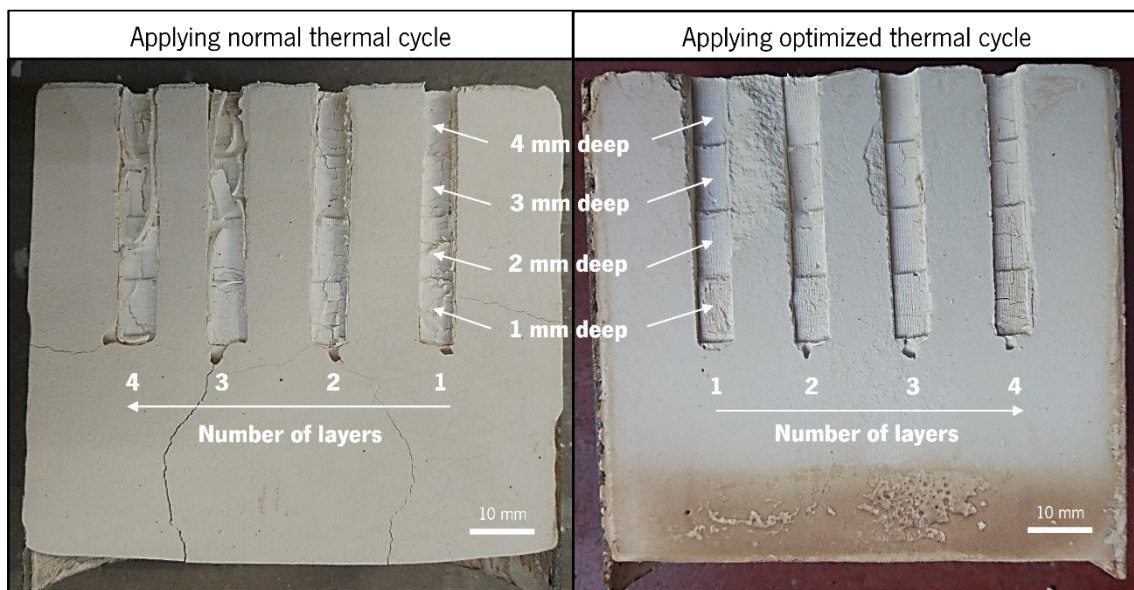


Figure 4.3: Application of both normal and optimized thermal cycles in plaster molding.

In this regard, and because the thermal cycle optimization applied to the plaster moldings arose as a result of the thermal instability of Yttria layers as a refractory between the liquid magnesium and the plaster from the molding walls, the optimized thermal cycle (Figure 4.2) can be included in the proposed methodology of this work when the use of Y_2O_3 coating is necessary.

4.2. Casting Parameters

After thermal treatment, the plaster moldings are put inside the furnace at the adequate pouring temperature. Additionally, a graphite crucible is placed and can contain up to 12 grams of the alloy to be used. Figure 4.4 shows the experimental setup of the induction furnace used in this study (already illustrated for case study 1 in Figure 3.10), with its main characteristics shown in Table 4.1.

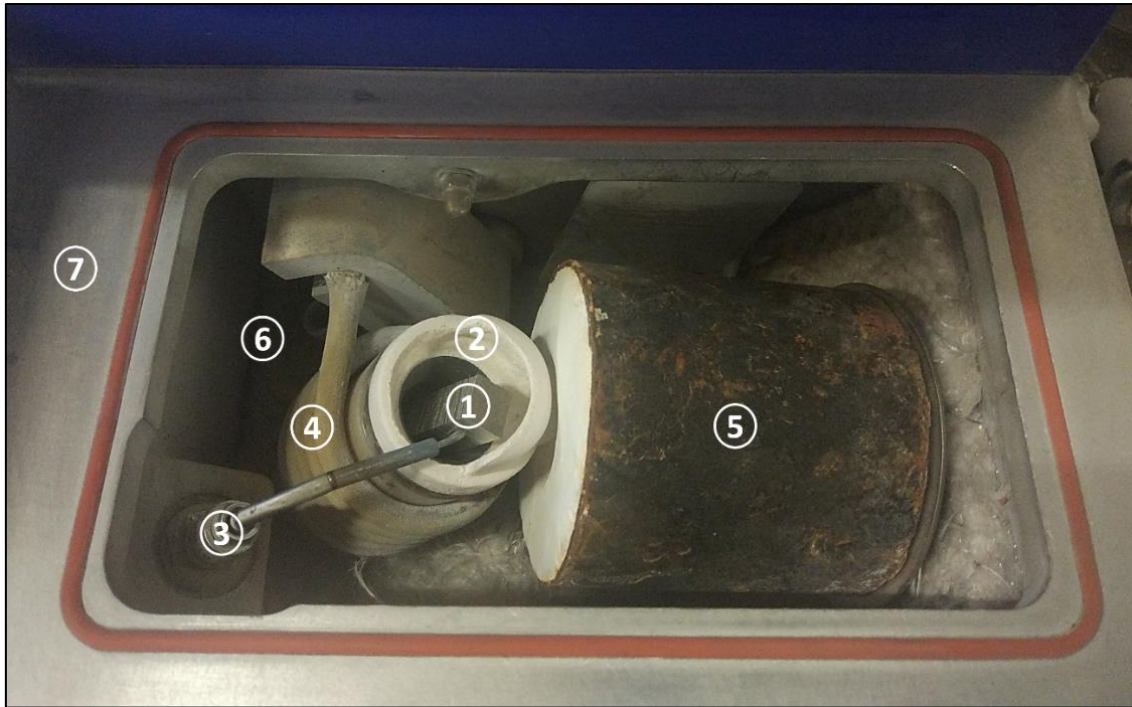


Figure 4.4: Induction furnace equipped with 1- 12 g of AZ91D-1 wt.% CaO, 2- crucible, 3- thermocouple, 4- induction coil, 5- plaster molding, 6- argon/vacuum atmosphere, and 7- external structure.

The magnesium alloy should be placed into the crucible in a single part in order to minimize the contact surface area of magnesium that can be susceptible to reactions. A melting charge is heated by induction in the used furnace (MC15+ from Indutherm). Inductive heating has the advantage of rapidly reaching melting temperatures due to direct heat transfer to the metal through a crucible with a graphite insert. The metal is thoroughly mixed by a magnetic field during the melting phase, ensuring homogeneous mixing. The magnesium alloy used in this study is AZ91D-1 wt.% CaO, as its composition is shown in Table 3.4. It has already been mentioned in Chapter 2 that the CaO addition turns this alloy into an Eco-Mg alloy, which is formed to avoid the use of SF_6 as a protective atmosphere. Thus, only argon is used as an inert element, overpressurized at 2 bar into the furnace when the metal is poured into the molding cavities to help the filling of the cavities.

Thereafter, and following a short period of metal solidification and cooling, the plaster molding is lowered into the water for demolding, and the resulting magnesium part is cleaned.

Table 4.1: Technical data of the experimental setup (according to the manual).

Parameters	Range
Crucible volume	10 cm ³ (with graphite inlay)
Crucible temperature	max. 2000 °C
Melting performance	3.5 kW
Main supply	230 V/ 16 A, 50 or 60 Hz
Cooling water supply	2.5 – 5 bar/min. 1.5 liter/minute
Cooling water recoil	Pressureless
Cooling water entry temperature	15 – 25 °C/59 – 77 °F
Ambient temperature	10 – 35 °C/50 – 95 °F
Relative atmospheric humidity	20 – 80 %
Weight	ca. 27 kg
Dimensions (width x depth x height)	400 x 400 x 450 mm

In subchapter 2.3, it is mentioned that the fluidity of liquid magnesium is greatly influenced by its pressure and temperature properties. These properties must be monitored to ensure successful magnesium castings, particularly for thin-walled applications. Several reference values were experimentally optimized in this study, as presented in Table 4.2, ensuring efficient and safe magnesium castings. However, it is important to note that the conditions are always dependent on the intended objectives for each casting, mainly pouring and molding temperatures. According to the literature review, pouring temperature has a greater effect on liquid metal fluidity and reaction propensity than molding temperature. Based on the defined safety values for both temperatures, there must be a compromise depending on the desired final magnesium part. Increasing the temperature results in greater fluidity and consequently greater cavity filling, but it also promotes the reaction of the liquid metals both with the surrounding atmosphere and with the molding walls. This will be discussed further in Chapter 5 for the manufacturing of stents in order to provide a better understanding of the effect of thermodynamic variables, namely pouring and molding temperatures.

Table 4.2: Optimal safe casting parameters (experimentally optimized).

Parameters	Range
Pouring temperature	660 – 720 °C
Molding temperature	350 – 450 °C
Protective Gas	Argon, 8 bar
Vacuum pressure	min. 8 m ³ /h, 0.1 mbar abs.
Pouring overpressure	2 bar
Melting time	150 s
Molding cooling time (inside furnace)	150 s
Molding cooling time (outside furnace)	7 min 30 s

The experimental setup is typically used to cast metal in the following manner: both the metal and molding are placed under full vacuum (melting), and the metal is poured into the molding cavities by tilting the entire chamber (pouring). Inside molding is also a vacuum atmosphere that guarantees a metal pouring without air counter pressure. During the pouring phase, the vacuum is rapidly replaced by argon overpressure, and the pressure impulse (the inside of the plaster molding is still under vacuum) will ensure a complete filling. The effect of vacuum in the molding and outside overpressure lasts for some time, long enough until the metal is already solid. An important feature of this system is the rapid creation of vacuum and the rapid build-up of pressure. It was spotted in Chapter 2 that the procedure of creating a vacuum atmosphere, followed by argon overpressure in this case, makes the process ideal for thin-walled castings, significantly aiding the cavity filling of most liquid metals. Nonetheless, due to the high reactivity of magnesium alloys, it is essential to determine the actual influence that vacuum pressure has on the entire system.

For these castings, a metallic molding was used with no pre-heating, and no protective coating is applied to the models. The cavity of the metallic molding corresponds to a cylindrical shape cavity with a diameter of 10 mm and 30 mm long. As described in the normal casting mode, the first casting (Figure 4.5a) was performed by vacuum melting and overpressure pouring with 2 bar argon. The second pouring (Figure 4.5b) was performed without vacuum, i.e., the metal was melted under ambient atmosphere and poured under argon overpressure of 2 bar. Then, the cylindrical pieces were removed from the moldings and cut for analysis and comparison, as shown in Figure 4.5.

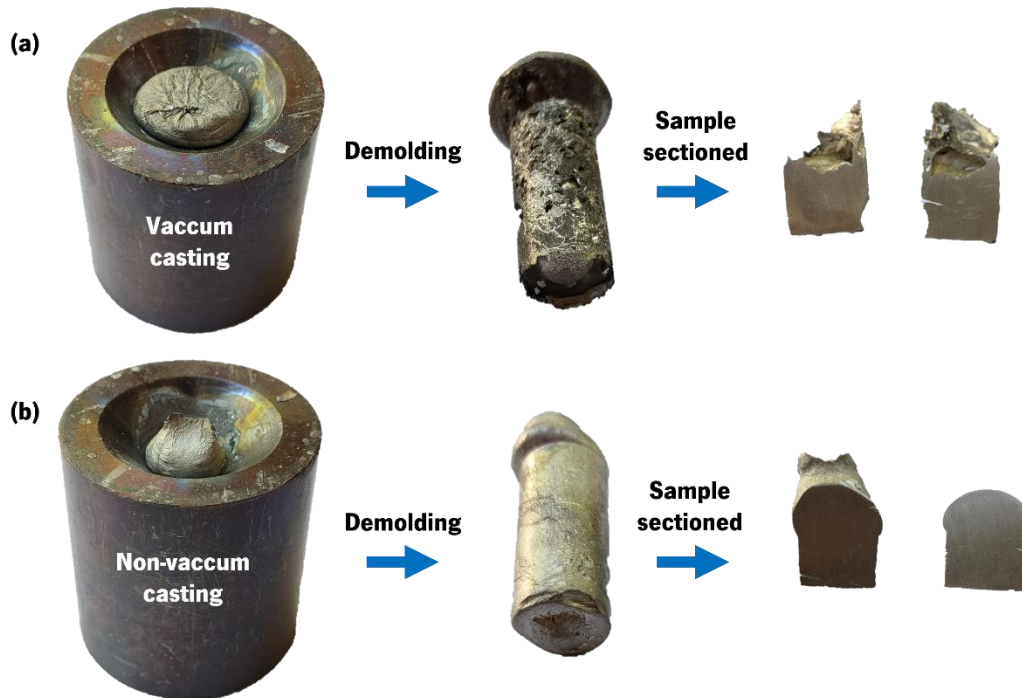


Figure 4.5: Magnesium investment casting in metallic molding: (a) vacuum casting and (b) non-vacuum casting.

An interesting and paradoxical result was obtained from this experiment. Although it seems counterintuitive, casting without the use of a vacuum atmosphere during the metal melting phase proved to be more beneficial than casting under negative pressure. A slightly darkened reacting zone was observed on the cast surface during vacuum casting. This phenomenon proves that reactions do not occur simply at the mold-metal interface as a consequence of the contact between the liquid magnesium and the silica from the plaster moldings. The reactions observed during the melting process suggest that the resultant oxidations can occur between magnesium and the surrounding environment. Since the mainly formed oxide - MgO - is characterized by white color, the formation of other reactions forming different reaction products, including carbon, can justify the black color on the casting's surface when using vacuum, as has already been reported by the scientific community in studies of Jafari *et al.* [103, 224]. The occurrence of Eq. 2.3 (see Table 3.6) can be used to justify a possible scenario during the melting phase, because of the direct interaction between the liquid magnesium and the atmospheric elements. Furthermore, the cavities are still under vacuum during the pouring phase, decreasing the surface tension of the metal and forcing it into the molding, which favors mold-metal adhesion. This phenomenon, together with the overpressure of argon, could cause turbulence in the metal pouring, causing air pockets to form, adversely affecting the pouring process and the surface quality of the metal. Casting without the

use of a vacuum atmosphere during the magnesium melting process, on the other hand, results in a cleaner melt, which presents no traces of reactions both during the melting and pouring phases and reveals a complete cavity filling.

There is limited literature on vacuum-assisted investment casting of magnesium alloys and even less information regarding thin-walled applications. Sin *et al.* [50] and Sin and Dube [114] have successfully produced thin-walled castings with a thickness of less than 2 mm, by improving the fluidity of the AZ91D magnesium alloy and ensuring a smooth surface finish. As demonstrated in case study 1 in Chapter 3 (using Yttria coating), it seems common sense to use vacuum pressure to improve cavity filling. According to the results from this study, using vacuum appears to be having a negative impact when applied to the AZ91D-1 wt.% CaO magnesium alloy in order to accentuate the interactions between the liquid magnesium and the surrounding atmosphere.

Figure 4.6 shows the microstructures of both samples in Figure 4.5. There seems to be a greater heterogeneity between the different phases in the sample in which the vacuum was used, as well as the formation of a finer microstructure of the matrix phase (α -Mg) and the intermetallic phase (β -Mg₁₇Al₁₂). Although the vacuum would improve the filling of the cavity, it would appear to accelerate metal solidification. It can be explained by the continuous pressure impulse created in the furnace atmosphere, which induces a more abrupt contact of the liquid magnesium with the molding walls.

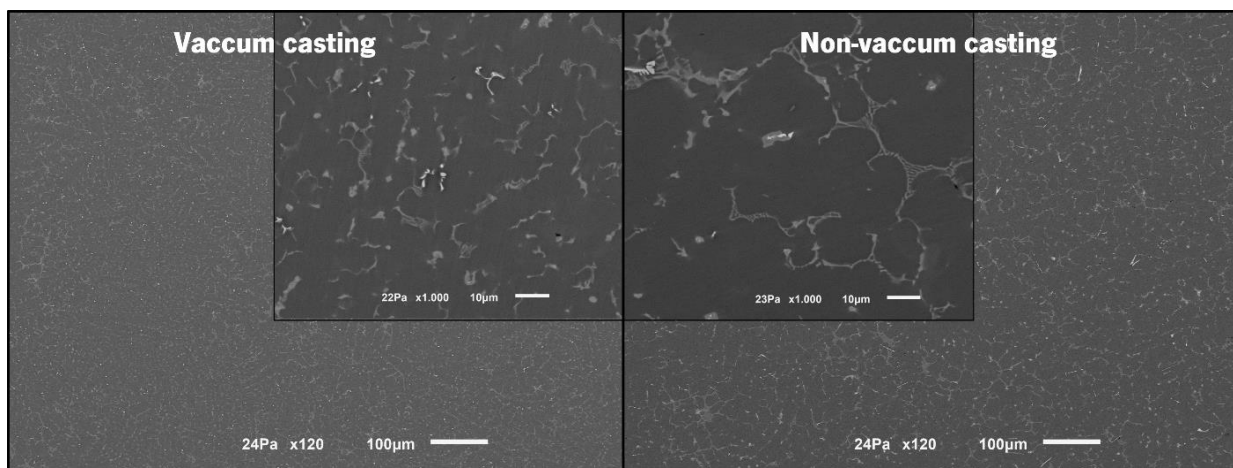


Figure 4.6: Microstructures of the vacuum and non-vacuum cast samples in Figure 4.5.

The effect of vacuum during the melting phase was also evaluated for stents' investment casting in plaster moldings, applying Yttria coating to the polymeric models for safety. The characteristics described in Table 4.2 were used for both castings, using pouring temperature of

720 °C and a temperature of 400 °C for molding plaster in order to enhance the filling. Two Y_2O_3 layers were applied to the models. The obtained results from these castings, as shown in Figure 4.7, agree with the previous magnesium experiments. It is quite visible that magnesium reactions were observed only in vacuum casting. Since Yttria was used as a protective coating at the mold-metal interface, the reactions observed in Casting I seemed to result from reactions beginning in the melting phase of metal and being accelerated by the vacuum atmosphere. Despite complete filling in this casting, the surface roughness of the stent was affected by the reactions, which resulted in the formation of a small dark layer over the most magnesium-surface area. There was a distinct scenario observed in Casting II, where no serious reactions seem to occur between the metal and the surrounding atmosphere during the melting process. However, even though the Yttria coating may have slightly increased the metal surface roughness, as described in case study 1 of Chapter 3, a complete cavity filling was achieved, which could be attributed to the high temperatures involved.

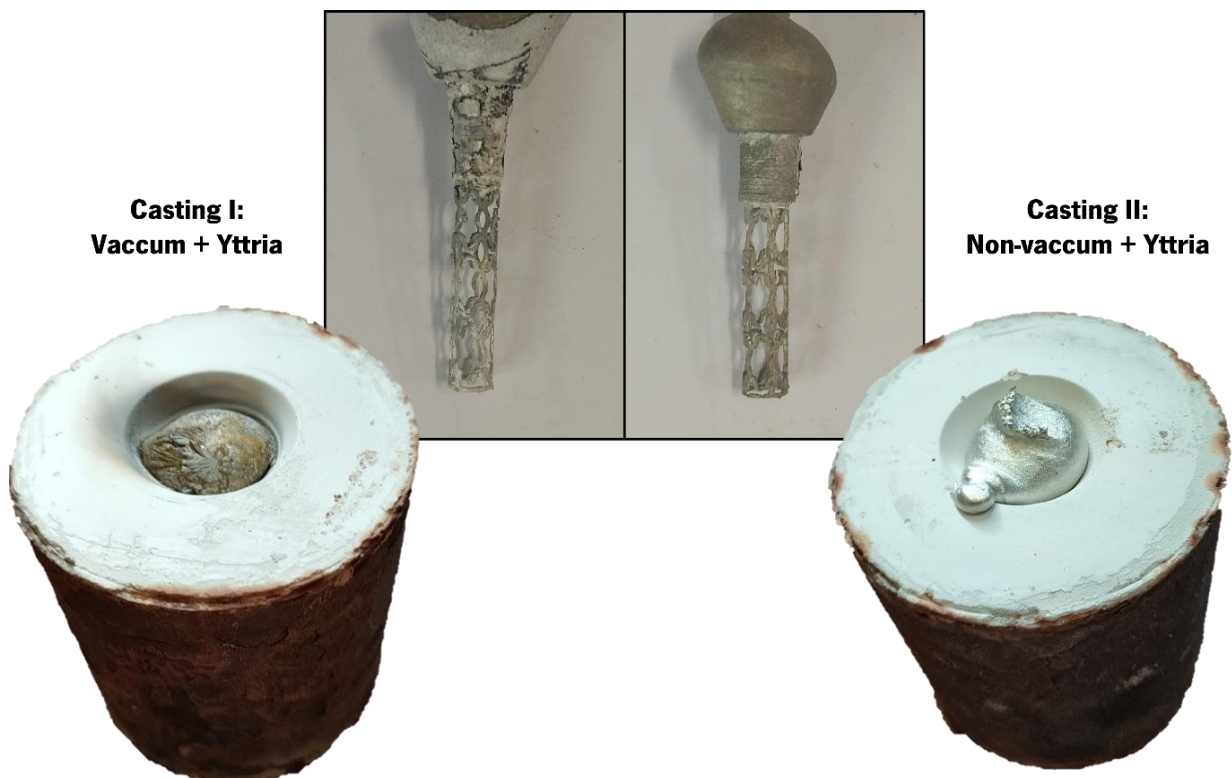


Figure 4.7: Mg stent investment casting in plaster molding of vacuum and non-vacuum castings.

The visual analysis of these obtained castings shows that the use of vacuum to assist investment casting of the AZ91D-1 wt.% CaO magnesium alloy has a negative impact on the quality of castings because of severe reactions between the liquid magnesium and the furnace

environment. As a result, a fluidity study on molten magnesium alloy was made and presented in the following chapter to examine the impact of some casting variables on the reaction rate that may occur and the filling length and quality of the final castings.

4.3. Case Study 2 – Enhancement of AZ91D-1 wt.% CaO Magnesium Alloy Fluidity in Thin-walled Investment Casting

4.3.1. Experimental procedure

To study the fluidity in thin-walled investment casting, the same experimental setup applied in case study 1 to investigate the mold-metal interface was used (Figure 2.6), applying the proposed methodology and adopting all process optimizations carried out so far. Hence, the process was based on five steps: (i) modeling of 3D CAD models; (ii) 3D printing and assembly; (iii) coating the models; (iv) preparation of the plaster moldings; (v) casting of the AZ91D-1 wt.% CaO magnesium alloy under different casting conditions.

Fluidity can be defined empirically as the ability of the molten metal to flow through and fill a molding cavity [118]. In Chapter 2, it is noted that this particular property is not one single physical characteristic. It is a complex attribute that is dependent not only on the composition of the molten alloy, casting parameters, and molding properties, but also on the testing method [114]. There is no universal test to measure the liquid metal fluidity, although several experiments have been developed to quantify this property [112-114, 118]. In the present case study, magnesium alloy fluidity was evaluated using the filling length capacity of the metal into the cavities of the plaster molding. Since these plaster moldings had a limited volume (80 x 80 mm² - see Figure 4.4), the model used for the fluidity tests consisted of a spiral specimen, as depicted in Figure 4.8. Based on the processing method, the influence of different variables presented in Table 4.3 were investigated.

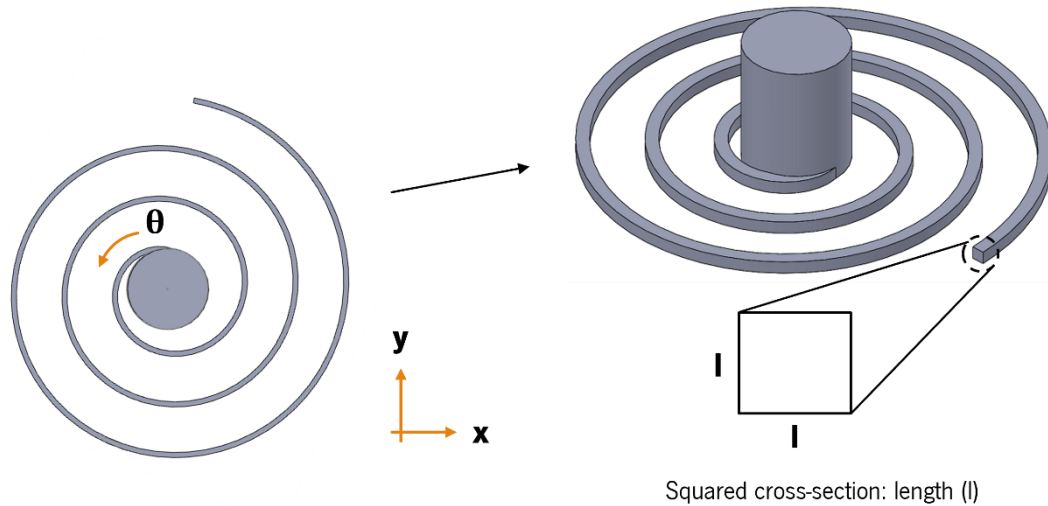


Figure 4.8: Spiral specimen for fluidity testing.

Table 4.3: The main variables and values used in evaluating fluidity.

	Value
Length of the squared cross-section, <i>l</i>	0.50 mm
	0.75 mm
	1.00 mm
	1.50 mm
Casting parameter	Condition N: No Yttria coating and no vacuum
	Condition Y: Yttria coating and no vacuum
	Condition YV: Yttria coating and vacuum
Pouring temperature	660 °C
	720 °C
Protective Gas	Argon, 8 bar
Vacuum pressure	min. 8 m ³ /h, 0.1 mbar abs.
Pouring overpressure	2 bar
Total: 24 castings	

Based on the model specimen, represented in Figure 4.8, the spiral path trajectory can be defined in the cartesian reference system through the following parametric equations:

$$x = R(\theta) \cdot \sin \theta \quad \text{Eq. 4.1}$$

$$y = R(\theta) \cdot \cos \theta \quad \text{Eq. 4.2}$$

where θ is the angular parameter along the spiral (measured by image analysis) and $R(\theta)$ denotes the radius of the spiral in position θ , which can be obtained by:

$$R(\theta) = R_0 + \frac{p}{2\pi} \cdot \theta \quad \text{Eq. 4.3}$$

in which R_0 corresponds to the initial radius of the spiral center, set to 4 mm, and p represents the spiral pitch, set to 5 mm. Thus, the filling length can be calculated through the integration of the arc length of the spiral path with respect to θ as follows:

$$L(\theta) = \int_0^\theta \sqrt{\frac{dx^2}{d\theta} + \frac{dy^2}{d\theta}} d\theta \quad \text{Eq. 4.4}$$

As integration of Eqs. 4.1-4.3 into Eq. 4.4, and solving the corresponding integral, the final filling length expression is given by:

$$L = \frac{\frac{p}{2\pi} \ln\left(\frac{p}{2\pi} \sqrt{\left(\frac{p}{2\pi}\theta + R_0\right)^2 + \left(\frac{p}{2\pi}\right)^2} + \frac{p}{2\pi}\left(\frac{p}{2\pi}\theta + R_0\right)\right)}{2} + \frac{\left(\frac{p}{2\pi}\theta + R_0\right) \sqrt{\frac{\left(\frac{p}{2\pi}\theta + R_0\right)^2}{\left(\frac{p}{2\pi}\right)^2} + 1}}{2} \quad \text{Eq. 4.5}$$

The initial models were made using additive manufacturing following the proposed methodology, based on FDM technology for each side length. After printing, only the models related to the **Y** and **YV** conditions were coated with two Yttria layers (according to the optimized procedures in Chapter 3), followed by the plaster molding fabrication. The Y_2O_3 coating application was reduced to two layers in order to reduce the cracking content. Since Yttria was used to coat most of the models, the optimized thermal cycle (Figure 4.2) was applied for plaster molding treatment. Regarding the casting parameters described in Table 4.2, the pouring temperature varies at the safe extremes, as indicated in Table 4.3. The same experimental setup, illustrated in Figure 4.4, was employed for melting 10 g of AZ91D-1 wt.% CaO (Table 3.4) in a SiC crucible for each casting. A total of 72 spiral castings were poured. For reproducibility purposes, three castings were performed for each condition. After pouring and demolding procedures, the measurement of the spiral angle was made.

4.3.2. Results and Discussion

Figure 4.9 displays the samples obtained for all performed castings according to variables: casting condition, pouring temperature, and edge length of the squared cross-section. For each casting, the spiral angle, θ , was measured using image analysis software (*ImageJ*), as described step by step in Figure 4.10. Considering a maximum angle of 952.5° for a total spiral length of 177 mm, which corresponds to 100 % filling, the final calculated results are presented in Table 4.4. The **0.5N660** sample, for instance, corresponds to the casting in which the model has a side

length of 0.5 mm, poured at 660 °C without the use of a model's coating and vacuum during the melting process (condition **N**). The process's reliability and the achievement of successful castings depend a lot on strict compliance with all the involved variables to reduce the effects of the user's handling sensitivity.

	Condition N		Condition Y		Condition YV	
0.5						
0.75						
1						
1.5						
	660	720	660	720	660	720

Figure 4.9: Experimental casting samples resulting from fluidity studies.

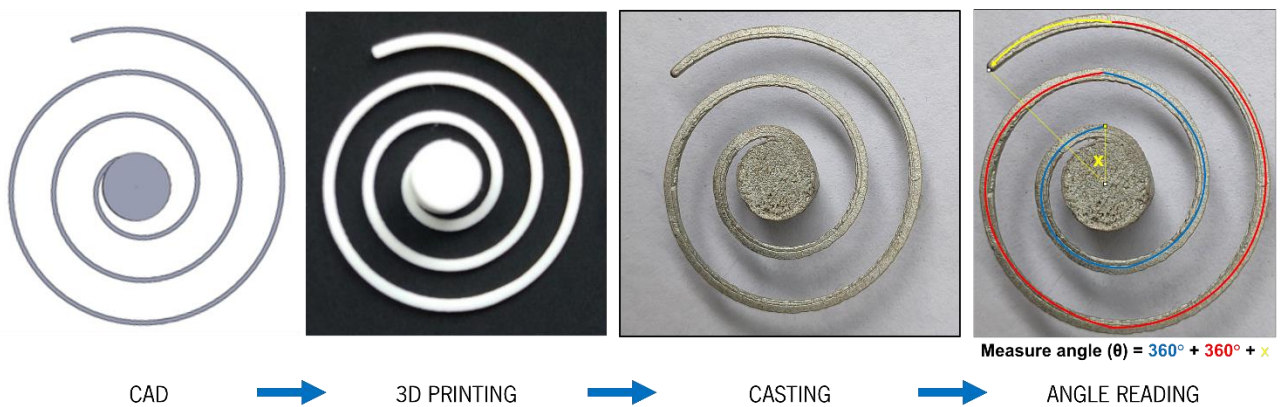


Figure 4.10: Steps for spirals' angle measurement.

Table 4.4: Calculated values from the experimental fluidity study.

Sample	Measured angle - Trial 1 (°)	Measured angle - Trial 2 (°)	Measured angle - Trial 3 (°)	Measured angle - average (°)	Filling length (mm)	Filling length percentage (%)
0.5N660	281.7	277.1	291.5	283.4	29.8	16.8
0.5N720	292.5	293.3	302.0	295.9	31.6	17.8
0.5Y660	277.3	269.2	293.2	279.9	29.3	16.6
0.5Y720	337.2	332.1	311.1	326.8	36.1	20.4
0.5YV660	403.5	417.2	391.9	404.2	48.4	27.3
0.5YV720	526.4	489.4	509.7	508.5	67.2	38.0
0.75N660	354.0	346.7	362.4	354.4	40.3	22.8
0.75N720	660.7	658.9	649.2	656.3	98.5	55.6
0.75Y660	184.0	169.1	183.6	178.9	16.6	9.4
0.75Y720	531.0	502.5	497.9	510.5	67.6	38.2
0.75YV660	484.0	483.7	460.3	476.0	61.1	34.5
0.75YV720	528.8	532.5	544.5	535.3	72.5	41.0
1N660	769.4	778.2	752.2	766.6	125.3	70.8
1N720	945.0	952.5	941.2	946.2	175.2	99.0
1Y660	285.5	296.5	320.3	300.8	32.2	18.2
1Y720	558.4	565.7	531.4	551.8	75.9	42.8
1YV660	476.8	457.0	433.1	455.6	57.3	32.4
1YV720	767.1	790.5	778.4	778.7	128.4	72.5
1.5N660	952.5	952.5	952.5	952.5	177.0	100.0
1.5N720	952.5	952.5	952.5	952.5	177.0	100.0
1.5Y660	691.7	683.6	714.3	696.5	107.9	61.0
1.5Y720	577.2	597.1	614.1	596.2	85.1	48.1
1.5YV660	942.7	927.5	916.3	928.8	170.0	96.0
1.5YV720	728.8	726.0	710.3	721.7	114.0	64.4

From the visual assessment of castings (Figure 4.9), some trends were noticeable, confirmed by the calculated values presented in Table 4.4. Overall, and as expected, it was evident that a longer filling length was achieved with an increase in the size of the squared cross-section and the pouring temperature, apart from a few exceptions. The obvious difference between the resulting metal reactions between the different casting conditions was also evident from visual observation, which corroborated the obtained results, discussed earlier in this chapter. The cast samples produced from condition **N**, in which protective coatings and vacuum atmospheres were not employed, resulted in clean metal parts with good dimensional accuracy and finish surface. When only a protective coating was applied to the initial models (condition **Y**), although it effectively prevented the liquid magnesium reactions, the dimensional accuracy and finish surface were affected, resulting in a worsened final quality of the castings. As discussed in case study 1 of Chapter 3, this phenomenon is caused by the deterioration of Ytria layers due to thermal instability.

Although the optimization of the thermal cycle (Figure 4.2) applied to the plaster moldings improves the stability of the Y_2O_3 layers and permits the mitigation of mold-metal reactions, there is still a slight degree of cracking, visible through the visual assessment of the castings' surface roughness. Moreover, the cracking of the outer layers of Yttria acts as a barrier to the metal's fluidity, thus reducing its filling length. As a final observation, contrary to the previous conditions, the obtained castings revealed the occurrence of reactions in the samples when the vacuum was applied during magnesium melting, even with Yttria as a refractory coating (condition **YV**). In these samples, the molten metal exhibited a black color in the superficial and middle zones of the spiral, due to the liquid remaining for a long time, leading to a longer reaction time with the plaster molding walls. Even though the Y_2O_3 coating is essential to the castings' success, it prevents strong exothermic reactions that are destructive to the process. Furthermore, these results suggest that vacuum assistance is an important factor in enhancing liquid magnesium reactions with the surrounding elements. Despite this, there was a higher percentage of cavity filling for shorter side length samples in the castings for condition **YV**, indicating that the vacuum resource effectively improves cavity filling for thin-walled samples.

The values presented in Table 4.4 were treated and graphically illustrated in the following figures for better perception and quantification of the obtained results. According to the increasing percentage of filling length for all the samples in Figure 4.11, it is easy to see that the samples with an edge of 1 mm and 1.5 mm long exhibited the highest percent of cavity filling as compared to the samples with a side length of 0.5 mm and 0.75 mm. Furthermore, only two samples were obtained with complete cavity filling: **1.5N660** and **1.5N720**. This fact is particularly noteworthy since it indicates the total effectiveness of the process in preventing reactions without requiring the use of protective coatings and vacuum protection. This is in opposition to current scientific knowledge regarding the effect of vacuum in reducing the Mg reactions. Figure 4.11 also demonstrates that the models with a lower percentage of cavity filling corresponded to the samples for condition **Y**. This highlights the Yttria obstruction of the magnesium pouring into the molding cavities. With respect to the obtained standard deviations, corresponding to three castings per sample, the registered values suggest no significant variation between samples, ensuring good casting repeatability. Despite that, it is evident that higher standard deviations are achieved in conditions **Y** and **YV**, which involve more uncontrollable variables due to the use of Yttria and vacuum.

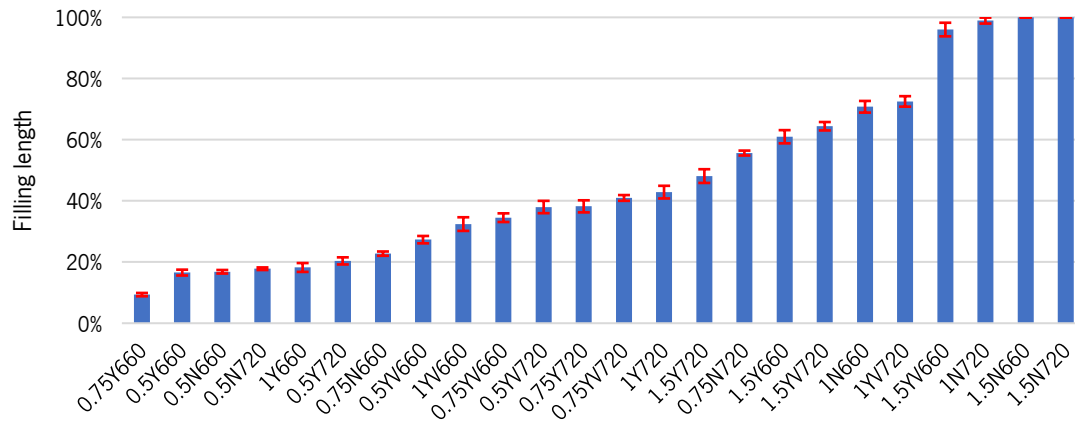


Figure 4.11: Filling length percentage for all samples obtained.

Figure 4.12 presents the results as a function of the edge of the squared cross-section and the casting conditions for the samples. It seems evident that the highest percentage of filling length was obtained in the spirals with the highest thickness and temperature for castings following the condition **N**. Indeed, this was the only case where the cavity filling followed an increasing orientation with increasing thickness and temperature. The obtained results were distinct in condition **Y**, and the lowest cavity filling percentages were achieved for almost all samples except for **0.75Y720** and **1Y720**. In addition, for this condition, the negative influence of the Y_2O_3 coating on the flow of liquid magnesium into the cavities was observed, being particularly evident for the **1.5Y720** sample.

There are two important pieces of evidence to highlight regarding the condition **YV**. In the first place, the vacuum effect appeared to significantly impact the cavity filling of thin-walled magnesium geometries, which allowed for an optimal filling rate for samples with a thickness of 0.5 mm at both temperatures studied. Secondly, the obtained value of 64.40 % filling for the **1.5YV720** sample, which is lower than the same condition at 660 °C, suggests a detrimental effect when the vacuum is used to assist higher thickness and temperature samples. Overall, considering the same casting condition, only three samples (marked in Figure 4.12 by the blue arrow) did not verify the tendency to rise the cavity filling with the increasing square cross-section. This occurred for conditions **Y** and **YV**, again related to the influence of Ytria coating and vacuum assistance.

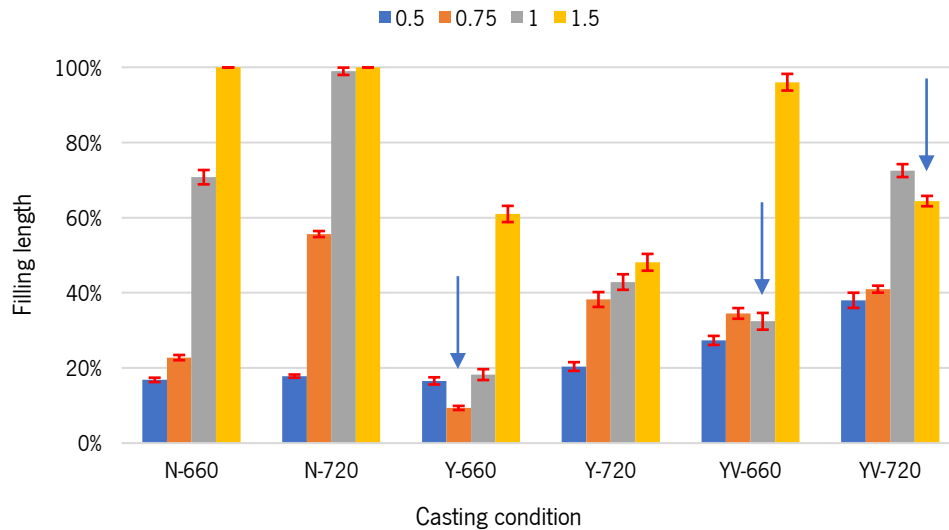


Figure 4.12: Filling length comparison between the different sizes of the squared cross-sections.

Additional statements can be traced from the obtained results when observing the cavity filling percentage concerning the temperatures used. In Chapter 2, it was mentioned that temperature is an essential factor affecting the fluidity of the liquid metal, inducing greater fluidity at higher temperatures. According to Figure 4.13, this fact was proven for most samples in this case study, although there was one point of inversion of the trend. With larger cross-sectional area spirals, the increase in temperature appears to have a negative effect on the filling length, which is particularly evident for condition **YV**. It can be explained by the action of the vacuum pressure, which seemed to enhance the mold-metal reactions, blocking the flow and decreasing the fluidity of the liquid magnesium. In these cases, the greater the sample thickness, the longer the mold-metal contact and the greater the rate of reaction.

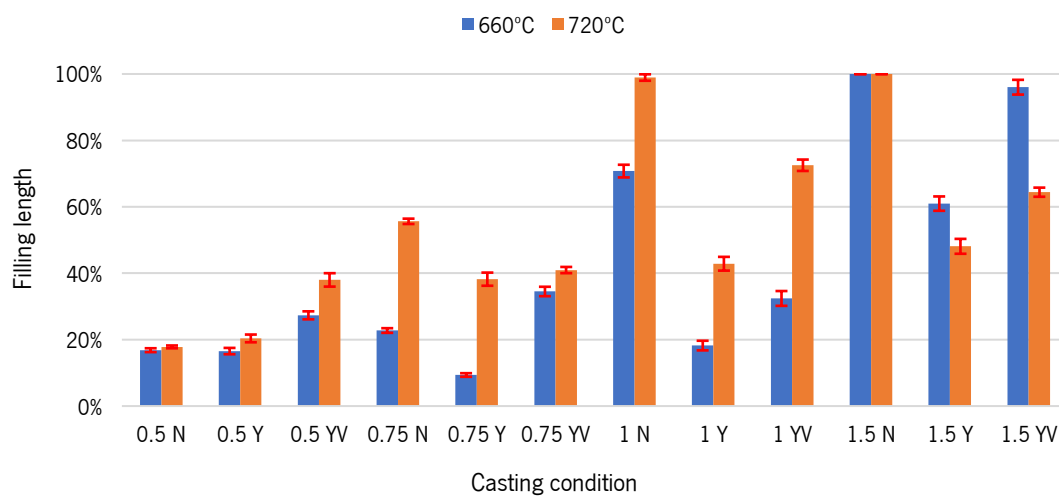


Figure 4.13: Filling length comparison between both temperatures.

Figure 4.14 illustrates the compilation of results for each casting condition. Here, it is also noticeable that higher filling length is achieved for thicker samples using condition **N**, and for thinner samples using condition **YV**. Additionally, the temperature increase only affects the cavity filling when Yttria and vacuum are used for thicker samples. Otherwise, there is a visible increase in cavity filling. As a final note, it must be noted once again the lower filling length percentages obtained in condition **Y**, which seems to be little affected by temperature variation.

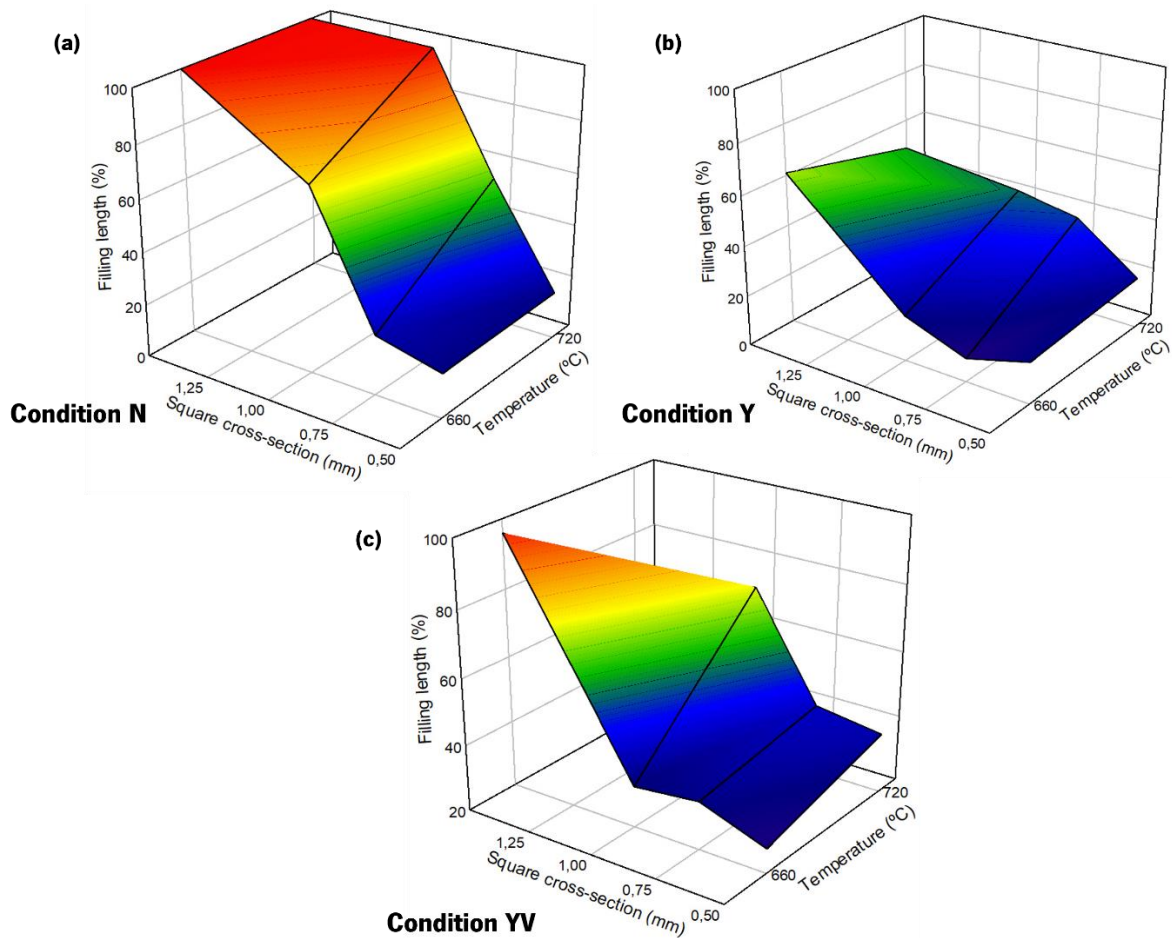


Figure 4.14: Filling length comparison between casting conditions: (a) condition N; (b) condition Y, and (c) condition YV.

To further analyze the different casting conditions and their influence on the filling length, an μ CT (X-ray Micro-computed Tomography) was conducted in order to validate the obtained results. The Bruker SkyScan 1275 (Bruker, Kontich, Belgium) used is an automated desktop laboratory system with an X-ray beam with peak energy from 20 kV to 100 kV, 10 W of the maximum power, small X-ray spot size ($>55 \mu\text{m}$), along with multiple filter options (aluminum and copper filters). The X-ray detector of this μ CT scanner is a 3 MP (1944 x 1536 pixels) active pixel CMOS flat-panel [225]. This equipment is composed of an X-ray source, a motor-controlled rotating

stage, and a detector. The specimen is mounted between the X-ray source and the detector panel, in the rotating stage. The radiation emitted by the X-ray source passes across the specimen and is projected on a digital detector, measuring the attenuation of the X-rays and producing a radiograph (known as 2D scanned or projection image). During acquisition, the object rotates over 180° or 360° with a fixed rotation step defined by the operator. At each angular position, a 2D scanned image is acquired. The sequentially acquired projection images are then processed using computer software, producing a series of reconstructed images (2D slices) that allow observing the object's internal structure. The reconstructed μ CT images can be used for volume rendering of tomographic data, creating 3D models using numerous available software tools (for example, CTAn, CTvox, CTVol, VGStudio) [226]. Image optimization comprises adjusting several μ CT parameters such as the magnification, the incident X-ray intensity, the filter type (e.g., no filter, copper, or aluminum), the rotation step and the acquisition time, and the threshold.

Through the 2D acquired projection images of the spirals with 1.5 mm of the squared cross-section regarding all casting conditions, as shown in Figure 4.15, both samples' good casting quality is notorious for condition **N** (Figures 4.15a and 4.15b), as mentioned early. Additionally, the appearance of a 'cracking husk' is noticed around the spiral specimens for the condition **Y** samples (Figures 4.15b and 4.15c) and condition **YV** samples (Figures 4.15e and 4.15f). It can be explained by the Y_2O_3 layers cracking, which, when detached from the molding walls, allow the liquid magnesium to penetrate through its interstices. This creates an outer Yttria shell that aggregates to the metal and is not naturally removed during demolding. As already mentioned in this work, this phenomenon can block the metal and affect the cavity filling, which may explain the results obtained in this case study. In addition, it appears that the formation of this Yttria "cracking husk" seems to be more evident in samples poured at 720 °C due to the greater fluidity of the liquid metal, and the latter samples for condition **YV** due to the vacuum effect.

The 3D models of the Yttria 'cracking husks' formed around metallic spirals can be created through a 3D analysis software (Avizo) by μ CT images reconstruction and observed separately due to the density difference between materials. In Figure 4.16, it is illustrated a higher magnification of the Yttria 3D models for **1.5Y660** and **1.5YV720** samples, demonstrating the existence of cracks in the Y_2O_3 coating. Comparing both samples, it is observed that the amount of aggregation to the metal is greater for condition **YV720**, demonstrating a direct correlation between the increase in pouring temperature and the use of vacuum with the greater penetration of the liquid metal into the coating interstices. A further consequence of the degradation of the Y_2O_3 coating

layer is the increased diffusion of elements at the mold-metal interface, which results in forming a reaction layer in the peripheral zone of the sample, as shown in Figure 4.17 (analysis SEM **1.5YV720** condition). The longer the cooling time, the greater the diffusion rate of elements and, consequently, the greater the formation of reaction layers. In conjunction with the vacuum effect, this phenomenon is responsible for the higher rate of surface reactions occurring in samples of condition **YV**.

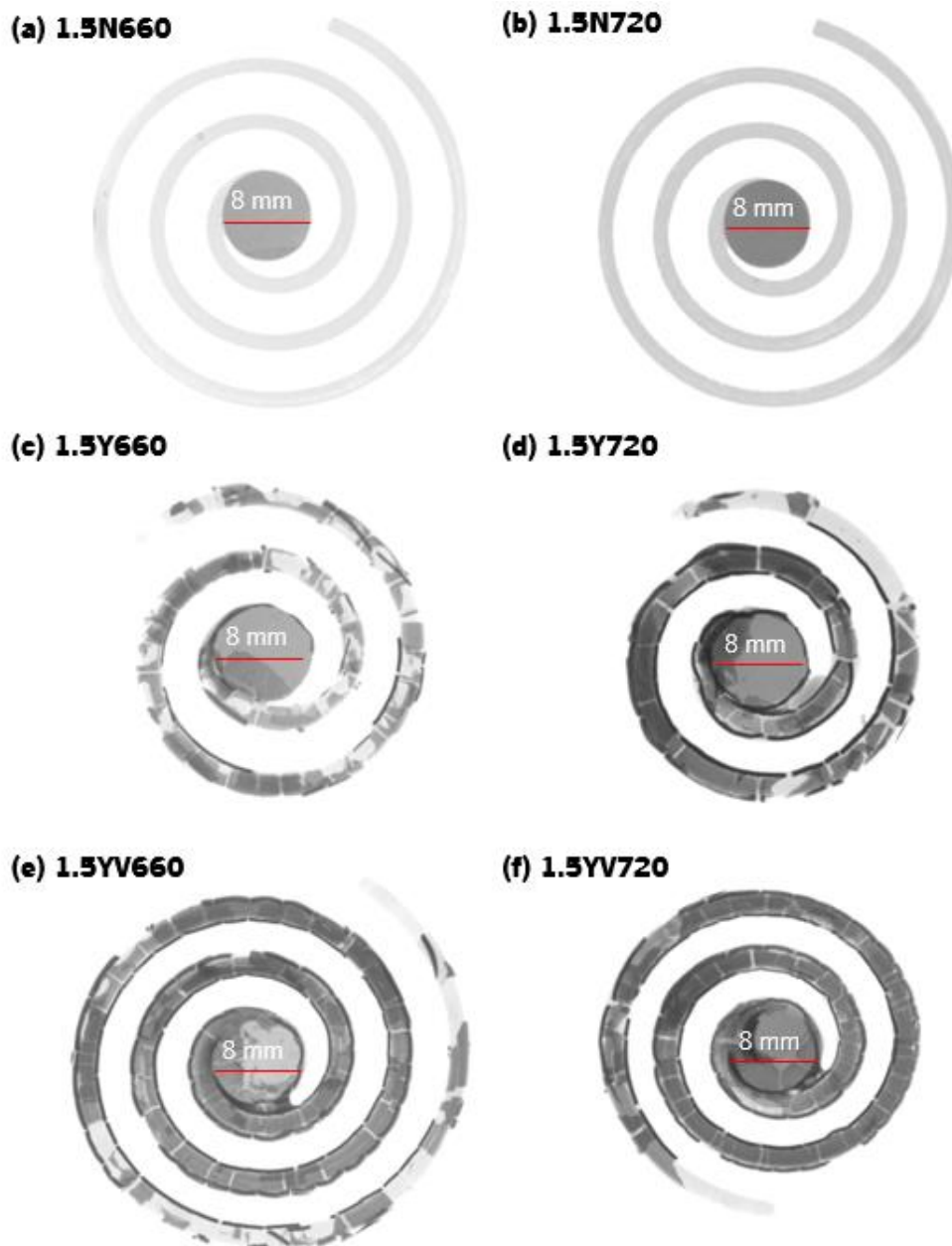


Figure 4.15: 2D μ CT images of the samples with 1.5 mm of thickness: (a) N660; (b) N720; (c) Y660; (d) Y720; (e) YV660, and (f) YV720.

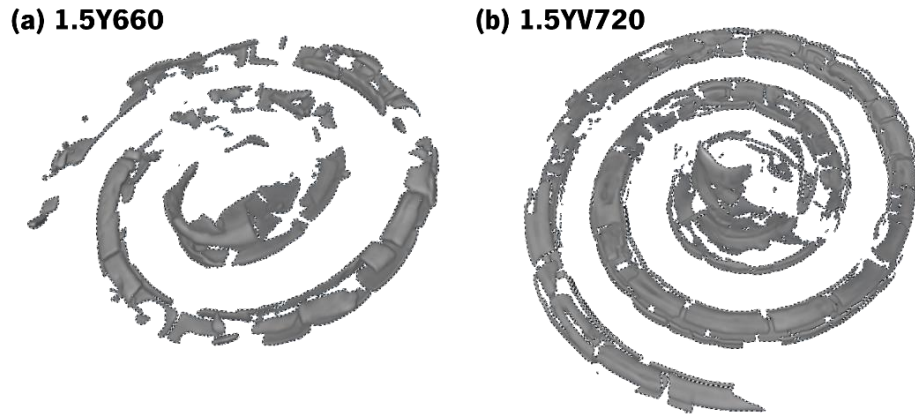


Figure 4.16: 3D μ CT models of the Yttria 'cracking husks' for samples: (a) 1.5Y660 and (b) 1.5YV720.

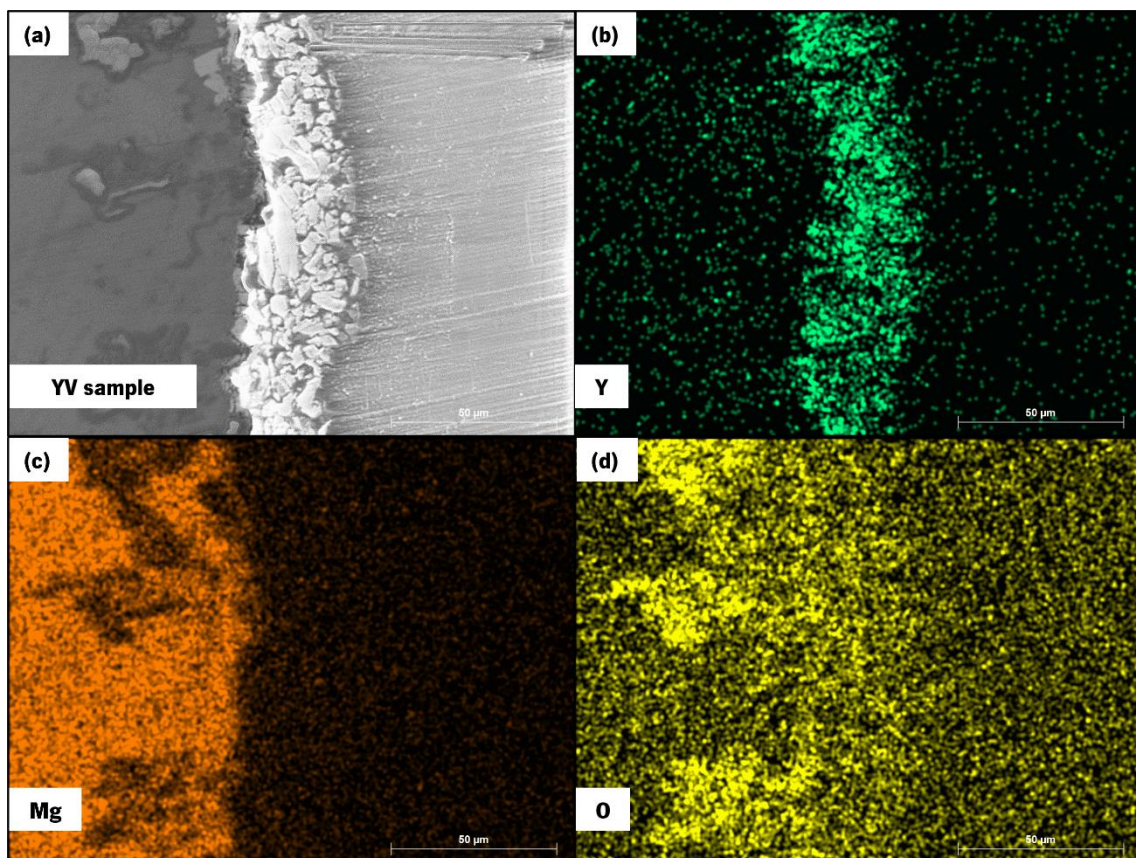


Figure 4.17: SEM analysis of the mold-metal interface of sample 1.5YV720: (a) backscattered FESEM image, and EDS elemental mapping of the element (b) Y, (c) Mg, and (d) O.

4.4. Influence of Casting Variables

DoE (Design of Experiments) is a relevant methodology applied to quantify effects, understand interactions between variables, model relationships, and measure experimental errors to obtain unambiguous answers to specific research questions, at minimum cost [227]. It has been

used in industry to enhance process performance, improve process yield, and decrease process variability [228]. Applying to this work, this methodology consists of the definition of the quality characteristics, the parameter that it intends to optimize, and the control factors and levels. The experiments were conducted based on a matrix of experiments, which comprised the total number of factors and levels. Based on the statistical analysis of the results, the average performance was computed, and an ANOVA (Analysis of Variance) was performed to determine the contribution of each factor on quality characteristics, which in this case consists of the filling length percentage, given by the obtained experimental data in case study 2 of the previous subchapter.

Considering that this analysis aims to study the influence of several process parameters on the cavity filling efficiency, the filling length was considered the quality characteristic to be optimized. As presented and discussed in Chapter 2, it is known that several factors have a significant influence on the magnesium alloy fluidity, and consequently on the filling length. However, the analysis of each parameter is too costly, due to the high number of possible combinations, considering that each factor has two or more levels. In that sense, the control factors selection consists of the ones known to have a significant effect on fluidity, which is in accordance with the filling optimization. So, the factors and levels selected in this study correspond to the studied variables, such as length of the squared cross-section, temperature, and casting condition (Table 4.3). In addition, the DoF (Degrees of Freedom) of each factor were also included, which correspond to the number of levels minus one. Regarding the factors and levels, and since there are non-numeric variables in this study, the matrix of experiments was designed (Table 4.5) considering all combinations, which correspond to the total defined samples. Thus, the values of the filling length for all angles' measurements, calculated and presented in Table 4.4, were used for this data analysis.

Table 4.5: Selected factors and their levels.

Control Factor	Level				DoF
	1	2	3	4	
Length of the squared cross-section, / (Factor A)	0.50	0.75	1.00	1.50	3
Temperature (Factor B)	660	720	-	-	1
Casting condition (Factor C)	N	Y	YV	-	2

To analyze the response of the quality characteristic to the variation of levels for each factor, the average performance of each factor was computed and presented in Figure 4.18. The data analysis was conducted using Minitab™ software.

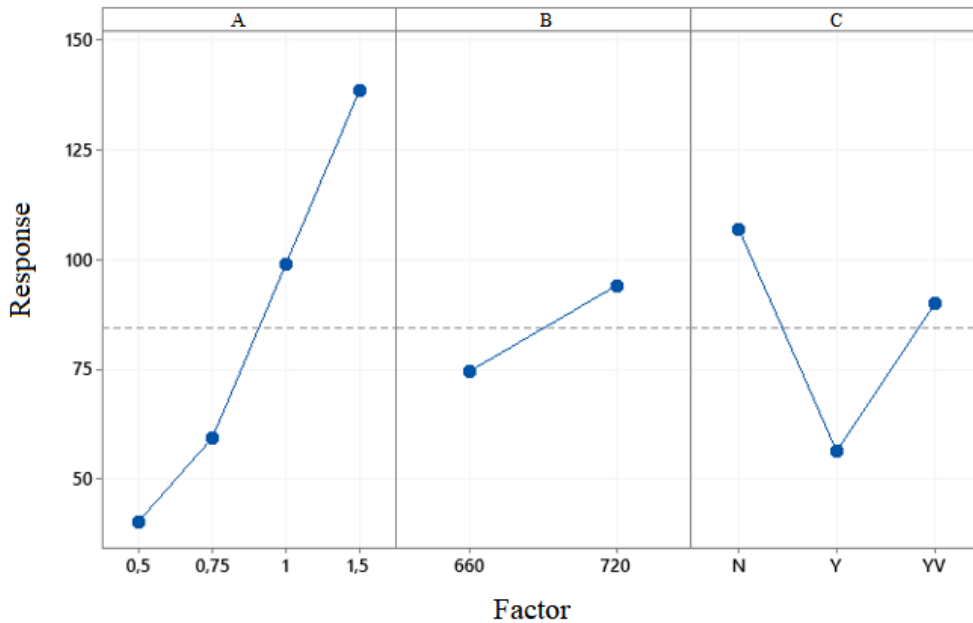


Figure 4.18: Response of the filling length to the variation of the factors.

Figure 4.18 shows that the higher the slope, the more influential is the factor. Thus, considering the filling length values obtained in this experiment, the graph shows that the side length of the cross-section (**Factor A**) seemed to be the most influential factor for the variance of final results, being the condition casting (**Factor C**) more influent than the temperature (**Factor B**). Although the temperature is considered one of the most determining variables in the foundry, the degree of influence of this property on the results of this study was smaller than the samples' thickness and the casting condition. In other words, the amplitude of the values for spiral thickness (between 0.5 mm and 1.5 mm) and the change in casting condition (condition **N**, **Y**, and **YV**) was, in this study, more significant for the magnesium filling length than the difference of the two used temperatures (660 °C and 720 °C).

To conduct a deeper analysis of the design parameters' contribution to the filling length, the data were analyzed by statistical treatment ANOVA. This method allowed determining the relative influence of a design parameter (on a percent basis) and separating the significant from those negligible [229]. The methodology and equations used for the analysis of variance are clearly expressed in [229, 230].

Table 4.6 presents the obtained results from ANOVA and shows the degrees of freedom of the experiments, the SS (Sequential Sum of Squares), which indicates the variation of the data for different factors, the V (Variance), the F (Variance Ratio), and the percentual contribution. The DoF of error is given by the difference between the total number of observations minus one and the number of factor levels minus one [229]. In this specific case, 24 values were conducted, so the subtraction between the total number of DoF (DoF Total = 23) and the DoF of each factor's levels (sum of DoF **Factor A** to **Factor C**) gives a DoF of error equal to 6. Variance can be obtained from the ratio between SS and DoF for each factor and error term. In its turn, F results from the ratio between the variance of the factor and the error variance. A computed value of F higher than the tabled F-values indicates a statistically significant factor [229]. Finally, the contribution of each factor to the filling length is presented in the last column of Table 4.6. This value is obtained from the ratio between the SS' (Pure Sum of Squares) of each factor and the total SS and expresses the impact of a factorial effect in percent [231]. SS' is the sum square of a factor minus the degrees of freedom times the error variance [229].

Table 4.6: Results of Analysis of Variance.

Factor	DoF	Pure sum of square (SS')	Variance (V)	F	Contribution (%)
A	3	34225.9	11408.6	13.2	55.4
B	1	2278.9	2278.9	2.6	3.7
C	2	10561.6	5280.8	6.1	17.1
Error	17	14669.9	862.9	-	23.8
Total	23	61736.2	-	-	100.0

Looking at the ANOVA results expressed in Table 4.4, the same evidence in Figure 4.18 can be drawn. It is clear that the parameter seeming to have the most significant influence on the sample's filling length was the side length of the squared cross-section (55.44 %), followed by the casting condition (17.11 %). The temperature was the factor with less effect on the filling length for this case than the others, presenting a contribution of 3.69 %. In terms of factor's significance, the F-ratios, expressed in the fifth column of Table 4.6, were compared with standard table values at a confidence level of the experiments equal to 95 % [229]. From the F-table, the F-value for factors A was equal to 3.1968, while for **Factors B** and **C**, F-table assumed a value equal to 4.4513 and

3.5915, respectively. Comparing the F-ratios obtained with the tabled F-values, it seems that **Factors A** and **C** were statistically significant for 95 % confidence, while **Factor B** was considered negligible in this analysis.

The results allow to conclude that, regarding the AZ91D-1 wt.% CaO fluidity, it was more effective to vary the cavity thickness and the casting conditions to enhance the filling length than to change the temperature. In this case, the selected range of temperatures varies between the minimum and maximum defined values that can ensure a suitable and safe Mg casting (660 °C - 720 °C), which can help to justify this evidence. Otherwise, temperature could play a more important role in the process. Additionally, the high value found for the error contribution in this analysis (23.76 %) seems to highlight that the heterogeneity of the levels of each factor, especially in this study, can influence the precision of the results.

4.5. Summary and Conclusions

The chapter aims to optimization of the final steps of the proposed casting methodology, specifically the optimization of the thermal cycle applied to the plaster moldings and the study of the casting variables' influence, both of which play a crucial role in successful castings. Furthermore, to assess the fluidity of liquid magnesium in molding cavities, a case study was conducted in order to understand and analyze the effect and contribution of every casting variable on the cavity filling capacity of the studied metal alloy.

The experimental perception of thermal instability of the Yttria coating when applied to the conventional casting method led to the need to optimize the thermal cycle. The TGA and DTG analysis of the materials used in the manufacturing process of plaster moldings allowed to conclude that, for the correct burning of polymeric materials (PLA and resin) and the stability of the Yttria solution, it was necessary to guarantee a maximum temperature of 450 °C, so the thermal cycle was adequate for these temperature conditions. The optimal casting parameters were experimentally optimized and the values to be adopted for safe castings using the AZ91D-1 wt.% CaO magnesium alloy in plaster molding were defined in this chapter. According to the desired outcome regarding cavity filling length and metal sanity (with more or fewer liquid magnesium reactions), those temperatures can be varied, considering that higher temperatures potentiate more reactions but ensure greater fluidity of the liquid magnesium. Even though pouring

temperature has a greater influence than molding temperature, a compromise between them is recommended for successful casting.

The use of a vacuum atmosphere during the process proved to be essential for the occurrence of liquid metal reactions. It is a result of both the potentiation of the mold-metal contact after the metal is poured as well as the interactions between the magnesium and the surrounding atmosphere during melting. The obtained castings suggest that even though it can positively contribute to the cavity filling into the molding, vacuum may significantly increase the occurrence of reactions between the liquid magnesium and the surrounding elements.

This chapter describes an experimental investigation of the fluidity of the AZ91D-1 wt.% CaO magnesium alloy, using a spiral specimen to evaluate the influence of certain casting conditions, including section thickness (0.5 mm, 0.75 mm, 1 mm, 1.5 mm), pouring temperature (660 °C and 720 °C) and casting conditions (condition **N** - no Yttria coating and no vacuum; condition **Y** - Yttria coating and no vacuum; and condition **YV** - use of Yttria coating and vacuum). Based on the experiments and analyzes carried out, the results of filling length, summarized in Figure 4.19, allow to conclude that:

- The overall analysis of all obtained castings revealed that an increase in the side length of the squared cross-section and the pouring temperature increases the magnesium filling length of the final samples. The exceptions concerning the thickness variable were the samples **0.75Y660**, **1YV660**, and **1.5YV720**, in which the cavity filling percentage decreased in relation to the previous smaller thicknesses. Regarding temperature, the exceptions were the samples **1.5Y720** and **1.5YV720**, which had a lower cavity filling than the same samples for the lowest temperature. These results were justified due to the blocking action of Yttria coating to the fluidity of magnesium in the condition **Y** samples, which was a consequence of the slight cracking level of the outer coating layers, and due to the vacuum assistance, potentiating the occurrence of metal-atmosphere and mold-metal reactions in the samples for condition **YV**.
- A complete cavity filling length was only achieved for **1.5N660** and **1.5N720** samples when neither Yttria coating nor vacuum were used. The lowest cavity filling percentage was obtained with the **0.75Y660** sample, corresponding to the sample with a thickness of 0.75 mm coated with Yttria and poured at 660 °C.

- Metal sanity and a good surface finish were achieved for condition **N** samples. This study confirmed that the process can be optimized even without using a model's coating and the use of vacuum atmosphere, as well as demonstrating the negative effects of vacuum assistance on the reaction occurrence. However, the filling length was affected in this condition, mainly for thinner samples.
- The filling length obtained for condition **Y** was below expectations. In addition to having low cavity filling percentages under most conditions, the Yttria coating's cracking into the cavity walls of the moldings appeared to act as a blocking barrier to cavity filling, which particularly affects thicker samples.
- For condition **YV** samples, two important pieces of evidence were concluded. On the one hand, through visual analysis, it was possible to verify that, for all castings, the use of vacuum seemed to act as an enhancer of magnesium reactions with the surrounding elements, contaminating the metal. A black color in the zones with a slower cooling rate was evidenced in this case. On the other hand, although this negative effect decreased the cavity filling percentage in samples with greater cross-section thickness, the vacuum positively improved the cavity filling for samples with smaller cross-section thickness.
- In general, only conditions **N** and **YV** have allowed obtaining satisfactory results, which are dependent on the final application. In thin-walled castings, the use of a vacuum atmosphere is essential for successful cavity filling, despite increasing reactions between the magnesium and the surrounding elements. The use of vacuum, therefore, requires Yttria coating on the model. On the other hand, Mg castings without the use of Y_2O_3 coating and vacuum resulted in clean metal castings presenting a good surface finish, despite affecting the fluidity of the liquid magnesium. So, this condition is recommended for thicker parts.
- Statistical analysis of the obtained results permitted to conclude that the thickness of the spiral section, which varied between 0.5 mm and 1.5 mm, had a greater effect on filling length than the other variables studied, such as the casting condition and the pouring temperature. In fact, this last variable, possibly because there are only two temperatures incorporated in this study (660 °C and 720 °C) that ensure safe castings of magnesium, appears to have the least influence on the filling length.

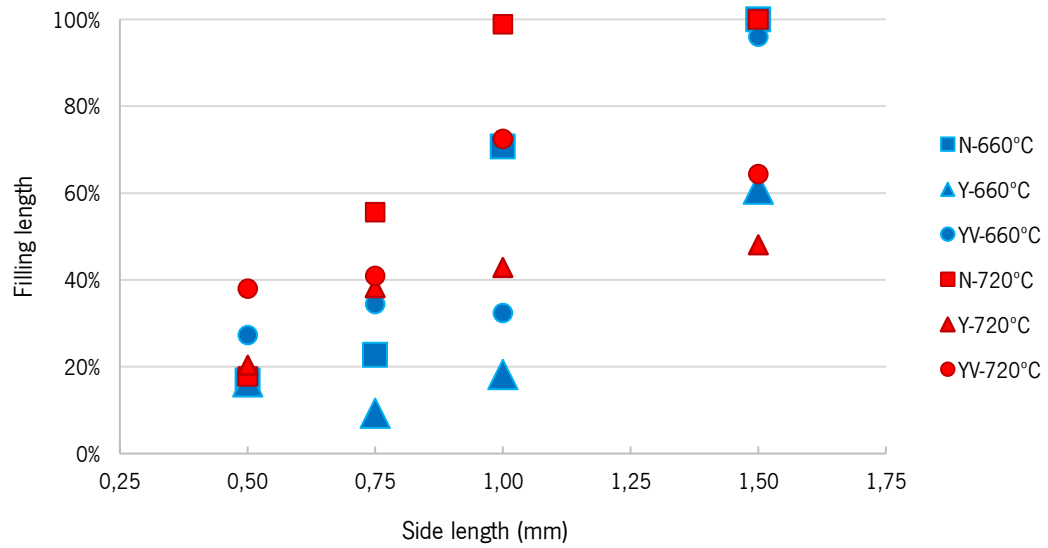


Figure 4.19: Evaluation of the filling length comparing all the studied variables.

No references are found in the literature to obtaining stents by investment casting. Even the available data about using this process to produce thin-walled magnesium components is scant.

Chapter 5. PROCESS VALIDATION: MAGNESIUM STENTS MANUFACTURING

As discussed in Chapter 2, the manufacture of stents, by laser cutting, is an expensive and complex process due to the particularities of geometrical shapes and the micro dimensions involved. In addition, this process is not feasible for magnesium alloys because of their high reactivity. Therefore, the objectivity of this doctoral thesis gains greater interest and significance, both in the scientific and industrial context.

This chapter discusses and characterizes the procedure for obtaining magnesium stents through investment casting in plaster molding. Based on all the optimizations made in the previous chapters of the various steps that comprise the methodology outlined in Chapter 2 (Figure 2.6), magnesium stents with a minimum thickness of up to 0.4 mm and a complex geometry were cast. Both casting conditions approved in the previous chapter, **YV** (Yttria and vacuum) and **N** (No Yttria and no vacuum), were applied and characterized for stent manufacturing. In the conclusion of this chapter, it will be possible to evaluate all the phenomena that occurred and determine what are the optimal casting conditions to guarantee the successful casting of the AZ91D-1 wt.% CaO magnesium alloy in plaster molding to obtain any magnesium part.

5.1. Model's Production: CAD and Printing

Following the proposed methodology described in Figure 2.6 (subchapter 2.5), and taking all previous processing optimizations into account, CAD modeling is the first step in stent production. Figure 5.1 illustrates the CAD stent model adopted in this study [232]. Throughout this chapter, and using a particular unit cell (Figure 5.1a) two different dimensions of the model have been used for different studies, as shown and described in Figure 5.1b. The thin-walled magnesium casting is evaluated using Model 1, which has a thickness of 0.4 mm. On the other hand, a detailed analysis of the microstructure has been carried out on Model 2, which has twice the thickness of the walls of Model 1.

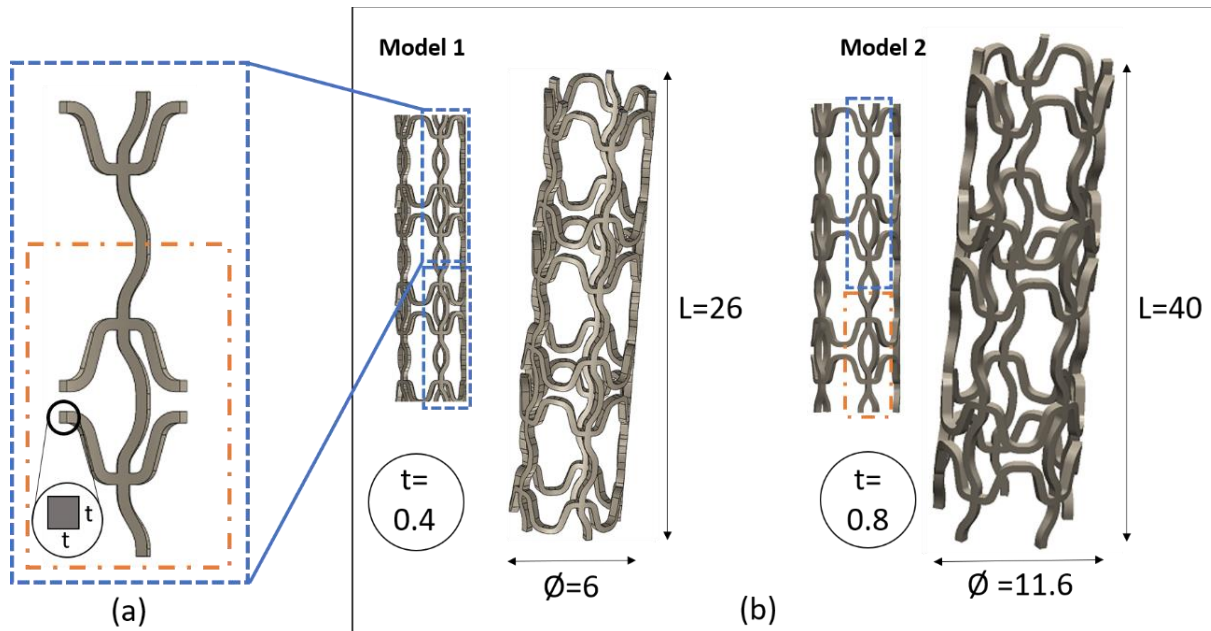


Figure 5.1: CAD stent geometry (mm): (a) design unit cell, and (b) models for testing.

For prototyping the stents' 3D models, SLA printing was used. The respective filling system was printed by FDM printing. Due to specific application requirements, both stent models were produced on the FabPro 1000 printer using the castable resin (JewelCast GRN) already described in Chapter 3. The optimal 3D printing of stents requires the use of support material and an angle of 20° for each stent system, as shown in Figure 5.2a. This printing optimized process results in an overall printing time of 2 hours and 4 minutes for Model 1 stent printing (Figure 5.2b).

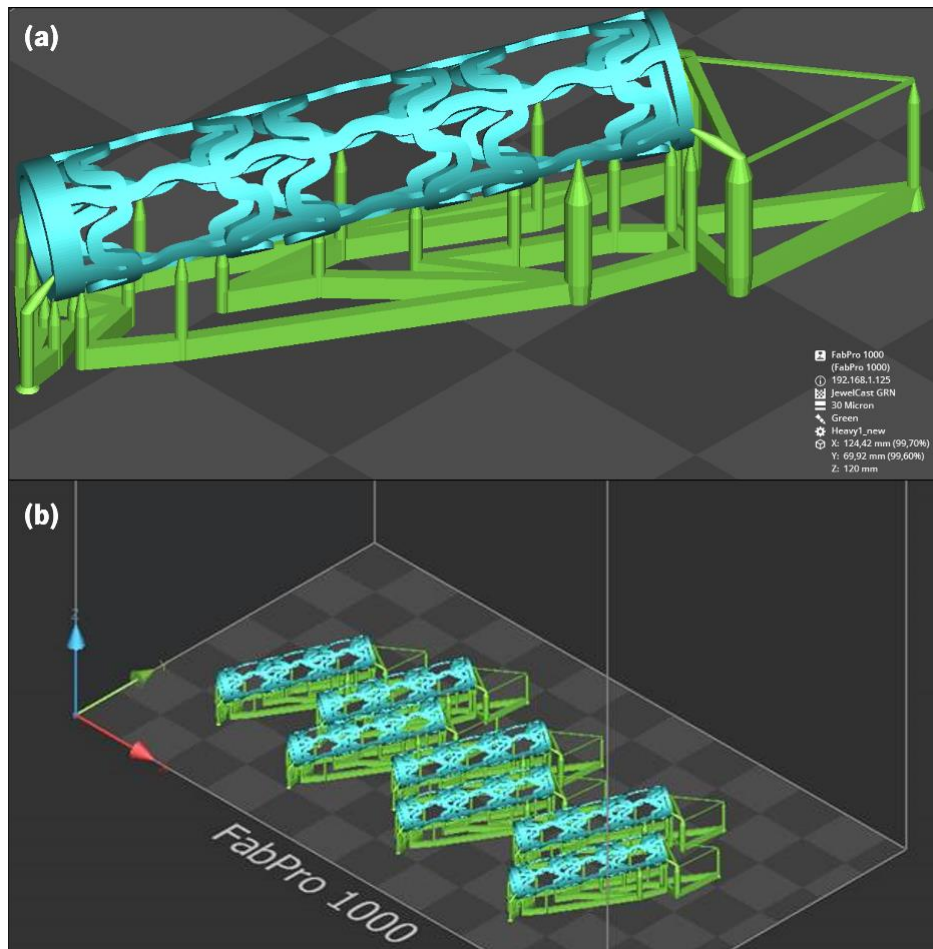

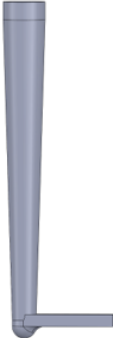
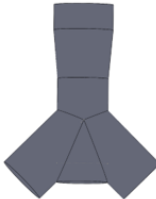



Figure 5.2: Additive manufacturing of stents Model 1: (a) construction of support material, and (b) printing maximization.

Regarding the stent design, the filling system was specifically investigated. As the investment casting process is widely used for large productions of small pieces, as is often the case in jewellery manufacturing, it is essential to maximize the filling tree of the initial models to ensure good metal flow and achieve the maximum number of parts for every casting.

To define the best filling method and determine the possibility of maximizing the stent's production, Table 5.1 shows the different approaches tested in this experimental research on the filling tree and the characteristics of each casting and the obtained results. The experimental setup and casting parameters of the previous case study 2 in Chapter 4 were applied to this process (Table 4.2). In addition to the use of Yttria to coat the samples and the vacuum assistance during melting, the pouring temperature of 720 °C was determined to increase magnesium fluidity into the molding cavities of the stent Model 1.

Table 5.1: Filling design optimization using condition YV and 720 °C pouring temperature.

Tree assembly design	Production	Type flow	Casting result
	1 stent	Direct filling	<p>Complete filling length. Medium surface quality. Occurrence of reaction gradient.</p>
	1 stent	Indirect filling	<p>Incomplete filling length. Poor surface quality. Metal stent without reaction.</p>
	2 stents	Direct filling	<p>Complete filling length with some defects. Poor surface quality. Occurrence of reaction gradient.</p>
	2 stents	Indirect filling	<p>Complete filling length with some defects. Medium surface quality. Metal stents without reaction.</p>

The results of the performed castings allow to conclude that no ideal condition existed for the design of the filling tree. As shown in Table 5.1, relating to the Model 1 stent castings, a more turbulent metal flow (direct filling) enhances the rate of reactions even when the cavity has been completely filled in both tree designs (1 and 2 stents). These castings revealed a black color gradient around the metal that was more evident in the zones closest to the filling basin corresponding to the zones in which the metal solidification rate was lower and, consequently, the metal stayed in contact with the molding walls longer. This phenomenon is consistent with the negative impact of vacuum highlighted in case study 2 of the previous chapter. In contrast, a uniform flow, promises greater magnesium purity from the bottom to the top (indirect filling), although complete stent cavity filling was not achieved. The cracking of the Yttria coating affected the surface finish of the metal, as expected, although it was less noticeable in the case of indirect filling for the casting of two stents.

Although the direct filling of liquid magnesium enhances the occurrence of reactions due to the vacuum influence, it was only in this condition that the cavity of the 0.4 mm thick stents was completely filled. Thus, the use of vacuum proved to be a fundamental condition for the effectiveness of the thin-walled filling length process, in conjunction with the metal flow by direct filling. In order to optimize the process, a thermal analysis was performed on the plaster moldings during the casting process (after the thermal cycle) to better comprehend the influence that the filling tree design has on the casting of the magnesium alloy. As illustrated in Figure 5.3a, three thermocouples were placed at distinct positions in the plaster molding (periphery, middle, and center). The temperatures in each position were then recorded at the defined molding temperature (400 °C) during the cooling phase.

The temperature readings in Figure 5.3b indicate that there was a significant temperature loss in the most peripheral zone of the plaster molding during the time of molding cooling. This temperature loss was more significant from periphery to the center. During the cooling time defined in Table 4.2, the peripheral zone decreases its temperature by about 100 °C to the surrounding atmosphere. This decrease begins almost immediately after the reading of the values. On the other hand, the heat transfer in the molding center was very low, which means that the central zone remained practically at the same temperature until demolding.

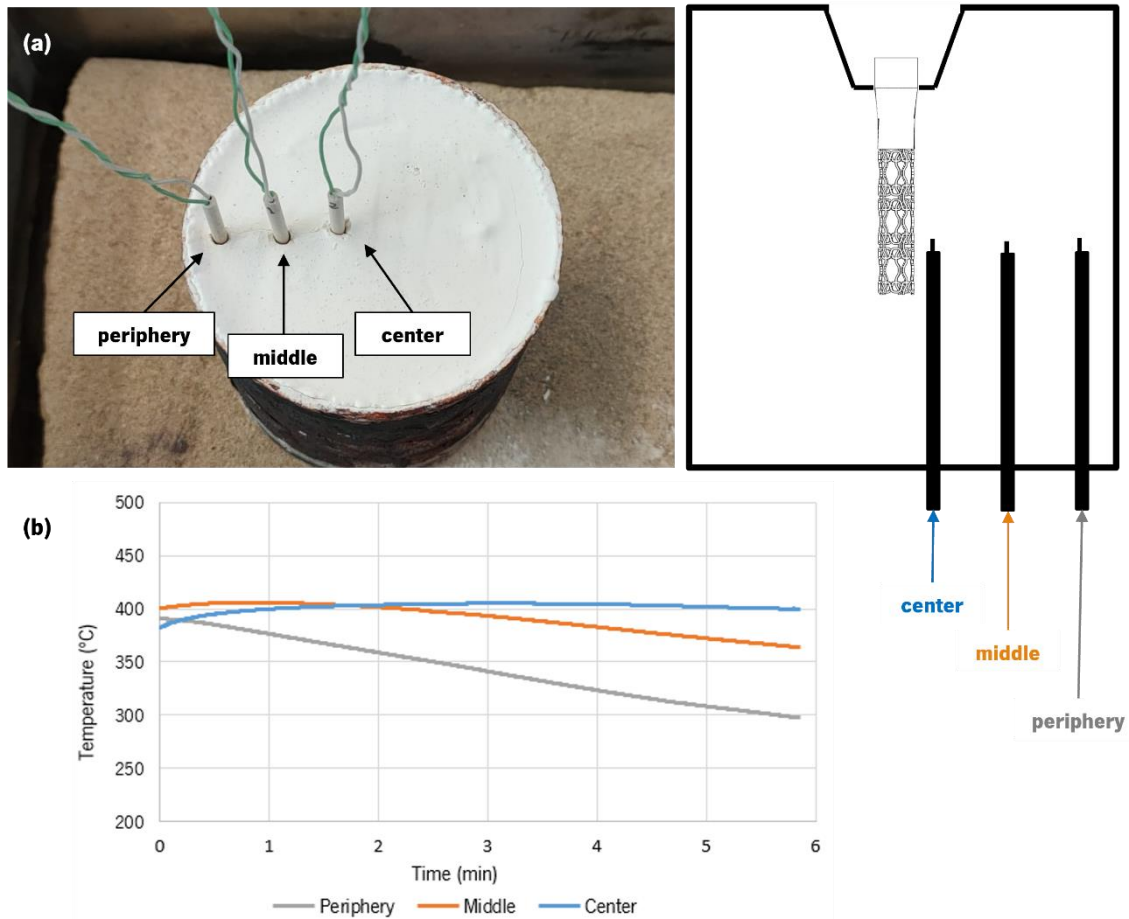


Figure 5.3: Molding cooling (after pouring): (a) placement of thermocouples, and (b) recording of temperatures.

The results allow to conclude that the solidification of the metal occurs faster in the peripheral areas of the molding, which can explain the cavity filling defects observed during the testing of a tree consisting of two stents when the thin-walled cavity filling is required close to the molding periphery. Therefore, to ensure greater metal fluidity and, consequently, a longer cavity filling length of thin-walled stents, the unitary tree system should be applied to each stent within each molding. Furthermore, a higher metallostatic pressure helps fill the cavity in this condition. Figures 5.4 and 5.5 illustrate the thermal gradient suffered by the plaster molding for both direct (1 stent) and indirect (2 stents) casting models at two distinct times: at the exact moment when magnesium is poured, and 3 minutes afterward. During this last condition, the temperature loss verified in the peripheral zones of the plaster molding was quite visible. This loss can significantly affect the stent cavity filling, especially in the areas farther from the molding center.

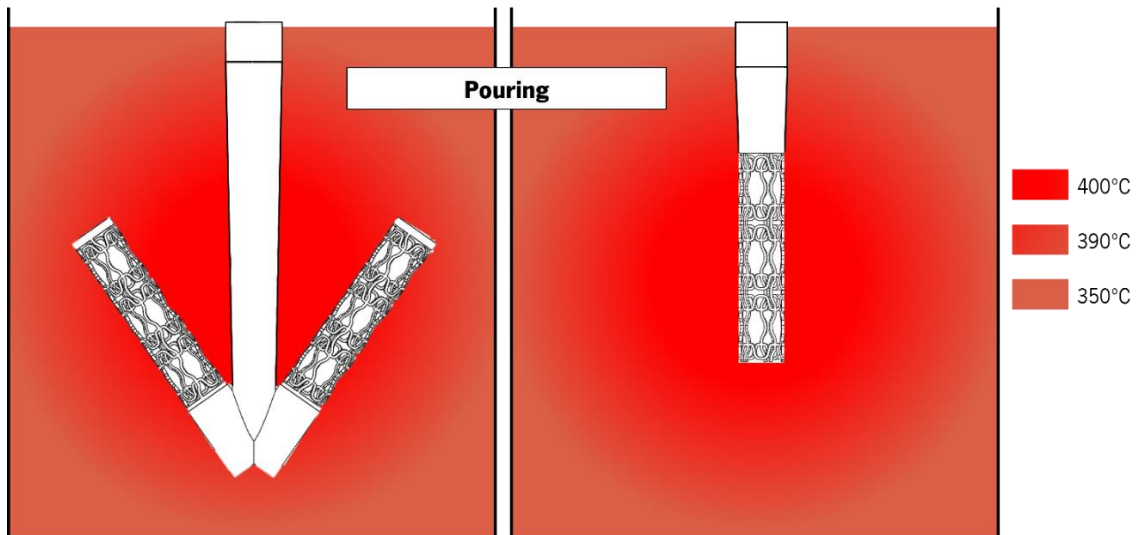


Figure 5.4: Schematic representation of molding temperature distribution during pouring.

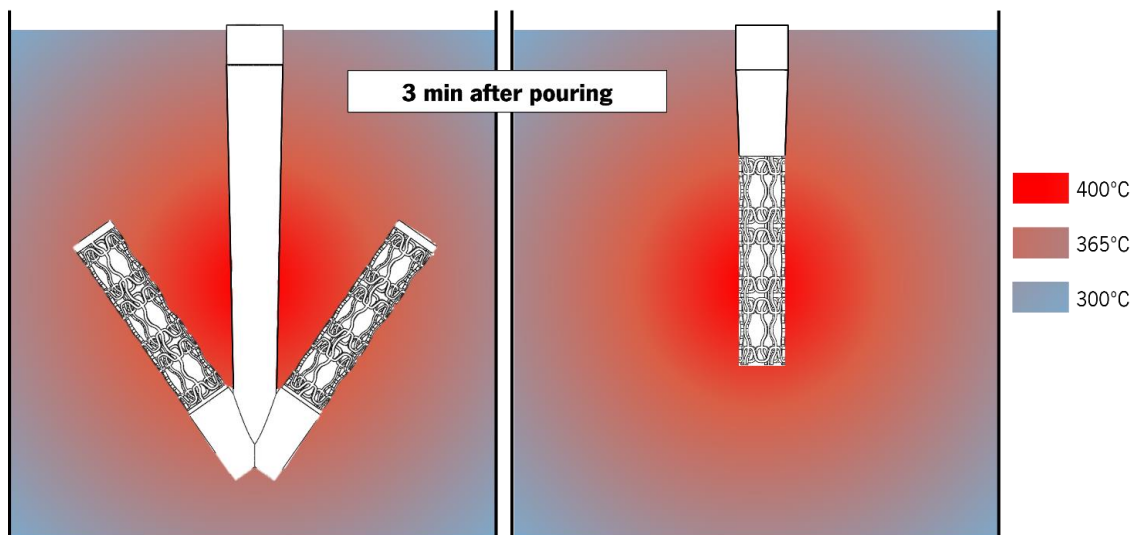


Figure 5.5: Schematic representation of molding temperature distribution 3 minutes after pouring.

5.2. Coating, Molding, and Casting Procedures

After modeling and printing the initial models and respective filling systems (Figure 5.6a), the steps of coating, fabrication of plaster moldings, melting, and casting are discussed below for both stent models (see Figure 5.1b), using both casting conditions defined in Chapter 4 (condition **YV** and condition **N**).

The casting condition **YV** was applied to the casting of stents almost like it was in the previous chapter for spirals (case study 2). After assembling the trees (Figure 5.6b), the coating of the models assumes a specific and essential step that should be more careful and homogeneous

as possible (Figure 5.6c). The stent models were immersed in liquid Y_2O_3 (99.99 wt.% purity - ZYP coating) and dried at a controlled temperature of 30 °C in a cubic chamber (800 x 400 x 400 mm³). The optimized painting characteristics for each model, shown in Table 5.2, were determined experimentally. Different coating layers and times between coatings were applied to each model as a result of different contact areas.

Table 5.2: Optimized painting characteristics.

Model	Coating layers	Immersion time	Time between coatings	Curing time after coatings
1	3	10 s	30 min	24 h
2	2	10 s	60 min	24 h

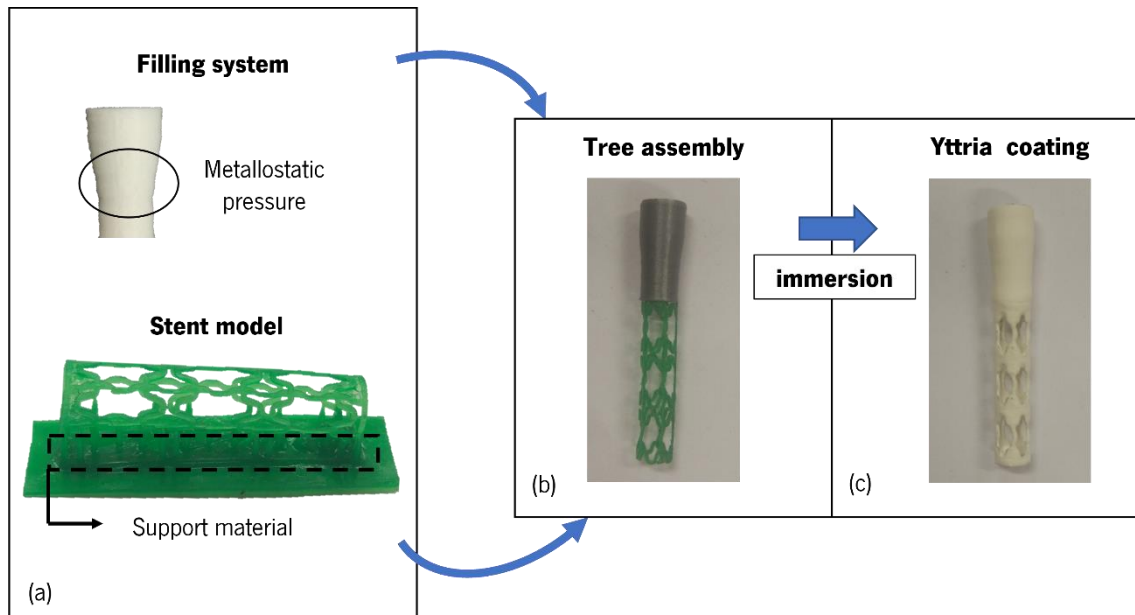


Figure 5.6: Model 1 processing: (a) additive manufacturing; (b) tree assembly; and (c) Yttria coating.

As the protective coating of the initial models is not used for condition **N** castings, the Yttria coating step is not incorporated into the process methodology.

After curing the model in condition **YV** and the assembly of the tree in condition **N**, the tree was put in plaster to produce the ceramic moldings according to the procedures outlined in the previous case studies. For that, a mixture of water and investment powder (Omega + from Gold Star) in a 40/100 (mass%) ratio was made according to the same conventional molding technique, and the moldings were dried at 30 °C before the thermal processing cycle to give consistency to

the plaster, eliminating the water content. Because of the thermal instability of the Yttria coating, the thermal cycle optimized in Chapter 4, and illustrated in Figure 5.7, was applied to the casting condition **YV** (see subchapter 4.1), using a molding temperature of 400 °C.

The casting process was performed for both casting conditions by applying the same experimental setup as in the previous case studies and using an induction melting furnace assisted by vacuum (condition **YV**) or without vacuum assistance (condition **N**), as illustrated in Figure 5.8. 10 g of AZ91D-1 wt.% CaO was cut, dried, and melted in a SiC crucible for each experiment. Table 3.4 shows the composition of the commercial alloy used in this study. As discussed in Chapter 2, this alloy was used to promote a no-SF₆ casting, which permits performing all tests under an argon-protected atmosphere and minimizes reactions during the melting stage. For the casting of condition **YV**, the metal was melted at 700 °C under a 1.0 bar vacuum atmosphere and kept isothermal inside the crucible for 1 minute for homogenization. In condition **N**, magnesium was melted at the same temperature in an air atmosphere. After this period, the melt was poured for both casting conditions at the same temperature into the preheated plaster molding cavities (400 °C) with an overpressure of 2.0 bar, which facilitates the metal pouring. Following a cooling period of 10 minutes, the stents were removed and cleaned after immersing the moldings in water for de-molding.

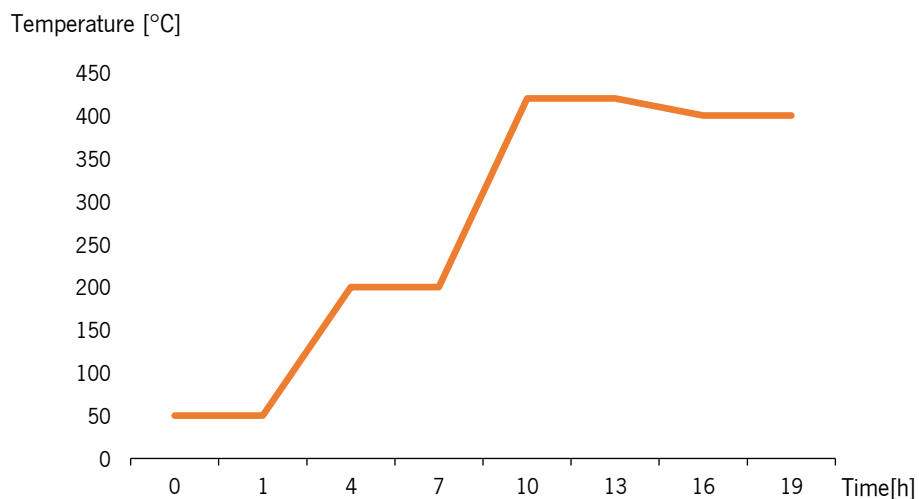


Figure 5.7: Thermal cycle optimized and applied to the plaster moldings when Yttria coating is used in stent manufacturing.

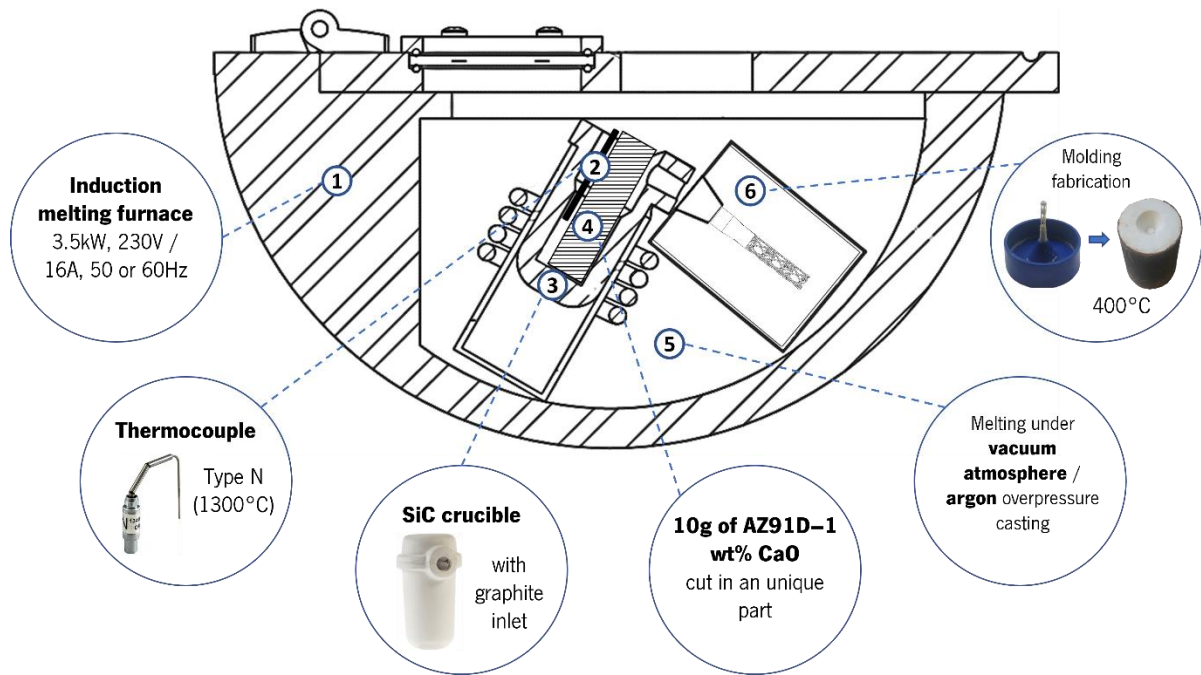


Figure 5.8: Experimental setup used for stent manufacturing.

5.3. Casting's Characterization

As part of the condition's validation, different analyzes and macro and microscopic characterizations were conducted. After de-molding and cleaning, the stents were initially evaluated by visual inspection, and volume loss analysis was performed using a precision digital scale throughout the process. The samples were cut and mounted on resin for further characterization following the weight evaluation. The samples were polished using SiC paper sizes (#320, #600, #800, and #1200) and cloths with a diamond suspension. Optical microscopy (OM) and scanning electron microscopy (SEM) equipped with energy-dispersive X-ray spectroscopy (EDS) and X-ray Diffraction (XRD) were performed to analyze the dimensional accuracy and chemical composition of the surface and matrix of the stents and to evaluate the extent of the mold-metal interface reactions. The XRD patterns were recorded between 30° and 50°, using 2θ as Cu $K\alpha 1$ radiation. A microhardness analysis was performed using a Vickers Microhardness Tester, applying a load of 15 grams. Additionally, X-ray Micro-computed Tomography (μ CT) was also performed in this study to analyze the stent's manufacturing details in-depth, helping to justify and validate the obtained results.

5.3.1. Yttria and Vacuum

Figure 5.9 presents the cast stents following the proposed casting method (Condition **YV**), using Y_2O_3 as refractory coating and vacuum assistance. Visual inspection confirmed both stent models' cavity filling, demonstrating the process's effectiveness for thin walls when using the Yttria-based coating and argon protection. Although no significant reactions or oxidations were detected throughout the entire process, a slight black layer was detected on the melts closest to the filling basin, as already demonstrated in case study 2 in Chapter 4 for fluidity study. However, this phenomenon was less evident with stent casting, which may be attributed to the different temperatures applied in this case (pouring temperature - 700 °C) compared to the fluidity case study (pouring temperature - 720 °C).

Comparing both cast models, a better cavity filling in castings corresponding to Model 2 was observed, which is expected since the solidification time is longer due to the larger thickness. The surface finish of Model 1 was, however, more satisfactory. It may be justified by the thermal instability of the Y_2O_3 coating with the molding walls when the volume models are larger and in which a thicker coating is applied (Model 2), affecting the surface roughness of the final castings. Additionally, both models appear to exhibit some failures along with the cavity filling, as indicated in red in Figure 5.9, which is consistent with the difficulty of cavity filling thin-walled geometries associated with this type of casting process.

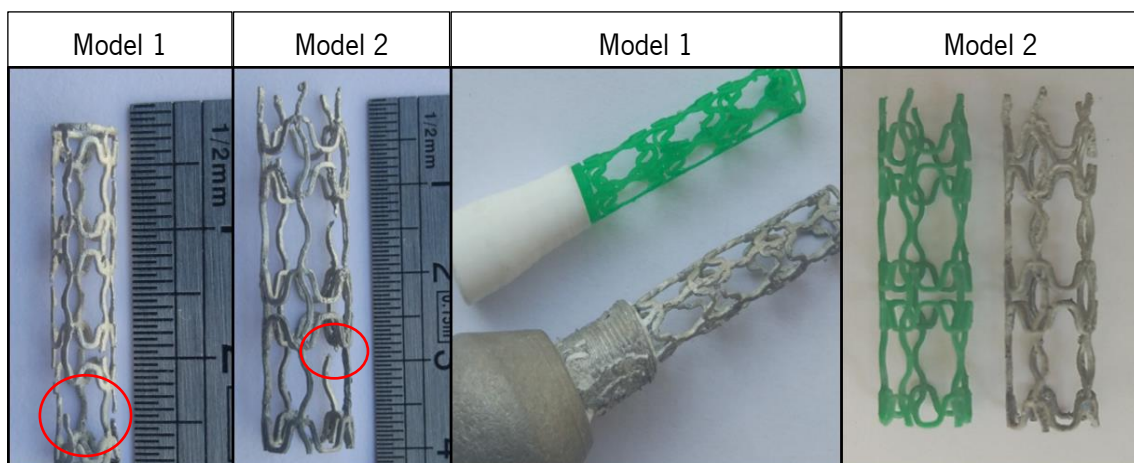


Figure 5.9: Yttria-coated cast stents.

The graph in Figure 5.10 presents the volume variation of the stents at different stages of the manufacturing process, considering six castings for each model. The results were obtained by measuring the mass difference for each model under analysis and using a digital scale. Considering the initial volume of the 3D CAD stents, the graphs show that the printing process induces a clear

increase in the volume, which is more evident in Model 1, due to the additional mass from support material (Figure 5.6a). Moreover, this type of additive manufacturing process implies dragging of material and the consequent increase in volume during printing operations, as confirmed by Carneiro *et al.* [233]. This phenomenon is more pronounced in smaller structures with thinner walls.

As a result of the transition from 3D printing to investment casting, there was a difference in volume between the two methods. Although the standard deviation of the measurements was higher in this process, the results show a decrease in the stents' volume for Model 1, suggesting being associated with an incomplete cavity filling. In Model 2, there is a slight increase in volume after casting, which permits to conclude that, although this model had a higher percentage of cavity filling, it may be related to the presence of impurities and reaction products in the final castings. The slight reaction rate can occur during the melting phase, but it is more pronounced for thicker walls since the solidification time is longer.

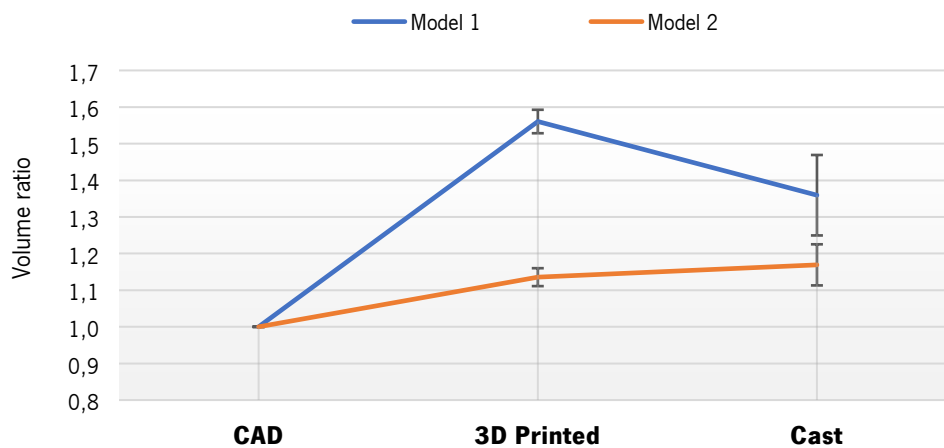


Figure 5.10: Volume ratio of coated stents during the process.

Figure 5.11 shows the result of pouring without a protective coating. The uncoated stents have an intense black color and non-uniform texture, which is quite different from the coated models (Figure 5.9). Cavity filling failures in these models have been notorious, mainly due to the accumulation of reaction products and oxides (white color). According to Jafari *et al.* [48] and to Sin *et al.* [50], the presence of strong exothermic reactions between the liquid metal and plaster molding, absent a protective coating, jeopardizes the process's safety, and reproducibility of these castings was not possible. Despite this, small metal fragments from these stents, marked in red in Figure 5.11, were recovered to conduct analyzes and comparisons.

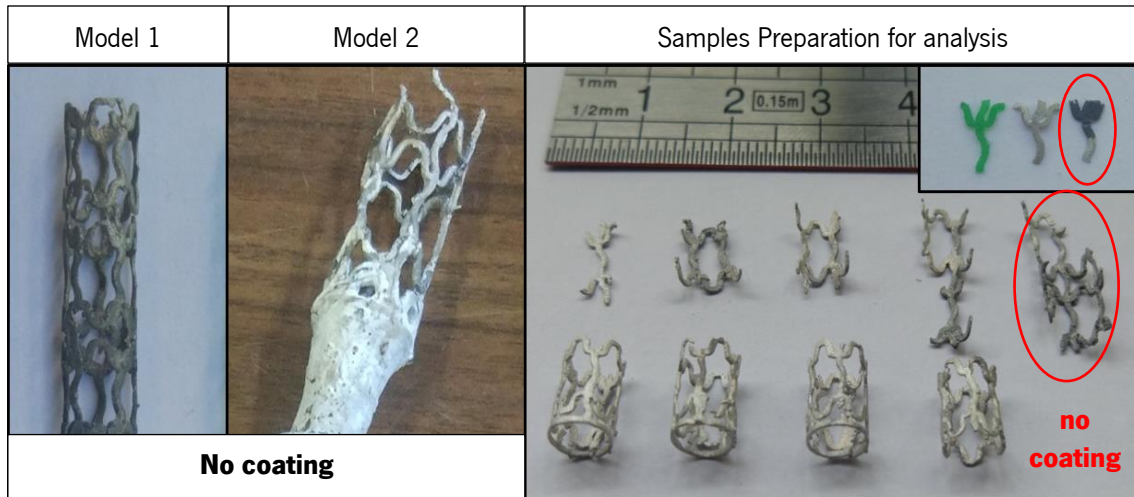


Figure 5.11: Uncoated cast stents and preparation of samples for microscopic characterization.

The SEM characterization of the microstructure of the cast models is presented in Figures 5.12 and 5.13. The pouring of the magnesium alloy into the plaster molding when no coating was applied suggests being greatly affected by the reactions occurring at the mold-metal interface, as the interface wall of the molding is compromised, affecting the surface roughness. Thus, the oxidized periphery, with the development of oxide layers and large porosities, the microstructure of both uncoated models was also affected. The oxidation processes and reaction processes in these cast samples resulted in a coarser microstructure with heterogeneous morphology, as well as a high concentration of inclusions and porosity. In contrast, coated stents for both models showed a clearly defined and unreacted periphery, as well as a uniform, clean, and refined microstructure. The microstructure comparison between the two poured models with the coating applied revealed no obvious differences between them, showing a clear definition of the predominant matrix (α -Mg) and the intermetallic (β -Mg₁₇Al₁₂) phase.

A comprehensive analysis was performed in Model 2 to understand the influence of the coating on the occurrence of reactions in which the metal remained liquid for a longer period of time and, consequently, the time of mold-metal contact was longer. Figures 5.14 and 5.15 illustrate a rib of the Model 2 unit cell (Figure 5.13), representing the stent's base area opposite the filling head (first zone to solidify). According to the SEM analysis, the differences between the coated and uncoated models were visible in terms of dimensions and microstructures. In the absence of coating (Figure 5.14), the molding walls were damaged by direct contact between the liquid metal and the molding walls, which resulted in serious reactions that contaminated the metal, blocked the metal pouring, and adversely affected the surface roughness and microstructure. On the other

hand, Figure 5.15 shows that the use of Y_2O_3 coating acted as a protective barrier, resulting in a smooth and well-defined casting of magnesium.

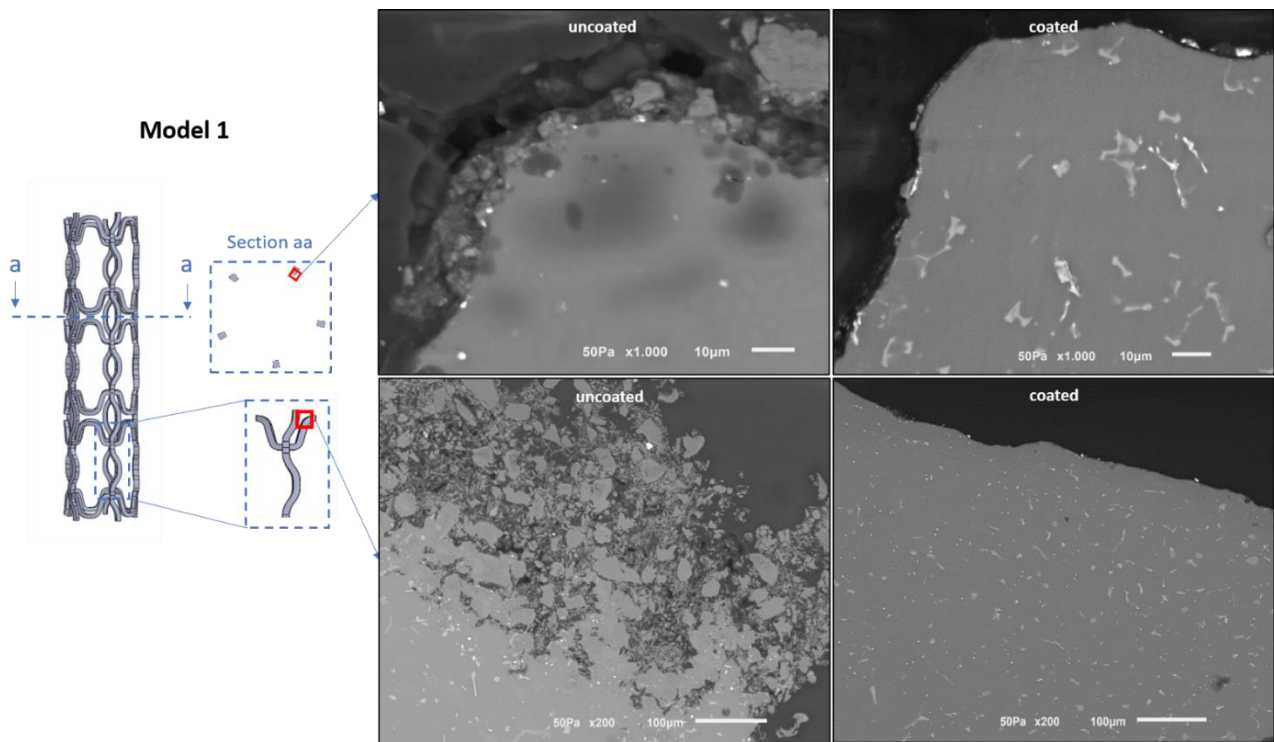


Figure 5.12: Model 1 SEM analysis.

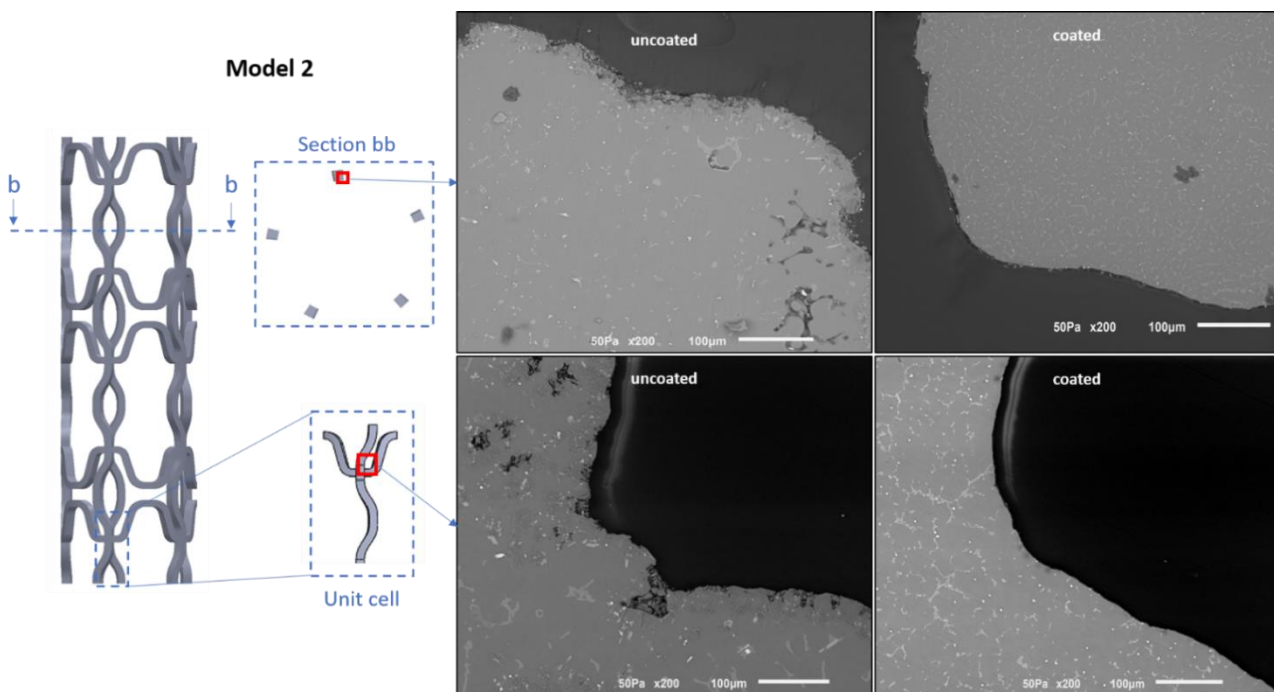


Figure 5.13: Model 2 SEM analysis.

The higher magnification highlights the perception of reaction occurrence and metal contamination in the uncoated model, favoring a coarse and non-uniform microstructure and the appearance of new phases and inclusions. A more uniform and refined microstructure was revealed in the coated model.

Tables 5.3 and 5.4 show the EDS analysis carried out on the microstructures for the different phases correctly identified in uncoated and coated models. Furthermore, an element analysis was performed along the rib of the stent from the center to the periphery. This was done to evaluate the depth of the reaction's products in each microstructure, as can be seen in Figures 5.14 and 5.15.

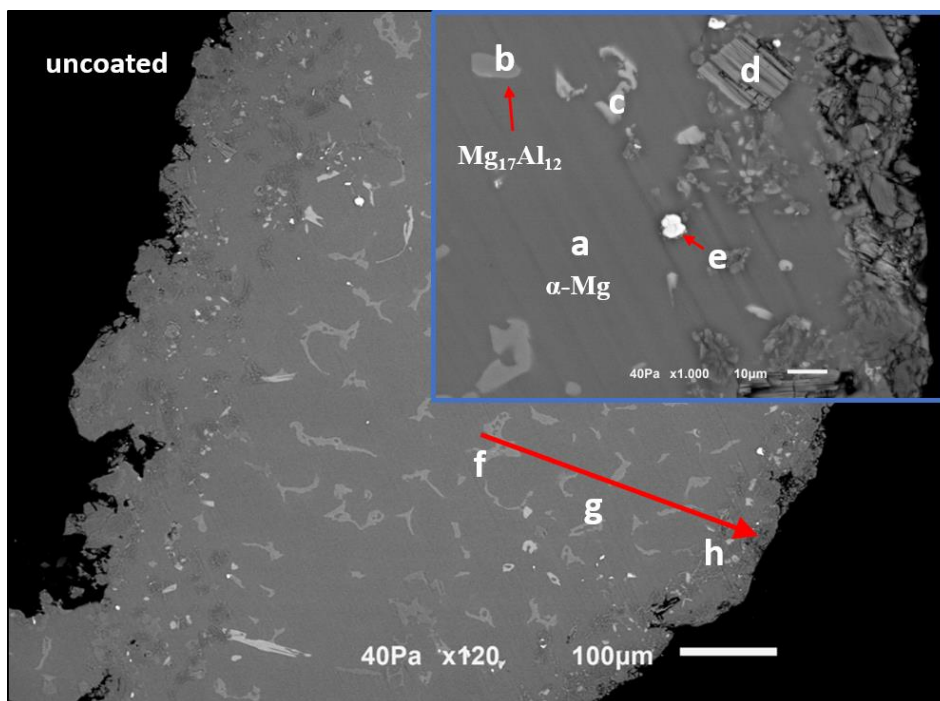


Figure 5.14: Backscattered FESEM images of the Model 2 uncoated unit cell.

Table 5.3: EDS analysis of the points indicated in Figure 5.14.

Element/ Point	Mg	Al	Mn	Ca	Y	Zn	O	Si	S
	Weight %								
a	89.8	6.5					3.7		
b	62.9	29.9		0.6		3.3	3.2		
c	52.2	1.7		19.6			7.0	19.4	
d	23.6	0.9		19.5			38.2	0.4	17.5
e	31.2	28.8	32.9	0.2			5.1	1.8	
f	90.1	6.8		0.2		0.6	2.3		
g	88.6	8.0				0.6	2.8		
h	81.6	6.3		0.5		0.3	6.7	4.3	0.3

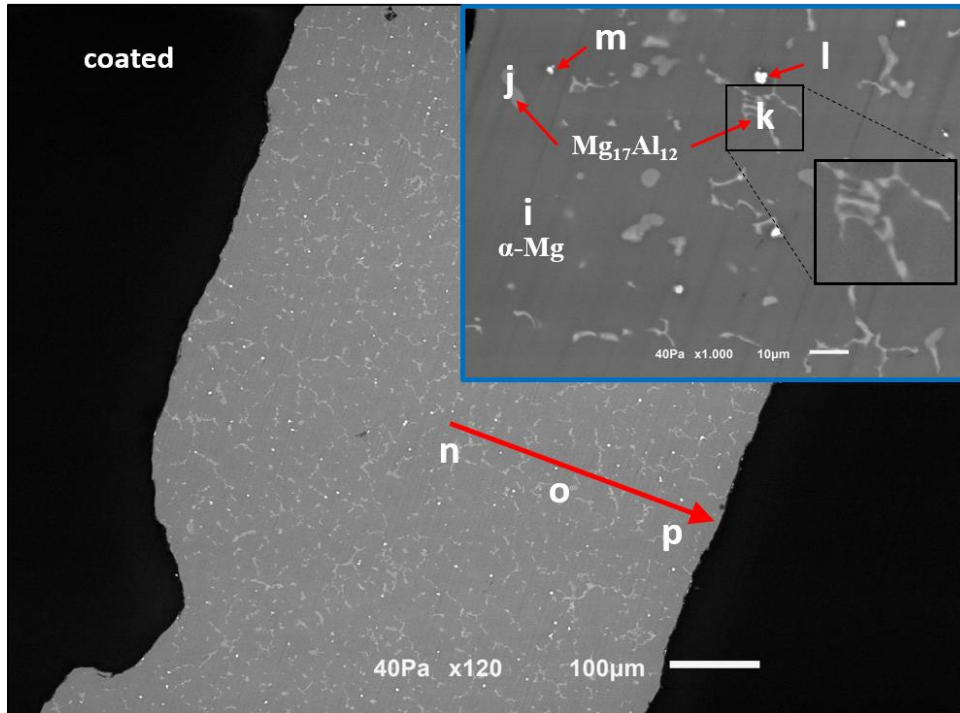


Figure 5.15: Backscattered FESEM images of the Model 2 coated unit cell.

Table 5.4: EDS analysis of the points indicated in Figure 5.15.

Element/ Point	Mg	Al	Mn	Ca	Y	Zn	O	Si	S
	Weight %								
i	90.9	6.0				0.5	2.6		
j	63.6	26.9		2.6		3.3	3.6		
k	63.1	23.9		8.5		0.2	4.3		
l	39.6	28.7	26.9	0.5		0.0	3.8	0.4	
m	26.2	31.0	0.8	1.5	32.8		7.7		
n	90.0	6.8		0.5		0.6	2.1		
o	89.3	7.1		0.7		0.8	2.1		
p	91.9	4.6					3.5		

EDS analysis confirmed the findings already described for coated and uncoated models. In addition to the well-defined α -Mg ('a' and 'i' points) and β -Mg₁₇Al₁₂ ('b' and 'j-k' points), the presence of an Al-Mn phase was found for both models, corresponding to the point 'e' on the uncoated model (Figure 5.14) and the point 'l' on the coated model (Figure 5.15). The presence of elements that do not compose the studied alloy, such as Si and S, provides evidence that reactions occur in the uncoated model involving the plaster from the ceramic molding. In contrast, these elements are virtually undetectable in the coated model.

As a result of the interaction between the metal and the plaster, the observation of 19.4 % Si at point 'c' suggests the formation of the Mg₂Si phase in the uncoated model, which is expected.

An intense degree of reactions occurred in the uncoated model periphery, as evidenced by the 'd' point values of 38.5 % O, 17.5 % S, and 4.3 % Si. Point 'k' suggests a shape change from strips to networks of the intermetallic $Mg_{17}Al_{12}$ due to the greater presence of Ca, as evidenced by the results of the EDS analysis and in accordance with research work reported Wang *et al.* [55]. This mechanism suggests contributing to the refinement of the intermetallic phase, being more noticeable in the coated model.

Additionally, the EDS analysis performed on coated model cast samples revealed that a Y trace was present within the alloy's microstructure ('m' point), near its periphery. As previously reported, this is directly related to the coating cohesion on the walls of plaster molding. If the same printing model is immersed in Ytria many times to thicken the protective layer, as was done with Model 2, small flaking may occur in the innermost layer of the molding walls due to the thermal cycle process. Due to this phenomenon, small Y_2O_3 particles detach from the molding wall, migrating towards the liquid metal close to the periphery due to their very high stability.

A possible cause of the oxidation rate that can occur during the entire process is the reaction between the liquid metal and the surrounding environment, as well as the contact between the liquid metal and the molding. Despite the controversy surrounding the quantification of oxygen (O) via EDS, in this study, the oxygen percentage values served only as a reference for the comparison of the different casting conditions, allowing to understand the relationship between oxidation rate and oxygen values. The higher oxygen values recorded in the uncoated model suggest that this kind of cast sample has a higher level of oxidation. More specifically, higher oxygen values were recorded in the 'f-g-h' points (uncoated model – Figure 5.14), varying from 2.3 % to 6.7 %, compared with 'm-n-o' points (coated model – Figure 5.15), which varied from 2.1 % to 3.5 %. The increase in oxygen in the uncoated microstructure is directly related to the decrease in Mg at the same points. In other words, and according to [234], the reaction between Mg and O seems to be a two-way diffusion reaction and thus, Mg_xO_y phases can be formed. The O percentages were also measured in other samples to guarantee the casting's reproducibility, both in the innermost zone and in the peripheral zone of the microstructure, as shown in Figure 5.16. The recorded values demonstrate and confirm the tendency for higher oxidation in uncoated models, mainly in peripheral zones. As can be seen in Figure 5.17, these facts were confirmed by the hardness analysis performed on both samples. On the coated sample periphery, higher hardness values were measured, justified by the rapid solidification of this zone. Conversely, no

significant differences were observed in hardness values between coated and uncoated samples in the center, indicating that the coating affects the mechanical properties of the metal.

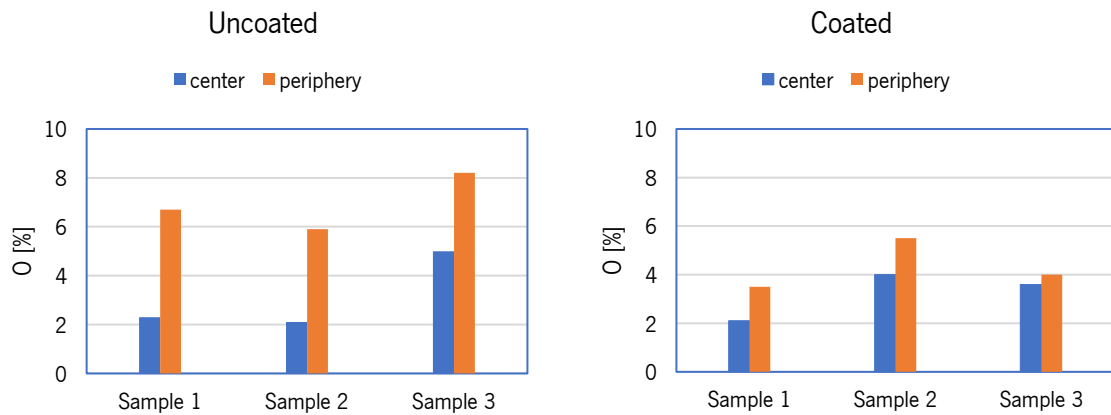


Figure 5.16: Values of oxygen concentrations in all castings.

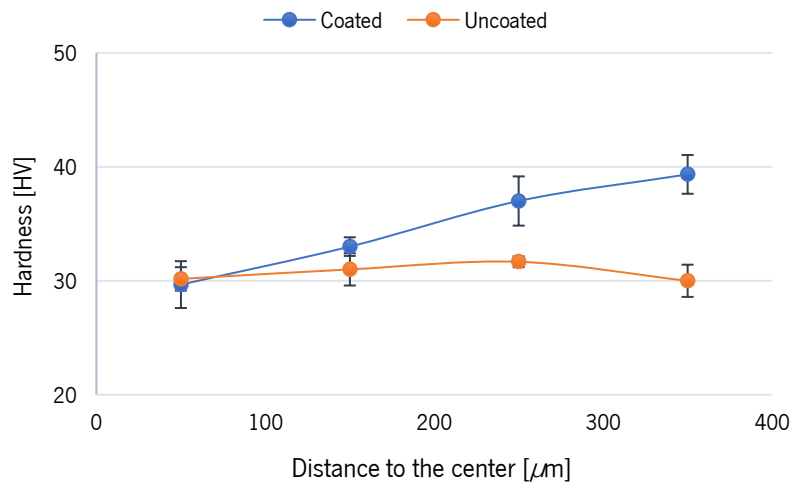


Figure 5.17: Hardness analysis of the Model 2 unit cell.

An XRD analysis was also performed on both cast samples of Model 2 (Figure 5.18). The obtained results were consistent with the previous analyzes, which showed that reaction products were generated only in the uncoated models at the mold-metal interface, such as MgO , SiO_2 , and Mg_2Si . In the coated model, besides $\alpha-Mg$ and $\beta-Mg_{17}Al_{12}$ phases, Y element was also registered, which proves the presence of Ytria traces particles in the microstructure. The CaO compound is a constituent present on the alloy and was only detected in the coated sample, which means it was decomposed and participated in the reactions that occurred in the uncoated sample.

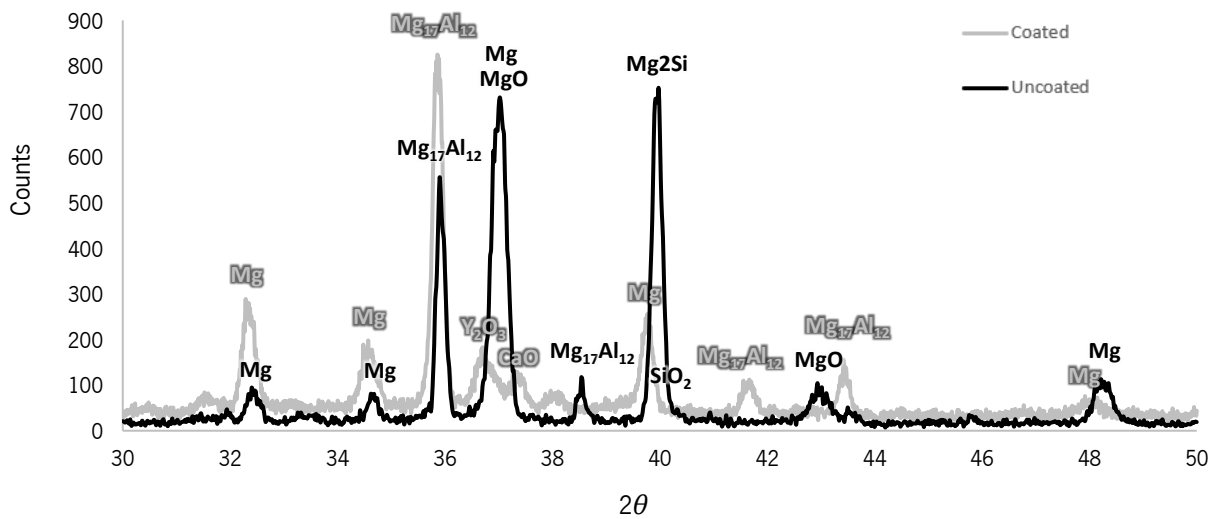


Figure 5.18: XRD analysis of the Model 2 unit cell.

5.3.2. No Ytria and no Vacuum

The castings for condition **N** were made without the vacuum atmosphere for melting and without the Ytria for coating the initial 3D models, albeit the same experimental setup was employed, as illustrated in Figure 5.8. The processing methodology for this condition was therefore limited to optimizations carried out along the various steps that can be applied to these castings, such as the printing of models and the optimization of casting variables, such as pouring and molding temperatures.

In the case of study 2 reported in Chapter 4, concerning the AZ91D-1 wt.% CaO magnesium alloy fluidity, no reactions between metal and the surrounding elements were observed for condition **N**. Therefore, an experimental study was conducted to investigate the effects of temperature on the process. For this purpose, four castings were performed at pouring temperatures of 600 °C and 800 °C and molding temperatures of 200 °C and 600 °C in order to obtain Model 1 stents. Figure 5.19 shows the resulting castings. Therefore, it can be concluded that temperature was a significant variable for this condition, both regarding cavity filling and the occurrence of reactions. The complete stent cavity filling was not achieved for any casting, which was almost non-existent at low casting temperatures for both molding temperatures; however, increasing the latter can slightly fill thin-walled ribs.

In contrast, the casting temperature of 800 °C was critical, and there was a severe occurrence of magnesium reactions aggravated by an increase in the molding temperature. The

occurrence of this phenomenon allowed to conclude that the existence of magnesium reactions in condition **YV** was not caused directly by the use of a vacuum atmosphere. This suggests that the vacuum atmosphere enhances the reactivity of magnesium and even its vaporization. Furthermore, mold-metal reactions also appear to be influenced by the behavior of the liquid metal at high temperatures. The effect of vacuum to assist the pouring enhances the mold-metal contact and, consequently, reactions between liquid magnesium and the plaster. Thus, since vacuum assistance is not used, a more extensive range of temperatures can ensure safe magnesium casting in plaster molding under condition **N**.

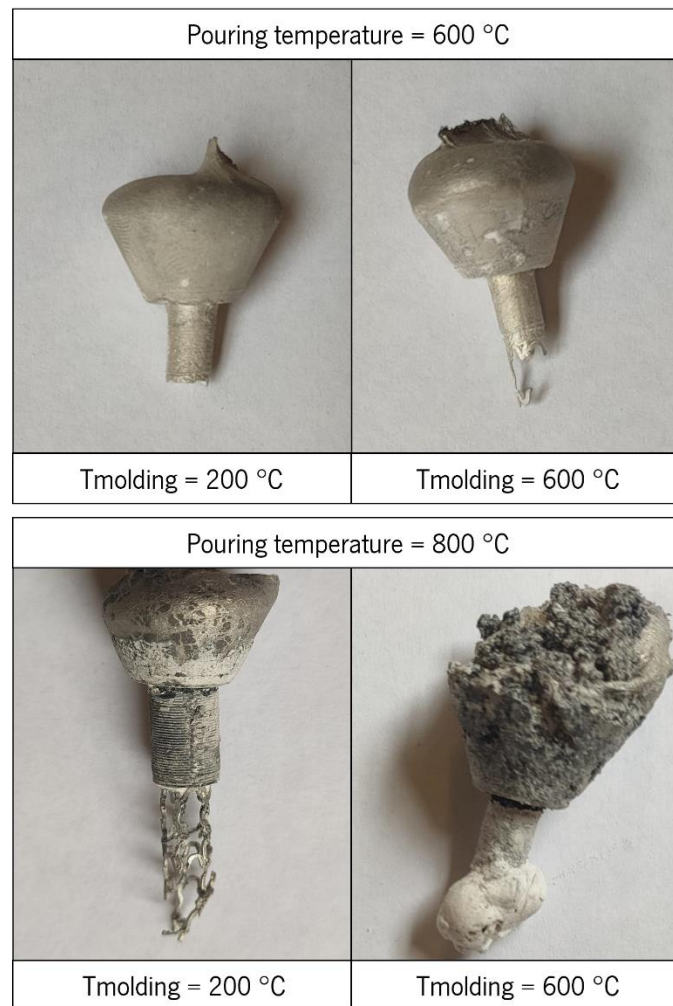


Figure 5.19: Study of the influence of the molding and pouring temperatures for condition **N**.

As Yttria was not used as a protective coating, the optimal thermal cycle for plaster moldings was not applied to this casting condition (condition **N**). Therefore, since a vacuum reduces the magnesium fluidity, this decrease can be compensated for by a small increase in the temperature involved. For that purpose, it was necessary to know the limit temperatures for the occurrence of reactions, thereby allowing to define the optimal casting conditions for condition **N**.

Applying the molding limit temperature of 450 °C, another experimental study was carried out to determine the optimal casting temperature for the casting of thin-walled stents through the condition **N**. The analysis of stent castings for different temperatures, shown in Figure 5.20, led to the conclusion that the mitigation of reactions was only possible for pouring temperature less than 720 °C. At temperatures higher than 720 °C, the necessary thermodynamic conditions for the occurrence of magnesium reactions appeared to be met, just as in condition **YV** at lower temperatures. Moreover, the complete cavity filling could only be achieved at temperatures higher than 720 °C, although it seems to be the limit temperature that inhibits reactions. The casting parameters should therefore be defined based on the characteristics of the final product considering the linear relationship between the filling length and the occurrence of reactions. In the case of Model 1, a complete casting without reactions was achieved by defining molding temperature at 450 °C and pouring at 720 °C. These results are consistent with those obtained in case study 2 (Chapter 4), in which melts occur in condition **N** without any magnesium reactions occurring at a pouring temperature of 720 °C.

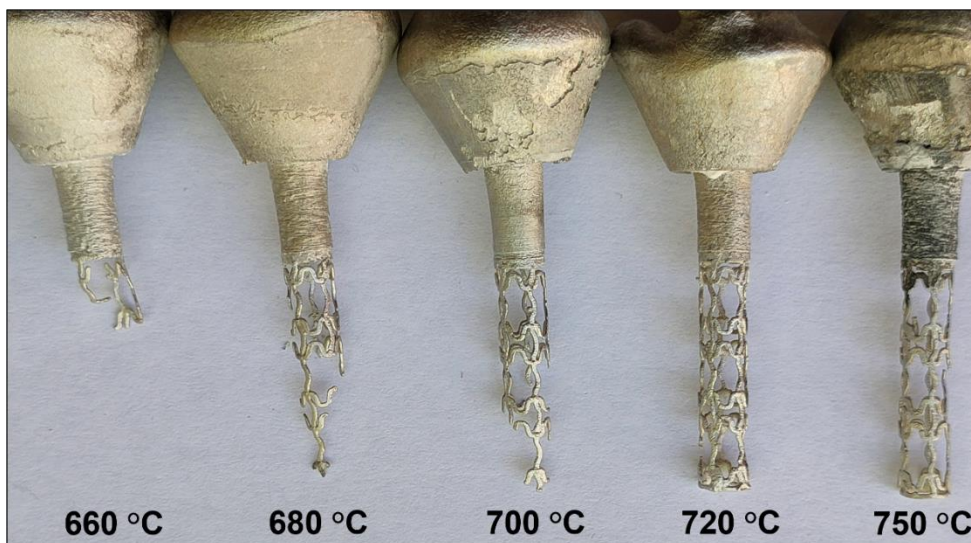


Figure 5.20: Influence of pouring temperature for condition N.

By applying the same processing method and all the optimizations performed during this work, both stent models were successfully obtained for condition **N**, as shown in Figure 5.21. Consistent with the results from the previous chapter, and contrary to what was expected for these casting conditions, the stents demonstrated good geometric rigor, and good surface finish, as well as high metal sanity. In addition to the complete filling length, the dimensional and geometric accuracy were quite faithful to those of the initial models, revealing only some imperfections due

to the associated geometric complexity. It was also reflected in the early stages of 3D printing and was agreed upon by all analyzed conditions.

A compromise must be struck between the used temperatures to ensure reaction-free castings and sufficient fluidity for complete stent cavity filling. In the case of stent Model 2, good results were achieved using a molding temperature of 400 °C and a pouring temperature of 700 °C, which were a little lower than those for stent Model 1. This can be explained by the larger dimensions of stent Model 2.

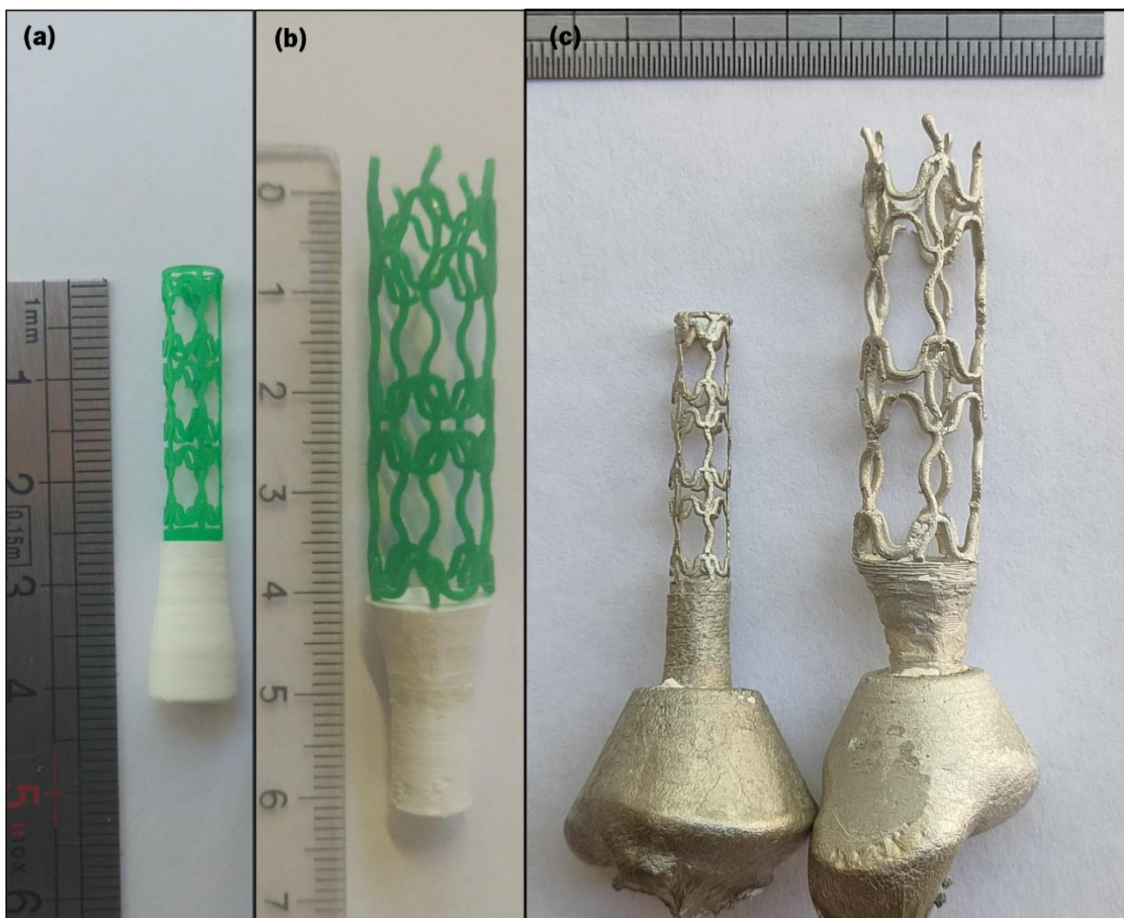


Figure 5.21: Stent obtained for both models through casting condition N: (a) printed Model 1; (b) printed Model 2, and (c) cast stents for both models.

The most surprising aspect of casting condition **N** was the absence of magnesium reactions throughout the entire process, despite the absence of a vacuum atmosphere that greatly facilitates cavity filling, especially in cavities of 0.4 mm thickness as in the case of stent Model 1. During the melting and pouring phases (with argon at 2 bar overpressure), liquid magnesium appeared to remain chemically stable, with no reactions occurring that could affect the alloy composition and the metal casting. The magnesium did not show significant reactions during the

cavity filling and solidification of the metal within the plaster molding, suggesting that direct mold-metal contact is not detrimental to the casting and sanity of the molten metal.

Likewise, condition **N** was tested for an indirect pouring metal design in order to obtain two stents, which had been more successful in condition **YV**, and both conditions were compared (Figure 5.22). According to the obtained castings, conditions **N** allowed achieving better metal sanity provided by reactions, although condition **YV** did not permit achieving a complete stent cavity filling. Therefore, although vacuum enhanced the fluidity of the magnesium, thereby promoting greater cavity filling, it also enhanced reactions that affected the sanity of the melt surface.

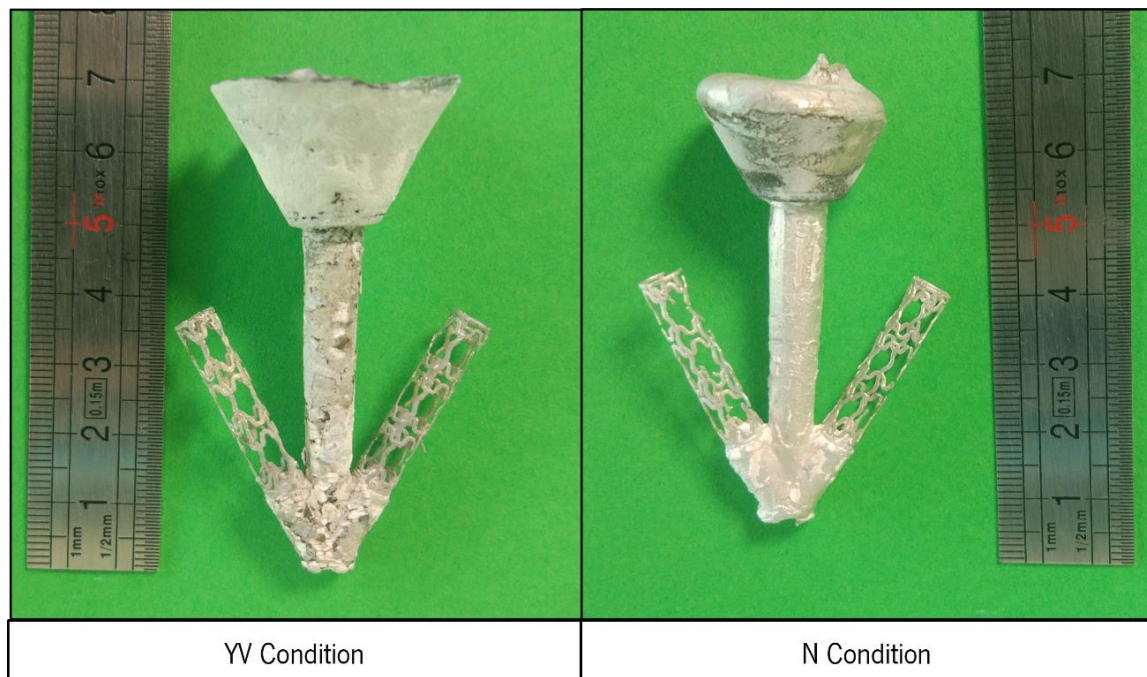


Figure 5.22: Comparison of conditions YV and N for indirect filling stent casting.

The microstructural analysis of the stent metal for condition **N** is presented in Figure 5.23 and Table 5.5. Observing the microstructures for both indicated areas, a good surface finish and higher dimensional rigor were notorious, showing a clear definition of the predominant matrix (α -Mg) and intermetallic (β -Mg₁₇Al₁₂) phases. The rapid metal solidification in these castings explains the small growth of the intermetallic phase, although it was evenly distributed throughout the microstructure. The EDS analysis provided additional support to the obtained results. In one sense, the absence of the elements Si and S in the samples appeared to indicate the absence of severe reaction products in the castings, as shown in the samples of condition **YV** presented in the previous subchapter. On the other hand, in addition to the known matrix (α -Mg) and intermetallic

(β -Mg₁₇Al₁₂) phases, it was observed the formation only of phases involving Al and other predominant elements from the studied alloy, forming for instance Al₄Mn and Al₂Ca phases.

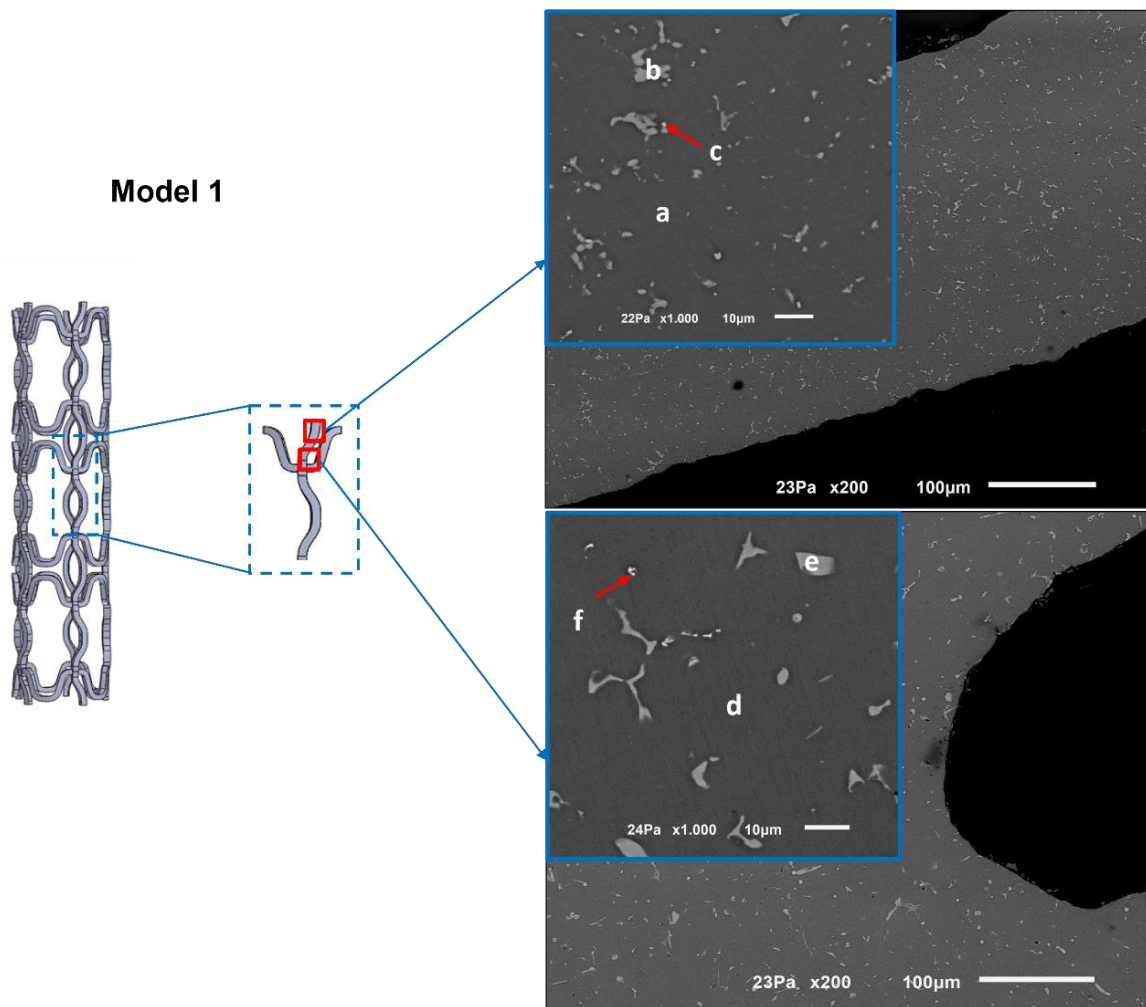


Figure 5.23: SEM analysis of the Model 1 unit cell for condition N.

Table 5.5: EDS analysis of the points indicated in Figure 5.23.

Element/ Point	Mg	Al	Mn	Ca	Zn	O
	Weight %					
a	89.9	6.2			0.8	3.1
b	43.4	36.7		15.7	0.8	3.4
c	41.5	37.4	12.4	4.7		4.0
d	87.8	8.9			0.9	2.3
e	36.0	43.1		16.9	0.6	3.5
f	41.0	26.9	23.1	1.3	0.2	7.4

5.4. Processing Methodology Overview

Experimental casting studies have been carried out during this study to optimize the proposed methodology for thin-walled magnesium investment casting, taking into account all the defined steps (see subchapter 2.5). Based on the intended purpose and the final casting characteristics, the investment casting process of AZ91D-1 wt.% CaO magnesium alloy in plaster molding covered a variety of approaches. Specific to the manufacture of stents, different process conditions were investigated and optimized in order to obtain castings with high metal sanity. Figure 5.24 illustrates the Model 1 stent casting fabricated under the conditions **YV**, **Y**, and **N**, and using the optimal casting variables for each one. In comparing the cast stents, and although both conditions **YV** and **Y** resulted in successful thin-walled cavity filling, the casting following condition **N** produced a 0.4 mm magnesium stent that presented a better surface finish and metallic sanity, which followed the discussion line of the previous subchapters. Using vacuum for condition **YV** produced a slight level of superficial magnesium reactions in the filling system zone, whereas Y_2O_3 layers slightly affected the dimensional accuracy of the molding cavities in condition **Y**.

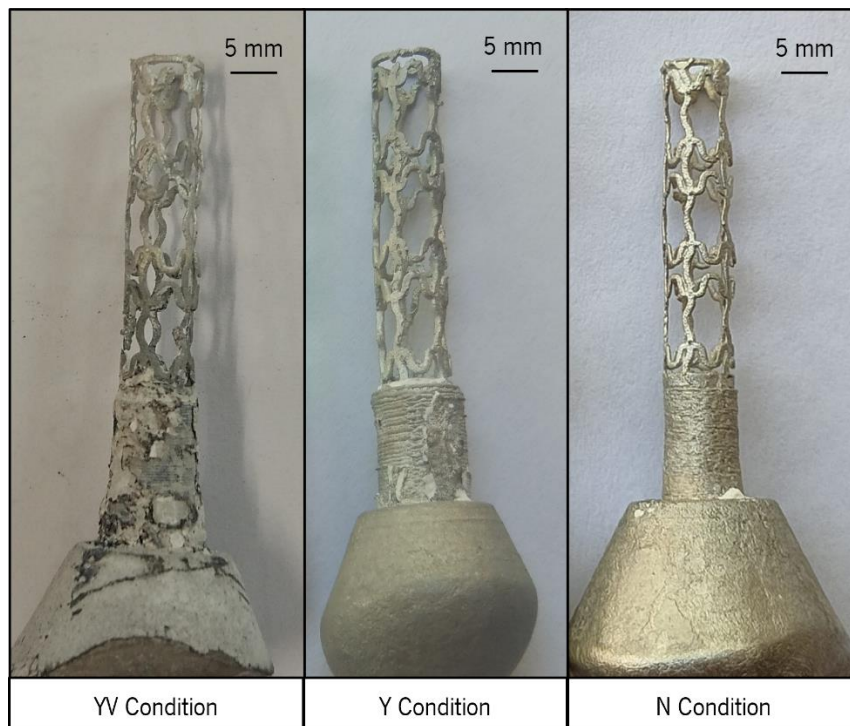


Figure 5.24: Comparison of Model 1 stent casting applying different casting conditions.

For a better understanding of the cavity filling quality when condition **N** was applied, an X-ray μ CT analysis was performed for both cast stent models, as shown in Figure 5.25. The analysis was performed according to the software used in case study 2 of Chapter 4 (Avizo) and using the

μ CT equipment from SkyScan 1275 (Bruker, μ CT, Kontich, Belgium). With this technique, images can be reconstructed with realistic definition, which allows for the inspection of the stent in a volumetric view. Table 5.6 summarizes the main parameters employed in acquiring the image shown in Figure 5.25.

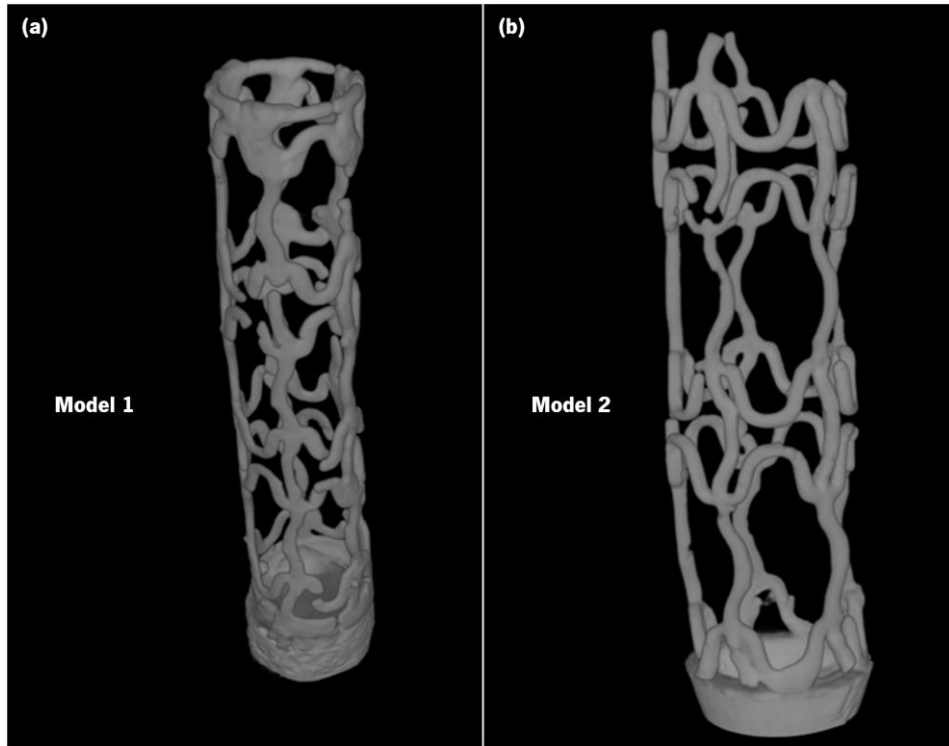


Figure 5.25: Micro-CT for both cast stents: (a) Model 1, and (b) Model 2.

Table 5.6: X-ray μ -CT scan parameters in Figure 5.25.

Stent model	Object to Source (mm)	Camera to Source (mm)	Source Voltage (kV)	Source Current (μ A)	Image Pixel Size (μ m)	Exposure time (ms)	Rotation Step (deg)	Frame Averaging	Filter
1	70.539	286.0	65	153	20.00	58	0.500	5	Al 1 mm
2	105.809	286.0	65	153	30.00	58	0.500	3	Al 1 mm

A more realistic view of the casting quality can be seen in Figure 5.25, which demonstrates the high geometric and dimensional rigor of the stent cavity filling compared to the initial 3D model fabricated by additive manufacturing. While there are some cavity filling failures and volume deficiencies in some stent ribs, these problems may result from the casting process and the imperfect 3D printing of the initial models. Additive manufacturing is often associated with printing

defects and material accumulation during the printing procedure. Figures 5.26 and 5.27 highlight some printing issues resulting from the additive manufacturing process, which were recorded through the X-ray microcomputed tomography analysis. The plaster investment casting process further reproduces part of these defects in the final metallic samples.

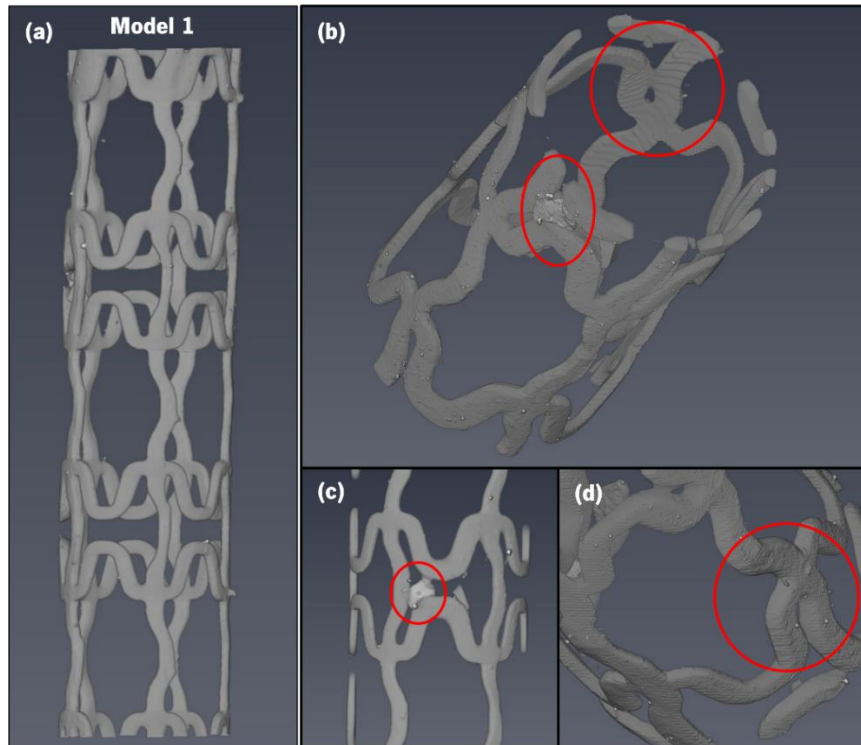


Figure 5.26: Micro-CT of the Model 1 printed stent: (a) 3D model reconstruction showing printing failures, such as (b) scars, (c) excess material, and (d) small pits.

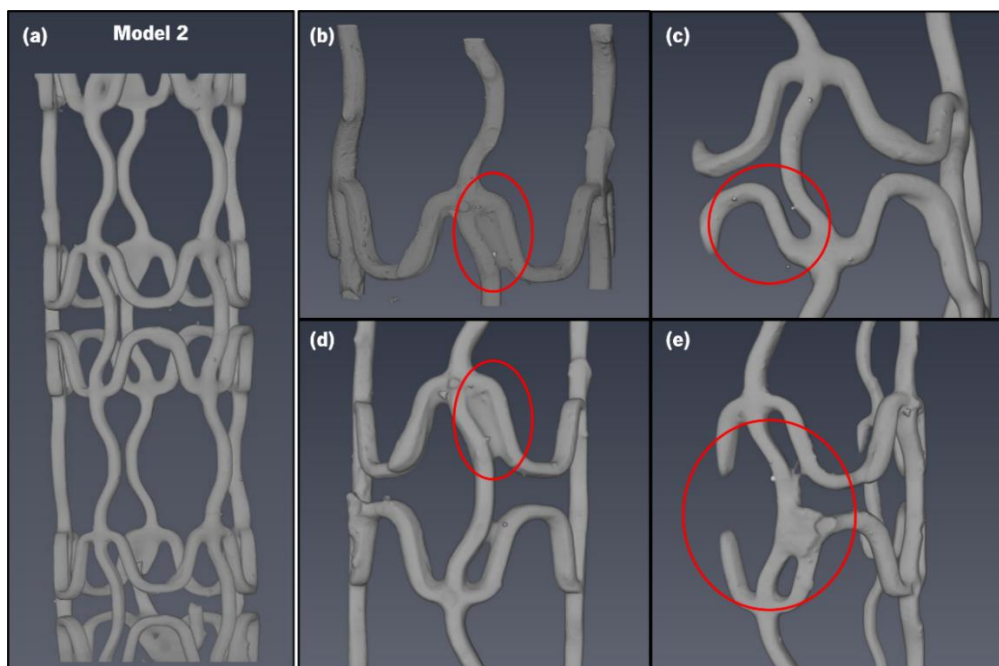


Figure 5.27: Micro-CT of the Model 2 printed stent: (a) 3D model reconstruction showing printing failures, such as (b)(d) excess material, (c) small pits, and (e) dimensional inaccuracies.

This research discusses at length the importance of using the Yttria coating, either for its positive influence on the mitigation of mold-metal reactions, or its negative impact on thermal stability, which adversely damages the molding cavities and ultimately affects the quality of the final castings.

In order to understand in-depth the effect of applying the optimized thermal processing to the plaster moldings on the investment casting of stents, an X-ray μ CT analysis was performed in one casting under the condition **YV**. The molding was analyzed with penetrative X-rays of 80 kV and 125 μ A, in high-resolution mode with a pixel size of 40 μ m and 38 ms of exposure time. Figure 5.28 illustrates how the Yttria remains inside the molding cavities after the 3D model elimination. Although the Yttria layers are more stable along the cavities (Figure 5.28a and d), the X-Y plane of the molding (Figure 5.28c) shows a break in the Y_2O_3 layer, which compromises the mold-metal barrier and interferes with Mg casting effectiveness. Moreover, it was found through 3D reconstruction (Figure 5.28b) that some discontinuities were visible along the length of the stent, indicating that the coating layer had been damaged. It is possible that Yttria's thermal instability causes this phenomenon as a result of the thermal cycle, although to a lesser extent, as expected, or by the poor adhesion between the coating and the resin model. Castings processed under conditions **Y** and **YV** revealed that, in addition to the decreased effectiveness of mold-metal protection, the breaking of the Y_2O_3 layers also caused a poorer surface finish.

As a result, the present study suggests that the use of Y_2O_3 as a refractory is dependent on the casting conditions. It shows positive results in castings in which vacuum is required since it can significantly increase the cavity filling. As shown in case study 2 of Chapter 4 for the fluidity study of thin-walled samples, the use of Yttria is, therefore, a mandatory requirement for castings of lower thickness. In the case of fabricating Model 1 stents, even though the ribs are only slightly thinner, their length is sufficient to achieve a successful casting without using a vacuum atmosphere and without using a Yttria coating.

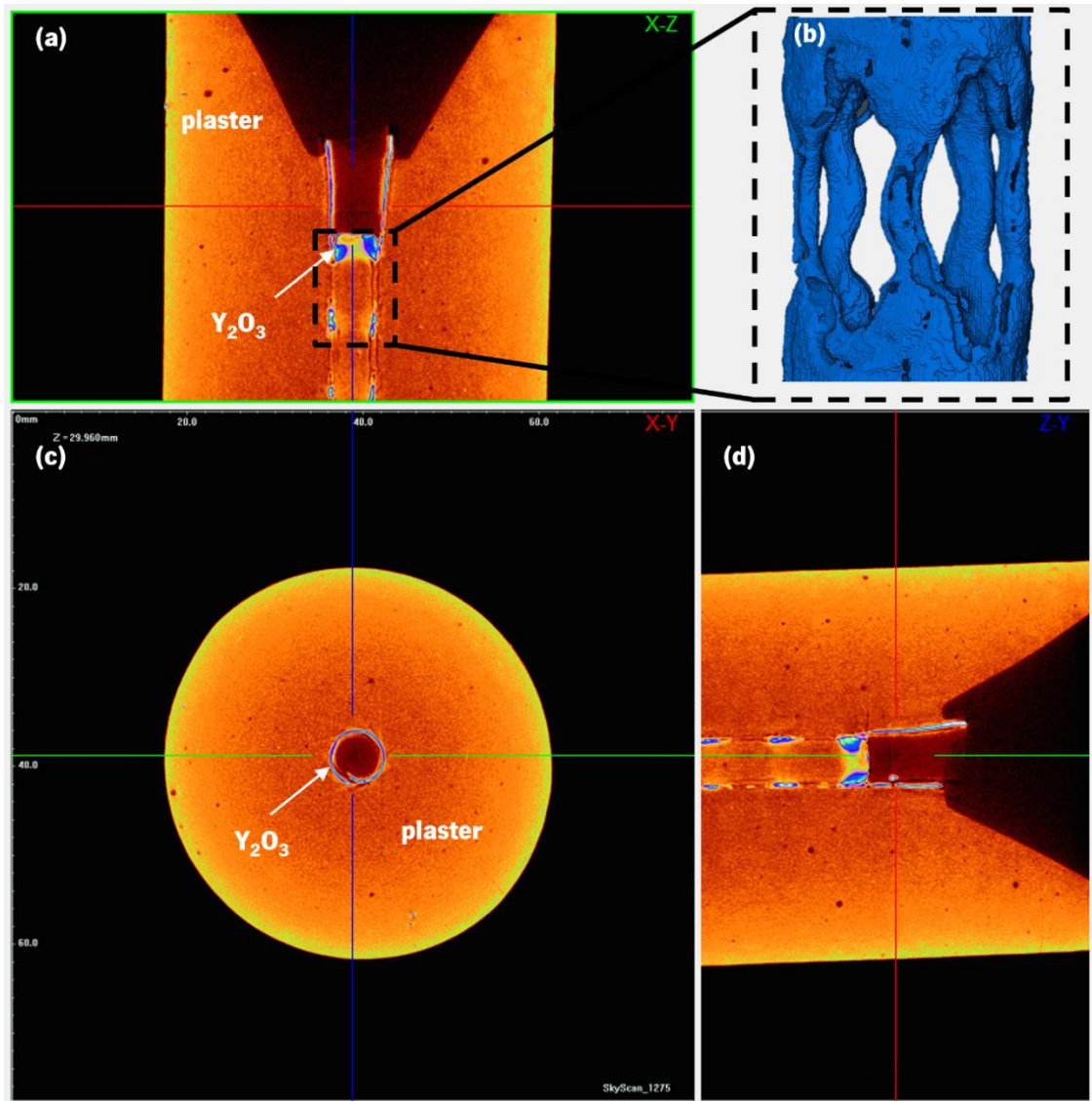


Figure 5.28: micro-CT of the Model 1 cast stent for condition YV: (a) X-Z plane, (b) isometric view of X-Z plane, (c) X-Y plane, and (d) Z-Y plane.

Contrasting conditions **N** and **YV**, despite the increase of knowledge about investment casting of magnesium alloys in recent years, there are no comparable studies in the scientific literature that enable to understand and justify the obtained results. Based on the practical sensitivity acquired throughout this work, the successful application of this process under both conditions seems to be attributed essentially to two important factors: (i) the casting parameters applied, and (ii) the magnesium alloy used.

Regarding the (i) casting parameters, the use of a vacuum atmosphere seems to be the predominant factor for the existence of reactions in the condition **YV**, which is not observed for condition **N**. The phenomena observed experimentally led to the formulation of a theory that requires further analysis and verification as quantitative evidence, but which is in conformity with

the obtained results. This study reports that during the melting phase of the used magnesium alloy, under the condition **N**, an appropriate metal melting temperature, between 650 °C and 720 °C, ensures that the liquid metal remains chemically stable. Consequently, there is no vaporization of magnesium and no reaction between the magnesium and the atmosphere within the furnace, as would be expected. In the absence of a vacuum atmosphere, the stability of the liquid metal can be explained due to the formation of a small protective oxide film, formed at the metal surface, by the reaction of magnesium with oxygen to form magnesium oxide. Several advantages are associated with the formation of this surface oxide layer in light metals, mainly aluminum, as described by Czerwinski [223, 235] and Tan *et al.* [236]. In this case, since the used furnace has a volume of about 2 dm³, the percentage of oxygen available in its atmosphere, approximately 20 % (ambient atmosphere), seems to correspond to the ideal amount of free oxygen needed to react with the surface magnesium to form MgO, which constitutes a protective barrier for the liquid metal. Once all the oxygen has been consumed to form the protective oxide film, there is no more oxygen available to produce undesirable reactions in the system.

Further, magnesium oxide acted as a barrier to the passage of other elements, both in diffusion and penetration, leading to harmful reactions. Therefore, the molten metal gains greater stability, resulting in higher surface tension. During the metal pouring process, this increase in surface tension of the liquid Mg appears to be sufficient to prevent the contact mold-metal, avoiding exothermic reactions involving the Mg and the SiO₂ from the plaster. The small amount of magnesium poured in each casting, as well as the involved thin-walled cavities, result in rapid metal solidification, which diminishes the time available for reactions to occur. Thus, Mg remains stable from melting to solidification, showing good metal purity and allowing successful castings. As long as there is oxygen available, Mg will react with oxygen. So, a limited amount of oxygen in the melting atmosphere seems to be one of the most crucial factors in preventing undesirable reactions. On the other hand, the presence of an adequate amount of O₂ is also a necessary condition for forming of the protective layer of MgO that guarantees protection to the liquid metal.

Considering the condition YV, and as shown by the results of case study 2 (fluidity study - Chapter 4), the vacuum atmosphere seems to constitute the critical condition for the occurrence of reactions. For this casting condition, as opposed to condition **N**, the formation of the protective layer of MgO is compromised by the action of the vacuum pump. This phenomenon can be observed experimentally during the magnesium melting process. After reaching the melting point, the liquid metal devoid of an adequate protective oxide layer, and after the incubation period of the

first oxidation stage [236], exhibits very reactive response to the increase in temperature and begins to react with the residual elements inside the furnace. Additionally, the vacuum may be significantly altering the thermodynamic properties of the furnace interior and the alloy, causing more vaporization of magnesium and the occurrence of reactions at temperatures lower than expected. Although a slight formation of MgO can be formed on the surface of the liquid metal, due to the residual O existing, it is quickly pulled by the vacuum pump and transported to the crucible and molding walls, as shown in Figure 5.29. Under these circumstances, and since the liquid metal is relatively reactive and unprotected, the occurrence of reactions with other residual elements in the atmosphere and with the molding walls is inevitable. Furthermore, the zones in which the metal remains liquid for a longer period of time allow for greater rates of reactions. This is evidenced by the formation of small superficial reaction layers in castings under the condition **YV**, being substantially reduced if Yttria coatings are used.

These phenomena point to the fact that the action of vacuum prevents the liquid metal from forming the protective oxide it needs to prevent reactions between magnesium and the surrounding elements, as well as decreases the surface tension of the molten metal. Even though a vacuum atmosphere contributes positively to the prevention of reactions, in particular in high vacuum systems, the present research work demonstrates the necessity of a limited amount of oxygen to permit the formation of a protective layer of magnesium oxide. The scientific community still does not have a perfectly formulated theory that describes the concept of surface tension of liquid metals. This is due to the high reactivity of liquid metals at high temperatures, as well as the high sensitivity of surface tension to impurities. Thus, mainly for magnesium casting, other tests and analyzes are necessary to justify and validate the obtained results.

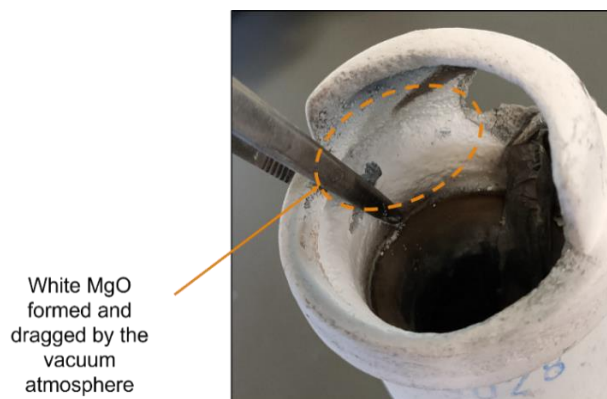


Figure 5.29: MgO formed on the crucible during the investment casting for condition YV.

Considering the (ii) magnesium alloy used, Figure 5.30 represents an experimental attempt to apply the same processing methodology to the commercial AZ91D magnesium alloy. The casting was performed under the casting condition **N** (no vacuum and no Yttria coating), which inhibited the occurrence of reactions in the handling of the AZ91D-1 wt.% CaO magnesium alloy during this work. This casting, however, was seriously compromised by severe reactions and high vaporization of magnesium, both during the melting phase (Figure 5.30a) as well as after magnesium pouring, as the result of reactions at the mold-metal interface. In this case, no protective oxide surface layer was formed. Instead, magnesium was continuously oxidized with elements from the furnace atmosphere, later leading to a reactive casting that resulted in oxide nodules with cauliflower structure (Figure 5.30b), as reported by Tan *et al.* [236]. As a result of this evidence, it can be concluded that the magnesium alloy used is also an important factor for the process's effectiveness.

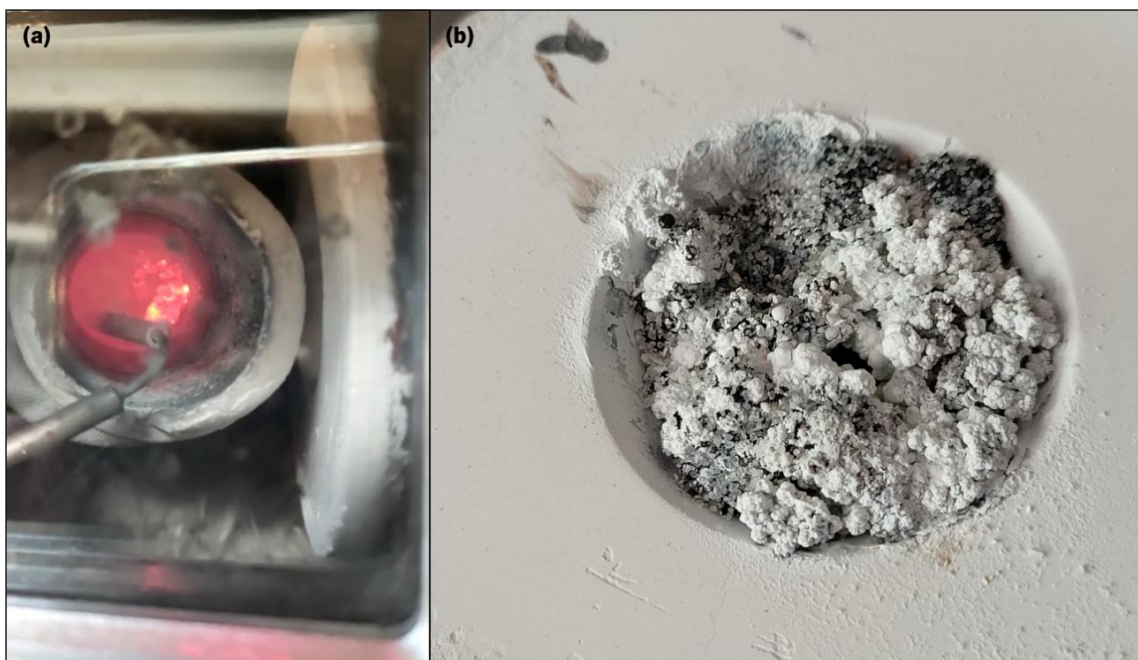


Figure 5.30: Stent investment casting using the commercial AZ91D magnesium alloy for condition YV: (a) during melting, and (b) after pouring.

5.5. Summary and Conclusions

This chapter applied the optimized methodology for the investment casting of AZ91D-1 wt.% CaO magnesium alloy in plaster molding to obtain stents, applying the casting conditions defined in the previous chapter. Two stent models with rib thicknesses of 0.4 mm and 0.8 mm

were successfully cast, demonstrating complete cavity filling, good surface finish, and high dimensional and geometrical accuracy. In order to characterize the surface and microstructure of the castings, OM and SEM were used to perform EDS and XRD analyzes. Different behaviors were reported by comparing different casting conditions, and different explanations were presented to justify the observed phenomena and the obtained results. Based on the experiments and analyzes carried out, the following conclusions can be drawn:

- The optimization of the filling design in investment casting using plaster moldings is detrimental to the manufacture of stents. The analysis of the molding cooling behavior showed significant temperature losses at the periphery a few minutes following the thermal cycle, which negatively influenced the flow of the liquid metal in the molding cavities in these areas, affecting especially the filling length of thin-walled parts. Thus, a single and direct filling method results in a more successful stent casting.
- The use of vacuum assistance to improve the fluidity of the alloy, in combination with the application of the casting condition **YV**, led to the casting of stents with a higher rate of cavity filling and an almost complete absence of reactions during the process, as well as high geometric rigor compared to the initial 3D models fabricated by additive manufacturing. Coated samples with Y_2O_3 layers revealed better metal purity in addition to a more uniform and refined microstructure. In the case of uncoated sample castings, several defects were observed affecting fluidity, dimensional and surface quality, as well as microstructure sanity. In Chapter 3, it was shown that severe reactions and oxidation occurred at the mold-metal interface in which no Yttria coating was applied (condition **N**). This resulted in the formation of reaction products that contaminated the microstructure of the magnesium alloy. According to these results, Y_2O_3 coatings should always be used in vacuum-environment castings.
- It should be noted that the registered values for oxygen concentrations (O) were only a complementary part of the analysis. Nevertheless, it shows a more pronounced degree of oxidation in the peripheral zones for both models analyzed, especially in those models in which no coating was applied.
- The casting of stents can be successfully achieved in any of the three conditions tested (**Y**, **YV**, and **N**). However, condition **N** guarantees the highest quality castings for both stent models. According to the stent model, successful Mg casting is dependent on the balance

between pouring and molding temperatures, which can vary according to defined safe values, as shown in Figure 5.31.

- In Chapter 4, it was concluded that condition Y was ineffective in this type of application. The obtained results confirmed that Yttria should only be used for castings in which a vacuum atmosphere is required, such as for the manufacturing of thin-walled magnesium parts. If the samples are thicker, the Y_2O_3 layers can create resistance to the metal flow and affect the castings' final surface roughness. Furthermore, the Yttria degradation phenomenon allows the liquid magnesium to penetrate through the coating interstices, creating a "cracking husk" around the metallic sample and increasing the diffusion of elements in the mold-metal interface. As a result, the surface samples react faster, particularly when the vacuum is applied.
- Although the proposed methodology provides effective thin-walled magnesium castings, the final samples revealed some defects. According to the analyzes carried out, these imperfections are a consequence of the casting process and the original 3D samples, which were created through additive manufacturing.
- The obtained results for conditions **N** and **YV** are based on two important factors: (i) the casting parameters implemented and (ii) the magnesium alloy used. Pressure and temperature were the key factors determining the greater or lesser occurrence of magnesium reactions, both during the melting and pouring phases. On the other hand, AZ91D-1 wt.% CaO Mg-Eco alloy has shown greater chemical and thermal stability than the commercial AZ91D magnesium alloy, which is critical to successfully applying the investment casting process in plaster molding. The use of a vacuum atmosphere (condition YV) for the casting of AZ91D-1 wt.% CaO magnesium alloy seems to inhibit the liquid metal from forming and preserving the protective oxide layer of MgO along the surface, which happens in castings under the condition **N**. For this condition, the oxide layer ensures the chemical stability of the molten metal, increases its surface tension, and prevents further magnesium reactions.

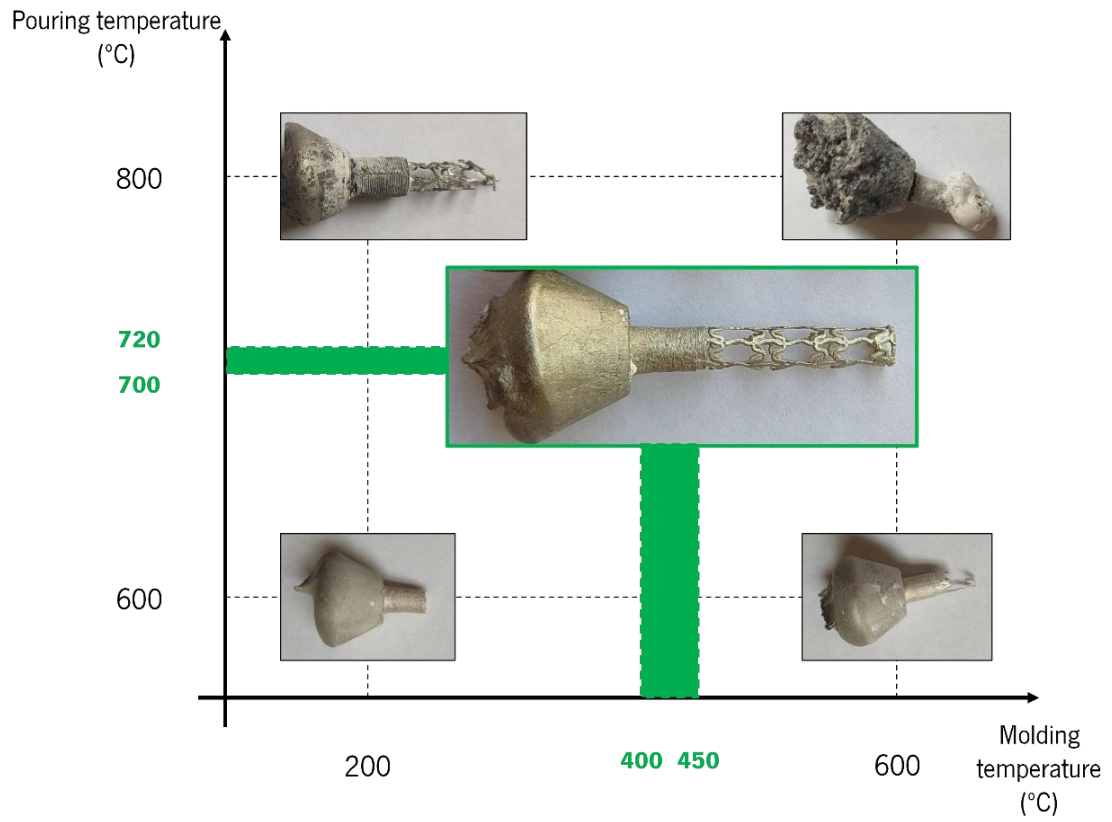


Figure 5.31: Optimal range of temperatures for stent manufacturing under the casting condition N.

The present thesis reflects extensive experimental work. In total, 4.5 kilograms of magnesium alloy were consumed. Since it was indicated that 10 grams of magnesium were required for each thin-walled casting, it means performing 450 castings!

Chapter 6. CONCLUDING REMARKS

6.1. Final Conclusions

An innovative methodology for manufacturing biodegradable magnesium stents has been presented in this thesis. The method consisted of the combination of additive manufacturing with investment casting of AZ91D-1 wt.% CaO magnesium alloy using plaster molding. Several aspects have been discussed throughout this research, including the printing of the 3D model, the application of the coating, the manufacture of the molding, and the casting processing. Novel methods and approaches have been proposed and considered throughout the document as well. The main conclusions are emphasized in this section, seeking to respond to the Research Objectives (**RO's**) initially outlined in Chapter 1.

Chapter 2 reviews the literature on the most pertinent issues related to the handling of magnesium alloys and the fabrication of stents. This chapter describes different magnesium alloy processing approaches, emphasising the addition of elements and the liquid metal treatment through the application of an ultrasound technique. Such approaches can significantly contribute to the development of new magnesium alloys with enhanced physical, chemical, and mechanical properties. These alloys can be utilized to replace the most commonly used metallic structural materials, such as iron, steel, and aluminum. Regarding the investment casting of magnesium alloy in ceramic molding, it is known that a number of methods have been developed and applied to mitigate the effects of reactions that occur during melting and pouring. Besides ceramic shell molding, other methods have also been reported to minimize the reaction issue, such as refractory coatings and protective fluxes and gases. However, none of these studies provided effective solutions to overcome the reactivity in the process, which is still poorly understood. Concerning stent manufacturing, various procedures are detailed, including different materials and conventional and non-conventional processes. Considering the main limitations associated with the use of permanent stents, the need for biodegradable stents manufactured with biodegradable

materials is adequately explored, although some important properties must be taken into account in order to ensure the reliable functional performance of the biomedical devices. Regarding the stent fabrication, laser cutting is the primary method of manufacturing stents. However, it is a process that involves several steps and introduces thermal issues that may later compromise the effectiveness of these devices, especially those made from magnesium alloys. In addition to some advantageous characteristics of most processes presented in Table 2.1, a clear opportunity for progress in the evolution of stent models and their fabrication was found. This is why a hybrid methodology combining additive manufacturing and investment casting in plaster molding is proposed in this work for magnesium casting, allowing time and cost savings.

Different methods for printing thin-walled parts are discussed in Chapter 3. It has been demonstrated that SLA printing offers better results than FDM printing, namely in terms of surface roughness and detail accuracy. In regard to printing materials, the resin used in SLA has a better surface wettability than PLA used in FDM, which leads to better coating adhesion. FDM technology, however, provides time and cost savings. Therefore, this study presents an optimization technique combining both printing processes, using SLA for the printing of stent models and FDM for the printing of the filling gating system. The mold-metal interface between liquid metal and plaster moldings is also characterized in this chapter through an experimental case study. Different protective coatings for magnesium investment casting in plaster molding are studied and analyzed. The Yttria coating was found to be more effective than Alumina and Sand-based slip coatings in preventing mold-metal reactions. As a result, it should be applied by the dipping method in a few layers due to its unstable stability at higher temperatures. Based on the obtained castings, the effectiveness of Y_2O_3 is investigated and confirmed in the case study. The samples using Yttria as a refractory coating evidenced a cleaner surface and a more uniform microstructure. In contrast, extreme reaction products and porosity defects have been detected in castings in which no coating has been applied to the 3D printed models.

Considering the Yttria instability at elevated temperatures, a thermal cycle optimization is proposed in Chapter 4 for thin-walled magnesium investment castings. Based on TGA and DTG analyzes, a new thermal cycle is recommended that involves a maximum temperature of 450 °C in order to ensure the proper burning of polymeric materials and the stability of the plaster solution. Furthermore, the optimal casting parameters for the AZ91D-1 wt.% magnesium alloy are experimentally optimized in this work through a fluidity case study. The use of a vacuum atmosphere during melting and pouring (condition **YV**) is shown to be vital to the occurrence of

magnesium reactions. Even though it contributes positively to cavity filling, especially for thin-walled parts, it also appears to significantly enhance the reaction between liquid magnesium and the surrounding elements. In general, vacuum is necessary for successful cavity filling of thin-walled castings, although Yttria coating plays a crucial role in mitigating this reaction rate. The casting of magnesium without Y_2O_3 coating and vacuum (condition **N**) is recommended for thicker parts. The result is a lower level of surface contamination and a better surface finish, although their fluidity may be affected. In general, a compromise between the molding and pouring temperatures is recommended for successful magnesium casting, since higher temperatures may potentiate more reactions, but will also guarantee a greater cavity filling length. The application of Yttria coating without vacuum assistance (condition **Y**) reveals to be ineffective for magnesium investment casting because the cracking into the molding cavities acts as a barrier to the cavity filling.

The process of manufacturing magnesium stents through investment casting in plaster molding is described and characterized in Chapter 5. In this work, magnesium stents with thicknesses of 0.4 mm and 0.8 mm are successfully fabricated using the proposed methodology, with a good surface finish, high degree of geometric and dimensional rigor, as well as being free of any reaction content. For that, a single and direct filling casting must be adopted. Despite the fact that complete cavity filling can be achieved for any tested casting condition, the highest quality final casting is achieved when Yttria coating and vacuum are not used during the processing (condition **N**). In this condition, oxygen does not react with the surrounding elements. The residual oxygen present in the furnace produces MgO, which acts as a protective oxide on the melt surface, thereby increasing the surface tension of the metal and preventing mold-metal contact. As demonstrated in Chapter 4, the use of vacuum presupposes the application of a Yttria coating, which improves the fluidity of the alloy and the cavity filling, although a surface reaction layer can be created in the process. This means that the casting condition to be used depends on the final application, as using vacuum guarantees better thin-wall cavity filling, while the absence of vacuum inhibits magnesium reactions. The same compromise exists for pouring and molding temperatures since higher temperatures ensure better cavity filling and lower temperatures mitigate reactions.

To sum up, it was demonstrated and proved that the proposed methodology is effective for the thin-walled investment casting of AZ91D-1 wt.% CaO magnesium alloy in plaster molding, optimized for stent manufacturing. This research work offers an opportunity to fill some gaps in the literature on the processing of magnesium alloys, which are important for the necessary expansion of these alloys into the foundry sector. This methodology also allows a more realistic assessment

of the potential of investment casting in plaster molding, which has received relatively scant attention in the industrial field.

6.2. Future Work

This work examined and discussed the main issue associated with magnesium investment casting in plaster molding, namely for thin-walled applications. The obtained experimental results constitute advances in the state-of-the-art, however further developments are needed to complement the existing facts and address some of their limitations, extending their applicability. In that sense, some suggestions for future research activities in this field are presented below.

The mold-metal interaction evaluated in this work can be extended to other experimental cases, including thicker samples. Thus, higher solidification times would be expected and its influence on the occurrence of reactions after the pouring could be more deeply exploited.

This work has demonstrated the process's effectiveness; however, further mechanical and corrosion characterization is required in order to validate the proposed methodology and understand its range of applications. There is a lack of information in the literature regarding investment casting magnesium alloys in plaster molding. Therefore, the mechanical properties and degradation rate of magnesium alloy samples obtained in this thesis are of particular significance.

Regarding the previous point, other strategies can be employed to improve the properties of the cast samples. Applying the proposed methodology of this work, methods such as liquid metal treatment by ultrasonic technique and chemical refinement by addition of elements could be tested to analyze their influence on the final cast parts.

In this study, it was observed that thermodynamic characteristics play an important role during the processing of magnesium alloys. Even though the cavity filling simulation is a challenging task given the large number of factors involved, a numerical study of the processing performed in this research would provide an additional tool for understanding all phenomena. Additionally, it would be possible to reduce the experimental content and save time and money.

Lastly, it was seen that the use of vacuum seems to directly influence the surface tension of the magnesium alloy for different casting conditions, which seems to be related to the reaction rate that can occur during the melting and pouring phases. Characterization of the surface tension of the liquid magnesium under different casting conditions is therefore necessary in order to better explain the obtained results.

REFERENCES

- [1] M. Hedin, 'The origin of the word *stent*', *Acta Radiol.*, vol. 38, no. 6, pp. 937–939, Nov. 1997, doi: 10.1080/02841859709172106.
- [2] World Health Organization, 'The top 10 causes of death', 2020. <https://www.who.int/news-room/fact-sheets/detail/the-top-10-causes-of-death> (accessed Jul. 15, 2021).
- [3] D. N. Ghista and F. Kabinejadian, 'Coronary artery bypass grafting hemodynamics and anastomosis design: a biomedical engineering review', *Biomed. Eng. Online*, vol. 12, no. 1, p. 129, 2013.
- [4] T. Simard, B. Hibbert, F. D. Ramirez, M. Froeschl, Y.-X. Chen, and E. R. O'Brien, 'The Evolution of Coronary Stents: A Brief Review', *Can. J. Cardiol.*, vol. 30, no. 1, pp. 35–45, Jan. 2014, doi: 10.1016/j.cjca.2013.09.012.
- [5] S. Amani, G. Faraji, H. Kazemi Mehrabadi, K. Abrinia, and H. Ghanbari, 'A combined method for producing high strength and ductility magnesium microtubes for biodegradable vascular stents application', *J. Alloys Compd.*, vol. 723, pp. 467–476, Nov. 2017, doi: 10.1016/j.jallcom.2017.06.201.
- [6] A. Schuesseler, 'Manufacturing of stents: optimize the stent with new manufacturing technologies', *New Technol. Vasc. Biomater. Fundam. Stent II*, pp. 93–106, 2007.
- [7] D. Mazzaccaro, M. T. Occhiuto, S. Stegher, P. Righini, G. Malacrida, and G. Nano, 'New technologies in vascular surgery: San Donato's experience in the last decades', *Eur. Heart J. Suppl.*, vol. 18, no. suppl E, pp. E37–E41, Apr. 2016, doi: 10.1093/eurheartj/suw021.
- [8] Lim Ing Haan Cardiology Clinic, 'Coronary Angioplasty and Stenting'. <http://drliminghaan.com/treatments-and-services/coronary-angioplasty-and-stenting/>
- [9] S. Garg and P. W. Serruys, 'Coronary Stents', *J. Am. Coll. Cardiol.*, vol. 56, no. 10, pp. S43–S78, Aug. 2010, doi: 10.1016/j.jacc.2010.06.008.
- [10] A. G. Demir and B. Previtali, 'Additive manufacturing of cardiovascular CoCr stents by selective laser melting', *Mater. Des.*, vol. 119, pp. 338–350, Apr. 2017, doi: 10.1016/j.matdes.2017.01.091.

- [11] L. Wang, G. Fang, L. Qian, S. Leeflang, J. Duszczek, and J. Zhou, 'Forming of magnesium alloy microtubes in the fabrication of biodegradable stents', *Prog. Nat. Sci. Mater. Int.*, vol. 24, no. 5, pp. 500–506, Oct. 2014, doi: 10.1016/j.pnsc.2014.08.006.
- [12] L. Mao *et al.*, 'A promising biodegradable magnesium alloy suitable for clinical vascular stent application', *Sci. Rep.*, vol. 7, p. 46343, Apr. 2017, doi: 10.1038/srep46343.
- [13] H. Matsuoka *et al.*, 'Bare metal stent implantation for in-stent restenosis with a drug-eluting stent', *J. Cardiol.*, vol. 55, no. 1, pp. 135–138, Jan. 2010, doi: 10.1016/j.jjcc.2009.04.006.
- [14] H. Hermawan, D. Dubé, and D. Mantovani, 'Developments in metallic biodegradable stents☆', *Acta Biomater.*, vol. 6, no. 5, pp. 1693–1697, May 2010, doi: 10.1016/j.actbio.2009.10.006.
- [15] M. Moravej and D. Mantovani, 'Biodegradable Metals for Cardiovascular Stent Application: Interests and New Opportunities', *Int. J. Mol. Sci.*, vol. 12, no. 12, pp. 4250–4270, Jun. 2011, doi: 10.3390/ijms12074250.
- [16] H. Meng, J. Liao, Y. Zhou, and Q. Zhang, 'Laser micro-processing of cardiovascular stent with fiber laser cutting system', *Opt. Laser Technol.*, vol. 41, no. 3, pp. 300–302, Apr. 2009, doi: 10.1016/j.optlastec.2008.06.001.
- [17] R. Erbel *et al.*, 'Temporary scaffolding of coronary arteries with bioabsorbable magnesium stents: a prospective, non-randomised multicentre trial', *The Lancet*, vol. 369, no. 9576, pp. 1869–1875, 2007.
- [18] J. Wiebe, H. M. Nef, and C. W. Hamm, 'Current Status of Bioresorbable Scaffolds in the Treatment of Coronary Artery Disease', *J. Am. Coll. Cardiol.*, vol. 64, no. 23, pp. 2541–2551, Dec. 2014, doi: 10.1016/j.jacc.2014.09.041.
- [19] D. Lim *et al.*, 'Suggestion of Potential Stent Design Parameters to Reduce Restenosis Risk driven by Foreshortening or Dogboning due to Non-uniform Balloon-Stent Expansion', *Ann. Biomed. Eng.*, vol. 36, no. 7, pp. 1118–1129, Jul. 2008, doi: 10.1007/s10439-008-9504-1.
- [20] R. A. Byrne, M. Joner, and A. Kastrati, 'Stent thrombosis and restenosis: what have we learned and where are we going? The Andreas Grüntzig Lecture ESC 2014', *Eur. Heart J.*, vol. 36, no. 47, pp. 3320–3331, Dec. 2015, doi: 10.1093/eurheartj/ehv511.

- [21] G. Lemesle, C. Delhaye, L. Bonello, A. de Labriolle, R. Waksman, and A. Pichard, 'Stent thrombosis in 2008: Definition, predictors, prognosis and treatment', *Arch. Cardiovasc. Dis.*, vol. 101, no. 11, pp. 769–777, Nov. 2008, doi: 10.1016/j.acvd.2008.10.006.
- [22] J. Kakadiya, 'Causes, symptoms, pathophysiology and diagnosis of atherosclerosis—a review', *PharmacologyOnline*, vol. 3, pp. 420–442, 2009.
- [23] M. Azaouzi, A. Makradi, and S. Belouettar, 'Deployment of a self-expanding stent inside an artery: A finite element analysis', *Mater. Des.*, vol. 41, pp. 410–420, Oct. 2012, doi: 10.1016/j.matdes.2012.05.019.
- [24] W. Wu, W.-Q. Wang, D.-Z. Yang, and M. Qi, 'Stent expansion in curved vessel and their interactions: A finite element analysis', *J. Biomech.*, vol. 40, no. 11, pp. 2580–2585, Jan. 2007, doi: 10.1016/j.jbiomech.2006.11.009.
- [25] A. J. Guerra, J. Farjas, and J. Ciurana, 'Fibre laser cutting of polycaprolactone sheet for stents manufacturing: A feasibility study', *Opt. Laser Technol.*, vol. 95, pp. 113–123, Oct. 2017, doi: 10.1016/j.optlastec.2017.03.048.
- [26] Y. Zhu *et al.*, 'The current status of biodegradable stent to treat benign luminal disease', *Mater. Today*, May 2017, doi: 10.1016/j.mattod.2017.05.002.
- [27] H. Y. Ang, H. Bulluck, P. Wong, S. S. Venkatraman, Y. Huang, and N. Foin, 'Bioresorbable stents: Current and upcoming bioresorbable technologies', *Int. J. Cardiol.*, vol. 228, pp. 931–939, Feb. 2017, doi: 10.1016/j.ijcard.2016.11.258.
- [28] Magnesium Elektron Ltd, 'An Introduction to Machining Magnesium', Luxfer MEL Technologies, 2017. [Online]. Available: www.magnesium-elektron.com
- [29] Leszek A. Dobrzanski, Menachem Bamberger, and George E. Totten, Eds., *Magnesium and Its Alloys: Technology and Applications*. 2019.
- [30] H. Friedrich and S. Schumann, 'Research for a “new age of magnesium” in the automotive industry', *J. Mater. Process. Technol.*, vol. 117, no. 3, pp. 276–281, 2001.
- [31] T. Xu, Y. Yang, X. Peng, J. Song, and F. Pan, 'Overview of advancement and development trend on magnesium alloy', *J. Magnes. Alloys*, vol. 7, no. 3, pp. 536–544, Sep. 2019, doi: 10.1016/j.jma.2019.08.001.
- [32] G. Arruebarrena *et al.*, 'Development of Investment-Casting Process of Mg-Alloys for Aerospace Applications', *Adv. Eng. Mater.*, vol. 9, no. 9, pp. 751–756, Sep. 2007, doi: 10.1002/adem.200700154.

- [33] E. Piyush, R. Raghu, M. S. Rakesh, and S. G. Sriram, 'Magnesium Alloy Casting Technology for Automotive Applications- A Review', vol. 04, no. 10, p. 7.
- [34] F. Pan, M. Yang, and X. Chen, 'A Review on Casting Magnesium Alloys: Modification of Commercial Alloys and Development of New Alloys', *J. Mater. Sci. Technol.*, vol. 32, no. 12, pp. 1211–1221, Dec. 2016, doi: 10.1016/j.jmst.2016.07.001.
- [35] F. Pan, M. Chen, J. Wang, J. Peng, and A. Tang, 'Effects of yttrium addition on microstructure and mechanical properties of as-extruded AZ31 magnesium alloys', *Trans. Nonferrous Met. Soc. China*, vol. 18, pp. s1–s6, Dec. 2008, doi: 10.1016/S1003-6326(10)60164-1.
- [36] Jiangxi Provincial Engineering Research Center for Magnesium alloys, GanNan Normal University, Ganzhou 341000, PR China and B. Han, 'Preparation of Yttrium-based Rare Earth Conversion Coating and Its Effect on Corrosion Resistance of AZ91D Magnesium Alloy', *Int. J. Electrochem. Sci.*, pp. 374–385, Jan. 2017, doi: 10.20964/2017.01.53.
- [37] A. Elsayed, E. Vandersluis, S. Lun Sin, and C. Ravindran, 'Inclusions in Permanent Mold Cast Magnesium ZE41A and AZ91D Alloys', *Int. J. Met.*, vol. 11, no. 4, pp. 749–765, Oct. 2017, doi: 10.1007/s40962-016-0119-2.
- [38] L. Wang, R. Lett, S. Felicelli, J. Berry, J. Jordon, and D. Penrod, 'Microstructure and Performance of Four Casting Processes for Magnesium Alloy AZ91', *Int. J. Met.*, vol. 5, no. 4, pp. 37–46, Oct. 2011, doi: 10.1007/BF03355521.
- [39] G. A. Lara-Rodriguez, I. A. Figueroa, M. A. Suarez, O. Novelo-Peralta, I. Alfonso, and R. Goodall, 'A replication-casting device for manufacturing open-cell Mg foams', *J. Mater. Process. Technol.*, vol. 243, pp. 16–22, May 2017, doi: 10.1016/j.jmatprotec.2016.11.041.
- [40] A. Kucharczyk, K. Naplocha, J. W. Kaczmar, H. Dieringa, and K. U. Kainer, 'Current Status and Recent Developments in Porous Magnesium Fabrication', *Adv. Eng. Mater.*, vol. 20, no. 1, p. 1700562, Jan. 2018, doi: 10.1002/adem.201700562.
- [41] R. Radha and D. Sreekanth, 'Insight of magnesium alloys and composites for orthopedic implant applications – a review', *J. Magnes. Alloys*, vol. 5, no. 3, pp. 286–312, Sep. 2017, doi: 10.1016/j.jma.2017.08.003.
- [42] G. Yuan, G. You, S. Bai, and W. Guo, 'Effects of heat treatment on the thermal properties of AZ91D magnesium alloys in different casting processes', *J. Alloys Compd.*, vol. 766, pp. 410–416, Oct. 2018, doi: 10.1016/j.jallcom.2018.06.370.

- [43] X.-Z. Yue, K. Kitazono, X.-J. Yue, and B.-Y. Hur, 'Effect of fluidity on the manufacturing of open cell magnesium alloy foams', *J. Magnes. Alloys*, vol. 4, no. 1, pp. 1–7, Mar. 2016, doi: 10.1016/j.jma.2015.11.007.
- [44] T. P. Duarte, F. J. L. Alves, and R. J. L. Neto, 'Utilização de Moldações Cerâmicas no Fabrico de Moldes Metálicos', *O Molde Rev. Assoc. Indústria Moldes*, vol. 12, pp. 32–41, 1999.
- [45] E. Willbold *et al.*, 'Biocompatibility of rapidly solidified magnesium alloy RS66 as a temporary biodegradable metal', *Acta Biomater.*, vol. 9, no. 10, pp. 8509–8517, 2013.
- [46] F. Witte, 'The history of biodegradable magnesium implants: A review☆', *Acta Biomater.*, vol. 6, no. 5, pp. 1680–1692, May 2010, doi: 10.1016/j.actbio.2010.02.028.
- [47] H. Jafari, M. H. Idris, and A. Ourdjini, 'A Review of Ceramic Shell Investment Casting of Magnesium Alloys and Mold-Metal Reaction Suppression', *Mater. Manuf. Process.*, vol. 28, no. 8, pp. 843–856, agosto 2013, doi: 10.1080/10426914.2013.811729.
- [48] H. Jafari, M. H. Idris, A. Ourdjini, and M. R. Abdul Kadir, 'An investigation on interfacial reaction between in-situ melted AZ91D magnesium alloy and ceramic shell mold during investment casting process', *Mater. Chem. Phys.*, vol. 138, no. 2–3, pp. 672–681, Mar. 2013, doi: 10.1016/j.matchemphys.2012.12.037.
- [49] H. Jafari, M. H. Idris, and A. Ourdjini, 'An alternative approach in ceramic shell investment casting of AZ91D magnesium alloy: In situ melting technique', *J. Mater. Process. Technol.*, vol. 214, no. 4, pp. 988–997, Apr. 2014, doi: 10.1016/j.jmatprotec.2013.11.004.
- [50] S. L. Sin, D. Dubé, and R. Tremblay, 'Interfacial reactions between AZ91D magnesium alloy and plaster mould material during investment casting', *Mater. Sci. Technol.*, vol. 22, no. 12, pp. 1456–1463, Dec. 2006, doi: 10.1179/174328406X148804.
- [51] C.-S. Chen, S.-Y. Lin, N.-K. Chou, Y.-S. Chen, and S.-F. Ma, 'Optimization of Laser Processing in the Fabrication of Stents', *Mater. Trans.*, vol. 53, no. 11, pp. 2023–2027, 2012.
- [52] M. Wang, D. H. Xiao, and W. S. Liu, 'Effect of Si addition on microstructure and properties of magnesium alloys with high Al and Zn contents', *Vacuum*, vol. 141, pp. 144–151, Jul. 2017, doi: 10.1016/j.vacuum.2017.04.005.
- [53] M. Razzaghi, H. Mirzadeh, and M. Emany, 'Unraveling the effects of Zn addition and hot extrusion process on the microstructure and mechanical properties of as-cast Mg–2Al magnesium alloy', *Vacuum*, vol. 167, pp. 214–222, Sep. 2019, doi: 10.1016/j.vacuum.2019.06.013.

- [54] H. Xue, G. Yang, D. Li, Z. Xing, and F. Pan, 'Effects of Yttrium Addition on Microstructure and Mechanical Properties of AZ80–2Sn Magnesium Alloys', *High Temp. Mater. Process.*, vol. 34, no. 8, Jan. 2015, doi: 10.1515/htmp-2014-0095.
- [55] F. Wang, J. Li, J. Liu, D. Lv, P. Mao, and Z. Liu, 'Influences of Ca and Y Addition on the Microstructure and Corrosion Resistance of Vacuum Die-Cast AZ91 Alloy', *Acta Metall. Sin. Engl. Lett.*, vol. 27, no. 4, pp. 609–614, Aug. 2014, doi: 10.1007/s40195-014-0101-z.
- [56] S. Agarwal, J. Curtin, B. Duffy, and S. Jaiswal, 'Biodegradable magnesium alloys for orthopaedic applications: A review on corrosion, biocompatibility and surface modifications', *Mater. Sci. Eng. C*, vol. 68, pp. 948–963, Nov. 2016, doi: 10.1016/j.msec.2016.06.020.
- [57] G. Eddy Jai Poinern, S. Brundavanam, and D. Fawcett, 'Biomedical Magnesium Alloys: A Review of Material Properties, Surface Modifications and Potential as a Biodegradable Orthopaedic Implant', *Am. J. Biomed. Eng.*, vol. 2, no. 6, pp. 218–240, Jan. 2013, doi: 10.5923/j.ajbe.20120206.02.
- [58] J. Koike, 'Dislocation Plasticity and Complementary Deformation Mechanisms in Polycrystalline Mg Alloys', *Mater. Sci. Forum*, vol. 449–452, pp. 665–668, Mar. 2004, doi: 10.4028/www.scientific.net/MSF.449-452.665.
- [59] A. C. Hänzi, A. S. Sologubenko, and P. J. Uggowitzer, 'Design Strategy for Microalloyed Ultra-Ductile Magnesium Alloys for Medical Applications', *Mater. Sci. Forum*, vol. 618–619, pp. 75–82, Apr. 2009, doi: 10.4028/www.scientific.net/MSF.618-619.75.
- [60] D. H. StJohn, M. Qian, M. A. Easton, P. Cao, and Z. Hildebrand, 'Grain refinement of magnesium alloys', *Metall. Mater. Trans. A*, vol. 36, no. 7, pp. 1669–1679, Jul. 2005, doi: 10.1007/s11661-005-0030-6.
- [61] Y. Ding, C. Wen, P. Hodgson, and Y. Li, 'Effects of alloying elements on the corrosion behavior and biocompatibility of biodegradable magnesium alloys: a review', *J. Mater. Chem. B*, vol. 2, no. 14, p. 1912–1933, Apr. 2014, doi: 10.1039/c3tb21746a.
- [62] G. Song, A. Atrens, X. Wu, and B. Zhang, 'Corrosion behaviour of AZ21, AZ501 and AZ91 in sodium chloride', *Corros. Sci.*, vol. 40, no. 10, pp. 1769–1791, Oct. 1998, doi: 10.1016/S0010-938X(98)00078-X.
- [63] F. Witte *et al.*, 'Degradable biomaterials based on magnesium corrosion', *Curr. Opin. Solid State Mater. Sci.*, vol. 12, no. 5, pp. 63–72, 2008.

- [64] Y. C. Li, M. H. Li, W. Y. Hu, P. D. Hodgson, and C. E. Wen, 'Biodegradable Mg-Ca and Mg-Ca-Y Alloys for Regenerative Medicine', *Mater. Sci. Forum*, vol. 654–656, pp. 2192–2195, Jun. 2010, doi: 10.4028/www.scientific.net/MSF.654-656.2192.
- [65] F. D'Errico, 'Bimodal Casting Process of Eco-Mg Series Alloys by Vertical High-Speed Press Machine', in *Magnesium Technology 2019*, V. V. Joshi, J. B. Jordon, D. Orlov, and N. R. Neelameggham, Eds. Cham: Springer International Publishing, 2019, pp. 25–31. doi: 10.1007/978-3-030-05789-3_5.
- [66] S. K. Kim, 'Design and Development of High-Performance Eco-Mg Alloys', *Magnes. Alloys*, p. 40.
- [67] J. K. Lee and S. K. Kim, 'Development of Novel Environment-Friendly Magnesium Alloys', *Adv. Mater. Res.*, vol. 47–50, pp. 940–943, Jun. 2008, doi: 10.4028/www.scientific.net/AMR.47-50.940.
- [68] J. Lee, H. Jo, and K. Kimshae, 'Effect of CaO addition on ignition behavior in molten AZ31 and AZ91D Magnesium alloys', *Rare Met.*, vol. 25, no. 6, pp. 155–159, Dec. 2006, doi: 10.1016/S1001-0521(08)60072-8.
- [69] S. K. Kim, 'Proportional Strength-Ductility Relationship of Non-SF6 Diecast AZ91D Eco-Mg Alloys', in *Magnesium Technology 2011*, W. H. Sillekens, S. R. Agnew, N. R. Neelameggham, and S. N. Mathaudhu, Eds. Cham: Springer International Publishing, 2011, pp. 131–136. doi: 10.1007/978-3-319-48223-1_25.
- [70] G. L. Song and A. Atrens, 'Corrosion Mechanisms of Magnesium Alloys', *Adv. Eng. Mater.*, no. 1, p. 23, 1999.
- [71] J. Walker, S. Shadanbaz, T. B. F. Woodfield, M. P. Staiger, and G. J. Dias, 'Magnesium biomaterials for orthopedic application: A review from a biological perspective: Magnesium Biomaterials for Orthopedic Application', *J. Biomed. Mater. Res. B Appl. Biomater.*, vol. 102, no. 6, pp. 1316–1331, Aug. 2014, doi: 10.1002/jbm.b.33113.
- [72] T. M. Pollock, 'Weight loss with magnesium alloys', *Science*, vol. 328, no. 5981, pp. 986–987, 2010.
- [73] H. X. Wang, S. K. Guan, X. Wang, C. X. Ren, and L. G. Wang, 'In vitro degradation and mechanical integrity of Mg–Zn–Ca alloy coated with Ca-deficient hydroxyapatite by the pulse electrodeposition process☆', *Acta Biomater.*, vol. 6, no. 5, pp. 1743–1748, May 2010, doi: 10.1016/j.actbio.2009.12.009.

- [74] T. J. Chen, R. Q. Wang, Y. Ma, and Y. Hao, 'Grain refinement of AZ91D magnesium alloy by Al-Ti-B master alloy and its effect on mechanical properties', *Mater. Des.*, vol. 34, pp. 637–648, Feb. 2012, doi: 10.1016/j.matdes.2011.05.020.
- [75] Y. Wang, X. Zeng, and W. Ding, 'Effect of Al-4Ti-5B master alloy on the grain refinement of AZ31 magnesium alloy', *Scr. Mater.*, vol. 54, no. 2, pp. 269–273, Jan. 2006, doi: 10.1016/j.scriptamat.2005.09.022.
- [76] M. Vlasceanu, S. Lun Sin, A. Elsayed, and C. Ravindran, 'Effect of Al-5Ti-1B on grain refinement, dendrite coherency and porosity of AZ91E magnesium alloy', *Int. J. Cast Met. Res.*, vol. 28, no. 1, pp. 39–46, Feb. 2015, doi: 10.1179/1743133614Y.0000000127.
- [77] T. J. Mason, 'Some neglected or rejected paths in sonochemistry – A very personal view', *Ultrason. Sonochem.*, vol. 25, pp. 89–93, Jul. 2015, doi: 10.1016/j.ultsonch.2014.11.014.
- [78] H. Puga, V. Carneiro, J. Barbosa, and V. Vieira, 'Effect of Ultrasonic Treatment in the Static and Dynamic Mechanical Behavior of AZ91D Mg Alloy', *Metals*, vol. 5, no. 4, pp. 2210–2221, Nov. 2015, doi: 10.3390/met5042210.
- [79] X. Liu *et al.*, 'Study on hydrogen removal of AZ91 alloys using ultrasonic argon degassing process', *Ultrason. Sonochem.*, vol. 26, pp. 73–80, Sep. 2015, doi: 10.1016/j.ultsonch.2014.12.015.
- [80] C. D. Lee, 'Effect of microporosity on tensile properties of as-cast AZ91D magnesium alloy', *Met. Mater. Int.*, vol. 8, no. 3, pp. 283–288, May 2002, doi: 10.1007/BF03186097.
- [81] B. A. Mikucki and J. D. Shearouse, 'Interdependence of Hydrogen and Microporosity in Magnesium Alloy AZ91', Mar. 1993, p. 930754. doi: 10.4271/930754.
- [82] G. I. Eskin and D. G. Eskin, *Ultrasonic treatment of light alloy melts*. CRC Press, 2014.
- [83] X. Du and E. Zhang, 'Microstructure and mechanical behaviour of semi-solid die-casting AZ91D magnesium alloy', *Mater. Lett.*, vol. 61, no. 11, pp. 2333–2337, May 2007, doi: 10.1016/j.matlet.2006.09.007.
- [84] H. Puga, J. Barbosa, S. Costa, S. Ribeiro, A. M. P. Pinto, and M. Prokic, 'Influence of indirect ultrasonic vibration on the microstructure and mechanical behavior of Al-Si-Cu alloy', *Mater. Sci. Eng. A*, vol. 560, pp. 589–595, Jan. 2013, doi: 10.1016/j.msea.2012.09.106.
- [85] H. Puga, 'Desenvolvimento de uma técnica de fundição de ligas de alumínio de alta resistência', Universidade do Minho, 2011.

- [86] R. Waksman, 'Current state of the absorbable metallic (magnesium) stent', *EuroIntervention J. Eur. Collab. Work. Group Interv. Cardiol. Eur. Soc. Cardiol.*, vol. 5 Suppl F, pp. F94-97, Dec. 2009, doi: 10.4244/EIJV5IFA16.
- [87] P. Lu, H. Fan, Y. Liu, L. Cao, X. Wu, and X. Xu, 'Controllable biodegradability, drug release behavior and hemocompatibility of PTX-eluting magnesium stents', *Colloids Surf. B Biointerfaces*, vol. 83, no. 1, pp. 23–28, Mar. 2011, doi: 10.1016/j.colsurfb.2010.10.038.
- [88] S. Asgari, C. Ag, and S. Asgari, *Biodegradable porous stent*. 2008. Accessed: Sep. 20, 2017. [Online]. Available: <https://www.google.com/patents/WO2008098922A3?cl=no>
- [89] 'Bioresorbable metal stent with controlled resorption', US20110076319 A1, Mar. 31, 2011 [Online]. Available: <http://www.google.ch/patents/US20110076319>
- [90] 'Degradable metal stent having agent-containing coating', US20090030507 A1, Jan. 29, 2009 [Online]. Available: <http://www.google.ch/patents/US20090030507>
- [91] J. A. Grogan, S. B. Leen, and P. E. McHugh, 'Computational micromechanics of bioabsorbable magnesium stents', *J. Mech. Behav. Biomed. Mater.*, vol. 34, pp. 93–105, Jun. 2014, doi: 10.1016/j.jmbbm.2014.01.007.
- [92] E. L. Boland, J. A. Grogan, C. Conway, and P. E. McHugh, 'Computer Simulation of the Mechanical Behaviour of Implanted Biodegradable Stents in a Remodelling Artery', *JOM*, vol. 68, no. 4, pp. 1198–1203, Apr. 2016, doi: 10.1007/s11837-015-1761-5.
- [93] J. Li, Q. Luo, Z. Xie, Y. Li, and Y. Zeng, 'Fatigue life analysis and experimental verification of coronary stent', *Heart Vessels*, vol. 25, no. 4, pp. 333–337, Jul. 2010, doi: 10.1007/s00380-009-1203-9.
- [94] S. Pattnaik, D. B. Karunakar, and P. K. Jha, 'Developments in investment casting process—A review', *J. Mater. Process. Technol.*, vol. 212, no. 11, pp. 2332–2348, Nov. 2012, doi: 10.1016/j.jmatprotec.2012.06.003.
- [95] A. Kumar, S. Kumar, and N. K. Mukhopadhyay, 'Introduction to magnesium alloy processing technology and development of low-cost stir casting process for magnesium alloy and its composites', *J. Magnes. Alloys*, vol. 6, no. 3, pp. 245–254, Sep. 2018, doi: 10.1016/j.jma.2018.05.006.
- [96] T. Wang, S. Yao, and W. Shen, 'A submerged-gate casting method', *J. Mater. Process. Technol.*, vol. 222, pp. 21–26, Aug. 2015, doi: 10.1016/j.jmatprotec.2015.02.034.
- [97] X. Li, W. Yu, J. Wang, and S. Xiong, 'Influence of melt flow in the gating system on microstructure and mechanical properties of high pressure die casting AZ91D magnesium

- alloy', *Mater. Sci. Eng. A*, vol. 736, pp. 219–227, Oct. 2018, doi: 10.1016/j.msea.2018.08.090.
- [98] M. Sahoo, *Technology for Magnesium Castings: Design, Products & Applications*. 2011.
- [99] A. A. Luo, 'Magnesium casting technology for structural applications', *J. Magnes. Alloys*, vol. 1, no. 1, pp. 2–22, Mar. 2013, doi: 10.1016/j.jma.2013.02.002.
- [100] J. M. G. Ferreira, *Tecnologia da Fundição*. Fundação Calouste Gulbenkian, 1999.
- [101] S. Lun Sin, D. Dubé, and R. Tremblay, 'An investigation on microstructural and mechanical properties of solid mould investment casting of AZ91D magnesium alloy', *Mater. Charact.*, vol. 59, no. 2, pp. 178–187, Feb. 2008, doi: 10.1016/j.matchar.2007.04.026.
- [102] B. D. Lee, U. H. Beak, K. W. Lee, G. S. Han, and J. W. Han, 'Protective Properties of SF₆ under Various Carrier Gases for the Protection of Molten Mg', *Mater. Trans.*, vol. 54, no. 1, pp. 66–73, 2013, doi: 10.2320/matertrans.M2012057.
- [103] H. Jafari, M. H. Idris, A. Ourdjini, and M. R. A. Kadir, 'Effect of Flux on In-Situ Melting Shell Investment Casting of AZ91D Magnesium Alloy', 2012, p. 6.
- [104] Z. Zhang and G. Morin, 'Effect of Inhibitor Gas on Mould-Magnesium Reactions in Investment Casting', *Magnes. Technol. 2004*, p. 7, 2004.
- [105] J. J. Barbosa and C. S. Ribeiro, 'Influence of crucible material on the level of contamination in TiAl using induction melting', *Int. J. Cast Met. Res.*, vol. 12, no. 5, pp. 293–301, Mar. 2000, doi: 10.1080/13640461.2000.11819366.
- [106] F. Gomes, H. Puga, J. Barbosa, and C. S. Ribeiro, 'Effect of melting pressure and superheating on chemical composition and contamination of yttria-coated ceramic crucible induction melted titanium alloys', *J. Mater. Sci.*, vol. 46, no. 14, pp. 4922–4936, Jul. 2011, doi: 10.1007/s10853-011-5405-z.
- [107] C. Cingi, *Mold-metal reactions in magnesium investment castings*. Helsinki University of Technology, 2006.
- [108] W. Ha and Y.-J. Kim, 'Effects of cover gases on melt protection of Mg alloys', *J. Alloys Compd.*, vol. 422, no. 1–2, pp. 208–213, Sep. 2006, doi: 10.1016/j.jallcom.2005.12.003.
- [109] M. P. Sealy, Y. B. Guo, J. F. Liu, and C. Li, 'Pulsed Laser Cutting of Magnesium-Calcium for Biodegradable Stents', *Procedia CIRP*, vol. 42, pp. 67–72, 2016, doi: 10.1016/j.procir.2016.02.190.

- [110] Paolo A. Netti, *Biomedical Foams For Tissue Engineering Applications*. Oxford: Elsevier, 2014.
- [111] A. V. Vyas and M. P. Sutaria, 'Investigation on Influence of the Cast Part Thickness on Interfacial Mold–Metal Reactions During the Investment Casting of AZ91 Magnesium Alloy', *Int. J. Met.*, vol. 15, no. 3, pp. 1021–1030, Jul. 2021, doi: 10.1007/s40962-020-00530-2.
- [112] S. Saxena, P. K. Sharma, and P. G. Student, 'Casting Fluidity of Metals and Alloys', *Int. J. Innov. Res. Sci. Eng. Technol.*, vol. 6, no. 2, p. 14, 2007, doi: 10.15680/IJIRSET.2017.0602171.
- [113] H. Huang, Y. X. Wang, P. H. Fu, L. M. Peng, H. Y. Jiang, and W. Y. Xu, 'Fluidity of AZ91D and Mg–3Nd–0.2Zn–Zr (wt-%) magnesium alloys: response to pouring and mould temperature', *Int. J. Cast Met. Res.*, vol. 26, no. 4, pp. 213–219, Aug. 2013, doi: 10.1179/1743133613Y.0000000055.
- [114] S. Sin and D. Dube, 'Influence of process parameters on fluidity of investment-cast AZ91D magnesium alloy', *Mater. Sci. Eng. A*, vol. 386, no. 1–2, pp. 34–42, Nov. 2004, doi: 10.1016/S0921-5093(04)00940-2.
- [115] W. Qudong *et al.*, 'Study on the fluidity of AZ91+ xRE magnesium alloy', *Mater. Sci. Eng. A*, vol. 271, no. 1, pp. 109–115, 1999.
- [116] B. S. Mitchell, *An Introduction to Materials Engineering and Science for Chemical and Materials Engineers*. John Wiley & Sons, 2004.
- [117] S. S. Khan, N. Hort, E. Subasic, and S. Schmauder, 'Fluidity of Magnesium alloys, an Experimental & Numerical approach', 2008. Accessed: Jul. 18, 2017. [Online]. Available: http://www.academia.edu/download/45611186/Fluidity_of_Magnesium_alloys_an_Experime20160513-906-6rrwxu.pdf
- [118] Y. Fu, H. Wang, X. Liu, and H. Hao, 'Effect of calcium addition on microstructure, casting fluidity and mechanical properties of Mg-Zn-Ce-Zr magnesium alloy', *J. Rare Earths*, vol. 35, no. 5, pp. 503–509, May 2017, doi: 10.1016/S1002-0721(17)60940-2.
- [119] Q. Hua, D. Gao, H. Zhang, Y. Zhang, and Q. Zhai, 'Influence of alloy elements and pouring temperature on the fluidity of cast magnesium alloy', *Mater. Sci. Eng. A*, vol. 444, no. 1, pp. 69–74, Jan. 2007, doi: 10.1016/j.msea.2006.08.060.
- [120] H. M. M. van Beusekom and P. W. Serruys, 'Drug-Eluting Stent Endothelium', *JACC Cardiovasc. Interv.*, vol. 3, no. 1, pp. 76–77, Jan. 2010, doi: 10.1016/j.jcin.2009.10.016.

- [121] S. N. David Chua, B. J. Mac Donald, and M. S. J. Hashmi, 'Finite element simulation of stent and balloon interaction', *J. Mater. Process. Technol.*, vol. 143–144, pp. 591–597, Dec. 2003, doi: 10.1016/S0924-0136(03)00435-7.
- [122] G. Mani, M. D. Feldman, D. Patel, and C. M. Agrawal, 'Coronary stents: A materials perspective', *Biomaterials*, vol. 28, no. 9, pp. 1689–1710, Mar. 2007, doi: 10.1016/j.biomaterials.2006.11.042.
- [123] C. Di Mario *et al.*, 'Drug-eluting bioabsorbable magnesium stent', *J. Intervent. Cardiol.*, vol. 17, no. 6, pp. 391–395, 2004.
- [124] K. Hanada, K. Matsuzaki, X. Huang, and Y. Chino, 'Fabrication of Mg alloy tubes for biodegradable stent application', *Mater. Sci. Eng. C*, vol. 33, no. 8, pp. 4746–4750, Dec. 2013, doi: 10.1016/j.msec.2013.07.033.
- [125] F. Liu *et al.*, 'The processing of Mg alloy micro-tubes for biodegradable vascular stents', *Mater. Sci. Eng. C*, vol. 48, pp. 400–407, Mar. 2015, doi: 10.1016/j.msec.2014.12.024.
- [126] E. P. Ivanova, K. Bazaka, and R. J. Crawford, 'Metallic biomaterials: types and advanced applications', in *New Functional Biomaterials for Medicine and Healthcare*, Elsevier, 2014, pp. 121–147. doi: 10.1533/9781782422662.121.
- [127] Y. Shimizu *et al.*, 'Medical application of magnesium and its alloys as degradable biomaterials', in *Interface Oral Health Science 2009*, Springer, 2010, pp. 318–320.
- [128] U. Sigwart *et al.*, 'Emergency stenting for acute occlusion after coronary balloon angioplasty.', *Circulation*, vol. 78, no. 5, pp. 1121–1127, 1988.
- [129] NIH - National Heart, Lung, and Blood Institute, 'What Are the Risks of Having a Stent?' <https://www.nhlbi.nih.gov/health/health-topics/topics/stents/risks#>
- [130] W.-Q. Wang, D.-K. Liang, D.-Z. Yang, and M. Qi, 'Analysis of the transient expansion behavior and design optimization of coronary stents by finite element method', *J. Biomech.*, vol. 39, no. 1, pp. 21–32, Jan. 2006, doi: 10.1016/j.jbiomech.2004.11.003.
- [131] C. Rogers, D. Y. Tseng, J. C. Squire, and E. R. Edelman, 'Balloon-artery interactions during stent placement', *Circ. Res.*, vol. 84, no. 4, pp. 378–383, 1999.
- [132] M. De Beule, R. Van Impe, B. Verheghe, P. Segers, and P. Verdonck, 'Finite element analysis and stent design: Reduction of dogboning', *Technol. Health Care Off. J. Eur. Soc. Eng. Med.*, vol. 14, no. 4, pp. 233–241, 2006.

- [133] J. Li, F. Zheng, X. Qiu, P. Wan, L. Tan, and K. Yang, 'Finite element analyses for optimization design of biodegradable magnesium alloy stent', *Mater. Sci. Eng. C*, vol. 42, pp. 705–714, Sep. 2014, doi: 10.1016/j.msec.2014.05.078.
- [134] D. E. Cutlip *et al.*, 'Clinical End Points in Coronary Stent Trials: A Case for Standardized Definitions', *Circulation*, vol. 115, no. 17, pp. 2344–2351, May 2007, doi: 10.1161/CIRCULATIONAHA.106.685313.
- [135] A. M. Sammel, D. Chen, and N. Jepson, 'New Generation Coronary Stent Technology—Is the Future Biodegradable?', *Heart Lung Circ.*, vol. 22, no. 7, pp. 495–506, Jul. 2013, doi: 10.1016/j.hlc.2013.02.008.
- [136] T. Muramatsu *et al.*, 'Progress in treatment by percutaneous coronary intervention: the stent of the future', *Rev. Esp. Cardiol. Engl. Ed*, vol. 66, no. 6, pp. 483–496, Jun. 2013.
- [137] P. Erne, M. Schier, and T. J. Resink, 'The Road to Bioabsorbable Stents: Reaching Clinical Reality?', *Cardiovasc. Intervent. Radiol.*, vol. 29, no. 1, pp. 11–16, Feb. 2006, doi: 10.1007/s00270-004-0341-9.
- [138] S. Saito, 'New horizon of bioabsorbable stent', *Catheter. Cardiovasc. Interv.*, vol. 66, no. 4, pp. 595–596, Dec. 2005, doi: 10.1002/ccd.20590.
- [139] J. A. Grogan, S. B. Leen, and P. E. McHugh, 'Comparing coronary stent material performance on a common geometric platform through simulated bench testing', *J. Mech. Behav. Biomed. Mater.*, vol. 12, pp. 129–138, Aug. 2012, doi: 10.1016/j.jmbbm.2012.02.013.
- [140] A. Ernst and J. Bulum, 'New generations of drug-eluting stents—a brief review', *EMJ Int Cardiol*, vol. 1, pp. 100–6, 2014.
- [141] S. A. Wayangankar and S. G. Ellis, 'Bioresorbable Stents: Is This Where We Are Headed?', *Prog. Cardiovasc. Dis.*, vol. 58, no. 3, pp. 342–355, Nov. 2015, doi: 10.1016/j.pcad.2015.08.011.
- [142] D. Chamié and A. Abizaid, 'Stent cronus: chegou o momento de adotarmos um stent nacional', *Rev Bras Cardiol Invas*, vol. 17, no. 3, pp. 300–4, 2009.
- [143] P. Ramadugu and K. Latha Alikatte, 'A Review on Biodegradable and Bioabsorbable Stents for Coronary Artery Disease', *J. Bioequivalence Bioavailab.*, vol. 08, no. 2, 2016, doi: 10.4172/jbb.1000269.

- [144] R. Waksman *et al.*, 'Safety and efficacy of bioabsorbable magnesium alloy stents in porcine coronary arteries', *Catheter. Cardiovasc. Interv.*, vol. 68, no. 4, pp. 607–617, Oct. 2006, doi: 10.1002/ccd.20727.
- [145] H. Hermawan and D. Mantovani, 'Process of prototyping coronary stents from biodegradable Fe–Mn alloys', *Acta Biomater.*, vol. 9, no. 10, pp. 8585–8592, Nov. 2013, doi: 10.1016/j.actbio.2013.04.027.
- [146] B. D. Ratner, Ed., *Biomaterials science: an introduction to materials in medicine*, Nachdr. San Diego: Academic Press, 2001.
- [147] X.-N. Gu and Y.-F. Zheng, 'A review on magnesium alloys as biodegradable materials', *Front. Mater. Sci. China*, vol. 4, no. 2, pp. 111–115, Jun. 2010, doi: 10.1007/s11706-010-0024-1.
- [148] P. Poncin and J. Proft, 'Stent tubing: understanding the desired attributes', in *Medical Device Materials: Proceedings of the Materials & Processes for Medical Devices Conference. Materials Park, OH: ASM International*, 2004, pp. 253–259.
- [149] W. D. Callister, *Materials science and engineering: an introduction*, 7. ed. New York, NY: Wiley, 2007.
- [150] J. G. Wall, H. Podbielska, and M. Wawrzńska, Eds., *Functionalized cardiovascular stents*. Duxford, United Kingdom: Woodhead Publishing, 2017.
- [151] W.-J. Ai, G. Fang, J. Zhou, M. A. Leeflang, and J. Duszczyc, 'Effect of twinning on the deformation behavior of an extruded Mg–Zn–Zr alloy during hot compression testing', *Mater. Sci. Eng. A*, vol. 556, pp. 373–381, Oct. 2012, doi: 10.1016/j.msea.2012.06.101.
- [152] T. Furushima and K. Manabe, 'Experimental and numerical study on deformation behavior in dieless drawing process of superplastic microtubes', *J. Mater. Process. Technol.*, vol. 191, no. 1–3, pp. 59–63, Aug. 2007, doi: 10.1016/j.jmatprotec.2007.03.084.
- [153] K. Yoshida and A. Koiwa, 'Cold drawing of magnesium alloy tubes for medical', *J. Solid Mech. Mater. Eng.*, vol. 5, no. 12, pp. 1071–1078, 2011.
- [154] S. Supriadi, T. Furushima, and K. Manabe, 'Real-time process control system of dieless tube drawing with an image processing approach', *Mater. Trans.*, vol. 53, no. 5, pp. 862–869, 2012.
- [155] G. Fang, W. Ai, S. Leeflang, J. Duszczyc, and J. Zhou, 'Multipass cold drawing of magnesium alloy minitubes for biodegradable vascular stents', *Mater. Sci. Eng. C*, vol. 33, no. 6, pp. 3481–3488, Aug. 2013, doi: 10.1016/j.msec.2013.04.039.

- [156] A. G. Demir *et al.*, 'Biodegradable magnesium coronary stents: material, design and fabrication', *Int. J. Comput. Integr. Manuf.*, vol. 27, no. 10, pp. 936–945, Oct. 2014, doi: 10.1080/0951192X.2013.834475.
- [157] F. Klocke, M. Schwade, A. Klink, and A. Kopp, 'EDM Machining Capabilities of Magnesium (Mg) Alloy WE43 for Medical Applications', *Procedia Eng.*, vol. 19, pp. 190–195, 2011, doi: 10.1016/j.proeng.2011.11.100.
- [158] A. Azushima *et al.*, 'Severe plastic deformation (SPD) processes for metals', *CIRP Ann.*, vol. 57, no. 2, pp. 716–735, 2008, doi: 10.1016/j.cirp.2008.09.005.
- [159] Z. J. Zheng, J. W. Liu, and Y. Gao, 'Achieving high strength and high ductility in 304 stainless steel through bi-modal microstructure prepared by post-ECAP annealing', *Mater. Sci. Eng. A*, vol. 680, pp. 426–432, Jan. 2017, doi: 10.1016/j.msea.2016.11.004.
- [160] D. Orlov, K. D. Ralston, N. Birbilis, and Y. Estrin, 'Enhanced corrosion resistance of Mg alloy ZK60 after processing by integrated extrusion and equal channel angular pressing', *Acta Mater.*, vol. 59, no. 15, pp. 6176–6186, Sep. 2011, doi: 10.1016/j.actamat.2011.06.033.
- [161] R. Z. Valiev and T. G. Langdon, 'Principles of equal-channel angular pressing as a processing tool for grain refinement', *Prog. Mater. Sci.*, vol. 51, no. 7, pp. 881–981, Sep. 2006, doi: 10.1016/j.pmatsci.2006.02.003.
- [162] A. Zhilyaev and T. Langdon, 'Using high-pressure torsion for metal processing: Fundamentals and applications', *Prog. Mater. Sci.*, vol. 53, no. 6, pp. 893–979, Aug. 2008, doi: 10.1016/j.pmatsci.2008.03.002.
- [163] Y. Zheng, *Magnesium alloys as degradable biomaterials*. CRC Press, 2015. [Online]. Available: <https://doi.org/10.1201/b18932>
- [164] G. Faraji, M. M. Mashhadi, and H. S. Kim, 'Tubular channel angular pressing (TCAP) as a novel severe plastic deformation method for cylindrical tubes', *Mater. Lett.*, vol. 65, no. 19, pp. 3009–3012, Oct. 2011, doi: 10.1016/j.matlet.2011.06.039.
- [165] Q. Ge, M. Vedani, and G. Vimercati, 'Extrusion of Magnesium Tubes for Biodegradable Stent Precursors', *Mater. Manuf. Process.*, vol. 27, no. 2, pp. 140–146, Feb. 2012, doi: 10.1080/10426914.2011.560231.
- [166] R. B. Figueiredo, S. Sabbaghianrad, A. Giwa, J. R. Greer, and T. G. Langdon, 'Evidence for exceptional low temperature ductility in polycrystalline magnesium processed by severe plastic deformation', *Acta Mater.*, vol. 122, pp. 322–331, Jan. 2017, doi: 10.1016/j.actamat.2016.09.054.

- [167] C. L. P. Silva *et al.*, 'Effect of severe plastic deformation on the biocompatibility and corrosion rate of pure magnesium', *J. Mater. Sci.*, vol. 52, no. 10, pp. 5992–6003, May 2017, doi: 10.1007/s10853-017-0835-x.
- [168] A. Yamashita, Z. Horita, and T. G. Langdon, 'Improving the mechanical properties of magnesium and a magnesium alloy through severe plastic deformation', *Mater. Sci. Eng. A*, vol. 300, no. 1, pp. 142–147, 2001.
- [169] Q. Ge, D. Dellasega, A. G. Demir, and M. Vedani, 'The processing of ultrafine-grained Mg tubes for biodegradable stents', *Acta Biomater.*, vol. 9, no. 10, pp. 8604–8610, Nov. 2013, doi: 10.1016/j.actbio.2013.01.010.
- [170] R. Kapoor, 'Severe Plastic Deformation of Materials', in *Materials Under Extreme Conditions*, Elsevier, 2017, pp. 717–754.
- [171] Y. F. Zheng, X. N. Gu, and F. Witte, 'Biodegradable metals', *Mater. Sci. Eng. R Rep.*, vol. 77, pp. 1–34, Mar. 2014, doi: 10.1016/j.mser.2014.01.001.
- [172] S. M. Fatemi-Varzaneh and A. Zarei-Hanzaki, 'Accumulative back extrusion (ABE) processing as a novel bulk deformation method', *Mater. Sci. Eng. A*, vol. 504, no. 1–2, pp. 104–106, Mar. 2009, doi: 10.1016/j.msea.2008.10.027.
- [173] H. Wang, Y. Estrin, H. Fu, G. Song, and Z. Zúberová, 'The Effect of Pre-Processing and Grain Structure on the Bio-Corrosion and Fatigue Resistance of Magnesium Alloy AZ31', *Adv. Eng. Mater.*, vol. 9, no. 11, pp. 967–972, Nov. 2007, doi: 10.1002/adem.200700200.
- [174] D. Song, A. Ma, J. Jiang, P. Lin, D. Yang, and J. Fan, 'Corrosion behavior of equal-channel-angular-pressed pure magnesium in NaCl aqueous solution', *Corros. Sci.*, vol. 52, no. 2, pp. 481–490, Feb. 2010, doi: 10.1016/j.corosci.2009.10.004.
- [175] M. Alvarez-Lopez *et al.*, 'Corrosion behaviour of AZ31 magnesium alloy with different grain sizes in simulated biological fluids☆', *Acta Biomater.*, vol. 6, no. 5, pp. 1763–1771, May 2010, doi: 10.1016/j.actbio.2009.04.041.
- [176] K. D. Ralston, N. Birbilis, and C. H. J. Davies, 'Revealing the relationship between grain size and corrosion rate of metals', *Scr. Mater.*, vol. 63, no. 12, pp. 1201–1204, Dec. 2010, doi: 10.1016/j.scriptamat.2010.08.035.
- [177] A. G. Demir *et al.*, 'Fiber laser micromachining of magnesium alloy tubes for biocompatible and biodegradable cardiovascular stents', Feb. 2012, p. 823730. doi: 10.1117/12.910131.

- [178] A. G. Demir, B. Previtali, and C. A. Biffi, 'Fibre Laser Cutting and Chemical Etching of AZ31 for Manufacturing Biodegradable Stents', *Adv. Mater. Sci. Eng.*, vol. 2013, pp. 1–11, 2013, doi: 10.1155/2013/692635.
- [179] D. Stoeckel, C. Bonsignore, and S. Duda, 'A survey of stent designs', *Minim. Invasive Ther. Allied Technol.*, vol. 11, no. 4, pp. 137–147, 2002.
- [180] C.-H. Chen and A. J. Kirtane, 'Stents, Restenosis, and Stent Thrombosis', *Interv. Card. Catheter. Handb. E-Book*, 2017.
- [181] K. Zeng, 'Optimization of support structures for selective laser melting.', University of Louisville, 2015. doi: 10.18297/etd/2221.
- [182] X. Zhao, B. Song, Y. Zhang, X. Zhu, Q. Wei, and Y. Shi, 'Decarburization of stainless steel during selective laser melting and its influence on Young's modulus, hardness and tensile strength', *Mater. Sci. Eng. A*, vol. 647, pp. 58–61, Oct. 2015, doi: 10.1016/j.msea.2015.08.061.
- [183] K. Takahata and Y. B. Gianchandani, 'A Planar Approach for Manufacturing Cardiac Stents: Design, Fabrication, and Mechanical Evaluation', *J. Microelectromechanical Syst.*, vol. 13, no. 6, pp. 933–939, Dec. 2004, doi: 10.1109/JMEMS.2004.838357.
- [184] M. Buehler and P. Molian, 'Nanosecond Laser Induced Periodic Surface Structures on Drug Elution Profiles in Stents', *J. Med. Devices*, vol. 6, no. 3, pp. 031002-031002–11, Jul. 2012, doi: 10.1115/1.4006539.
- [185] Eric Lundin, 'Small-scale laser cutting for stent, tube fabrication', *TUBE PIPE J.*, 2015.
- [186] S. O. Kim and J. S. Kwak, 'Magnetic force improvement and parameter optimization for magnetic abrasive polishing of AZ31 magnesium alloy', *Trans. Nonferrous Met. Soc. China*, vol. 18, pp. s369–s373, 2008.
- [187] S. Chen *et al.*, 'In vivo degradation and bone response of a composite coating on Mg-Zn-Ca alloy prepared by microarc oxidation and electrochemical deposition', *J. Biomed. Mater. Res. B Appl. Biomater.*, vol. 100B, no. 2, pp. 533–543, Feb. 2012, doi: 10.1002/jbm.b.31982.
- [188] F. Witte *et al.*, 'In vivo corrosion of four magnesium alloys and the associated bone response', *Biomaterials*, vol. 26, no. 17, pp. 3557–3563, Jun. 2005, doi: 10.1016/j.biomaterials.2004.09.049.

- [189] N. Erdmann *et al.*, 'Biomechanical testing and degradation analysis of MgCa0.8 alloy screws: A comparative in vivo study in rabbits', *Acta Biomater.*, vol. 7, no. 3, pp. 1421–1428, Mar. 2011, doi: 10.1016/j.actbio.2010.10.031.
- [190] D. Pierson *et al.*, 'A simplified in vivo approach for evaluating the bioabsorbable behavior of candidate stent materials', *J. Biomed. Mater. Res. B Appl. Biomater.*, vol. 100B, no. 1, pp. 58–67, Jan. 2012, doi: 10.1002/jbm.b.31922.
- [191] X. L. Liu, W. R. Zhou, Y. H. Wu, Y. Cheng, and Y. F. Zheng, 'Effect of sterilization process on surface characteristics and biocompatibility of pure Mg and MgCa alloys', *Mater. Sci. Eng. C*, vol. 33, no. 7, pp. 4144–4154, Oct. 2013, doi: 10.1016/j.msec.2013.06.004.
- [192] H. Hermawan, D. Dubé, and D. Mantovani, 'Degradable metallic biomaterials: Design and development of Fe-Mn alloys for stents', *J. Biomed. Mater. Res. A*, vol. 9999A, p. NA-NA, 2009, doi: 10.1002/jbm.a.32224.
- [193] M. Bram, T. Ebel, M. Wolff, A. P. Cysne Barbosa, and N. Tuncer, 'Applications of powder metallurgy in biomaterials', in *Advances in Powder Metallurgy*, Elsevier, 2013, pp. 520–554.
- [194] C. Yan, L. Hao, A. Hussein, and D. Raymont, 'Evaluations of cellular lattice structures manufactured using selective laser melting', *Int. J. Mach. Tools Manuf.*, vol. 62, pp. 32–38, Nov. 2012, doi: 10.1016/j.ijmachtools.2012.06.002.
- [195] C. Yan, L. Hao, A. Hussein, P. Young, and D. Raymont, 'Advanced lightweight 316L stainless steel cellular lattice structures fabricated via selective laser melting', *Mater. Des.*, vol. 55, pp. 533–541, Mar. 2014, doi: 10.1016/j.matdes.2013.10.027.
- [196] Y. Wessargues *et al.*, 'Additive manufacturing of vascular implants by selective laser melting', *Biomed. Tech.*, vol. 59, pp. S401–S404, 2014, doi: 10.1515/bmt-2014-5005.
- [197] P. Mariot, M. A. Leeftang, L. Schaeffer, and J. Zhou, 'An investigation on the properties of injection-molded pure iron potentially for biodegradable stent application', *Powder Technol.*, vol. 294, pp. 226–235, Jun. 2016, doi: 10.1016/j.powtec.2016.02.042.
- [198] P. F. Santos *et al.*, 'Fabrication of low-cost beta-type Ti-Mn alloys for biomedical applications by metal injection molding process and their mechanical properties', *J. Mech. Behav. Biomed. Mater.*, vol. 59, pp. 497–507, Jun. 2016, doi: 10.1016/j.jmbbm.2016.02.035.
- [199] M. F. F. A. Hamidi *et al.*, 'A review of biocompatible metal injection moulding process parameters for biomedical applications', *Mater. Sci. Eng. C*, vol. 78, pp. 1263–1276, Sep. 2017, doi: 10.1016/j.msec.2017.05.016.

- [200] Y. Li, L. Li, and K. A. Khalil, 'Effect of powder loading on metal injection molding stainless steels', *J. Mater. Process. Technol.*, vol. 183, no. 2, pp. 432–439, Mar. 2007, doi: 10.1016/j.jmatprotec.2006.10.039.
- [201] A. Royer, T. Barriere, and J. C. Gelin, 'The degradation of poly(ethylene glycol) in an Inconel 718 feedstock in the metal injection moulding process', *Powder Technol.*, vol. 284, pp. 467–474, Nov. 2015, doi: 10.1016/j.powtec.2015.07.032.
- [202] D. Y. Park, S. W. Lee, S. J. Park, Y.-S. Kwon, and I. Otsuka, 'Effects of Particle Sizes on Sintering Behavior of 316L Stainless Steel Powder', *Metall. Mater. Trans. A*, vol. 44, no. 3, pp. 1508–1518, Mar. 2013, doi: 10.1007/s11661-012-1477-x.
- [203] B. Hausnerova, *Powder injection moulding-An alternative processing method for automotive items*. InTech, 2011.
- [204] A. Romero, G. Herranz, and A. L. Morales, 'Study of magnetoelastic properties of pure nickel parts produced by metal injection moulding', *Mater. Des.*, vol. 88, pp. 438–445, Dec. 2015, doi: 10.1016/j.matdes.2015.08.137.
- [205] A. Fayyaz, N. Muhamad, A. B. Sulong, J. Rajabi, and Y. N. Wong, 'Fabrication of cemented tungsten carbide components by micro-powder injection moulding', *J. Mater. Process. Technol.*, vol. 214, no. 7, pp. 1436–1444, Jul. 2014, doi: 10.1016/j.jmatprotec.2014.02.006.
- [206] S. Antusch *et al.*, 'Mechanical and microstructural investigations of tungsten and doped tungsten materials produced via powder injection molding', *Nucl. Mater. Energy*, vol. 3–4, pp. 22–31, Jul. 2015, doi: 10.1016/j.nme.2015.04.002.
- [207] L. Zhang, D. Li, X. Qu, M. Qin, X. He, and Z. Li, 'Microstructure and tensile properties optimization of MIM418 superalloy by heat treatment', *J. Mater. Process. Technol.*, vol. 227, pp. 71–79, Jan. 2016, doi: 10.1016/j.jmatprotec.2015.08.001.
- [208] H. O. Gulsoy, S. Pazarlioglu, N. Gulsoy, B. Gundede, and O. Mutlu, 'Effect of Zr, Nb and Ti addition on injection molded 316L stainless steel for bio-applications: Mechanical, electrochemical and biocompatibility properties', *J. Mech. Behav. Biomed. Mater.*, vol. 51, pp. 215–224, Nov. 2015, doi: 10.1016/j.jmbbm.2015.07.016.
- [209] X. Kong, T. Barriere, and J. C. Gelin, 'Determination of critical and optimal powder loadings for 316L fine stainless steel feedstocks for micro-powder injection molding', *J. Mater. Process. Technol.*, vol. 212, no. 11, pp. 2173–2182, Nov. 2012, doi: 10.1016/j.jmatprotec.2012.05.023.

- [210] A. T. Sidambe, I. A. Figueroa, H. G. C. Hamilton, and I. Todd, 'Metal injection moulding of CP-Ti components for biomedical applications', *J. Mater. Process. Technol.*, vol. 212, no. 7, pp. 1591–1597, Jul. 2012, doi: 10.1016/j.jmatprotec.2012.03.001.
- [211] 'Stent made by rotational molding or centrifugal casting and method for making the same', 6574851, Jun. 2003
- [212] Y. B. Guo and M. Salahshoor, 'Process mechanics and surface integrity by high-speed dry milling of biodegradable magnesium–calcium implant alloys', *CIRP Ann.*, vol. 59, no. 1, pp. 151–154, 2010, doi: 10.1016/j.cirp.2010.03.051.
- [213] J. A. Nordin, A. K. Nasution, and H. Hermawan, 'Can the Current Stent Manufacturing Process be Used for Making Metallic Biodegradable Stents', *Adv. Mater. Res.*, vol. 746, pp. 416–421, Aug. 2013, doi: 10.4028/www.scientific.net/AMR.746.416.
- [214] P. Chalermkarnnon, A. Manonukul, N. Muenya, H. Nakayama, and M. Fujiwara, 'Minimizing Contamination in Commercial Mass Production of Metal Injection Molded Pure Titanium', *J. Manuf. Sci. Eng.*, vol. 133, no. 5, p. 054502, 2011.
- [215] V. Lopes, H. Puga, J. Barbosa, and J. C. Teixeira, 'Effect of Ytria Mould Coating on the Investment Casting of AZ91D-1 wt% CaO Magnesium Alloy', *Int. J. Met.*, vol. 14, no. 1, pp. 98–107, Jan. 2020, doi: 10.1007/s40962-019-00339-8.
- [216] V. Lopes, H. Puga, I. V. Gomes, N. Peixinho, J. C. Teixeira, and J. Barbosa, 'Magnesium stents manufacturing: Experimental application of a novel hybrid thin-walled investment casting approach', *J. Mater. Process. Technol.*, vol. 299, p. 117339, Jan. 2022, doi: 10.1016/j.jmatprotec.2021.117339.
- [217] B. A. Ramachandran M, 'Effect of Process Parameters on Roughness and Hardness of Surface and Dimensional Accuracy of Lost Wax Process Casting', *J. Mater. Sci. Eng.*, vol. 04, no. 04, 2015, doi: 10.4172/2169-0022.1000175.
- [218] C. Frueh, D. R. Poirier, M. C. Maguire, and R. A. Harding, 'Attempts to develop a ceramic mould for titanium casting—a review', *Int. J. Cast Met. Res.*, vol. 9, no. 4, pp. 233–239, Nov. 1996, doi: 10.1080/13640461.1996.11819664.
- [219] R. L. Saha, T. K. Nandy, R. D. K. Misra, and K. T. Jacob, 'On the evaluation of stability of rare earth oxides as face coats for investment casting of titanium', *Metall. Trans. B*, vol. 21, no. 3, pp. 559–566, Jun. 1990, doi: 10.1007/BF02667869.

- [220] T. Phetrattanarangsi *et al.*, 'The behavior of gypsum-bonded investment in the gold jewelry casting process', *Thermochim. Acta*, vol. 657, pp. 144–150, Nov. 2017, doi: 10.1016/j.tca.2017.09.008.
- [221] M. E. Moussa, M. A. Waly, and A. M. El-Sheikh, 'Effect of Ca addition on modification of primary Mg₂Si, hardness and wear behavior in Mg–Si hypereutectic alloys', *J. Magnes. Alloys*, vol. 2, no. 3, pp. 230–238, Sep. 2014, doi: 10.1016/j.jma.2014.09.005.
- [222] M. Lotfpour, M. Emamy, C. Dehghanian, and B. Pourbahari, 'Ca Addition Effects on the Microstructure, Tensile and Corrosion Properties of Mg Matrix Alloy Containing 8 wt.% Mg₂Si', *J. Mater. Eng. Perform.*, vol. 27, no. 2, pp. 411–422, Feb. 2018, doi: 10.1007/s11665-017-3121-9.
- [223] F. Czerwinski, 'The oxidation behaviour of an AZ91D magnesium alloy at high temperatures', *Acta Mater.*, vol. 50, no. 10, pp. 2639–2654, Jun. 2002, doi: 10.1016/S1359-6454(02)00094-0.
- [224] H. Jafari, M. H. Idris, and A. Ourdjini, 'High temperature oxidation of AZ91D magnesium alloy granule during in-situ melting', *Corros. Sci.*, vol. 53, no. 2, pp. 655–663, Feb. 2011, doi: 10.1016/j.corsci.2010.10.012.
- [225] Bruker, *Desk-Top X-Ray Microtomograph SkyScan 1275 User Manual*, vol. 1.2. Kontich: Belgium, 2016.
- [226] I. Duarte, T. Fiedler, L. Krstulovic-Opara, and M. Vesenjak, 'Brief Review on Experimental and Computational Techniques for Characterization of Cellular Metals', *Metals*, p. 726, 2020.
- [227] C. Yuangyai and H. B. Nembhard, 'Chapter 8 - Design of Experiments: A Key to Innovation in Nanotechnology', in *Emerging Nanotechnologies for Manufacturing*, William Andrew, 2010, pp. 207–234. doi: 10.1007/978-3-642-28882-1_11.
- [228] S. M. Zahraee, A. Memari, G. Rezaei, J. Afshar, and J. B. M. Rohani, 'Teaching the Design of Experiment and Response Surface Methodology Using Paper Helicopter Experiment', p. 11.
- [229] R. K. Roy, *A Primer on The Taguchi Method*. USA: Society of Manufacturing Engineers, 2010.
- [230] N. Celik and E. Turgut, 'Design analysis of an experimental jet impingement study by using Taguchi method', *Heat Mass Transf.*, vol. 48, no. 8, pp. 1407–1413, 2012, doi: 10.1007/s00231-012-0989-7.

- [231] G. Taguchi, S. Chowdhury, and Y. Wu, *Taguchi's Quality Engineering Handbook*. New Jersey, USA: John Wiley & Sons, Inc., 2005.
- [232] I. V. Gomes, H. Puga, and J. L. Alves, 'Shape and functional optimization of biodegradable magnesium stents for manufacturing by ultrasonic-microcasting technique', *Int. J. Interact. Des. Manuf. IJIDeM*, Dec. 2017, doi: 10.1007/s12008-017-0442-8.
- [233] V. H. Carneiro, S. D. Rawson, H. Puga, J. Meireles, and P. J. Withers, 'Additive manufacturing assisted investment casting: A low-cost method to fabricate periodic metallic cellular lattices', *Addit. Manuf.*, p. 101085, Jan. 2020, doi: 10.1016/j.addma.2020.101085.
- [234] M. Amiri Farsani and R. Gholamipour, 'Silica-Free Zirconia-Based Primary Slurry for Titanium Investment Casting', *Int. J. Met.*, vol. 14, no. 1, pp. 92–97, Jan. 2020, doi: 10.1007/s40962-019-00335-y.
- [235] F. Czerwinski, 'Oxidation Characteristics of Magnesium Alloys', *JOM*, vol. 64, no. 12, pp. 1477–1483, Dec. 2012, doi: 10.1007/s11837-012-0477-z.
- [236] Q. Tan, A. Atrens, N. Mo, and M.-X. Zhang, 'Oxidation of magnesium alloys at elevated temperatures in air: A review', *Corros. Sci.*, vol. 112, pp. 734–759, Nov. 2016, doi: 10.1016/j.corsci.2016.06.018.

SCIENTIFIC CONTRIBUTIONS

Papers in Scientific Journals

1. **V. Lopes**, H. Puga, J. Barbosa, and J. C. Teixeira, 'Effect of Yttria Mould Coating on the Investment Casting of AZ91D-1 wt.% CaO Magnesium Alloy', *Int. J. Met.*, vol. 14, no. 1, pp. 98–107, Jan. 2020, doi: 10.1007/s40962-019-00339-8.240.
2. **V. Lopes**, H. Puga, I. V. Gomes, N. Peixinho, J. C. Teixeira, and J. Barbosa, 'Magnesium stents manufacturing: Experimental application of a novel hybrid thin-walled investment casting approach', *J. Mater. Process. Technol.*, vol. 299, p. 117339, Jan. 2022, doi: 10.1016/j.jmatprotec.2021.117339.
3. V. H. Carneiro, J. Pereira, **V. Lopes**, C. Jesus, and H. Puga, 'Inverse engineering approach to determine the elastic properties of lightweight expanded clay', *Constr. Build. Mater.*, vol. 216, pp. 11–18, Aug. 2019, doi: 10.1016/j.conbuildmat.2019.04.264.
4. H. Puga, V. H. Carneiro, C. Jesus, J. Pereira, and **V. Lopes**, 'Influence of particle diameter in mechanical performance of Al expanded clay syntactic foams', *Compos. Struct.*, vol. 184, pp. 698–703, Jan. 2018, doi: 10.1016/j.compstruct.2017.10.040.

Papers in Scientific Conferences

1. **V. Lopes**, J. Pereira, V. H. Carneiro, and H. Puga, 'Magnesium alloy biodegradable scaffolds: Simulation of casting and manufacturing', in *Bioengineering (ENBENG), 2017 IEEE 5th Portuguese Meeting on*, 2017, pp. 1–4.